DISINFECTION OF SOLID SURFACES BY COMBINATIONS OF UV LIGHT AND OXIDATION TREATMENTS

by

Douglas Walter McGregor Gardner

A Doctoral Thesis

Submitted in partial fulfilment of the requirements
for the award of

Doctor of Philosophy of Loughborough University

March 1997

ABSTRACT

Combinations of ultraviolet light (UV) and the oxidising agents, hydrogen peroxide (H_2O_2) and ozone (O_3), were evaluated for disinfecting solid surfaces. Studies were conducted using spores of the bacterium *Bacillus subtilis* (ATCC 6633) attached to materials ranging from filter papers and membranes to aluminium and PTFE. Techniques were developed for depositing, recovering and enumerating spores from these surfaces.

Treatment of spore-laden surfaces was carried out both with bench-top mounted UV sources and in a specially designed irradiation chamber. Objects for treatment in the latter were suspended in the UV field created by four symmetrically arranged sources. The chamber was equipped with an air-atomising nozzle so that objects could be treated with sprays of aqueous oxidants whilst undergoing irradiation. Provision was also made for electrostatically charging the nozzle.

Kinetic data was collected on the inactivation of spores by various combinations of UV and oxidising agents. Synergistic inactivation of spores was observed for UV and H_2O_2, with a particularly high rate of inactivation being recorded for H_2O_2 concentrations in the range 0.5 - 1.0 % w/v H_2O_2. Aqueous ozone did not exhibit sporicidal action under the conditions investigated. Some evidence was obtained to show that electrostatic charging of sprays did result in enhanced rates of surface impact, but the results obtained were inconclusive.

The structure of the surface on which spores were present was shown to influence the disinfection levels obtained when the surface was exposed to UV. A zonal shielding model was developed in which the surface was assumed to comprise of a finite number of zones in which the spores were afforded specific protection to incident UV. This model was fitted to the experimental data with good results.

Modelling of the UV intensity fields created by UV sources and the intensities produced on the surfaces of objects within UV fields was conducted. These models were combined with experimentally-derived kinetic expressions to predict the disinfection rates on objects of regular geometry undergoing treatment either with UV or with UV in combination with H_2O_2 .

ACKNOWLEDGEMENTS

TABLE OF CONTENTS

3. DISINFECTION EXPERIMENTS

5. UV FIELD MODELLING

6. COMBINED UV-H₂O₂ DISINFECTION MODEL

7. OVERALL CONCLUSIONS AND SUGGESTIONS FOR FURTHER WORK

APPENDIX 1. COMPUTER PROGRAMS

APPENDIX 2. IMPACT TESTS IN THE SPRAY CHAMBER

APPENDIX 3. STATISTICS

REFERENCES

LIST OF TABLES

TABLE OF FIGURES

1. INTRODUCTION

1.1 Surface disinfection

1.1.1 Definition of Terms

'Sterilisation' is commonly understood as implying the total destruction or elimination of *all* forms of life. 'Disinfection', on the other hand, has an altogether more restricted meaning i.e. that of freeing from infection. Block (1983) defines the term more specifically as 'destroying disease germs or other harmful micro-organisms or inactivating viruses'. He further goes on to state that disinfection agents are generally 'those that kill the growing forms, but *not necessarily,* the resistant spore forms of bacteria, *except* when the intended use is specifically against an organism forming spores'.

The context in which the term disinfection will be used throughout this work is simply in terms of processes or agents that result in either the total or partial elimination of certain organisms but not others. This definition maintains the distinction between sterilisation and disinfection without providing unnecessary constraints on the use of the latter term.

1.1.2 Scope of Application

Attention will be focused here on the disinfection of solid objects, as opposed to liquids or gases, which might harbour populations of harmful or otherwise unwanted micro-organisms. The particular concern of this work is those objects which human beings might come into contact with and which might act as potential sources of infection. Such objects in effect act as vehicles of infection. Excluded from consideration here is human skin; whilst frequently implicated as a vehicle of infection, particularly in hospital environments (Springthorpe and Sattar, 1990), its sensitivity requires specialised treatment which lies

outside the scope of this work.

In any consideration of the disinfection of a solid surface attention should be paid to the nature and properties of that surface. Contaminating micro-organisms will not necessarily be exposed at the top layers of contaminating surfaces. In porous materials for example, micro-organisms might be present deep in the body of the material, remote from the surface. Even surfaces which appear visibly smooth can contain microtopographic features which can provide protection to contaminating micro-organisms (Springthorpe and Sattar, 1990). Evidence exists to suggest that, in broad terms, the resistance of micro-organisms on a surface to disinfection treatments is often greater than the resistance of the same micro-organism when in suspension in liquid (Morris, 1972).

1.1.3 Disinfectants

There have been many techniques developed over several years for achieving sterilisation or disinfection of microbially-contaminated substances. These can be divided into two categories - physical agents and chemical agents. Table 1.1 lists the more common agents.

Physical agents	Chemical agents
Dry heat (hot air)	Salts
Moist heat (steam)	Acids and alkalis
Non-ionising radiation (UV)	Halogens and halogen-forming compounds
Ionising radiation	Oxidising agents
Filtration	Ether
	Alcohols
	Soaps and detergents
	Phenols
	Formaldehyde
	Glutaraldehyde
	Ethylene Oxide

Table 1.1 Common sterilants and disinfectants (After Thomas (1988))

2

Naturally, no single agent is likely ever to be universally applicable in all situations. Treatments based on the application of moist heat at a temperature of 121°C, though generally effective would be wholly unsuitable for the treatment of a heat-labile material. Likewise, the use of certain chemical agents on foods would be inappropriate in instances where residual agent might itself prove harmful to health. The primary purpose of presenting Table 1.1 is to provide an indication of the wide range of treatments and agents which are available. Attention will focus in this work on the use of ultraviolet light and the oxidising agents, hydrogen peroxide and ozone used either by themselves or in combination with one another. Full descriptions on the use and efficacy of the other agents mentioned in the table may be found in Block (1983). Treatments which feature combinations of these agents are referred to as 'advanced oxidation treatments'. These treatments will have particular advantages in certain applications but not in others. It is not the intention in what follows to identify every recorded application but generally to define broad areas where these techniques might hold future promise.

Food represents a particularly good example. Food can be a source of infection to humans due to contamination of the foodstuff by some external source or alternatively, the flora naturally associated with the surfaces of foods or within the foods can cause infection. Ingestion of microbially contaminated food can lead to food poisoning or food intoxication with consequences varying from gastric disturbances of varying degrees of severity to death. Much concern is being expressed in the microbiological contamination of fresh meat during slaughter and subsequent processing. This can be reduced by good sanitary practice but contamination of carcasses can still occur. Therefore there has been much interest in the disinfection of carcasses in abattoirs in order to maintain quality on storage, particularly in respect to beef (Reagan et al., 1973; Stermer et al., 1987; Greer and Jones, 1989; Kenney et al., 1995), although other studies have examined chicken (Banati et al., 1993), fish (Huang and Toledo, 1982) and pork (Fu et al., 1994).

Concern is not only directed towards meat; dried particulate foodstuffs, such as herbs and spices (Shama et al., 1994) and cereals and nuts (Andrews, 1996), can be a source of

infection due to micro-organisms present both within the particles and on their surfaces.

Food can also become contaminated by the packaging in which it is placed. A certain degree of contamination of the packaging might prove acceptable, as the levels on the product generally exceed those on the packaging by several orders of magnitude. However, the presence of even low numbers of certain pathogenic bacteria such as *Salmonella* are unlikely to be tolerated under any conditions. One area of food packaging that has received much attention is aseptic packaging, which is the process of placing a sterile product in a sterile container (Anon., 1980).

Considerable scope for UV and UV-associated disinfection treatments exists in hospitals and other health care environments. This ranges from instruments employed in general surgery and which may not, for whatever reason, be subjected to thermally treatment, such as endoscopes (Padial and Osborne, 1992), bone grafts and dialysis equipment (Thomas, 1988), equipment used in dental surgeries (Gurevich *et al.*, 1996) to more advanced video-imaging medical equipment (Duppler, 1992). In addition, there may be a role for UV-based disinfection treatments in controlling the spread in hospitals of nosocomial infections such as methicillin resistant *Staphylococcus aureus* (MRSA) which have been shown to be dependent on a number of environmental factors (Ruef, 1995).

1.2 UV irradiation

1.2.1 Introduction

The UV spectrum can be divided into 4 regions: UVA, from 400 to 315 nm, UVB, from 315 to 280 nm, UVC, from 280 to 200 nm, and Vacuum-UV, less than 200 nm (so termed because air strongly absorbs UV at wavelengths less than 200 nm, therefore making its use only practical under vacuum conditions; Meulemans, 1987).

The use of ultraviolet light for the destruction of micro-organisms was observed in the early 20th century but was never adopted at that time as a practical method of sterilisation due to the low power of the UV lamps available. In the 1970's UV sterilisation became of interest again as new legislation controlling chemical residues in food packaging came into force and new higher power UV lamps became available (Bachman, 1975; Sugawara *et al.*, 1981).

The germicidal effectiveness of different UV wavelengths for a particular organism may be directly compared in a so-called 'inactivation action spectrum'. Peak germicidal activity is generally found to be at a wavelength of 260 nm, which is close to the peak line of a mercury vapour lamp (Munakata *et al.*, 1991).

1.2.2 Disinfection with UV

Ultraviolet light (UV) is an effective disinfectant for a wide range of micro-organisms and is used for the disinfection of water (Shama, 1992) and the disinfection of air (Nakamura, 1987). There are many other potential applications for UV as a disinfectant. UV has been proposed as a disinfectant for food packaging (Bachman, 1975; Toledo *et al.*, 1973). It has also been proposed as a disinfectant for foodstuffs, including meat and fish.

Huang and Toledo (1982) investigated the use of UV as a disinfectant for the surface of whole fish. They found UV to be an effective disinfectant when applied to smooth-surfaced fish such as Spanish mackerel. However, UV was not very effective when used on rough-surfaced fish, such as mullet and croaker. The authors attributed this to shadow effects caused by the rough surface which shielded the natural flora from the incident UV.

In a study on the use of UV for the disinfection of beef carcasses, Stermer *et al.* (1987) found that UV reduced the concentration of natural flora on beef steaks. The natural flora, when cultured and grown on agar plates, was disinfected more quickly on agar plates than on the beef steaks, suggesting that the surface afforded some protection to the flora.

Reagan *et al.* (1973) showed that UV irradiation produced an increased lag phase in the microbial growth curve on beef tissue and also produced a reduced growth rate after the initial lag phase. Greater disinfection levels were achieved on fatty tissue than on lean muscle tissue. Kaess and Wiederman (1973) showed that UV was an effective disinfectant for chilled beef slices when the UV intensity was greater than 2 $\mu W/cm^2$. These workers found that the application of UV extended the initial lag phase in the growth of *Pseudomonas*, and the moulds *Tharnidium* and *Penicillium*. The microbial growth rate of *Pseudomonas* was also reduced but the growth rate of the moulds was unaffected.

Hirose *et al.* (1982) investigated the effects of high intensity UV (of between 2 - 60 mW/cm^2) on the disinfection of the surface of Wiener sausages. They found that whilst UV was an effective disinfectant against *E.coli* and *B.subtilis* spores in suspension, the disinfection rate for *E.coli* on the surface of the sausage obtained was only 0.019 times that obtained in suspension. In addition, it was observed that less disinfection was obtained at the ends of the sausage, which were creased. This was attributed to shadow effects.

Lee *et al.* (1989) showed that UV could be used to disinfect *Salmonella* in molten chocolate if the chocolate was less than 1 mm thick. It was found that the milk chocolate attenuated the UV, causing the disinfection level to be reduced as the thickness of the chocolate film increased even whilst keeping the UV intensity constant.

Shama *et al.* (1994) used UV to inactivate *B.subtilis* spores on ballotini which were pneumatically conveyed through a UV field. Such a method could be applied to the disinfection of herbs and spices, as well as various pharmaceuticals and cosmetics.

Van der Molen *et al.* (1980) showed that UV could be used to reduce the numbers of viable phototrophic bacteria growing in a biofilm on a stone church wall when applied continuously for one week. It was found that the UV had to be applied in one dose to be effective. If the UV was applied only during the night then the bacteria were able to repair themselves during the daytime and little reduction in viable bacterial numbers was achieved.

1.2.3 Disinfection Kinetics

Inactivation curves are typified by characteristic phases; the first of these is the initial lag phase. The disinfection rate then gradually increases and 1st order kinetics are generally obtained (order in this case being with respect to microbial concentration). The portion of the curve prior to the 1st order section is commonly referred to as the 'shoulder' of the curve. Disinfection curves are often referred to as being 'shouldered 1st order kinetic curves'. The shoulder of the disinfection curve is attributed to the presence of mechanisms natural to the micro-organisms which can repair a limited amount of cellular damage up to a certain level and beyond which inactivation ensues. At higher levels of disinfection (over 3 orders of reduction in the viability) the inactivation rate gradually reduces, sometimes giving rise to a stationary phase at between 4 and 5 orders of reduction in viability. This has been attributed to a small fraction of UV resistant cells (Sugawara *et al.*, 1981).

UV inactivation models assume light to be comprised of photons. Photons of UV light are considered to strike the medium in which the micro-organisms are present. Some of these photons hit the micro-organisms and are absorbed by them. Only a fraction of the photons absorbed will actually cause death or inactivation of cells. This fraction is known as the 'quantum yield' (Harm, 1980a). The 'observed quantum yield' is reduced by the repair mechanisms in the cells. Therefore the observed quantum yield is always lower than the underlying quantum yield.

In any irradiation event, the level of inactivation of micro-organisms is related to the quantity of UV that the micro-organisms are exposed to. The term 'fluence', has been adopted and is the product of UV intensity and time (Harm, 1980b).

Two types of UV inactivation kinetics have been proposed: 'multi-target' and 'multi-hit' kinetics. Multi-target kinetics assume that there are a certain number of targets in a cell that must each be struck by a photon to inactivate the cell (Harm, 1980c). Multi-target type inactivation curves are generally applied to cases where suspended cells exist naturally in small clusters or where cells contain multiple sets of their genetic material. Multi-hit kinetics

assume that a certain target must be hit a certain number of times for the cell to be inactivated (Harm, 1980c).

The following expression has been developed for multi-target kinetics (Harm, 1980c):

$$\left(\frac{N}{N_0}\right) = 1 - (1 - e^{-kF})^n$$

where

N = microbial count

N_0 = initial microbial count

K = inactivation rate coefficient

F = UV fluence = Intensity x Exposure time

n = number of targets

This expression can be simplified at low survival levels by applying the binomial theorem to obtain :

$$\left(\frac{N}{N_0}\right) \approx ne^{-kF}$$

This expression can be plotted on a semilog graph of surviving fraction against fluence. This gives the log of the number of targets, log n, as the intercept and the inactivation rate coefficient, k, as the gradient.

In practice not all inactivation curves follow the multi-target type. In some cases the target numbers obtained are not integers. This occurs as a result of the cells' repair mechanisms and no truly general equation for UV inactivation kinetics can be produced as the repair mechanisms active in any given situation will depend on many factors such as the species involved, the nature of the environment etc. UV inactivation kinetics are usually classified either by a decimal reduction time (the time taken to inactivate 90% of cells based on first order disinfection kinetics). This value is supplemented by an 'extrapolation number'. The extrapolation number is the intercept on the $LOG_{10}(N/N_0)$ axis of a semilog plot of

microbial survival against fluence when extrapolating the first-order part of the disinfection curve. This is equivalent to the target number if multi-target kinetics were observed.

It should be noted that these models do not account for the tailing of the inactivation curves which is sometimes observed. Sugawara *et al.* (1981) adapted a multi-hit model for the UV inactivation of *B.subtilis* spores by postulating that there existed a small fraction of UV resistant spores which had the same number of hits required for inactivation as the remainder of the population. This model was fitted successfully to their experimental data.

Caution must be exercised in using these data. For example, it has been shown that the growth medium can greatly affect the UV-resistance of *B.subtilis* spores. This could be due to proteins within the spore protoplast, either through direct absorption of UV or by binding to the DNA, thus affecting its UV absorption. The quantity of proteins in a spore will be affected by the growth medium (Bayliss *et al.*, 1981). Due to the variation in the disinfection performance of UV against the same micro-organisms in studies by different researchers such tables can only be used as a guide to the approximate UV dose required. An example of such a table is given by Chang *et al.* (1985).

1.2.4 Mechanism of UV-induced inactivation

The germicidal action of ultraviolet light has been shown to be due to absorption by the nucleotide bases in microbial DNA, mainly by the pyrimidine bases, causing the formation of harmful 'photoproducts'. These photoproducts alter the DNA of the micro-organism and prevent replication. The main photoproducts of biological effect are all pyrimidine derivatives - cyclobutyl-type dimers, pyrimidine adducts, pyrimidine hydrates, and DNA-protein crosslinks. One specific product, 5-thyminyl 5-6-dihydrothymine - often referred to as the spore photoproduct, is formed in spores and is the dominant cause of their inactivation (Harm, 1980d). For high intensity UV (10^{11} - 10^{13} Wm^{-2}) it has been shown that the dominant cause of inactivation in viruses and bacterial plasmids is single-strand DNA breaks (Gurzadyan *et al.*, 1981).

9

Most studies into the germicidal effects of UV have been concentrated at wavelengths below 300 nm. However it has been found that 365 nm UV (near UV) can have an inactivating effect on micro-organisms (Sammartano and Tuveson, 1985; Eisenstark *et al.*, 1986; Yallaly and Eisenstark, 1990). The mechanism involved must be different to that involved with far UV as nucleic acids only weakly absorb energy from near UV. It has been claimed that near UV causes the formation of hydrogen peroxide *in situ* in the micro-organisms (Yallaly and Eisenstark, 1990).

1.2.5 Repair and recovery of UV-induced damage

1.2.5.1 Repair mechanisms for UV-induced damage

Virtually all micro-organisms are capable of recovering from UV-induced injury due to the possession of mechanisms capable of repairing damage within the cells (Harm, 1980e). The cell component most vulnerable to damage is the DNA. This is because there is only one copy per cell and it is a large molecule. All known molecular repair processes act upon nucleic acids, in particular DNA. This is thought to be due to the fact that other important molecules in cells exist in many copies and therefore damage to a small fraction of these will not seriously affect cellular functions. Ultimately, repair of all cell components is governed by the cells genome.

The repair mechanisms for UV-induced damage of cell DNA can be classified according to the method by which the DNA is repaired. These are: reversal of the UV-induced alteration, replacement of UV-damaged nucleotides, and combination of undamaged regions in replicating DNA molecules.

10

1.2.5.2 Photoreactivation and Photoenzymatic repair

This class of repair mechanism reverses the UV-induced alteration. The damage caused to cells exposed to far UV irradiation can be reduced when the cells are exposed to light in the near UV or violet-blue range of the spectrum (310 - 480 nm), and is sometimes referred to as 'photoreactivating light' and the process of repair 'photoreactivation'. Exposure to far UV can result in the formation of cyclobutyl pyrimidine dimers. An enzyme, referred to as a 'photolyase', becomes activated when exposed to light of the appropriate wavelength and acts to hydrolyse the dimers. Other repair processes that do not use light are often referred to as 'dark repair' mechanisms, such as those mechanisms discussed in sections 1.2.5.3 and 1.2.5.4.

1.2.5.3 Excision - Resynthesis Repair

This class of repair mechanism involves the removal of the damaged sections of the DNA (excision), the resynthesis of the removed sections and rejoining those sections into the DNA. An example of this repair is in the removal of pyrimidine dimers from DNA damaged by far UV. The damaged regions of the cell DNA are recognised by a 'repair endonuclease' which cleaves the polynucleotide strand by the dimer. The cleaved sections of the DNA are soluble in acid and hence gradually dissolve, leaving single-stranded sections in the DNA. The complementary stand in the single-stranded DNA sections acts as the template for the resynthesis of the missing sections of the DNA. The resynthesised DNA sections are rejoined to the DNA by the enzyme polynucleotide ligase (Harm, 1980f).

These mechanisms are all enzyme-based and in total there are at least four enzymatic activities that have to be performed. The precise mechanisms comprising each of these stages of the excision-resynthesis repair process vary between organisms (Harm, 1980f).

1.2.5.4 Recombination repair

This class of repair mechanism combines separate parts of DNA strands to form one complete DNA molecule. For any damaged section of the DNA, if the adjacent section on the complementary strand is undamaged then the genetic code remains intact to resynthesise the damaged section of the DNA. Before recombination repair can take place it is necessary for the cell to replicate the DNA. When the cell attempts to replicate the DNA it is not possible to replicate the damaged sections of the DNA. This leads to the formation of separate sections of the DNA molecule, in addition to the strands of the original DNA molecule. The damaged sections along the DNA strands are then replaced by the newly created DNA sections and the two single strands of the DNA recombine.

As the recombination repair mechanism can only occur after replication of the damaged DNA it is sometimes referred to as 'postreplication repair' (Harm, 1980g).

1.2.5.5 Repair mechanisms for damage caused by other sterilants

The classes of DNA repair mechanisms described for UV-induced damage also apply to other sterilants which damage cell DNA, e.g. hydrogen peroxide or hydrogen peroxide combined with UV. Hydrogen peroxide and ozone are also known to act on other cell constituents, such as the cell wall or membrane (Block, 1983; Stevenson and Shafer, 1983). Naturally, repair to cellular constituents other than nucleic acids requires the cells' DNA to be intact.

1.3 Peroxidation

1.3.1 Introduction

Hydrogen peroxide (H_2O_2) has been used as a bactericidal and sporicidal agent for several decades. At low concentrations it is bactericidal but not sporicidal. The majority of studies have employed a hydrogen peroxide concentration greater than 10 w/v% to achieve a sporicidal effect, with one notable exception being Baldry (1983) who reported sporicidal action using 2.6 w/v% H_2O_2 for contact times of over four hours. In general, the sporicidal efficiency increases with hydrogen peroxide concentration (Stevenson and Shafer, 1983).

Hydrogen peroxide solutions have been recommended for the disinfection of surgical implant components, temperature-sensitive plastic equipment, hydrophilic soft contact lenses, commercial packing materials, water, and milk (Klapes and Vesley, 1990).

H_2O_2, like other chemical sterilants, is constrained in its use by legislation. For example, the 'FDA' set a maximum allowable H_2O_2 concentration in foods to be 0.1 ppm. Thus if H_2O_2 is used as a sterilant for food packaging, the residual H_2O_2 must be controlled. H_2O_2 is quite stable at ambient temperatures. Therefore processes using H_2O_2 as a surface sterilant often operate at temperatures above ambient and use hot air to remove residual hydrogen peroxide (Stevenson and Shafer, 1983).

Hydrogen peroxide vapour has also been proposed as a surface sterilant. Two methods for its production are given - sparging air through aqueous hydrogen peroxide (Wang and Toledo, 1986) or by injecting aqueous hydrogen peroxide into a low pressure chamber (Klapes and Vesley, 1990). The use of vapour-phase hydrogen peroxide has the advantage over liquid hydrogen peroxide that it will be applied more uniformly. Also, it avoids the problems of forming films and pools of hydrogen peroxide on the treated surface which can cause hydrogen peroxide to be adsorbed to the surface or to sub-surface material. Hydrogen peroxide vapour has the additional advantage that it is non-toxic in contrast to

previously used gaseous sterilants such as ethylene oxide and formaldehyde (Klapes and Vesley, 1990).

1.3.2 Disinfection using hydrogen peroxide

There has been a great deal of interest in the inactivation kinetics of micro-organisms using H_2O_2 as the sterilant e.g. (Toledo *et al.*, 1973; Bayliss and Waites, 1981; Stevenson and Shafer, 1983; Leaper, 1984). These papers proposed H_2O_2 as a surface sterilant for aseptic packaging. The test micro-organism used in these studies was typically *B.subtilis* spores (various strains) as this organism has been shown to be one of the most resistant to hydrogen peroxide (Toledo *et al.*, 1973). In these studies, spores were either used directly by suspending them in hydrogen peroxide solutions or else were placed on filter paper strips prior to immersion in hydrogen peroxide solutions.

The curves of H_2O_2-induced microbial inactivation are similar in shape to those of UV inactivation. H_2O_2-induced microbial inactivation has usually been described by decimal reduction times even though the disinfection kinetics (with respect to microbial concentration) are not first order. They are shouldered first order, sometimes with a stationary phase after 4-5 orders of inactivation (Toledo *et al.*, 1973; Cerf and Metro, 1977; Bayliss and Waites, 1981; Bayliss *et al.*, 1981; Stevenson and Shafer, 1983; Wang and Toledo, 1986). Cerf and Metro (1977) investigated the tailing of the inactivation curves of *B.licheniformis* spores treated with hydrogen peroxide. They were able to eliminate the possibility of a mutant H_2O_2-resistant strain being formed during cultivation by growing colonies from a single spore. They concluded that the tailing effect was due to clumping of the spores. The affinity which the spores had for each other led to the formation of clumps of more than one hundred spores, with diameters greater than six spore widths. Catalase naturally present in the spores decomposes H_2O_2; it was found that the catalase was inactivated but only at a very slow rate. Therefore, viable spores are afforded protection from hydrogen peroxide when they are surrounded by inactivated spores because the latter act as a sink for hydrogen peroxide due to the catalase still present in them.

14

The disinfection performance of hydrogen peroxide is greatly increased with temperature (Toledo *et al.*, 1973). The effect of a 10°C rise in temperature has been shown to cause the disinfection rate due to hydrogen peroxide to increase to between 1.6 and 2.5 times its original value. The temperature dependence of the microbial disinfection rate due to hydrogen peroxide can be described by the Arhenius equation.

The relationship between hydrogen peroxide concentration and the inactivation rate has repeatedly been shown not to be linear (Toledo *et al.*, 1973; Stevenson and Shafer, 1983; Leaper, 1984; Wang and Toledo, 1986). In the absence of a mechanistically-based model, Leaper (1984) fitted an empirical model to the relationship.

1.3.3 Mechanisms of microbial inactivation

Working with DNA extracted from *Bacillus subtilis (60009)*, Rhaese and co-workers (Rhaese and Freese, 1968; Rhaese *et al.*, 1968) found that hydrogen peroxide caused the breakage of double bonds in DNA causing the liberation of all four bases (some of which were altered), and broke the sugar-phosphate backbone. Massie *et al* (1972) also found base destruction by H_2O_2 in calf thymus DNA and in addition detected single-strand and double-strand breaks and cross-linking in the DNA. They found that base destruction was the dominant mechanism, proceeding at more than twenty times the rate of formation of single-strand breaks. Indeed, base destruction by H_2O_2 was so high that absorbance of 260 nm UV was reduced. H_2O_2 reacts more readily with adenine and thymine nucleotides than it does with guanine and cytosine nucleotides.

In addition to its effect on DNA, it has also been shown that hydrogen peroxide destroys proteins in spores (Stevenson and Shafer, 1983) with the primary target being the spore coat. Bayliss and Waites (1976) showed that treatment with sub-lethal doses of hydrogen peroxide actually stimulated germination.

The effect of metal ions, particularly cupric ions, on the disinfection performance of hydrogen peroxide has been widely reported. Massie $et\ al.$ (1972) found that the addition of $CuCl_2$ increased the rate of base destruction by H_2O_2 whilst $FeCl_2$ had little effect and $MgCl_2$ decreased the rates. Salts which are effective in increasing the oxidising ability of hydrogen peroxide will therefore increase the bactericidal effect of hydrogen peroxide. The most effective catalyst for hydrogen peroxide disinfection is Cu^{2+} ions, with Fe^{2+} ions also noted for a catalysing effect by some researchers (Stevenson and Shafer, 1983). Stark and Faber (1985) found that iron and copper ions were required for hydrogen peroxide to be lethal to cultured hepatocytes, whereas Bayliss and Waites (1981) found that the resistance of $Serratia\ marascens$ to H_2O_2 to be unaffected by the cellular iron content but demonstrated the additional lethality of H_2O_2 to $C.bifermentas$ spores in the presence of Cu^{2+} ions (Bayliss and Waites, 1976). Therefore the results of Bayliss and Waites agree with the findings of Massie $et\ al.$ (1972) that Cu^{2+} ions are a more important factor in H_2O_2 lethality than Fe^{2+} ions. The combination of hydrogen peroxide and Fe^{2+} ions is called 'Fenton's reagent'.

Several factors are known to influence the resistance of micro-organisms to hydrogen peroxide. One of these is the growth medium. Bayliss $et\ al$ (1981) grew $B.subtilis$ cultures using different growth media. They showed that the growth media had a marked effect on the surviving fraction of micro-organisms after treatment with hydrogen peroxide. However, no relationship between spore coat properties and hydrogen peroxide resistance could be found. The growth media was also shown to affect the number of cells surviving treatment with UV. However the effect of growth medium on survival was different for the two types of disinfection treatment.

1.4 Ozonation

1.4.1 Introduction

Ozone is a highly reactive oxidant and disinfectant in both gaseous and aqueous form. Aqueous ozone has been widely investigated for water treatment, both as a disinfectant and as an oxidant for the destruction of various pollutants. An intensive literature search only uncovered one previous study (that of Rickloff (1987)) in which aqueous ozone had been used specifically as a surface sterilant. One of the difficulties of working with aqueous ozone is that it is subject to losses through decomposition and reactions with various impurities in water. This has led to wide disagreement about disinfection rates and kinetics between previous researchers due to errors in controlling and measuring ozone concentration (Zhou and Smith, 1994).

1.4.2 Disinfection using ozone

Ozone inactivation has been described in terms of first order kinetics. Some researchers have observed an initial lag phase in the disinfection curves (Muraca *et al.*, 1987; Wickramanayake and Sproul, 1988). Tailing of the curves has also been noted (Zhou and Smith, 1994). The tailing of the inactivation curves from ozone is attributed to the formation of clumps of micro-organisms, as was the case for disinfection by hydrogen peroxide. This theory was given support by the work of Dahi (1976) who showed that after breaking up the clumps of micro-organisms by ultrasound, first order inactivation kinetics were obtained. The rate of disinfection using aqueous ozone is rapid and this makes it difficult to obtain kinetic data from the initial part of the curve. This might explain why some researchers have not reported the existence of an initial lag phase (Zhou and Smith, 1994). In general terms, inactivation curves obtained using O_3 show similar characteristics to those for UV and H_2O_2-induced microbial inactivation.

17

Whilst it has been shown that the inactivation kinetics are nearly first order with respect to microbial concentration, the order with respect to ozone is almost certainly much greater than one according to Zhou and Smith (1994). A figure in the region of 3 has been suggested (Glaze et al., 1987). It has been shown that the microbiocidal activity of ozone occurs at the surface of micro-organisms, leading to the disintegration of the cell wall (Zhou and Smith, 1994). Therefore the order of the inactivation kinetics will be governed by the interactions of ozone molecules and the microbial envelope. With other disinfectants where the microbiocidal activity is due to effects within the cytoplasm, the disinfection kinetics are often mass transfer limited and hence the order of the disinfection kinetics with respect to the disinfectant concentration are close to unity (Zhou and Smith, 1994). As ozone primarily acts at the surface, the disinfection rate will be determined by the reaction rate of ozone with the cell wall and this explains why the disinfection kinetics are so strongly dependent on ozone concentration. In contrast to this, Wickramanayake and Sproul (1988) found the order of the disinfection kinetics of *N.gruberi* cysts with respect to ozone concentration to be near unity. This would suggest that the biocidal effect of the ozone does not occur at the surface of the cysts.

Rickloff (1987) investigated the use of aqueous ozone for sterilising solid surfaces by immersing porcelain cylinders, onto which bacterial spores had been dried, into aqueous ozone. It was found that aqueous ozone of approximately 10 mg/L at 20°C was effective against spores in suspension and against spores dried onto a clean surface. However aqueous ozone proved ineffective for inactivating spores surrounded by organic material on a solid surface, such as soil. Raising the temperature to 60°C made the disinfection performance worse in the presence of soil.

The disinfection rate of micro-organisms by aqueous ozone has been shown to be influenced only slightly by temperature (Muraca et al., 1987; Zhou and Smith, 1994). Beltran et al. (1994) showed that increasing the temperature of aqueous ozone produced two conflicting effects. Increasing the temperature increased the reaction rate constant but this was countered by a decrease in the aqueous ozone concentration as the saturated concentration decreased with temperature. When the aqueous ozone concentration was

kept constant, an increase in the oxidation rate due to aqueous ozone was found. The inactivation rates' dependence on temperature has been adequately described using the Arhenius equation (Wickramanayake and Sproul, 1988; Zhou and Smith, 1994).

Ishizaki *et al* (1986) investigated the effect of ozone gas on six species of *Bacillus* spores. The inactivation kinetics observed were shouldered first order (except for *B.cereus* which displayed no shoulder). Using ozone concentrations of between 0.5 and 3.0 mg/l it was found that the relative humidity of the ozone gas used greatly influenced the inactivation rate. Relative humidities in excess of 50% were needed for significant inactivation at these ozone concentrations. Increasing the relative humidity increased the first order kill rate and decreased the lag time. These findings would seem to suggest ozone is only sporicidal in the presence of water.

1.4.3 Mechanism of disinfection

Whilst, as the foregoing suggests, the use of ozone as a disinfectant is now becoming widely established, the cellular targets against which ozone or its breakdown products act, have not been unambiguously identified. These cellular targets are in any event likely to be non-specific and to be dependent on cell type, the physiological state of the cell, etc. This is in sharp contrast to UV irradiation where the primary lethal effect is directed against the cells' genome. What is incontrovertible is that ozone exerts its lethality through the generation of free radicals. The processes by which this occurs has been extensively studied in relation to the oxidation of (relatively simple) chemical structures. Therefore it is appropriate to give some considerations to previous studies in which the mechanism of free radical generation has been investigated because such processes will be relevant to cellular inactivation.

Ozone and its breakdown products can react directly with chemical species present in water (Staehelln and Hoigne, 1985). The decomposition of aqueous ozone is due to a chain reaction involving $OH^{\bullet}$ radicals. This chain mechanism is affected by the presence of

species which scavenge the $OH^\bullet$ radicals and hence inhibit the chain mechanism, and also by species which promote the chain by converting $OH^\bullet$ radicals (which react with many chemical species) to $O_2^{-\bullet}$ radicals. The latter mainly react with O_3, hence promoting further reaction. In very pure water, hydroxyl radicals react with ozone so that the chain propagating steps shown can be repeated several times. It has been postulated that many hundreds of ozone molecules may be decomposed by a single initiation step (Glaze *et al.*, 1987).

The presence of these promoters and inhibitors greatly influences the rate of ozone decomposition and, as a consequence, the concentration of the ozone and its decomposition products, which in turn affects the reaction rates of the processes of interest. The nature of specific promoters and inhibitors and their concentrations will vary between different water sources. Therefore results conducted by different groups do not generally agree well, even with respect to the kinetic orders of the reactions. Typical promoters are formic acid, methanol and phosphate ions. Typical $OH^\bullet$ radical scavengers include alkyl groups, t-Butyl alcohol, and bicarbonate/carbonate ions (Staehelln and Hoigne, 1985). By treating the effects of promoters and inhibitors in general, these workers show that the rate of ozone decomposition is first order with respect to ozone, independent of the number of promoters and inhibitors. This was not the case where the radical formation becomes fast, e.g. under high alkaline conditions or in the presence of UV. The rate of ozone decomposition with respect to ozone concentration can be between half to second order under such conditions (Staehelln and Hoigne, 1985). The relative rates of these reactions, in conjunction with the decomposition rate of ozone, will affect the inactivation kinetics obtained. Thus, unless identical conditions are employed every time, it will be difficult to make an accurate prediction of ozone-induced microbial inactivation kinetics.

The mechanism for the decomposition of aqueous ozone proposed by Staehelln and Hoigne (1985) is shown below :

Initiation step :

$$O_3 + OH^- \rightarrow HO_2^{\bullet} + O_2^{-\bullet} \tag{1}$$

Propagation steps :

$$HO_2^{\bullet} \Leftrightarrow O_2^{-\bullet} + H^+ \tag{2}$$

$$O_2^{-\bullet} + O_3 \rightarrow O_3^{-\bullet} + O_2 \tag{3}$$

$$O_3^{-\bullet} + H^+ \rightarrow HO_3^{\bullet} \tag{4}$$

$$HO_3^{\bullet} \rightarrow OH^{\bullet} + O_2 \tag{5}$$

$$OH^{\bullet} + O_3 \rightarrow HO_2^{\bullet} + O_2 \tag{6}$$

Termination steps :

$$2OH^{\bullet} \rightarrow H_2O_2 \tag{7}$$

$$OH^{\bullet} + M \rightarrow products \tag{8}$$
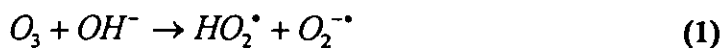
where M is a radical scavenger

Aqueous ozone decomposes to several oxidising species e.g. hydrogen peroxide, hydroxyl radicals and superoxide radicals. Much of the work conducted into disinfection has not concerned itself with the particular chemical species responsible for the oxidation of the biological material. However such studies have been undertaken for the oxidation of various pollutants in water. Although these studies are not concerned with disinfection, they provide useful information about the oxidation mechanisms of ozone, which is relevant because the disinfection properties of ozone are attributed to its oxidising micro-organisms, rendering them inactive.

Beltran *et al.* (1994) investigated the oxidation of azatrine by ozone. By employing the radical scavenger, t-butanol, it was found that oxidation was primarily due to radicals, even at pH 2 where the radical concentration is much lower than at pH 7. Consequently increasing the pH increases the oxidation rate for a given aqueous ozone concentration.

21

Nonetheless, these workers showed that ozone reacted directly with azatrine but the reaction rate was much lower than that for the radicals.

When employing aqueous ozone as a sterilant it is necessary to know the decomposition rate of the aqueous ozone so that a suitable aqueous ozone concentration and contact time can be maintained. The decomposition rate of aqueous ozone can be accurately predicted under acidic conditions using the equation developed by Morooka *et al.* (1978).

1.5 Combined treatments (Advanced oxidation methods)

1.5.1 Introduction

Interest has been shown in the use of combinations of UV, H_2O_2 and O_3 as sterilants. These combinations have been shown to have a greater oxidising effect than the sum of the oxidising effects of the individual oxidants, i.e. a synergistic effect is produced. From studies of these processes, the synergism has been attributed to the formation of intermediate hydroxyl radicals which are highly reactive and hence short-lived. The hydroxyl radical is the most powerful oxidising species after fluorine. Its oxidising action is mostly brought about by hydrogen abstraction (Legrini *et al.*, 1993). Due to the very fast reaction rate coefficients for reactions involving hydroxyl free radicals, the reaction rate is often controlled by the rate of formation of hydroxyl radicals (Wolfrum *et al.*, 1994).

Processes that form hydroxyl radicals as a result of a combination of treatments are referred to as 'Advanced Oxidation Processes'. This class of process covers all the permutations of UV, H_2O_2 and O_3 and also includes other processes in which hydroxyl radicals are formed. The latter include aqueous ozone at high pH values and ozone or hydrogen peroxide with other hydroxyl radical initiators such as metals and metal oxides (Glaze *et al.*, 1987).

The hydroxyl free radical is difficult to detect directly because it is so short-lived. It has

been detected by electron paramagnetic resonance (EPR) spectroscopy when employing a 'trap' for the hydroxyl radicals (Wolfrum *et al.*, 1994). It should be noted though that direct evidence for the existence of the hydroxyl free radical has not been obtained but there is a body of indirect evidence for its existence.

1.5.2 UV and hydrogen peroxide

1.5.2.1 Disinfection

Bayliss and Waites (1979) investigated the simultaneous use of hydrogen peroxide and far UV. They found that the simultaneous use of hydrogen peroxide and UV produced a synergistic inactivation effect against *Bacillus subtilis* spores. Interestingly, no synergistic effect was obtained when hydrogen peroxide and UV were used successively. Bayliss and Waites (1981) noted that when hydrogen peroxide was used after UV, the resulting level of inactivation was less than the sum of the 2 individual treatments. They explained this effect by the breaking of spore clumps and possible reversal of DNA damage by H_2O_2.

Bayliss and Waites (1979) found an optimum inactivation rate was obtained with a H_2O_2 concentration of 0.3 M (= 1.0 w/v%) for the combined treatment for *B.subtilis (NCDO 2129)* spores. Although the UV intensity employed was not stated, it can be taken to have been about 260 μW/cm^2 as the physical arrangement appears identical to previous work of theirs (Bayliss and Waites, 1980). In this work, the combined treatment was used against vegetative cells. Results from H_2O_2 concentrations above 1.0 w/v% were not presented but the authors claimed that 1.0 w/v% was the optimum concentration for the UV + H_2O_2 process for vegetative cells. The UV intensity will affect the quantum yield of H_2O_2 decomposition (Lunak and Sedlak, 1992) and so 1.0 w/v% H_2O_2 may not represent a universal optimum for all UV intensities. However Bayliss and Waites (1982) did investigate the UV + H_2O_2 process with a much higher intensity UV source giving an intensity of 1.8 mW/cm^2 compared to the 260 uW/cm^2 used previously. For spores from the same strain of *B. subtilis*, the optimum H_2O_2 concentration was found still to be about

1.0 w/v%. For a different strain of *B.subtilis* spores (NCDO 2130) a weaker optimum existed in the range 1.0 - 2.5 w/v%. On the basis of this result, similar H_2O_2 concentrations were henceforth used in their studies. Bayliss and Waites attributed this optimum to the fact that at higher hydrogen peroxide concentrations more UV would be absorbed by the hydrogen peroxide, thus reducing the UV intensity near the spores. This is supported by their finding that doubling the volume of liquid reduced the kill. For hydrogen peroxide concentrations of over 5 w/v%, Bayliss and Waites showed that combining UV with H_2O_2 gave a lower disinfection performance than UV alone.

Stannard *et al.* (1983) showed that synergism was observed when combining UV with hydrogen peroxide when used against four micro-organisms which had been applied to the surfaces of food cartons. Hydrogen peroxide was sprayed onto the inside of the cartons which were subsequently exposed to 10 seconds of UV (dose not given). The maximum level of synergism was achieved with hydrogen peroxide concentrations in the range of 0.5 to 1.0 w/v%.

1.5.2.2 Mechanisms of microbial inactivation and hydroxyl radical formation

The synergistic inactivation effect has been attributed to the formation of hydroxyl radicals. It is known that hydroxyl radicals attack DNA in cells (Adinarayana *et al.*, 1988; Dirksen *et al.*, 1988). A large number of products from both the sugar moiety and the heterocyclic bases in DNA have been isolated and identified. Hydroxyl radicals induce both DNA strand breaks and base release (Glaze *et al.*, 1987).

The inactivation kinetics obtained using UV and hydrogen peroxide are due to at least three separate sterilants - UV and hydrogen peroxide and the decomposition products of hydrogen peroxide - notably hydroxyl free radicals. To understand the mechanism of inactivation using UV and hydrogen peroxide it is necessary to understand the decomposition of hydrogen peroxide in the presence of UV (sometimes referred to as 'photodecomposition').

24

It has been known for several decades that hydrogen peroxide decomposes in the presence of ultraviolet light to water and oxygen. Urey *et al.* (1929) suggested that this was due to the formation of hydroxyl radicals.

$$H_2O_2 \xrightarrow{h\nu} 2OH^{\bullet} \tag{1}$$

Haber and Weiss suggested that the hydroxyl radicals formed should bring about a radical chain mechanism in which the propagation cycle gives high quantum yields (Lunak and Sedlak, 1992) :

$$OH^{\bullet} + H_2O_2 \rightarrow H_2O + HO_2^{\bullet} \tag{2}$$

$$HO_2^{\bullet} + H_2O_2 \rightarrow O_2 + H_2O + OH^{\bullet} \tag{3}$$
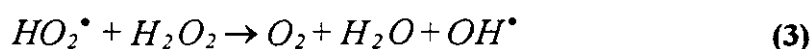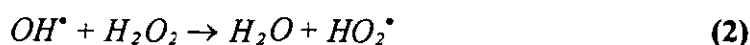
However high quantum yields are not always obtained due to the following termination steps :

$$HO_2^{\bullet} + OH^{\bullet} \rightarrow O_2 + H_2O \tag{4}$$

$$2HO_2^{\bullet} \rightarrow H_2O_2 + O_2 \tag{5}$$

$$2OH^{\bullet} \rightarrow H_2O + O \tag{6}$$

$$2OH^{\bullet} \rightarrow H_2O_2 \tag{7}$$

$$OH^{\bullet} + X \rightarrow \text{interruption of the chain} \tag{8}$$
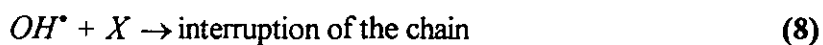
where X is a radical scavenger.

A linear dependence of quantum yield both on the concentration of hydrogen peroxide and on the reciprocal value of the square root of the intensity of absorbed radiation has been found but this relationship has only been tested over narrow ranges (Lunak and Sedlak, 1992).

The quantum yield of the photolysis of hydrogen peroxide is greatly dependent on the intensity of the radiation absorbed. High quantum yields (>>1) are only obtained at low radiation intensities. For high radiation intensities the quantum yields were between 1 and 2. Weiss attributed this to an effective termination of $OH^\bullet$ and $HO_2^\bullet$ radicals, caused by their high concentration.

Reaction (3) is known as the "Haber-Weiss reaction". It is of interest as it is the rate determining step in the photodecomposition of H_2O_2. Also, the reaction leads to the removal of $HO_2^\bullet$ radicals, which although not as powerful an oxidising species as hydroxyl radicals (Wolfrum et al., 1994), play an important role in reactions with enzymes and membranes and are thus of interest with respect to H_2O_2-induced microbial inactivation (Lunak and Sedlak, 1992).

Wolfrum et al. (1994) predicted the steady-state concentration of hydroxyl radicals to be proportional to the UV intensity. They found experimentally that the rate of formation of hydroxyl radicals was proportional to the hydrogen peroxide concentration at concentrations of up to 0.017 w/v% H_2O_2 (=5.0 mM).

The rates obtained by previous researchers for the photodecomposition of hydrogen peroxide show marked discrepancies. This is because other chemical species present can interact with free radicals present in the H_2O_2 decomposition chain. In addition, metal ions such as Fe^{2+} and Cu^{2+} are known to act as catalysts in the decomposition of hydrogen peroxide (in the absence of UV), causing the formation of free radicals. The presence of these free radicals also causes an increase in the decomposition rate of hydrogen peroxide in the presence of UV. Copper ions are the most effective catalyst of H_2O_2 lysis known so

26

A linear dependence of quantum yield both on the concentration of hydrogen peroxide and on the reciprocal value of the square root of the intensity of absorbed radiation has been found but this relationship has only been tested over narrow ranges (Lunak and Sedlak, 1992).

The quantum yield of the photolysis of hydrogen peroxide is greatly dependent on the intensity of the radiation absorbed. High quantum yields ($>>1$) are only obtained at low radiation intensities. For high radiation intensities the quantum yields were between 1 and 2. Weiss attributed this to an effective termination of $OH^{\bullet}$ and $HO_2^{\bullet}$ radicals, caused by their high concentration.

Reaction (3) is known as the "Haber-Weiss reaction". It is of interest as it is the rate determining step in the photodecomposition of H_2O_2. Also, the reaction leads to the formation of $HO_2^{\bullet}$ radicals, which although not as powerful an oxidising species as hydroxyl radicals (Wolfrum et al., 1994), play an important role in reactions with enzymes and membranes and are thus of interest with respect to H_2O_2-induced microbial inactivation (Lunak and Sedlak, 1992).

Wolfrum et al. (1994) predicted the steady-state concentration of hydroxyl radicals to be proportional to the UV intensity. They found experimentally that the rate of formation of hydroxyl radicals was proportional to the hydrogen peroxide concentration at concentrations of up to 0.017 w/v% H_2O_2 (=5.0 mM).

The rates obtained by previous researchers for the photodecomposition of hydrogen peroxide show marked discrepancies. This is because other chemical species present can interact with free radicals present in the H_2O_2 decomposition chain. In addition, metal ions such as Fe^{2+} and Cu^{2+} are known to act as catalysts in the decomposition of hydrogen peroxide (in the absence of UV), causing the formation of free radicals. The presence of these free radicals also causes an increase in the decomposition rate of hydrogen peroxide in the presence of UV. Copper ions are the most effective catalyst of H_2O_2 lysis known so

26

far. The effect of copper sulphate has been detected at concentrations as low as 10^{-7} M (Lunak and Sedlak, 1992). In order to accurately predict the inactivation kinetics from theory one would need to know the precise mechanisms behind the microbial inactivation and the kinetics of the formation and destruction of the relevant chemical species. Such an approach is not currently possible due to the multitude of factors affecting the decomposition of H_2O_2. Therefore the rate coefficients for the reactions involved in the photodecomposition of hydrogen peroxide must be determined every time a different water source is employed. The concentrations of the intermediate free radicals may then be calculated by assuming that the free radicals reach a steady state concentration.

Bayliss and Waites (1979) tested their hypothesis that the synergistic inactivation effect obtained with UV and hydrogen peroxide was due to hydroxyl radicals by adding free radical scavengers L-cysteine and mannitol to the spore suspensions 30 minutes before treatment to allow time for them to permeate into the cells. It was found that none of the radical scavengers had any effect on disinfection performance. They concluded that if hydroxyl radicals were responsible for the synergistic effect then they must be formed at sites within the spores that the radical scavengers could not reach.

Waites *et al.* (1988) found that the optimum UV wavelength was different for the combined UV + H_2O_2 process to that for UV alone. For UV induced microbial inactivation, the optimum wavelength is about 260 nm, due to absorption by the nucleic acid bases in the DNA. For UV + 1.0 w/v% H_2O_2 a maximum rate of microbial inactivation was obtained with 270 nm UV (intensity not stated). Waites *et al.* (1988) explained the wavelength shift as being due to the absorption of UV by the H_2O_2. Whilst it is necessary for H_2O_2 to absorb UV to produce the synergistic effect, if UV is absorbed significantly in the hydrogen peroxide the average UV intensity at the cells' surface (or inside the cells) will be reduced. This both reduces the disinfection rate due to UV solely and the concentration of hydroxyl radicals at the cells' surface and inside the cells, thus reducing the inactivation rate.

Bayliss *et al.* (1982) investigated the mechanism of microbial damage by the combined effects of UV and H_2O_2 treatment using strains of *B.subtilis* spores some of which were

deficient in two specific repair mechanisms. These repair mechanisms were capable of removing the spore photoproduct and of performing excision/resynthesis repair. The results showed that the spores' UV resistance was important in determining the spores' resistance to the combined treatment whilst the spores' resistance to hydrogen peroxide did not influence the resistance to the combined treatment. This shows that the combined treatment, like UV alone, primarily attacks the spores' DNA whereas hydrogen peroxide alone does not primarily attack DNA because the loss of excision/resynthesis repair made no difference to the spores' hydrogen peroxide resistance. However there might be other, as yet unidentified, repair mechanisms for H_2O_2-induced DNA damage. Bayliss and Waites (1981) also demonstrated that microbial resistance to H_2O_2 and UV + H_2O_2 combined is related to the total catalase activity within cells. Changes in growth media can affect catalase synthesis and hence microbial resistance.

1.5.3 Ozone and hydrogen peroxide

1.5.3.1 Disinfection using aqueous O_3 and H_2O_2

Wolfe *et al.* (1989) first gave the combination of O_3 + H_2O_2 the name 'Peroxone'. Most of the published work in this area deals with the oxidation of organic material present in surface waters and as for previously described oxidation treatments, there have been few published disinfection studies using this process. Wolfe *et al.* (1989) found that the use of hydrogen peroxide in combination with aqueous ozone did not change, or even slightly reduced, the inactivation level of *E.coli* in river water over a range of $O_3 : H_2O_2$ ratios. This they attributed to the formation of hydroxyl radicals which react with a wide range of compounds and therefore might well react with other organics present in the river water which ozone would not react with in any significant quantity. They also noted that the ozone residuals were lower in the peroxone process and postulated that the lower ozone residual might cause a worse disinfection performance.

1.5.3.2 Mechanisms of inactivation and hydroxyl radical formation

As with aqueous ozone, the chemistry of the hydrogen peroxide-aqueous ozone system is dominated by free radical chemistry and for the reasons previously stated, a short review of free radical generation mechanisms will be given. The conjugate base of hydrogen peroxide can initiate the ozone decomposition chain by the following reaction (Glaze *et al.*, 1987):

$$HO_2^- + O_3 \rightarrow HO_2 + O_3^-$$ (1)
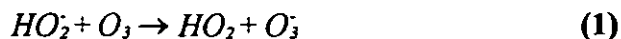
Peyton described different products from the same reactants:

$$HO_2^- + O_3 \rightarrow OH^\bullet + O_2^{-\bullet} + O_2$$ (2)
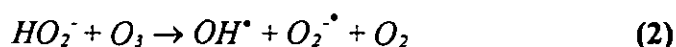
Staehelln and Hoigne (1985) stated that $O_2^{-\bullet}$ radicals can be formed in the reaction between the HO_2^- ion and O_3, which is in agreement with Peyton. The other reaction mechanisms are the same as for the decomposition of aqueous ozone (see section 1.4). Once the ozone decomposition chain is started, hydroxyl radicals will be produced. Staehelln and Hoigne showed that hydrogen peroxide was formed in the decomposition of aqueous ozone and plays an important role in the formation of hydroxyl radicals.

Namba and Nakayama (1982) provided evidence that hydroxyl radicals are formed in ozone/hydrogen peroxide mixtures. Using a single $H_2O_2 : O_3$ ratio, they found that the degradation rates of 8 different alcohols (relative to that of ethanol) in the ozone/hydrogen peroxide mixture to be virtually identical to those due to hydroxyl radicals in aqueous solutions, as determined by Dorfman and Adams (1973).

There is disagreement between previous researchers about the ratio of $H_2O_2 : O_3$ needed to optimise the oxidation rate. For example, Glaze *et al.* (1987) found the optimum ratio to be equimolar with respect to the rate of destruction of trichloroethylene in well water. In contrast, Wolfe *et al.* (1989) found that hydrogen peroxide did not increase the disinfection performance of aqueous ozone in river water. The differences between results from

previous studies might possibly be explained by the fact that the studies were conducted in different waters. As the oxidation mechanisms of the peroxone process are attributed to free radicals it is likely that the concentrations of these radicals will strongly depend on the nature and the concentrations of the various promoters and scavengers present in each water. Therefore, optimum production of the hydroxyl radical appears to depend on a combination of factors: ozone dosage, the H_2O_2 : O_3 ratio, the contact time, and the composition of the water in which the sterilants are dissolved (Wolfe *et al.*, 1989; Ferguson *et al.*, 1990).

1.5.4 UV and ozone

1.5.4.1 Introduction

The combination of aqueous ozone and UV has been widely investigated for the oxidation of organic compounds in water treatment (Legrini *et al.*, 1993). However, as for the other combined treatments considered, there have not been many published studies of the disinfection performance of the UV + O_3 system. One exception was Francis *et al.* (1988) who studied the inactivation of *E.coli* in aqueous ozone and UV. They found the inactivation kinetics to be first order with some tailing of the curve. The disinfection rate for the UV + O_3 system was faster than the disinfection rates obtained using UV or O_3 separately as sterilants (ozone concentration not stated).

1.5.4.2 Mechanisms of hydroxyl radical generation

When used together, UV and aqueous ozone produce hydroxyl radicals (Beltran *et al.*, 1994). The decomposition mechanism of aqueous ozone in the presence of UV consists of the same pathways as for aqueous ozone alone with the addition of the following reactions:

$$O_3 + H_2O \xrightarrow{hv} H_2O_2 + O_2 \qquad (1)$$

$$H_2O_2 \xrightarrow{hV} 2OH^\bullet \qquad\qquad (2)$$
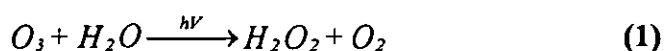
The second reaction has been shown to be much slower than the first and is considered negligible when considering the oxidation mechanisms of aqueous ozone (Beltran *et al.*, 1994). The conjugate base of the hydrogen peroxide formed from the photolysis of aqueous ozone can then form hydroxyl radicals from the same pathways as described in section 1.4.3.

Beltran *et al.* (1994) showed that oxidation from the UV + O_3 process was almost solely due to oxidising radicals, with the contribution from direct ozonation even lower than in the case of using aqueous ozone solely. Denis *et al.* (1992) showed that oxidising radicals were formed in the UV + O_3 process. The oxidation rate increased with aqueous ozone concentration up to 4 mg O_3/L. These workers also showed that increasing the temperature increased the rate of oxidation .

From stoichiometry, the yield of hydroxyl radicals from the UV + H_2O_2 process is greater than that for the UV + O_3 process (1.5 moles of O_3 consumed to provide 1 mole of hydroxyl radicals compared to 0.5 moles of H_2O_2 consumed to produce 1 mole of hydroxyl radicals). However aqueous ozone absorbs UV far more strongly than hydrogen peroxide (molar extinction coefficients : O_3 = 3300 $M^{-1}cm^{-1}$, H_2O_2 = 20 $M^{-1}cm^{-1}$). Therefore for the same molar concentration of H_2O_2 and O_3 exposed to UV, a higher concentration of hydroxyl radicals will be formed in aqueous ozone (Glaze *et al.*, 1987). Theoretically this makes aqueous ozone a more effective disinfectant than hydrogen peroxide of the same molar concentration when combined with UV.

As was the case for aqueous ozone, it is useful to know the degradation rate of aqueous ozone in the presence of UV so that one can apply doses of aqueous ozone suitable to maintain the required aqueous ozone concentration and exposure time. No practical equations for the rate of photolytic decomposition of ozone are currently available.

1.6 Aims and Objectives

The preceding review of the literature provided evidence that the inactivation of micro-organisms in liquid media by UV and, to a lesser extent, advanced oxidation processes, had been extensively studied. However, relatively little work had been done on microbial inactivation on the surfaces of solid objects. In particular, the literature highlighted a deficiency in any coherent data which could be used to accurately predict the rates of inactivation of micro-organisms on surfaces for the purposes of evaluating these technologies for applications in such fields as food processing and the disinfection of medical items.

The well-documented synergistic disinfective action of UV in combination with hydrogen peroxide merited particular attention as it could offer operating advantages such as reduced treatment times. In considering how best to apply liquid disinfectants to surfaces, attention focused on sprays. The application of liquids in the form of sprays represents one method of obtaining even coverage of the surfaces of an object. Indeed, one such combination, UV and hydrogen peroxide sprays, has been patented as a disinfection treatment for the cardboard-based material from which drinks cartons are fabricated (Peel and Waites, 1983). A refinement of this type of technology is the electrostatic charging of liquid sprays to obtain enhanced surface coverage whilst minimising liquid consumption. Charged sprays have demonstrated definite advantages for car body painting and crop spraying (Bailey, 1986) and such an approach could be useful in controlling residual levels of the disinfectants, an important consideration for foodstuffs.

On the basis of these considerations, the principal objectives of this research programme were formulated thus :-

- To devise methods for studying the efficacy of UV either alone or in combination with aqueous hydrogen peroxide and ozone for disinfecting the surfaces of solid

objects.

- To obtain data on the rates of inactivation of a model organism by these methods and to apply appropriate kinetic expressions to the data.

- To establish whether the electrostatic charging of liquid sprays resulted in enhanced surface coverage and improved disinfection kinetics.

- To investigate the effects on microbial survival of disinfecting surfaces having different surface characteristics or 'micro-topographies'.

- To devise mathematical models which would permit the UV intensities on the surfaces of objects of regular geometry placed in a UV field to be predicted.

- To combine model predictions with experimentally determined inactivation data to enable an evaluation of a hypothetical process for the disinfection of objects by UV in combination with spray disinfection.

2. METHODS AND APPARATUS

2.1 Micro-organisms

2.1.1 Source

E.coli MGa was isolated from Mogden Sewage Treatment Works (near Kew, Surrey) and is further described by Shama (1992). *Micrococcus luteus* (ATCC 4698, NCIMB 9278), and *Bacillus subtilis* (ATCC 6633, NCIMB 8054) were purchased from the National Collection of Industrial and Marine Bacteria (NCIMB), Aberdeen.

2.1.2 Cultivation of organisms

All three organisms used were cultivated using similar techniques. Stock cultures were prepared from freeze-dried ampoules by aseptically transferring culture to 250 ml Erlenmeyer flasks which contained 100 ml Nutrient Broth (Oxoid) using a flamed inoculation loop. One loopful of organisms was used to inoculate the nutrient broth. The Erlenmeyer flasks were incubated at 30°C in a rotary incubator at 200 rpm until the organisms had reached the stationary phase in their growth cycle. This was determined by the measurement of the absorbance at 600 nm of samples using a spectrophotometer (Shimadzu UV-1201 UV-VIS Spectrophotometer, Shimadzu Europa, Duisburg, Germany). Samples (1 ml) were taken aseptically from the flasks using a micropipette (Gilson) and transferred to cuvettes suitable for use in the spectrophotometer. The stationary phase was deemed to have been reached when there was no further increase in the absorbance at 600 nm. The incubation periods required for the three organisms to reach the stationary phase were : *E.coli* MGa - 12 hours, *M.luteus* (ATCC 4698, NCIMB 9278) - 35 hours, *B.subtilis* (ATCC 6633, NCIMB 8054) - 24 hours. Growth curves for these micro-organisms are shown in Figure 2.1. The 3 micro-organisms used were stored as cultures on Nutrient Agar slopes in a refrigerator at 4°C.

34
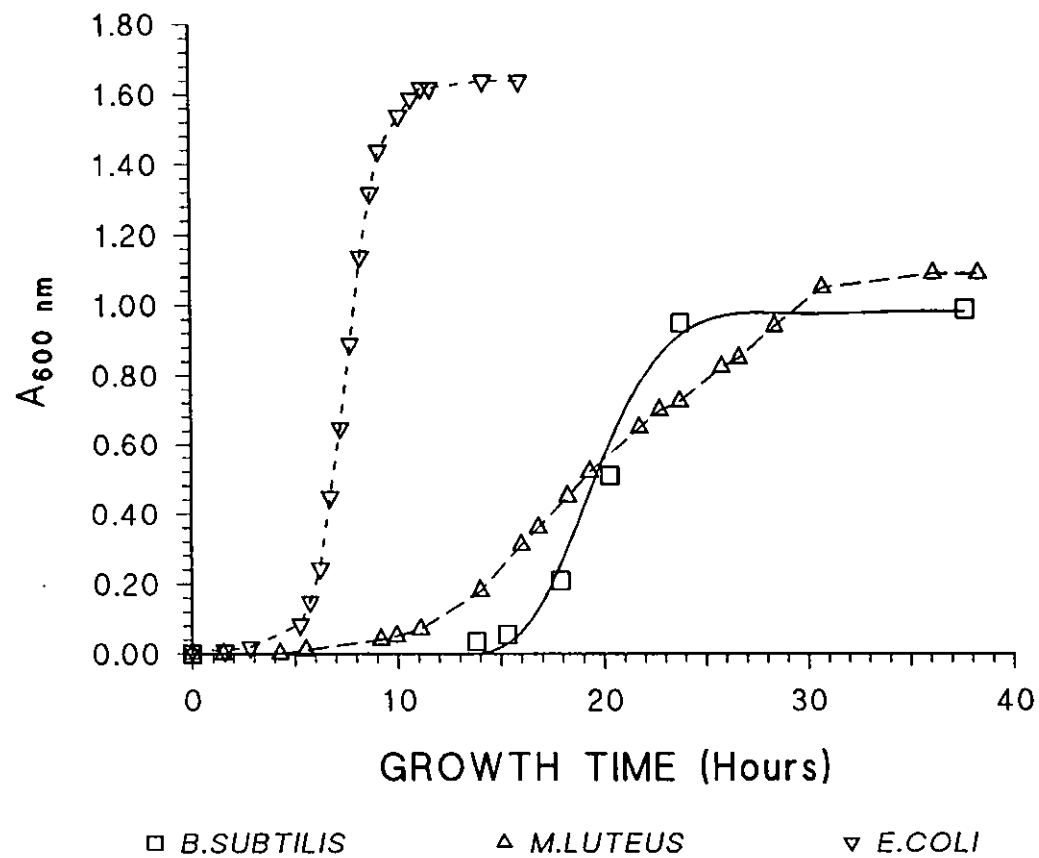
FIGURE 2.1   Microbial growth curves

2.1.3 *B.subtilis* spore production

(a) Introduction

Chang *et al.* (1985) and Bayliss *et al.* (1981) demonstrated that the UV resistance of *B.subtilis* spores depended on the growth medium in which the cells were grown and also the degree to which they were heat-shocked (Toledo *et al.*, 1973). Therefore it was critically important to use a standard method to generate *B.subtilis* spores. The method used for the cultivation of *B.subtilis* spores was based on the approach of Harnulv and Snygg (1972).

(b) Procedure

An Erlenmeyer flask containing 100 ml Nutrient Broth (Oxoid Ltd., Basingstoke, Hants.) was inoculated with one loopful of *B.subtilis* from a Nutrient Agar slope. The Erlenmeyer flask was incubated at 30 °C for 24 hours in a rotary incubator at 200 rpm. The resulting *B.subtilis* culture was then used to inoculate the Sporulation Agar (SA) plates (Harnulv and Snygg, 1972) :

Ingredient	% w/v
Nutrient broth (Oxoid)	0.8
Yeast extract (Oxoid)	0.4
$MnCl_2.4 H_2O$ (BDH)	0.001
Agar technical grade 3 (Oxoid)	2.0
adjusted to pH	7.2

SA plates were inoculated with 0.2 ml of *B.subtilis* culture which was spread over the plates using a flamed glass spreader. The plates were incubated for 14 days at 30 °C.

After 14 days incubation the growth of the *B.subtilis* was confluent. Harnulv and Snygg found that over 95% of the *B.subtilis* were in the form of spores after 3 days of incubation. *B.subtilis* spores were harvested from sporulation plates by pipetting 5 ml sterile distilled water onto the surface of the plate and scraping the surface with a flamed inoculation loop

in order to detach the spores. The resulting suspension was pipetted into sterile Universal bottles and then immediately washed in order to remove small pieces of agar. The *B.subtilis* spore suspension was transferred to sterile centrifuge tubes and centrifuged at 8000 g for 20 minutes. The supernatant was poured off and 10 ml sterile distilled water added. The pellet was resuspended by vigorous mixing using a vibratory mixer ('Whirlimixer', Fisons Scientific Apparatus, Loughborough, Leics.). This procedure was repeated a further 2 times.

In order to inactivate any vegetative cells that might still have been present, the *B.subtilis* spore suspension was subjected to a 'heat shock'. Universal bottles containing the spore suspension were placed in a water bath at ambient temperature. The temperature of the water bath was then raised to 70 °C (typically this took approximately 30 minutes) and the spore suspension kept at that temperature for 30 minutes. The Universals were then removed from the water bath and transferred to a refrigerator at 4 °C where they were kept until required.

2.1.4 Determination of UV resistance of spores

In order to eliminate variability, batches of spore stock were made in sufficient quantities to last for several months experimental work. Tests were carried out to determine the UV resistance of spore stocks as they were produced. This was done by coating Grade 2 filter paper (Whatman) with spores, as described in section 2.2, and exposing to UV. The UV source used was the high intensity lamp described in section 2.3.2.

The disinfection results obtained with Grade 2 filter paper were plotted onto a graph including all previous disinfection studies for *B.subtilis* spores on this surface. If the disinfection results obtained lay within the range of results previously determined then the spore batch was deemed suitable for use. An example is shown in Figure 2.2 where the disinfection data for a new spore batch, created on 29/11/94, was compared to that obtained from previous spore batches. This new spore batch was deemed suitable for use.
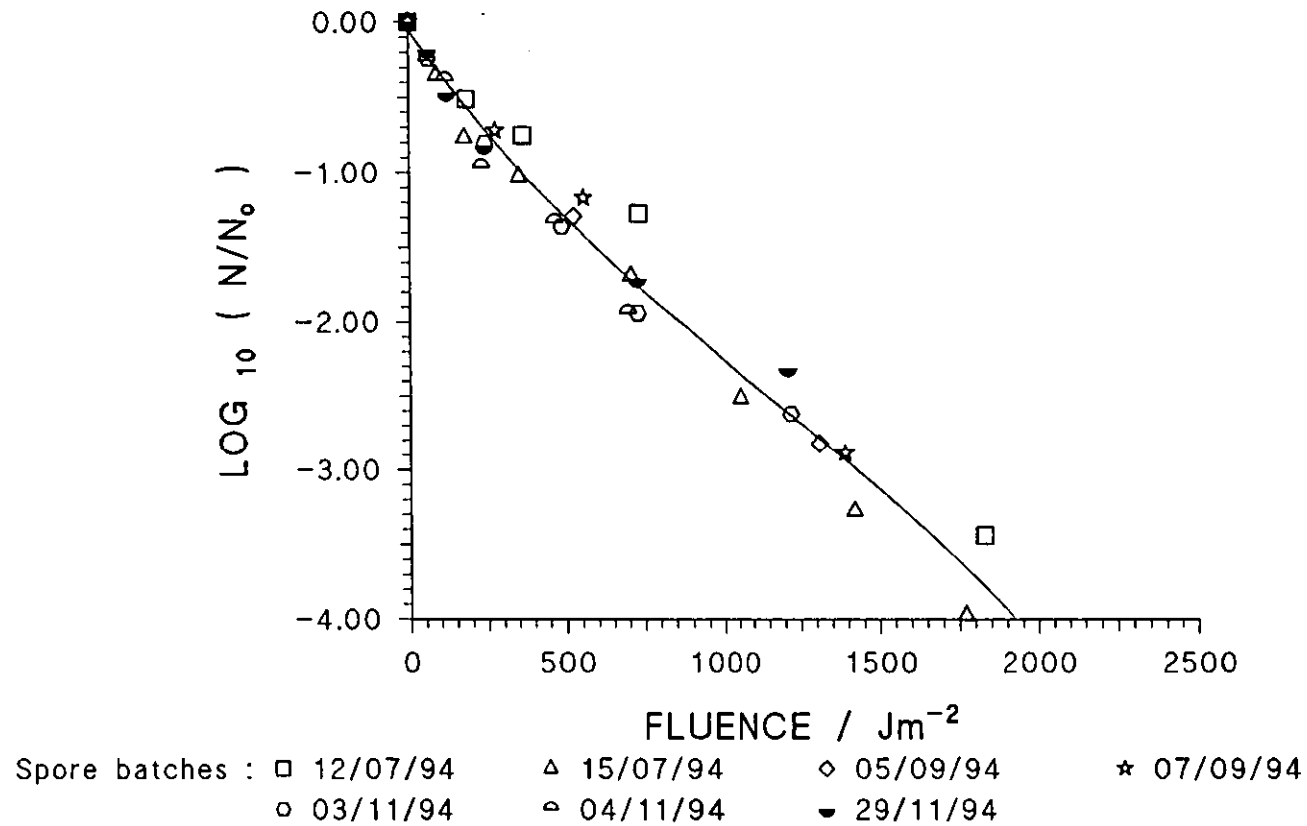
FIGURE 2.2 *B.subtilis* **spores on Grade 2 filter paper exposed to UV using the high intensity lamp**

2.2 Coating of surfaces

2.2.1 Introduction

The principle objective of the work described here was to study the performance of a spray sterilisation chamber when test objects of different geometries were placed within it. To assess the level of disinfection obtained it was necessary to know the number of viable organisms on the object before and after treatment. As the test objects could not be directly coated with micro-organisms, test surfaces were coated with micro-organisms and attached to the objects. The best results were obtained by either filtering spore suspensions through membranes or by allowing spore suspensions to dry directly onto surfaces, e.g. filter paper or aluminium sheet.

2.2.2 Filter paper strips

(a) Grades of paper used

Two grades of cellulose filter paper (Whatman (UK) Ltd., Maidstone, Kent) were used in this work - Grade 2 and Grade 6 filter paper (made from cotton linters; particle retention of 8 μm and 3 μm respectively). Grade 2 filter paper had a more open structure (8 μm retention) than Grade 6 filter paper (3 μm retention). In addition, Glass microfibre filter paper (Whatman) was also used in certain experiments.

(b) Inoculation of the filter paper

Filter paper strips (3 cm x 1 cm) were cut out by hand and placed in sterile Petri dishes. Each strip was inoculated with the test organism by pipetting 40 μL of a microbial suspension onto the filter paper strip using a micropipette (Gilson). Eight aliquots of microbial suspension, total volume 40 μL, were applied over the surface area of the filter paper strip in a '4x2' pattern i.e. 4 aliquots along the 3 cm length and 2 aliquots along the 1 cm length. Once inoculated the filter paper strips were left in the Petri dishes to dry overnight and subsequently kept at ambient temperature in the dark and used the day after

inoculation.

(c) Recovery of spores / micro-organisms

In order to recover the micro-organisms from the filter paper strips it was necessary to return the spores to a suspension so that serial dilutions and platings could be performed. The filter paper strips were placed in sterile Universal bottles containing 10 ml sterile Ringers solution (Oxoid Ltd., Basingstoke, Hants.) and approximately 1 g ballotini (3 mm +/- 0.5 mm diameter, Jencons, Leighton Buzzard, Bedfordshire) and macerated by agitation using a vibratory mixer. Following this, the resulting fibrous suspension was allowed to settle for 40 seconds to leave a clear, fibre-free Ringers solution which yielded a full recovery of the spores from the filter paper strip. Supernatant was removed and subsequently used for serial dilutions and/or plating.

2.2.3 Membranes

(a) Types of membranes used

Two types of membranes were used in this work, both having 0.2 μm pore size - cellulose nitrate membranes (Whatman) and Anodisc membranes (Whatman). Anodisc membranes retain a smaller electrostatic charge on their surfaces than cellulose nitrate membranes, and have a regular, 'honeycomb' appearance when viewed under a scanning electron microscope. The Anodisc membrane is constructed of a patented inorganic material, ANOPORE^{TM}.

(b) Inoculation of the membranes

B.subtilis spore suspension (10 ml), diluted 1 in 250, was vacuum-filtered through each membrane, which was then placed in a sterile Petri dish and left to dry overnight in a dark cupboard at ambient temperature. Dilution was necessary in order to make the microbial count per membrane the same as the count per filter paper strip in the technique described in section 2.2.2.

40

(c) Recovery of spores

It was found that the sampling technique described above for filter paper strips (see section 2.2.2(b)) provided full recovery of *B.subtilis* spores from membranes.

2.2.4 Non-porous materials

B.subtilis spore suspension was also deposited onto the surface of 'coupons' and allowed to dry. This method was used by Wang and Toledo (1986) when investigating the disinfection performance of hydrogen peroxide vapour. Aluminium, stainless steel, and PTFE coupons were coated using this technique.

(a) Inoculation of the surfaces

Coupons of the required material were cut into 15 mm x 15 mm squares from virgin material. In total 0.10 ml *B.subtilis* spore suspension was pipetted onto the surface of the coupon by placing 9 aliquots of 11.1 µL each across the surface of the coupon in an evenly spaced '3 by 3' pattern. The coupons were then transferred to sterile Petri dishes and placed in a 60°C incubator for 40 minutes to dry.

(b) Spore recovery

Full recovery was achieved by placing the coupons in sterile Universal bottles containing 10 ml sterile Ringer's solution and mixing vigorously for 1 minute using a vibratory mixer (Fisons, Loughborough, Leics.).

2.2.5 Attachment to objects

Filter paper strips, membranes and coupons of non-porous materials were all attached to test objects using 3 pieces of adhesive tape. The spore-impregnated test surface was stuck to one piece of tape whilst the other two pieces of tape were used to stick the tape to the

41

object. The tape held the test surface firmly in position so it was possible to use it on the vertical surfaces of objects. This method enabled the test surface to be removed from the tape by the use of tweezers, thus allowing fast sampling of the test surface.

2.3 Lab-based inactivation studies

2.3.1 Introduction

A number of small-scale experiments were carried out in the laboratory where better control of key parameters, such as UV intensity, quantity of sterilant applied and exposure time could be exercised.

2.3.2 Exposure to UV

The UV lamps used were either a 6 W low intensity source (TUV 6 W, Phillips Ltd, Croyden, Surrey) or a high intensity source (UV LUX 30 W, Voltarc Tubes Inc., USA) with reflector. Test materials were placed in Petri dishes and exposed to the UV lamp at a known intensity. The intensity was measured using a UV radiometer (Model 'UVX', UVP Inc., Cambridge, Cambs.). Preparation and sampling of test surfaces was as described in section 2.2. Figures 2.3 and 2.4 show the arrangements for the UV irradiation of samples with both lamps.

2.3.3 Exposure to liquid sterilants

These experiments were performed with *B.subtilis* spore impregnated Grade 2 filter paper strips. Liquid sterilant (40 µl) was applied to each strip by a pipette in 8 aliquots, evenly distributed over the filter paper surface. In measuring exposure times, these were taken as commencing from the instant the entire filter paper strip had been wetted. The filter paper strips were sampled as previously described (see section 2.2.2).
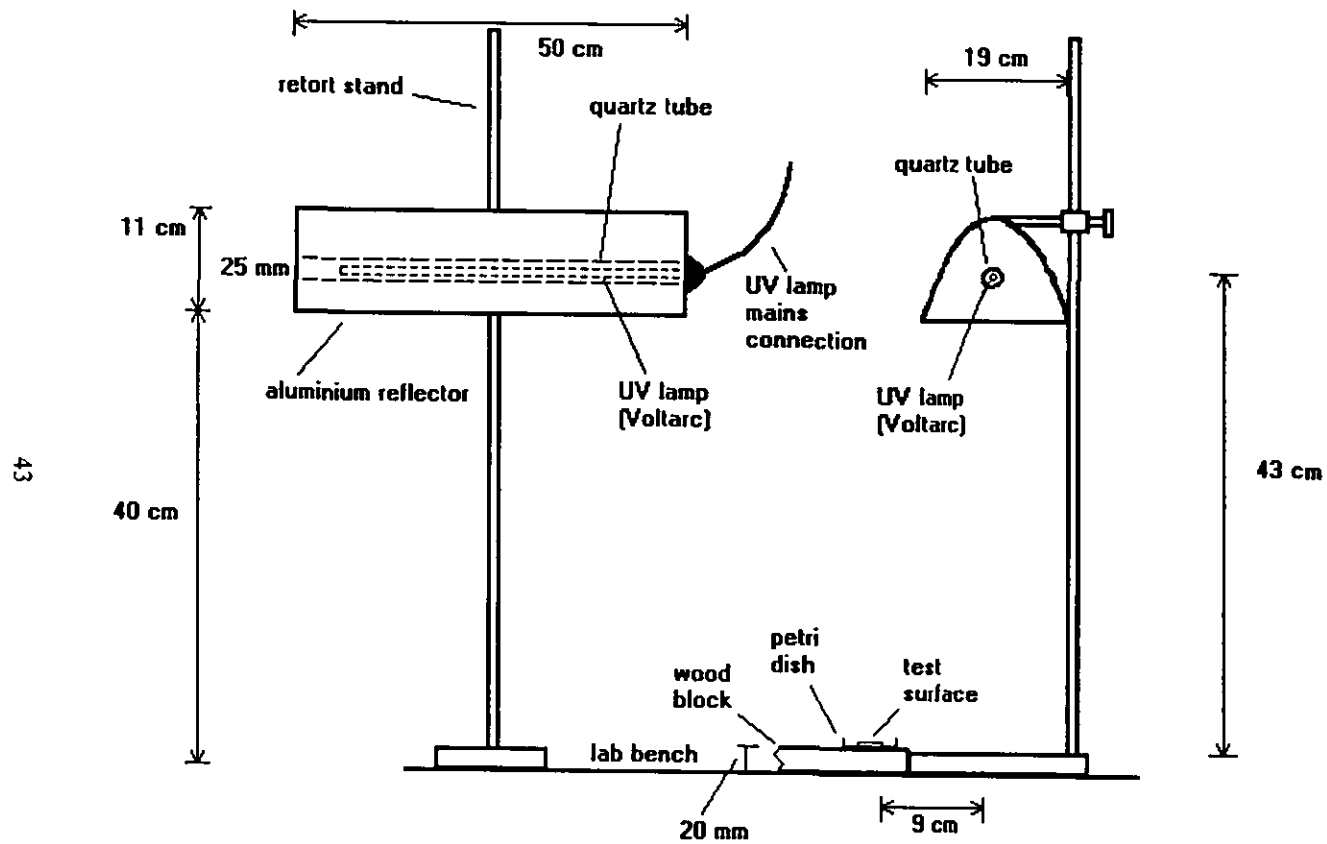
FIGURE 2.3   High intensity UV lamp arrangement
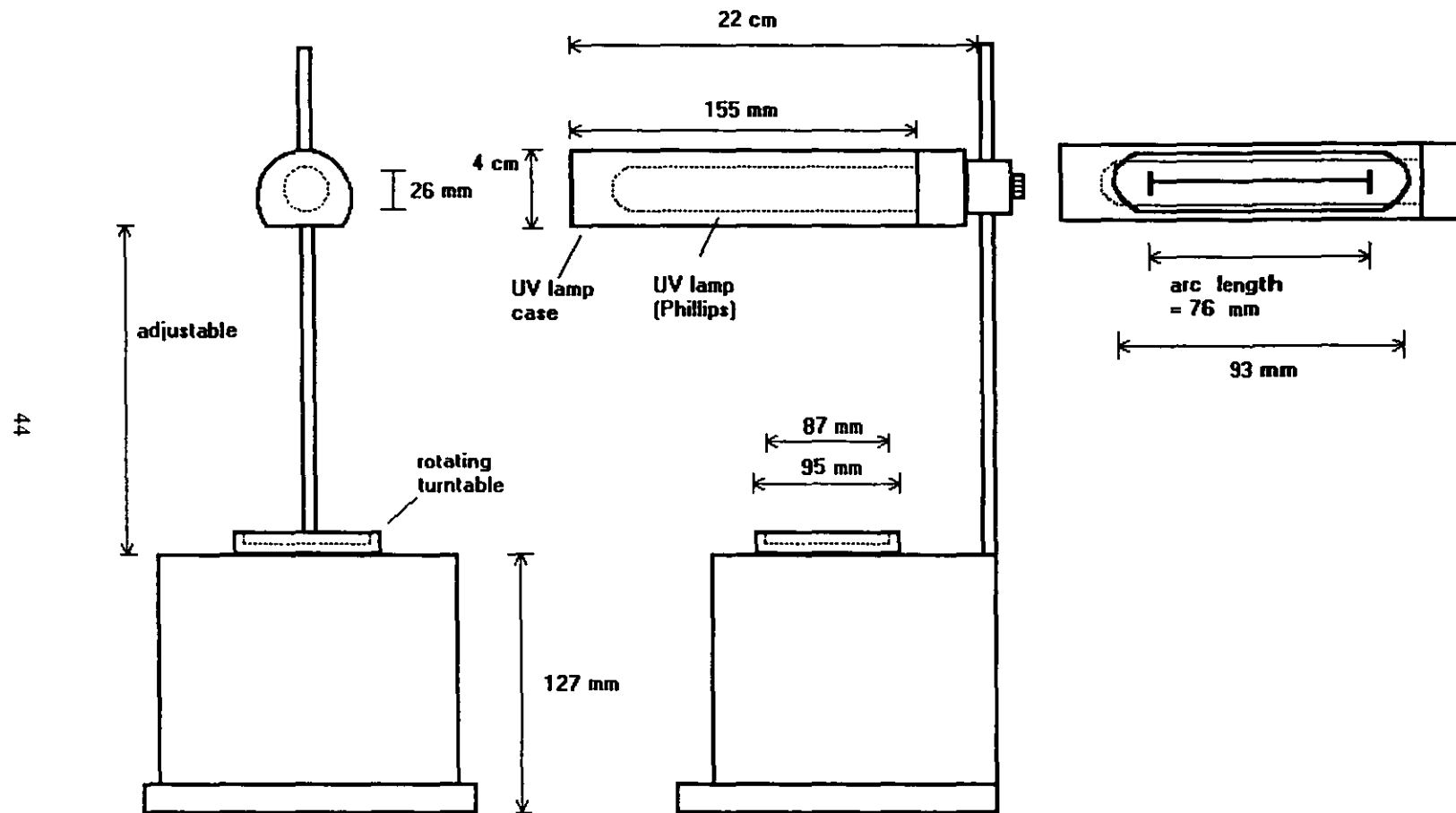
FIGURE 2.4   Low intensity UV lamp arrangement

2.3.4 Exposure to gaseous ozone

The output from an air-fed ozoniser (EA Technology, Capenhurst, Cheshire) was passed into a sealed, 0.5 L glass reaction vessel. The volumetric flowrate was measured by a rotameter and was approximately 0.5 L/min. Ten minutes were allowed for the ozone concentration to reach steady-state, after which *B.subtilis* spore impregnated aluminium coupons (prepared and sampled according to the method described in section 2.2.4) were placed in turn in the reaction vessel (using flamed tweezers) for specified exposure times and then immediately sampled.

2.4 Assessment of microbial survival following disinfection

2.4.1 Serial dilutions

Serial dilutions were performed in Eppendorf tubes by adding 0.1 ml of the sample to 0.9 ml of Ringers solution (Oxoid) and mixing the contents for ten seconds using a vibratory mixer (Fisons).

2.4.2 Plating

Typtone Soya Agar (TSA) (Oxoid) was used to estimate microbial survival. The Miles and Misra (1938) plating technique was used with the modification that 6 aliquots of 20 μL microbial suspension, rather than 5 aliquots of 20 μL, were placed on a single agar plate using a micropipette (Gilson). The plates were left until the agar had absorbed the microbial suspension. They were then inverted and placed in a 30°C incubator. The plates were incubated until visible microbial colonies formed. These were counted and the plates returned to the incubator. When no further increase in the number of microbial colonies occurred, this count was taken to be the final result. For *B.subtilis* spores this incubation time depended on the level of damage incurred by the spores. For undamaged spores 17 hours incubation was typically sufficient to produce countable microbial colonies. The longest incubation period required was for spores treated with 29 w/v% H_2O_2 which required a 48 hour incubation period.

2.4.3 Sampling precautions

(a) Experiments using UV

Micro-organisms possess a number of mechanisms for repairing UV-induced damage (see section 1.2.5). Post recovery procedures were standardised in order to minimise repair to damaged cells. This entailed storing samples in the dark to avoid light-induced repair mechanisms and plating samples out with the minimum of delay to avoid light-independent ('dark') repair from occurring.

(b) Experiments using hydrogen peroxide

In order to exercise careful control over exposure times to H_2O_2 following treatment, test surfaces were rapidly transferred to Universal bottles, containing 10 ml Ringer's solution, and shaken vigorously. This resulted in rapid dilution; at the highest concentration of H_2O_2 applied, 40 µl of 29 w/v%, this procedure resulted in a final H_2O_2 concentration of 0.12 w/v%. Concentrations below 10 w/v% have been shown not to be sporicidal (Stevenson and Shafer, 1983). This was confirmed by a series of experiments.

2.5 Chamber description

The spray disinfection chamber used in this work to treat test objects is shown in Figure 2.5. The chamber was equipped with four UV sources which were situated at the top of the chamber and which formed a UV field in which objects to be treated were slowly rotated. At the lower end of the chamber was located a spray nozzle which permitted spraying with either aqueous ozone or hydrogen peroxide during irradiation.

The body of the spray disinfection chamber comprised a cylindrical piece of glass (9" diameter QVF with buttressed ends; Corning Glass Ltd., Stone, Staffs.). The glass body was sealed by means of two circular PVC plates which were bolted into place (Figure 2.6). A circular aperture was cut into the top plate in order to introduce test objects into the chamber. This aperture was sealed by means of a removable solid PVC plug. Objects to be
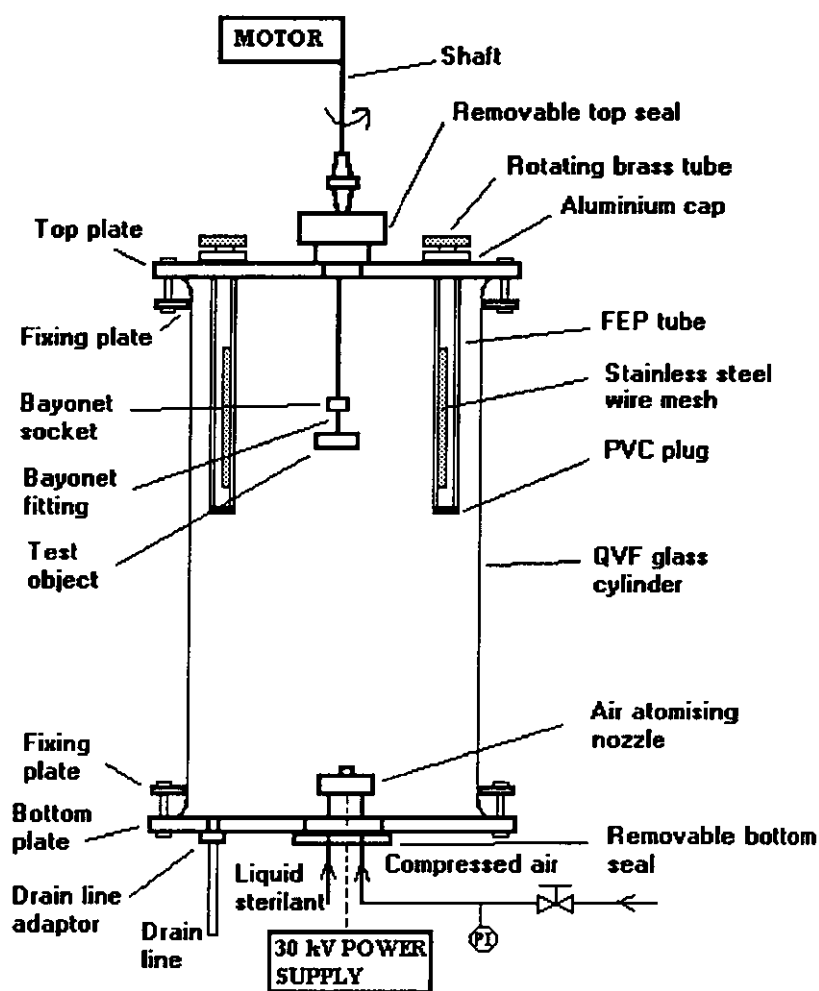
FIGURE 2.5   Spray sterilisation chamber

8 cm

76 mm

35 cm

8.5 cm

35 mm

32 mm

TOP END PLATE   BOTTOM END PLATE
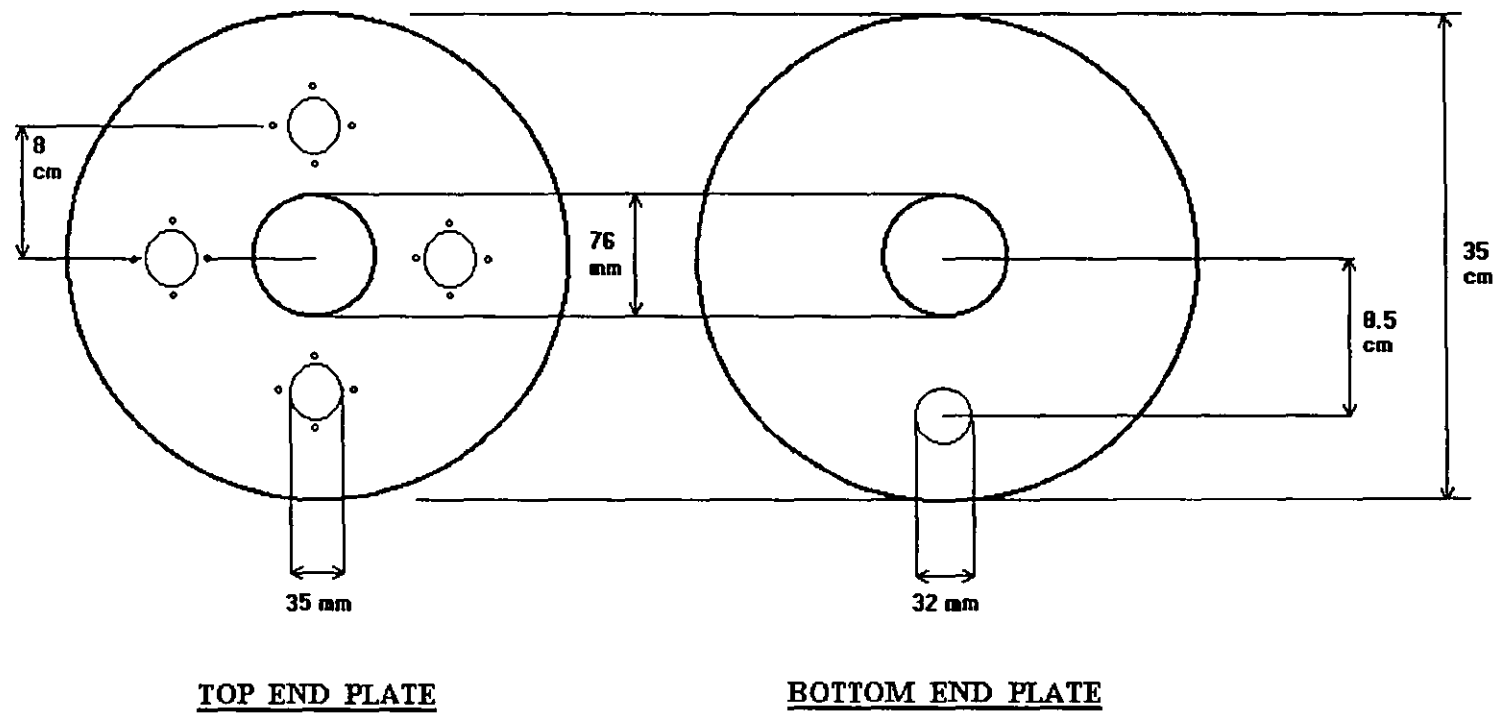
FIGURE 2.6   End plates of the spray disinfection chamber

irradiated were coupled to a stainless steel shaft which penetrated the PVC plug by means of a bayonet fitting (see Figure 2.7). The shaft was in turn connected to the shaft of a small electric motor (Citenco Ltd, Boreham Wood, Herts.). During normal operation the object was rotated at approximately 30 rpm.

The top plate was bored to permit four low pressure mercury vapour UV sources (UV LUX 30W, Voltarc Tubes Inc., USA) to be suspended in the chamber. The sources were housed in shrouds made of clear Fluorinated Ethylene Propylene (FEP) tubing (32 mm ID, 0.5 mm thickness; Adtech Ltd, Stroud, Gloucs). FEP is transparent to short wave UV and is far more robust than quartz glass which is traditionally used. The FEP tubes were sealed at their lower ends with circular push-fitted PVC caps. The FEP tubes were attached to circular aluminium caps which provided the means of suspension in the chamber. This arrangement gave a spray proof seal whilst enabling the tubes to be securely held in place (Figure 2.8).

In order to control irradiation times without interrupting power to the UV sources, brass tubular shields were placed inside the FEP tubes. (Interruption of the power supply would have delayed experimentation as the sources required a period of several minutes in order to reach stable emission). Circumferential windows (arc 180°) were cut into the brass tubes and rings were attached to the ends of the brass tubes protruding from the FEP tubes so that the brass tubes could be conveniently and rapidly rotated, either to irradiate the object or to cease irradiation.

Initial studies revealed that the intensity of the UV field was very high and spores on test surfaces were inactivated within seconds. This arrangement would have made the collection of inactivation data over time impossible. It was therefore necessary to reduce the UV intensity. This was done by introducing stainless steel meshes (Plain Dutch Weave, nominal aperture 0.125 mm; Incamesh Filtration, Warrington, Cheshire) inside the brass tubes.

The consequences of confining the UV sources as described above was that the temperatures inside the FEP tubes rose to over 100°C, whilst the chamber temperature reached 50 °C. The emission of the UV lamps would have been considerably reduced at such temperatures. Also, as it was intended to investigate disinfection performance at near ambient temperatures, such temperatures in the chamber could not be tolerated. In order to dissipate the heat generated, compressed air was introduced into the FEP tubes via ¼"

14 mm

I 2 mm

6 mm

50 mm

43 mm

31 mm

20 mm

X SECTION AA

BAYONET FITTING

BAYONET SOCKET

A   A
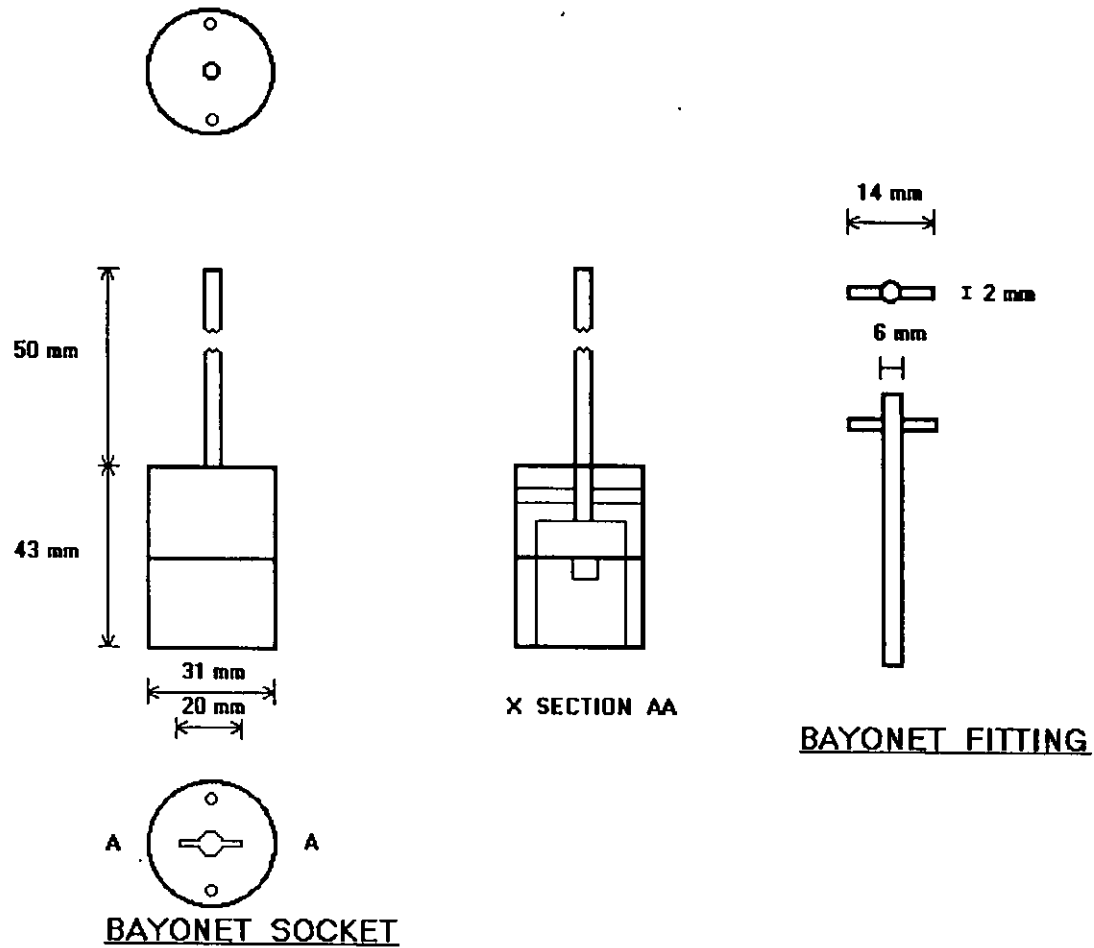
FIGURE 2.7   Method of attachment of test object to rotating shaft
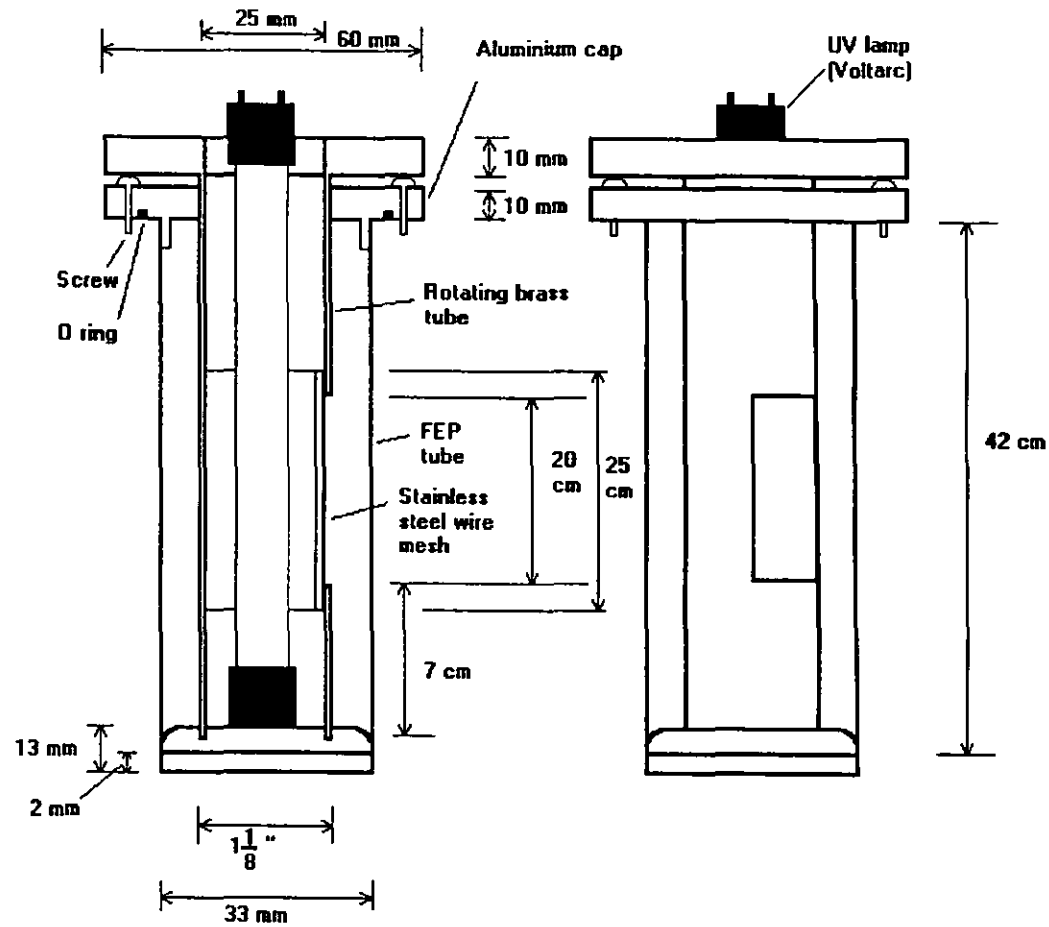
FIGURE 2.8   UV lamp holder for spray sterilisation chamber

brass tubing. These tubes ran alongside the UV sources to which they were attached by means of fine wire. The same air flowrate was used in all the disinfection experiments, which was controlled by setting the air pressure on the feed line to 2.0 bar. This air flowrate was sufficient to maintain temperatures of 40°C inside the FEP tubes. Moreover the chamber temperature remained relatively stable, increasing by under 5°C after one hour of operation.

Three test objects were made for use in the spray sterilisation chamber. These were a cylinder (hollow from the bottom to 1 cm below the top) and a disc-shaped object, both made from PVC, and a hollow cylinder constructed from stainless steel. These objects are depicted in Figure 2.9.

2 air-atomising nozzles were used in the spray chamber. The first nozzle used was a BETE 1/4 XA series siphon/gravity feed air-atomising nozzle (Lurmark, Longstanton, Cambridge). This nozzle produced a venturi action which provided a pressure difference sufficient to convey liquid up into the nozzle body where the liquid and compressed air were mixed internally to produce an atomised spray. The nozzle was made entirely from 303 grade stainless steel. The nozzle comprised separate air and fluid caps. (Table 2.1 shows manufacturer's data for the nozzle). An identical nozzle constructed from a non-metallic, oxidant-resistant material was also employed in this study. This nozzle was a 1/4" BSP siphon/gravity feed air-atomising nozzle with the same spray characteristics as the nozzle previously described (Spraying Systems Co., Godalming, Surrey) (Spray combination no. SU1A) and was manufactured from perspex.

The nozzles produced full cone spray patterns. When operating in the spray chamber the cone spray pattern only extended for 3-5 cm from the nozzle before the effect of eddies of air in the confined volume of the spray chamber destroyed the pattern, producing a chaotic, turbulent spray pattern.

In order to gain access to the spray nozzle without dismantling the spray chamber, the nozzles were located on mountings that could be inserted into the centre of the bottom end-plate. The removable seal on which the perspex nozzle was mounted is shown in Figure 2.10.

Disc-shaped object   PVC cylinder   Hollow stainless steel cylinder
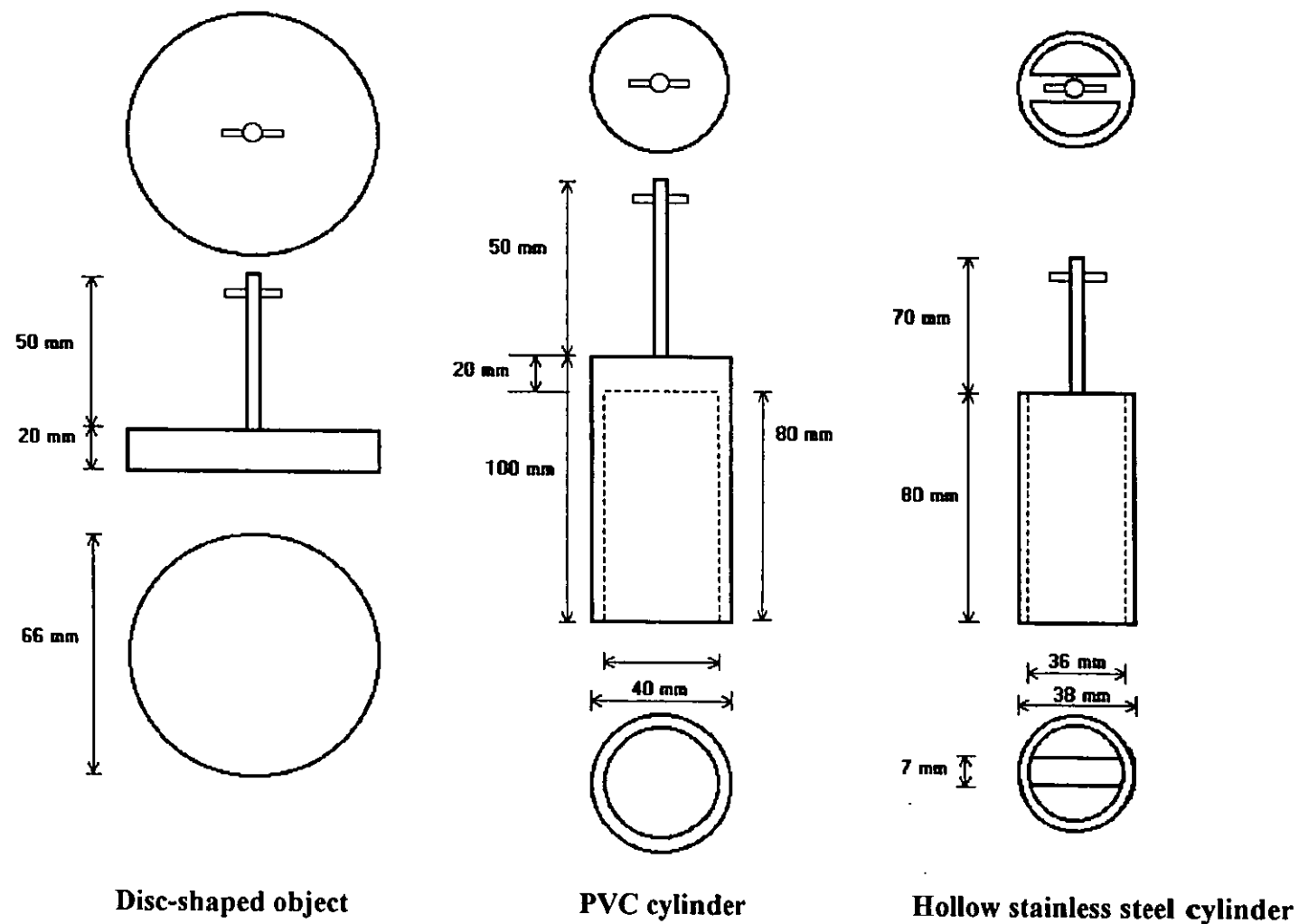
FIGURE 2.9   **Test objects for use in the spray sterilisation chamber**

Spray combination number	Air pressure / bar	Air capacity / l min⁻¹	Liquid capacity / l hour⁻¹ at 10 cm siphon height	.. at 20 cm siphon height	.. at 30 cm siphon height	.. at 60 cm siphon height
SR050	0.7	11.3	0.87	0.68	0.53	
SR050	1.5	17.0	1.3	1.2	1.1	0.62
SR050	3.0	28	1.5	1.4	1.3	1.1

Note   : Perspex nozzle spray characteristics identical to those of the SR050 combination

: Spray angle for nozzle SR050 = 18°

TABLE 2.1   Stainless steel air-atomising nozzle characteristics
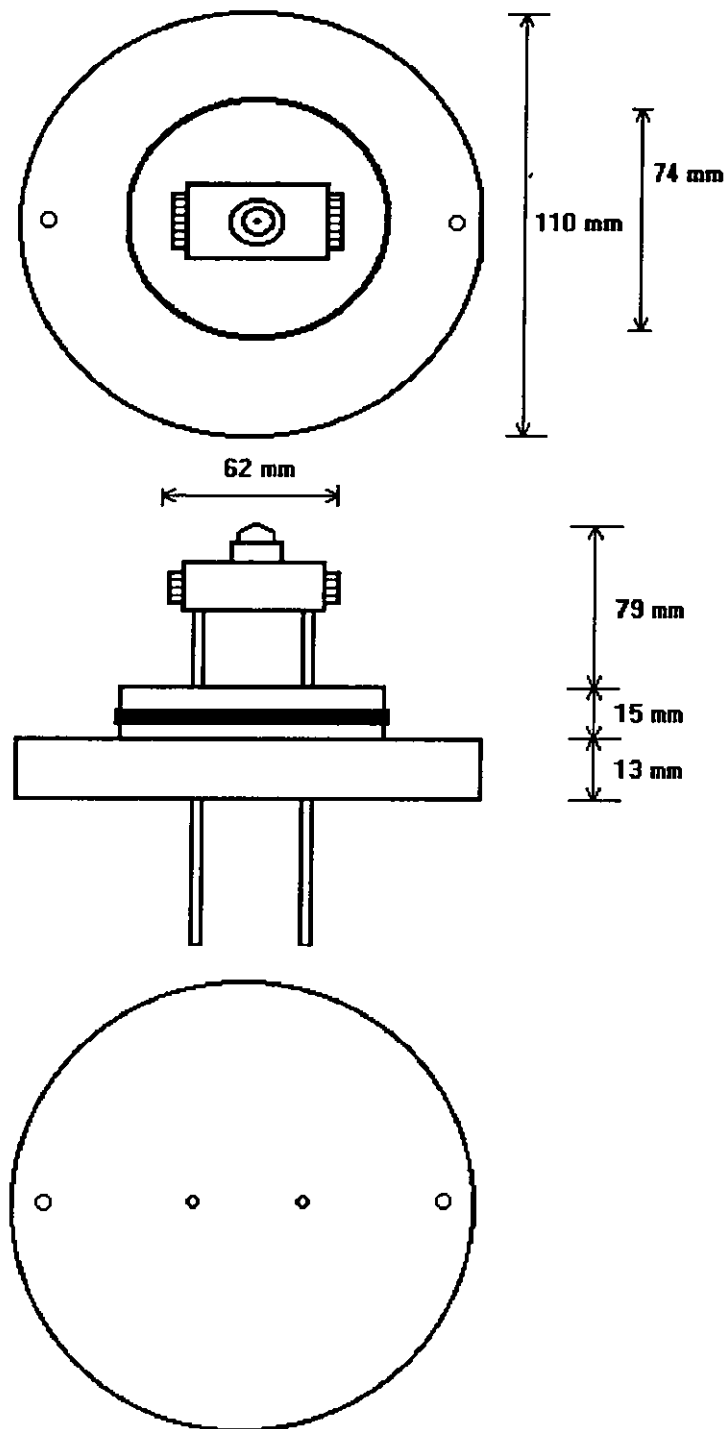
FIGURE 2.10 Removable mounting for perspex spray nozzle

Electrostatically-charged sprays were generated by using the stainless steel air-atomising nozzle connected to a 30 kV power supply (Alpha Series; Brandenburg Ltd., Thorton Heath, Surrey) (Figure 2.11).

2.6 Inactivation studies in the chamber

2.6.1 Exposure to UV

Prior to irradiation, the 4 UV lamps in the chamber were allowed 15 minutes to reach a temperature of approximately 40°C to ensure constancy of power output during the course of the experiment. When the UV lamps had reached the required temperature, the test object was placed in the chamber using the methods described in section 2.5.

The object was irradiated by rotating the brass tubes through 180° thus exposing the object to the output from the UV lamps. Either 2 or 4 lamps were used. Two lamps were used when a lower UV intensity was required, as in the case when UV was combined with 1.0 w/v% H_2O_2. At the end of the required exposure period the brass tubes were rotated such that no UV from the lamps could reach the object.

2.6.2 Exposure to sterilant sprays

Objects were exposed to sprays in the chamber by attaching them to the central shaft passing through the top plate as described in section 2.5. The vertical position of the object in the spray chamber could be adjusted by altering the position of the motor. A vessel containing the liquid sterilant was placed underneath the chamber at a known siphon height and the liquid feed line to the air atomising nozzle was placed in the liquid sterilant. The feed air pressure, the siphon height and the measured spray time duration were recorded. The spray duration time was measured from the time that the spray issued from the nozzle and not from when the air supply to the nozzle was turned on.

In the absence of UV, the exposure time to sterilant was taken as the duration from which the spray ceased to when the test surface was sampled; access to the test surface typically
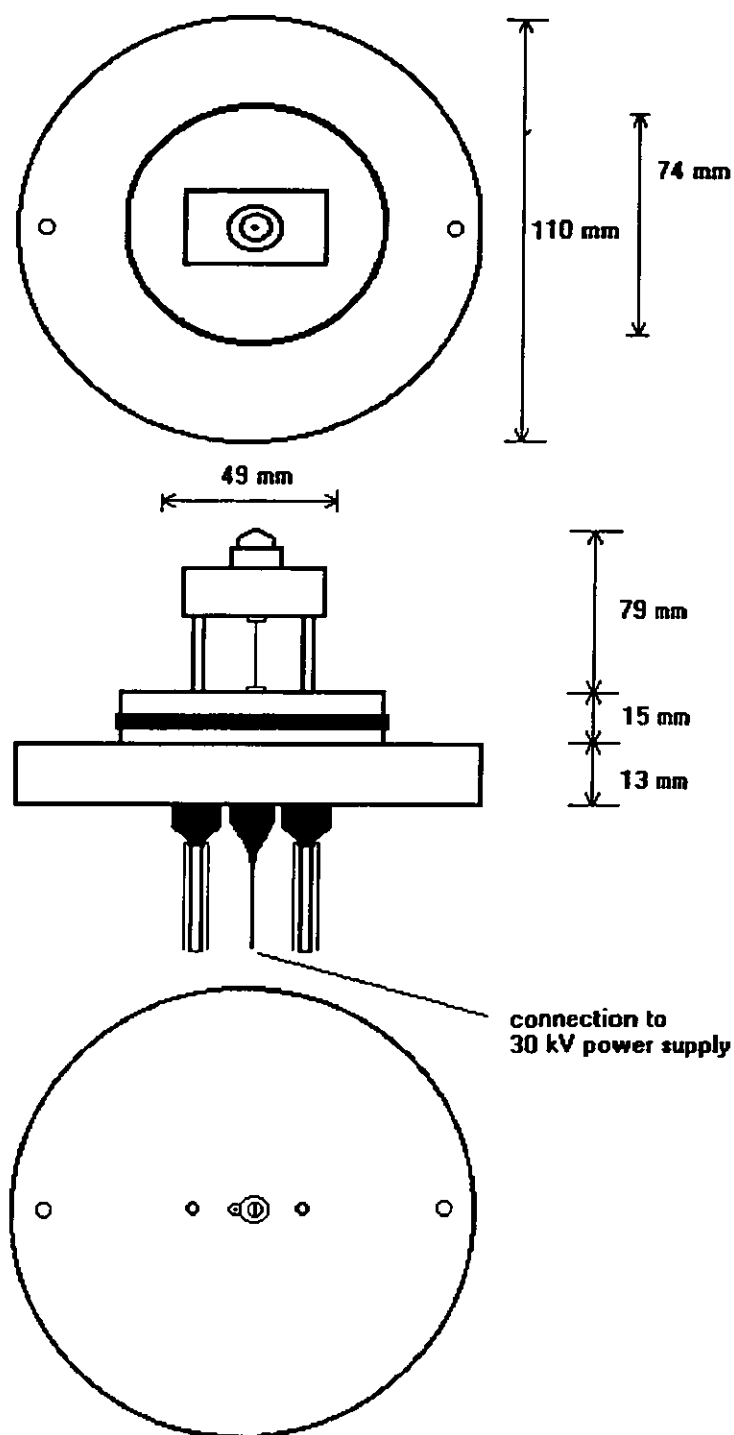
FIGURE 2.11 Electrostatic spray nozzle mounting

took 40 seconds. When using UV in combination with H_2O_2 sprays which were not sporicidal (e.g. 1.0 w/v% H_2O_2), the exposure time was taken to be the time that the surface was exposed to UV.

When an object was to be exposed to a combination of liquid sterilant and UV, the object was sprayed first with the UV sources shielded. Once the object was coated with spray, the brass tubes in the chamber were rotated in order to expose the object to the desired UV intensity. This procedure was developed because the inactivation rate due to combined treatments was rapid. This also allowed the test surface to be fully coated before irradiation.

Only one test surface was attached to the solid objects at any one time. By conducting a series of experiments for which the test surfaces were subjected to varying exposure times, it was possible to accumulate disinfection rate data.

2.6.3 UV Bioassay

UV fluences can be determined by reference to the dose-response characteristics of a particular organism. This technique has been referred to as a 'bioassay' (Qualls and Johnson, 1983).

With this information it is necessary only to establish the fraction of that organism surviving exposure to UV. The dose response curve for the organism enables the fractional survival to be 'translated' into an estimate of the UV fluence.

In this work, dry Grade 2 filter paper impregnated with *B.subtilis* spores were used. Seven disinfection experiments were performed to generate the dose response curve for the spores (Figure 2.12). A third-order polynomial curve was fitted to this data using a commercially available software package (Fig P, Biosoft, Cambridge, Cambs.) and its inverse function enabled UV fluence to be estimated directly once fractional survival of the spores were known.
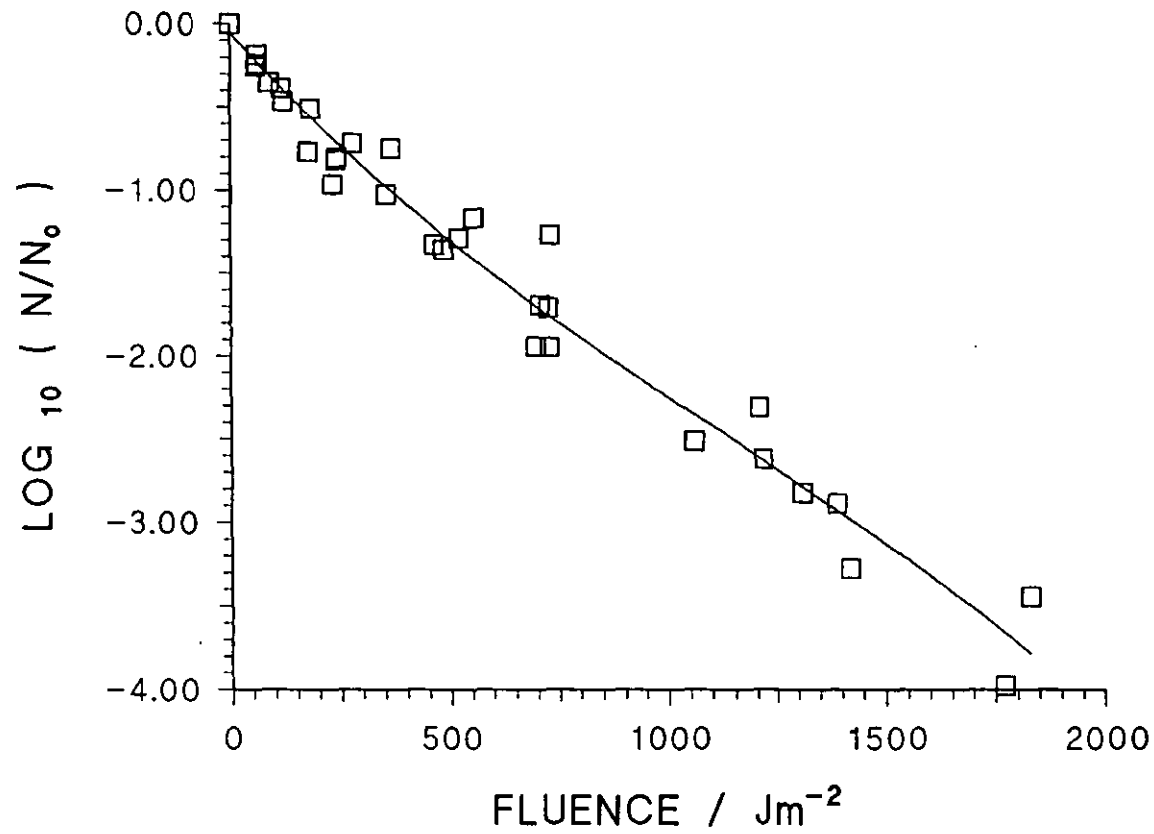
FIGURE 2.12   *B.subtilis* spore-based UV intensity bioassay (on dry Grade 2 filter paper)

2.7 Spray Impact Tests

2.7.1 Introduction

These experiments were performed to estimate the mass of spray deposited on a surface during spraying and are referred to here as 'impact tests'. Two variations of impact tests were employed - attaching paper strips to the object and weighing them after spraying (attached filter paper method), and wiping the surface of an object with paper after spraying and then weighing the paper (absorbance method).

2.7.2 Absorbance method

2 cm x 2 cm squares of filter paper (Whatman, Grade 2) were cut out, labelled and weighed on a precision balance (Metler AJ100, Mettler Instruments Ltd, High Wycombe, Berks) just prior to use. After spraying, the object was quickly removed and the object surface wiped with the filter paper square. The filter paper was then weighed immediately on the precision balance which was positioned next to the spray chamber. It was important to minimise the delay between spraying the object, wiping the object and weighing the filter paper because evaporation, either from the object surface or from the filter paper squares, was found to be significant.

2.7.3 Attached filter paper method

3 cm x 1 cm strips of filter paper (Whatman, Grade 2) were cut out and weighed on a precision balance (Mettler AJ100). The strips were then attached to the object by adhesive tape. After spraying the object, the strips were removed from the adhesive tape and weighed.

2.8 Production and measurement of ozone

2.8.1 Production of ozone

(a) Gaseous ozone

Two ozonisers were available for the production of gaseous ozone, made by BOC and EA Technology respectively. The feeds to these ozonisers were either compressed air or compressed oxygen (BOC). When oxygen-fed, the ozonisers produced a higher concentration of gaseous ozone. Previous researchers (Rickloff, 1987; Bader and Hoigne, 1981) have quoted figures of between 4 and 8 v/v% ozone for oxygen-fed ozonisers. When air-fed, the EA Technology ozoniser produced gaseous ozone of a concentration about 1.0 v/v% (determined using the method described in section 2.8.2).

(b) Aqueous ozone

Aqueous ozone was produced by bubbling gaseous ozone produced from the ozoniser through distilled water. The experimental arrangement for the production of aqueous ozone is shown in Figure 2.13. In order to obtain a saturated concentration of aqueous ozone (40 mg/L) it was necessary to use an oxygen feed to the ozoniser. When an air feed was used the highest aqueous ozone concentration that could be obtained in distilled water at 1-2 °C was about 7 mg/L. A number of precautions were necessary to ensure consistency of production. First, prior to being exposed to ozone gas, a 200 ml charge of distilled water was placed in a 250 ml capacity Dreschel bottle and stored in a refrigerator at 4°C for one hour. The Dreschel bottle was then placed in a beaker filled with ice and then gaseous ozone was bubbled through it for one hour. This was sufficient to produce a saturated concentration of aqueous ozone. The Dreschel bottle, still in the beaker filled with ice, was transferred to the refrigerator at 4°C until required. When aqueous ozone was needed, the required volume was pipetted into a chilled Universal bottle. The Dreschel bottle was then sealed and the beaker replaced in the refrigerator.

Gaseous ozone emerging from the gas outlet of the Dreschel bottle was disposed of by bubbling it through a solution of potassium iodide. As a further precaution the equipment for aqueous ozone production was placed inside a fume cupboard.

PI

OZONISER → to atmosphere

O₂

Dreschle
bottle

Aqueous
ozone

ice   beaker

Dreschle
bottle

KI solution
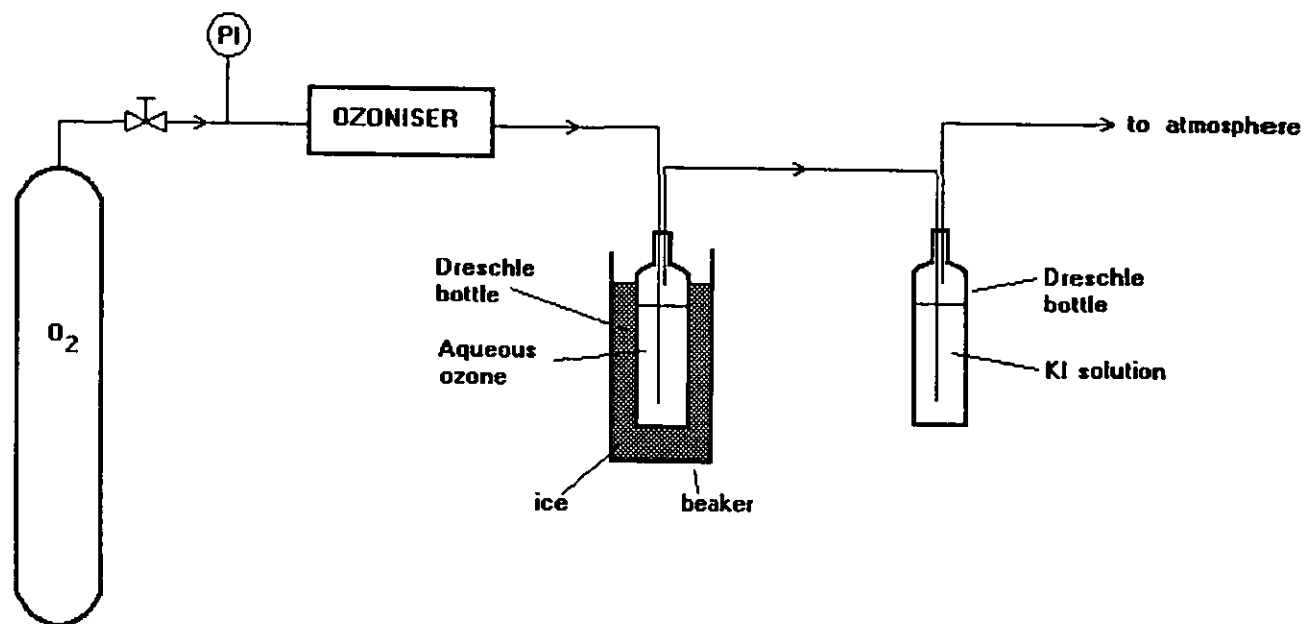
FIGURE 2.13 Production of aqueous ozone

2.8.2 Measurement of gaseous ozone concentration

Gaseous ozone concentration was determined using the method described by the APHA Intersociety Committee (Anon., 1977). This iodometric method involved reaction between potassium iodide and ozone. The ozone gas was bubbled into an alkaline potassium iodide solution at a known flowrate for a certain period of time. The resulting solution was neutralised with phosphoric acid which allowed the liberation of iodine into solution, producing a yellow colour. The absorbance at 352 nm of this solution was measured using a spectrophotometer (Shimadzu UV-1201). The ozone concentration in the solution was calculated from this result using an experimentally-determined calibration graph (see Anon. (1977) for details). As the volume of gas sampled was known, the gaseous ozone concentration could be calculated.

2.8.3 Measurement of aqueous ozone concentration

The method used was that described by Bader and Hoigne (1981). (All reagents used were purchased from Fisons Scientific Apparatus, Loughborough, Leics.). Approximately 30 ml of 0.4 M sulphuric acid was poured into a 50 ml volumetric flask. Five ml of aqueous ozone was pipetted into the volumetric flask and the volume made up to 50 ml with 0.4 M sulphuric acid. The contents of the volumetric flask were poured into a 200 ml beaker. Five ml of 0.4 M potassium iodide solution was added to this mixture. The ozone reacted with the potassium iodide to liberate iodine into solution, producing a yellow colour. Five ml of a 1.0 w/v% starch solution was added, producing a blue-coloured starch-iodine complex. Sodium thiosulphate solution was titrated against this solution. The end point was assessed to be when the solution became clear. Sodium thiosulphate solution (10^{-3} M) was used for determining aqueous ozone concentrations of about 40 mg/L. Sodium thiosulphate solution (10^{-4} M) was used for aqueous ozone concentrations of about 7 mg/L.

The aqueous ozone concentration was calculated using the relationships that 1 mole of ozone liberates 0.65 moles of I_2 (Anon., 1977) and that 2 moles of sodium thiosulphate react with 1 mole of I_2.

3. EXPERIMENTAL DISINFECTION STUDIES

3.1   Introduction

In this Chapter are reported experiments in which the disinfection performance of UV, H_2O_2 and ozone, either alone or in combination, were investigated using *B.subtilis* spores on a variety of test surfaces. Exposure of the test surfaces to the disinfection agents were conducted using both the spray chamber and bench top mounted UV sources.

The effects of varying the intensity of UV light and of H_2O_2 and aqueous ozone concentrations were investigated in order to find combinations of these disinfectants which gave synergistic disinfection levels. Kinetic expressions were fitted to the experimentally obtained disinfection data in order to develop equations which could subsequently be used to predict disinfection performance for larger scale spray disinfection chambers.

3.1.1 Inactivation Kinetics

The quantitative treatment of disinfection data was reviewed in Chapter 1 but it might prove helpful to briefly reiterate the main features here.

First-order kinetics represent the simplest form of kinetic expression applicable to disinfection data. These kinetics are infrequently observed for UV inactivation and are typical only for viruses whose sensitive material is single-stranded DNA or RNA. The interaction of other factors can lead to pseudo first-order kinetics being observed (Harm, 1980h).

First-order disinfection kinetics are described by the equation:

$$\left(\frac{N}{N_0}\right) = e^{-kF} \qquad \textbf{(3.1)}$$

where   k   =   inactivation rate coefficient

             F   =   fluence

             N   =   microbial concentration

             N_0 =   initial microbial concentration

In the work described below, first order kinetics were fitted to the disinfection data using conventional linear regression techniques.

Also discussed earlier were multi-target and multi-hit kinetics. In the former, the cell is visualised as containing multiple targets which must all be struck by UV photons for cell death to occur whereas in the latter, the cell is seen as containing a single susceptible target which must be struck a certain number of times for death to ensue. Multi-target kinetics were chosen for use in this study in preference to multi-hit kinetics because the former are more easily fitted to experimental data and also because they have successfully been applied to UV-induced inactivation of *B.subtilis* spores (Sugawara *et al.*, 1981).

Multi-target kinetics are described by the equation:

$$\left(\frac{N}{N_o}\right) = 1 - (1 - e^{-kF})^n \qquad \textbf{(3.2)}$$

where   N   =   microbial concentration

             N_o =   initial microbial concentration

             k   =   inactivation rate constant

             F   =   UV fluence

             n   =   number of targets

Equation (3.2) describes a 'shouldered first-order' disinfection curve of the type first described in section 1.1.2. At low microbial survival, equation (3.2) can be simplified to:

$$\left(\frac{N}{N_0}\right) \approx ne^{-kF}$$

(3.2a)

Multi-target kinetics were fitted to experimental data by the method described by Harm (1980c). On a plot of LOG_{10} (N / N_0) vs. F , the intercept of the linear asymptote on the LOG_{10} (N / N_0) axis will be LOG_{10} n and the gradient will be -0.434k. In certain cases a degree of judgement may have to be applied in determining precisely where to delineate the first order part of the curve, but once that has been achieved it is a matter of applying linear regression techniques to obtain the gradient.

3.2 UV Irradiation

3.2.1 Results

Results obtained during the UV inactivation of *B.subtilis* spores in distilled water are shown in Figure 3.1. The data shown represents results from six separate experiments conducted over a two year period. The data displays a shouldered first-order response with 'tailing' at higher UV fluences. Although partly occluded by data points, the 'shoulder' itself is not particularly prominent. Notwithstanding, multi-target kinetics were deemed to be appropriate and were fitted to the data obtained at UV fluences below 900 Jm^{-2} and the parameters are displayed in Table 3.1.

Figure 3.2 shows the inactivation data obtained on coupons of aluminium, stainless steel and PTFE. The inactivation data obtained was similar for each of these surfaces.

66
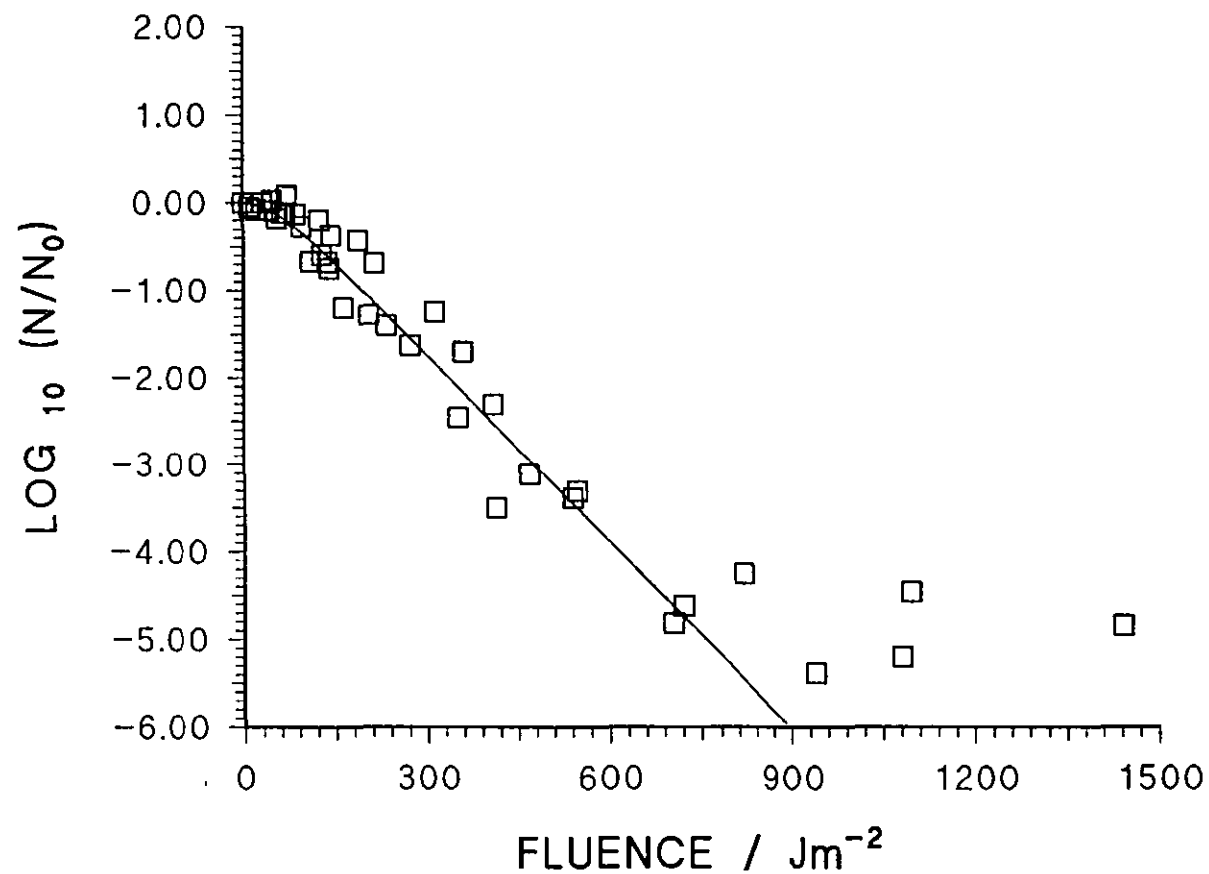
FIGURE 3.1   Exposure of *B.subtilis* spores suspended in distilled water to UV
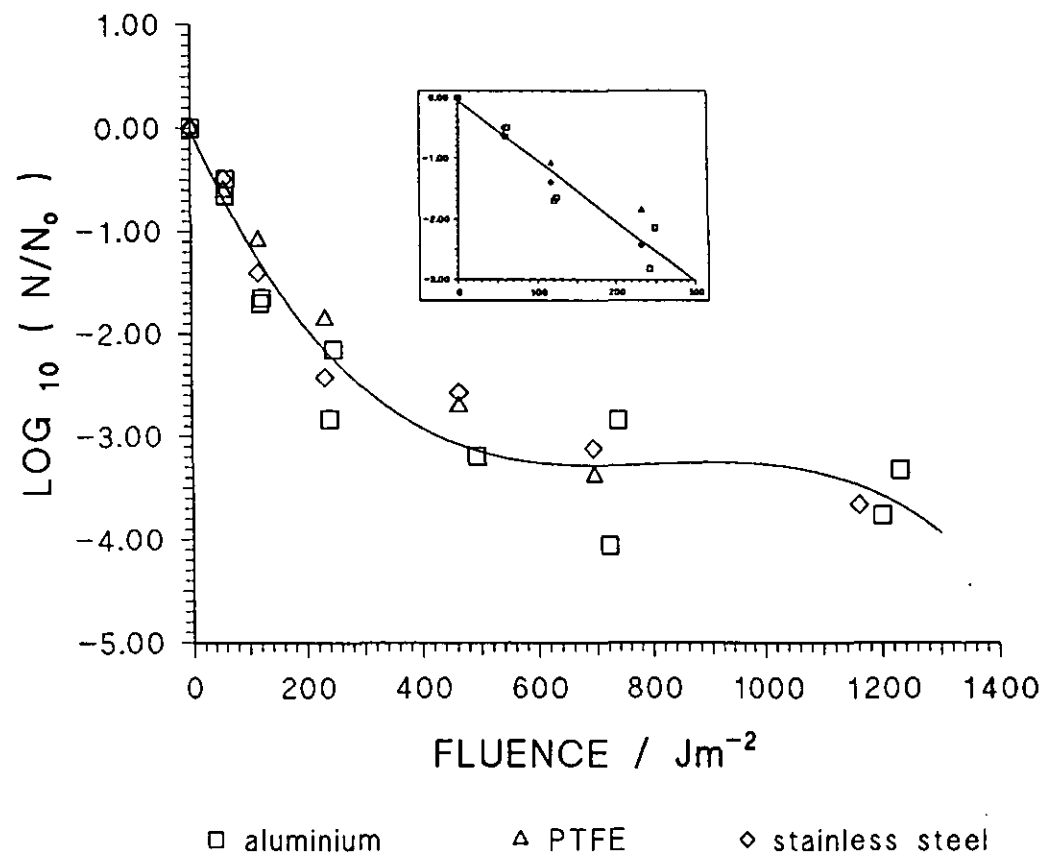
FIGURE 3.2 Exposure of *B.subtilis* spores on impervious surfaces to UV

First order kinetics were fitted to the early data (i.e. for fluences less than 500 Jm^{-2}) using linear regression and the rate constants are shown in Table 3.2.

The disinfection data obtained for aqueous spore suspensions filtered through Anodisc membranes and subsequently irradiated with UV are shown in Figure 3.3. First order kinetics were fitted to the data obtained at fluences below 400 Jm^{-2} and the rate constant is shown in Table 3.2. Although the membrane data displays a greater degree of scatter (particularly at high fluences) than that obtained for spores in aqueous suspension, comparison of the rate constants (Tables 3.1 and 3.2) reveals that the spores were inactivated at a faster rate when deposited on the membranes.

MEDIUM	INACTIVATION RATE CONSTANT $(Jm^{-2})^{-1}$	EXPONENT
Distilled water	1.65×10^{-2}	2.65
Wet Grade 2 filter paper	3.22×10^{-2}	2.00
Wet Grade 6 filter paper	9.34×10^{-3}	2.00

TABLE 3.1   Multi-target kinetic constants for *B.subtilis* spore inactivation by UV   (see Appendix 3 for standard deviations)

MEDIUM	INACTIVATION RATE CONSTANT $(Jm^{-2})^{-1}$
Glass microfibre filter paper	1.10×10^{-3}
Impervious materials (PTFE, aluminium and stainless steel)	2.28×10^{-2}
Anodisc membranes	2.13×10^{-2}
Dry Grade 2 filter paper	4.79×10^{-3}
Dry Grade 6 filter paper	8.77×10^{-4}

TABLE 3.2   First-order kinetic constants for *B.subtilis* spore inactivation by UV   (see Appendix 3 for standard deviations)

Figure 3.4 shows spore inactivation on dry Grade 2 filter and dry Grade 6 filter paper and a comparison of first order rate constants (Table 3.2) reveals that a slower rate of inactivation was obtained on the Grade 6 filter paper strips.

69
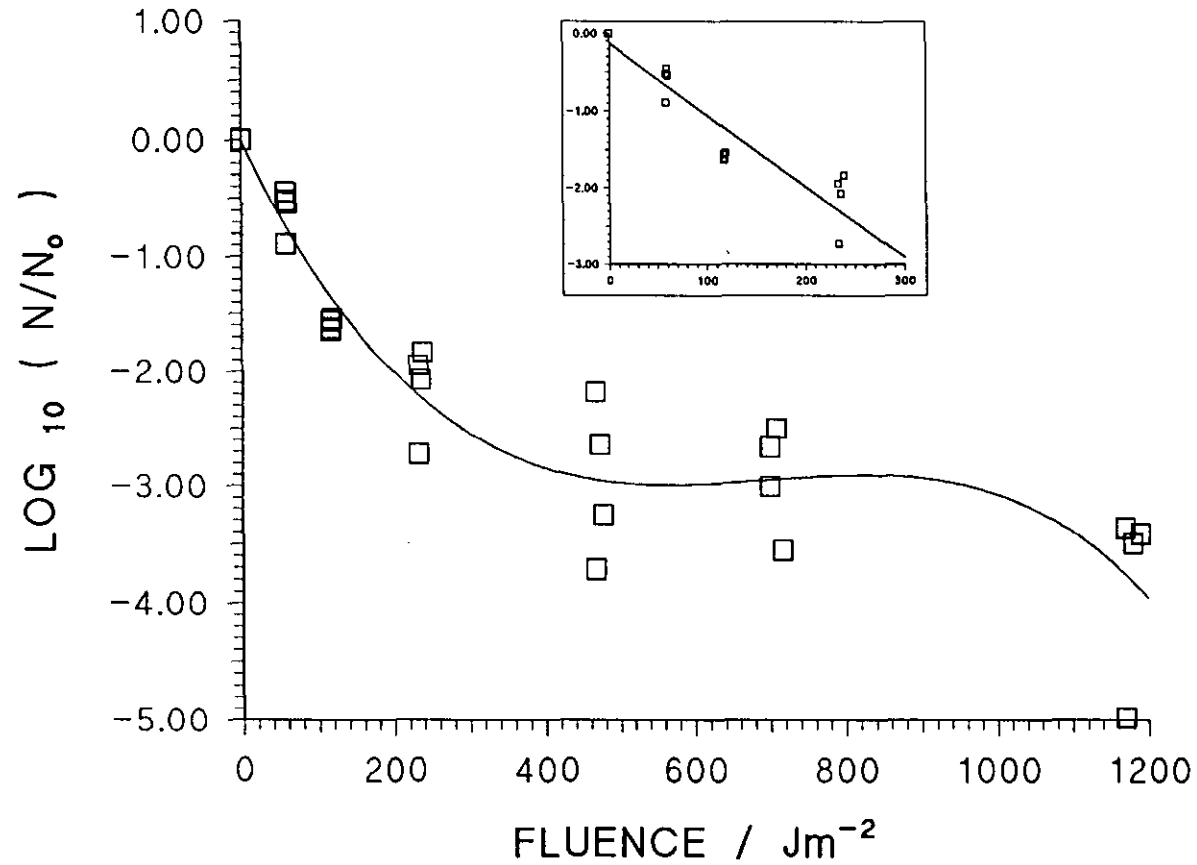
FIGURE 3.3 Exposure of *B.subtilis* spores on Anodisc membranes to UV
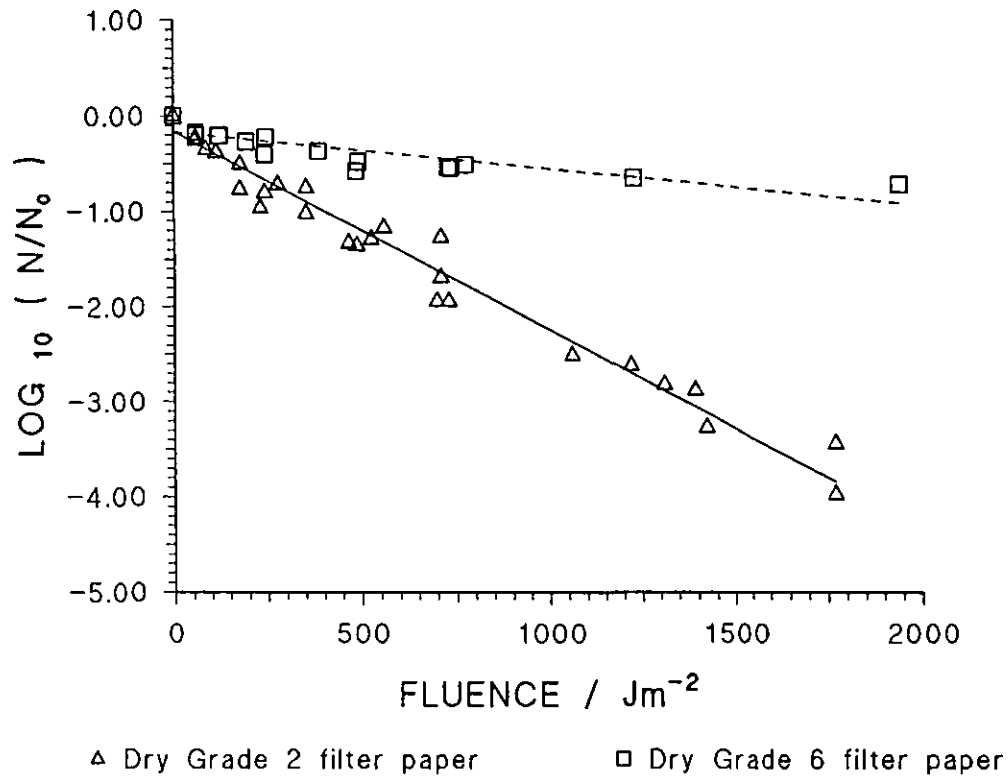
FIGURE 3.4   Exposure of *B.subtilis* spores on dry Grade 2 and dry Grade 6 filter papers to UV

Data showing the inactivation of *B.subtilis* spores on Glass Microfibre filter paper, when exposed to UV light using the high intensity UV source, are presented in Figure 3.5. This data displays considerable scatter but first order kinetics were applied in order to obtain some quantitative measure of the disinfection rate for comparison with the other materials (see Table 3.2). Overall, a much lower level of spore inactivation was achieved at fluences identical to those used for spores in aqueous suspension.

Scanning electron microscope (SEM) images were obtained for Anodisc membranes, Grade 2 filter paper, and glass microfibre filter paper coated with *B.subtilis* spores, and are shown in Figures 3.6 - 3.8. The higher magnification photographs (a) reveal the spores in relation to the different surface features whilst the low magnification photographs (b) enable comparisons of surface structure to be made.

Figure 3.9 shows inactivation data obtained using Grade 2 filter paper strips, wetted with 40 μl distilled water prior to irradiation. Also included are the results obtained with dry filter paper for comparison. The results clearly show that a greater rate of inactivation was obtained in filter paper strips when they were wetted with distilled water prior to irradiation. This result was unexpected and is commented upon in the Discussion. The curve fitted to the inactivation data for wet Grade 2 filter paper is described by multi-target kinetics and the kinetic parameters are shown in Table 3.1.

An increase in the disinfection rate (relative to dry filter paper) was also observed when Grade 6 filter paper strips were wetted with 40 μl of distilled water prior to UV irradiation. This is shown in Figure 3.10 which also shows the results obtained with dry Grade 6 filter paper. Multi-target kinetics were applied to the inactivation data for wet Grade 6 filter paper strips and the kinetic parameters are displayed in Table 3.1.

3.2.2 Discussion

B.subtilis (ATCC 6633) spore inactivation in water has been previously investigated and the results obtained here show the same shape of inactivation curve as that
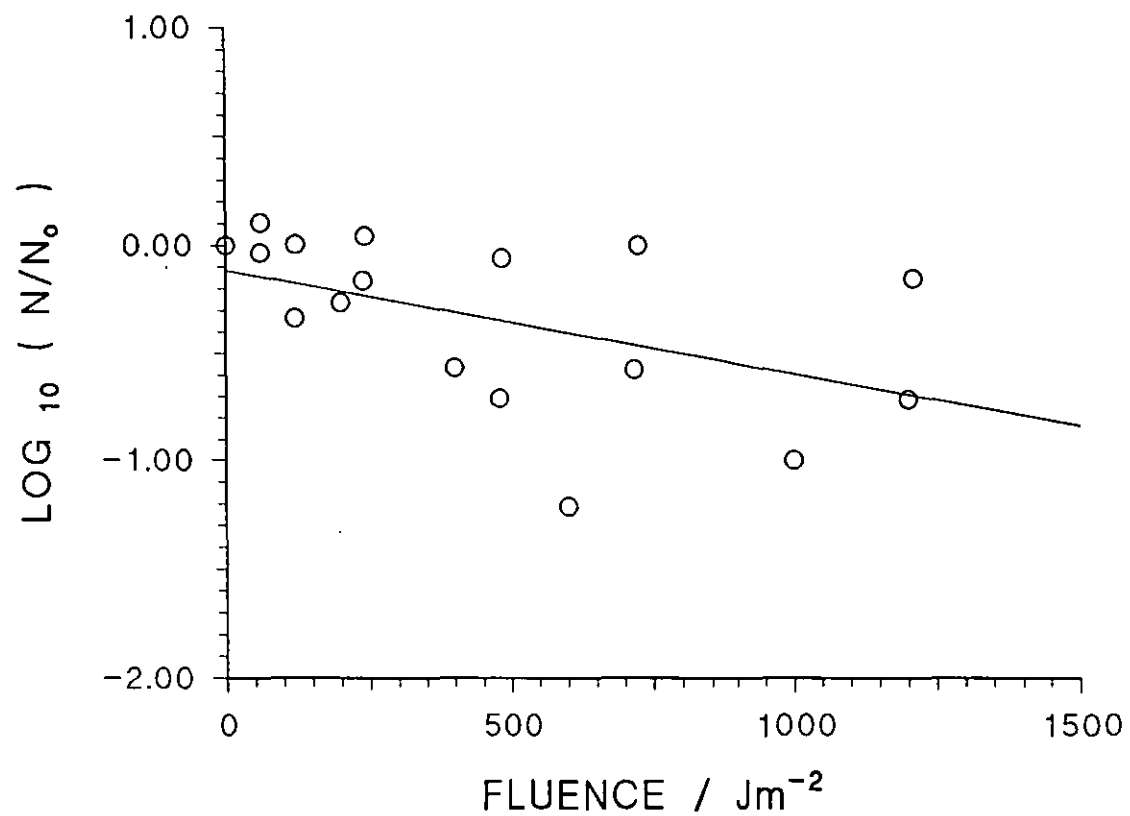
FIGURE 3.5 Exposure of *B.subtilis* spores on glass microfibre filter paper to UV
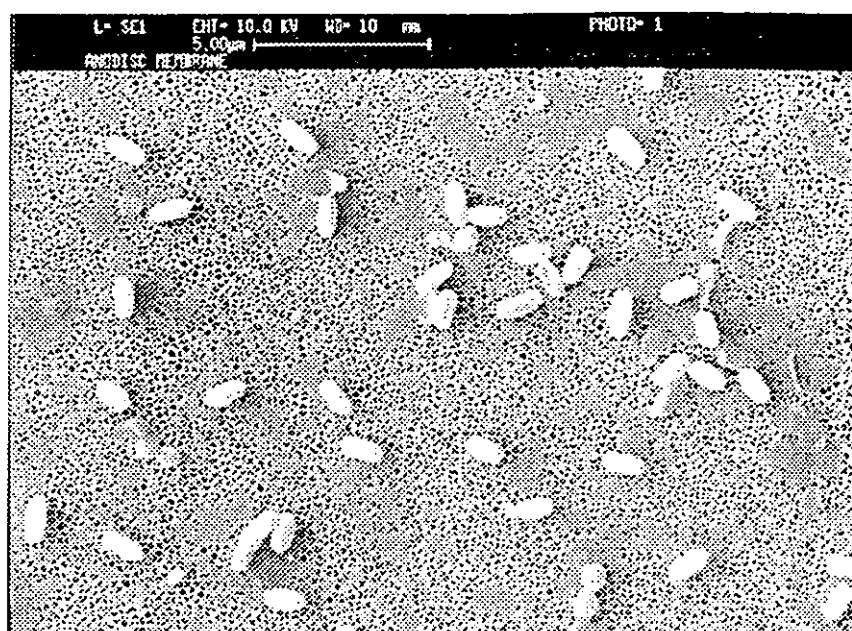
(a) High magnification
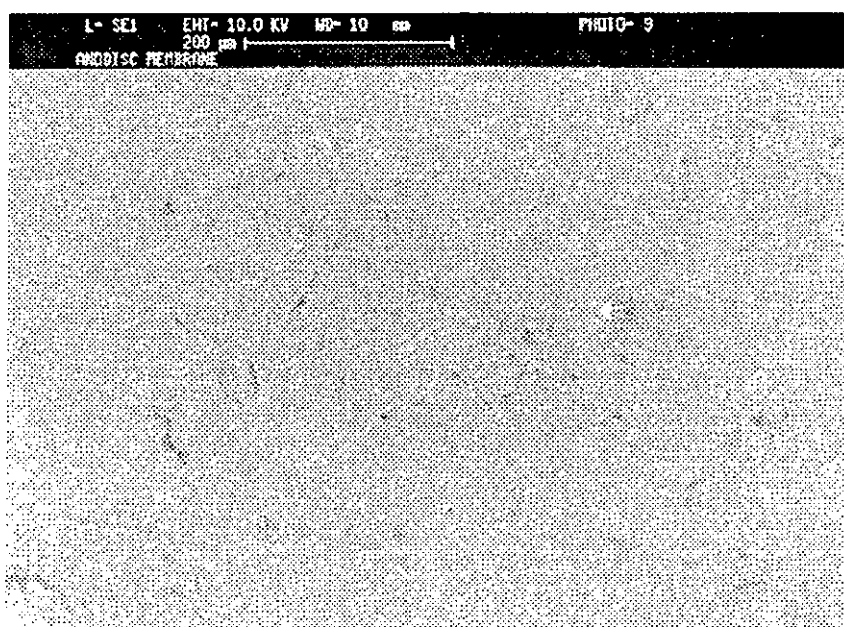
(b) Low magnification

FIGURE 3.6 *B.subtilis* spores on Anodisc membranes
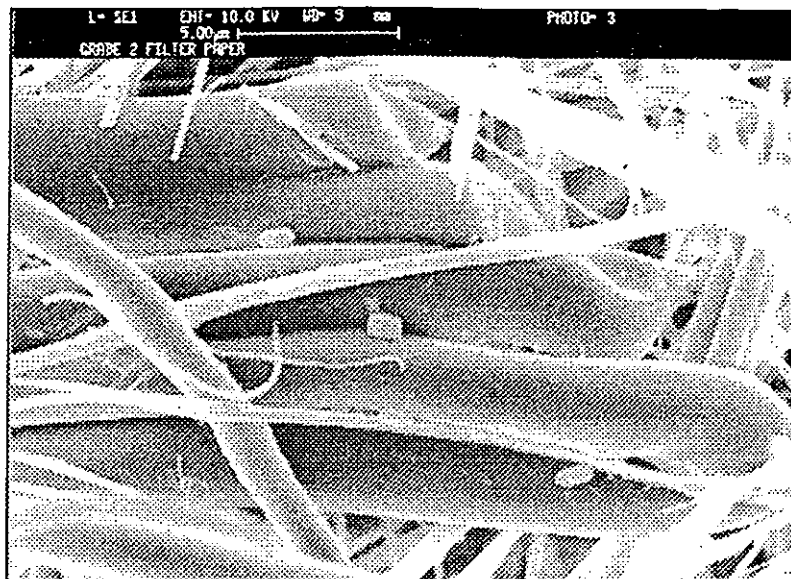
(a) High magnification
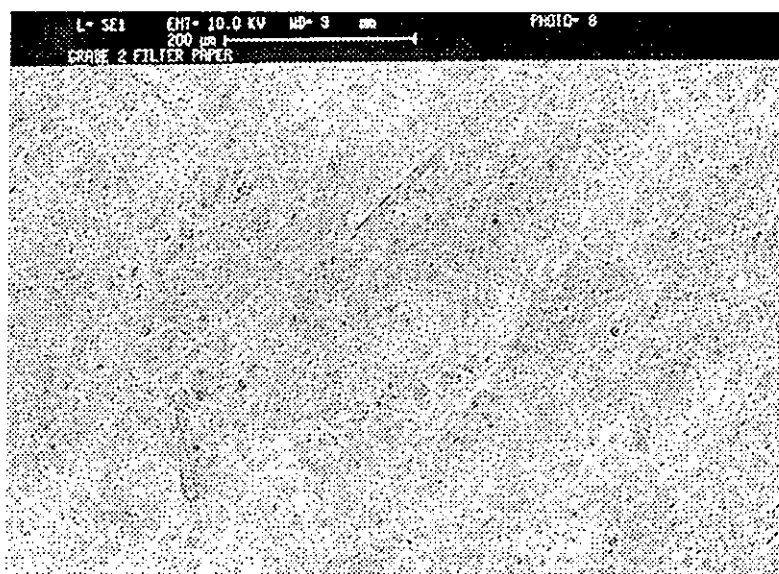
(b) Low magnification

FIGURE 3.7 *B.subtilis* spores on Grade 2 filter paper
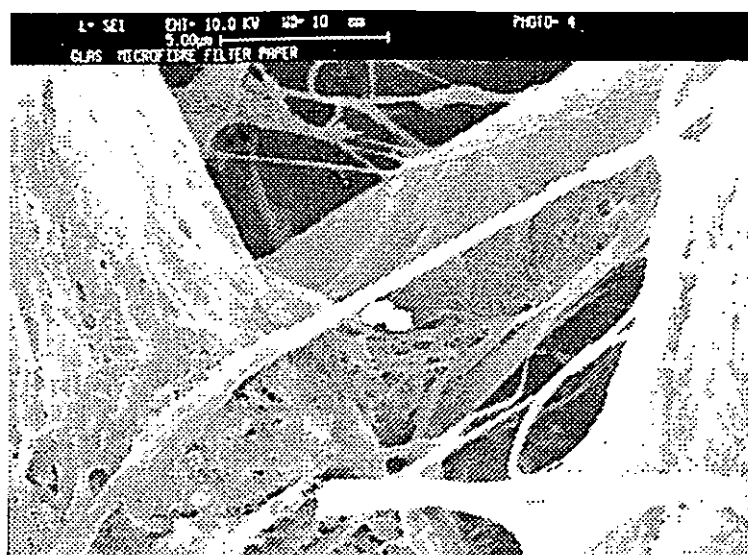
(a) High magnification
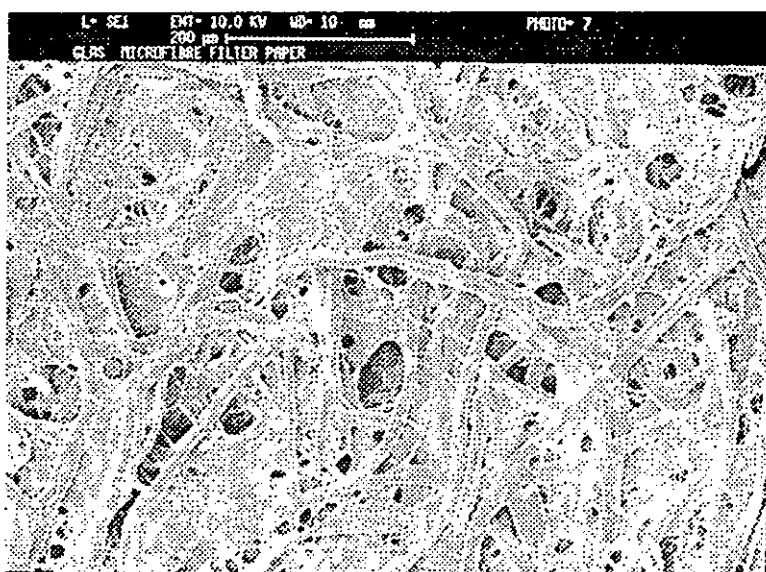
(b) Low magnification

FIGURE 3.8   *B.subtilis* spores on Glass microfibre filter
paper
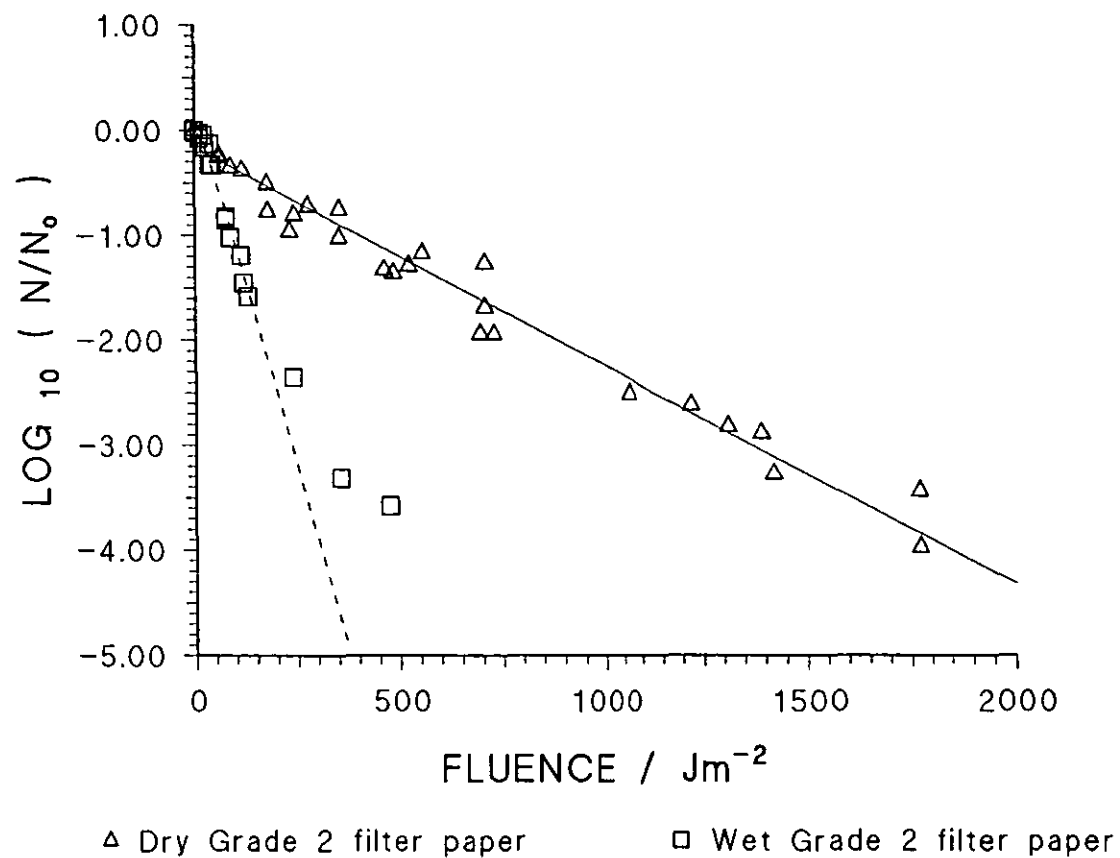
FIGURE 3.9 **Exposure of *B.subtilis* spores to UV on wet and dry Grade 2 filter paper**
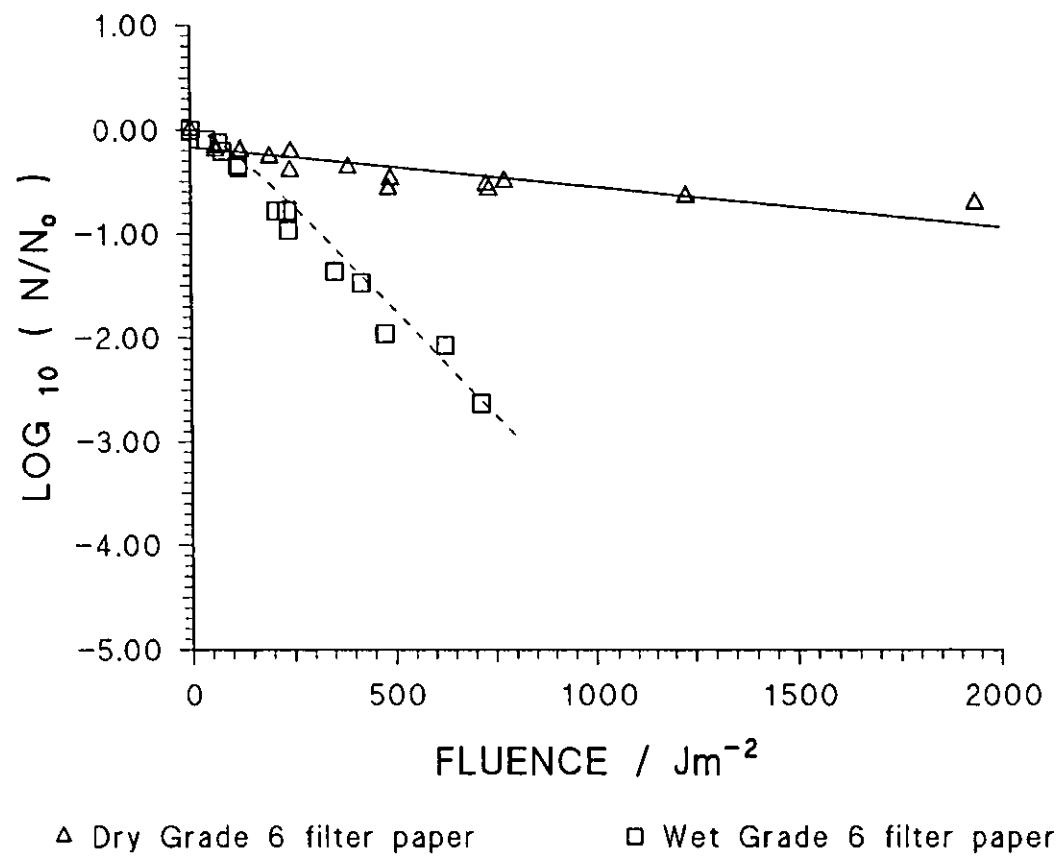
FIGURE 3.10   Exposure of *B.subtilis* spores to UV on wet and dry Grade 6 filter paper

obtained by Qualls and Johnson (1983), Chang *et al.* (1985) and Sommer and Cabaj (1993). Multi-target kinetics were applied to the experimental data from these studies and the kinetic parameters obtained are displayed in Table 3.3 along with the kinetic parameters obtained in this work. The rate constants (k) are comparable in all the studies and vary from 1.15×10^{-2} to 3.85×10^{-2} $(Jm^{-2})^{-1}$. The principal difference was in the value of the exponent (n); the value for the results obtained here being the lowest of all the comparable previous studies. One possible cause might lie in the method of generating the spores; all of the previous workers employed different methods to that employed here and Bayliss *et al.* (1981) have shown that method of cultivation can affect the UV resistance of the spores. Additionally, when comparing n values between disinfection curves, it should be remembered that n is based on a logarithmic scale - i.e. $LOG_{10}n$ is the intercept of the LOG axis of the semi-log disinfection graph so small changes in the intercept can produce large changes in the n value obtained.

Spore inactivation on coupons of aluminium, stainless steel and PTFE (Figure 3.2) seemed not to be affected by the specific nature of the material and it seemed logical to treat the data from all three materials in the same way. They are referred to as 'impervious materials' on subsequent figure legends. Disinfection rates on the Anodisc membranes are comparable to those obtained with spores on the impervious materials. Figure 3.6 reveals the spores to be present singly and in small clusters on the surface of an Anodisc membrane of 2μm pore size. Filtration of the spore suspension through the membrane proved to be an effective way of coating the membrane with spores.

Rate constant $k / (Jm^{-2})^{-1}$	Exponent n	Reference
1.65×10^{-2}	2.65	This work
1.15×10^{-2}	100	Chang *et al.* (1985)
3.85×10^{-2}	10.2	Qualls and Johnson (1983)
2.14×10^{-2}	6.31	Sommer and Cabaj (1993) - Method A
3.50×10^{-2}	6.31	Sommer and Cabaj (1993) - Method B
1.77×10^{-2}	4.68	Sommer and Cabaj (1993) - Method C

Table 3.3   **Comparison of multi-target parameters for *B.subtilis* spores in aqueous suspensions irradiated with UV**

Filter papers proved a useful medium with which to conduct experiments and preliminary experiments (results not shown) revealed spore recoveries approaching 100 %. The inactivation rates for spores deposited on the surface of both grades 2 and 6 filter papers was lower than for the aluminium coupons and the 2μm membrane, as comparison of the parameters in Table 3.2 shows. The rate constant for the Grade 2 and 6 filter papers is 0.22 and 0.041 times less than that for the Anodisc membrane respectively. Figure 3.7 shows spores on the surface of Grade 2 filter papers. The surface topography appears relatively open so that whilst *B.subtilis* spores might lodge beneath the surface, sufficient UV light could still penetrate to those regions and inflict at least some inactivation. The results obtained here showed that inactivation of spores to levels below that detectable was achieved with this grade of filter paper (i.e. no viable spores were recovered).

The inactivation rate constant for spores on glass microfibre paper was comparable (1.25 times greater) to that for Grade 6 filter paper. The results show a considerable amount of scatter (Figure 3.5) and whilst precautions were taken to minimise handling of the glass microfibre pads, they were relatively compressible and it is possible that the routine treatment employed in cutting strips, depositing spores etc. may have resulted in irreproducible alterations to the surface of this material. Figure 3.8 shows the structure of the glass microfibre paper. Highly labryrinthine channels are revealed with some spores visible inside the channels. Spores present at depths below the surface would only receive a fraction of the incident UV light.

The faster disinfection rate on Grade 2 and Grade 6 filter paper strips when wetted was unexpected and has not previously been reported. This phenomenon was first discovered when conducting preliminary experiments into the effects of combined UV irradiation and peroxidation (See Section 3.4). The reasons advanced for this phenomenon can only be speculative. Filter paper fibres expand when wet and it is possible that this expansion might result in spores being moved towards the surface, alternatively the presence of water might have led to UV light being reflected further down into the sub-surface layers.

In order to facilitate further comparison of the results obtained here with spores in a variety of media, all the data were combined and are shown in Figures 3.11a and 3.11b. In order to aid clarity, the individual data points are not shown and polynomial curves have been fitted to the data. One striking feature of presenting the data in this way is that differences in the shapes of the disinfection curves are highlighted and suggests that the surface itself can influence the disinfection performance obtained.

The extent of spore survival obtained is comparable for Anodisc membranes, distilled water and impervious surfaces at disinfection levels less than 3 orders. At higher fluences, *B.subtilis* spores appear to have a lower resistance to UV on Anodisc membranes and on impervious surfaces at low fluences (less than 400 Jm^{-2}) compared to *B.subtilis* spores in distilled water. On the remaining surfaces the disinfection levels were lower than in distilled water. However at higher fluences, greater disinfection of the *B.subtilis* spores was achieved in distilled water than on any of the other surfaces (as seen in Figures 3.11a and 3.11b).

The SEM photographs (Figures 3.6 - 3.8) revealed spores in association with a variety of surfaces, and it is possible to visualise each of the surfaces as offering different degrees of protection, or shielding, to the spores associated with any particular surface. Shielding effects due to surface irregularities have previously been reported. For example, in the use of UV to reduce the surface microbial count on beef steaks, Stermer *et al.* (1987) noted that substantial protection of the natural flora to incident UV occurred. Huang and Toledo (1982) investigated the inactivation of natural flora on the skin of whole fish by UV. They showed that UV was more effective in inactivating micro-organisms on the skin of smooth-surfaced fish, such as mackerel, than on rough-surfaced fish, such as mullet. If the degree of protection that a surface offers is not uniform over the whole surface then spores on the surface will receive different UV intensities at the same incident UV intensity. In such cases, changes to the shape of the disinfection curve are observed, and appear as disinfection curves for mixed populations (Harm, 1980i). This explains the range of shapes of disinfection curves observed for the same micro-organism, *B.subtilis* spores, when present on different surfaces but exposed to the same UV doses. The results obtained by Stermer

81
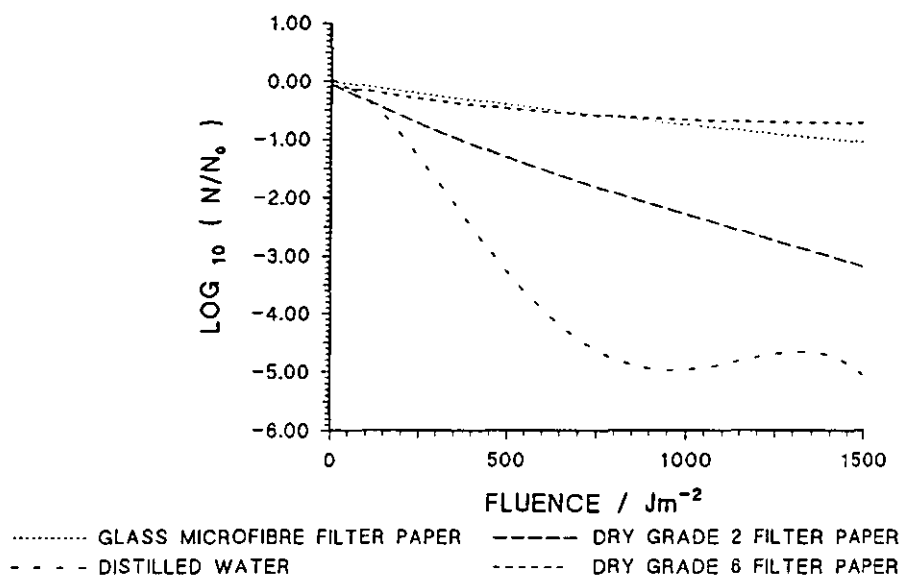
(a)
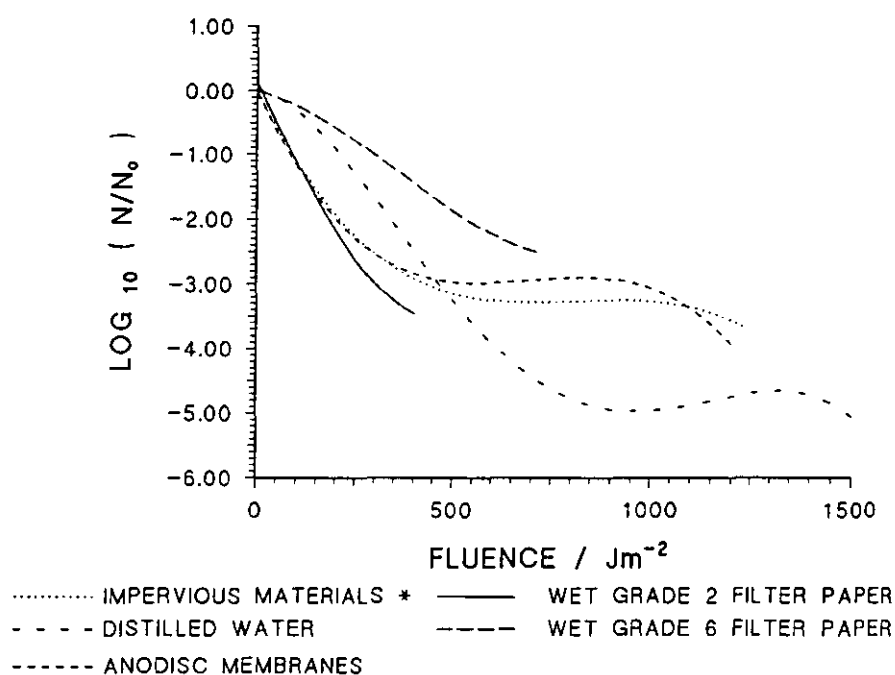
(b)

FIGURE 3.11 Summary of disinfection curves of *B.subtilis* spores exposed to UV

* PTFE, aluminium and stainless steel

82

et al. (1987) also showed a change in shape of the disinfection curve from agar plates to when the flora was present on beef steaks.

3.3 Disinfection using hydrogen peroxide

3.3.1 Introduction

The experiments described below were conducted with a variety of materials in the form of coupons which bore *B.subtilis* spores on their surfaces. Application of H_2O_2 was either by pipette, for laboratory-based studies or by atomisation nozzle in the spray disinfection chamber. All experiments were performed in triplicate.

3.3.2 Results

Disinfection experiments were performed in the spray chamber using 29 w/v% H_2O_2. PTFE coupons, onto which *B.subtilis* spores had been coated, were attached to the disc test object as shown in Figure 3.13 and subjected to a pulse of an atomised spray of H_2O_2 of between 10 and 30 seconds duration. The coupons were then left in the chamber for exposure times between 1 and 10 minutes before removal; Figure 3.12 shows this inactivation data. Identical experiments were conducted using *B.subtilis* spores on stainless steel coupons and the results obtained are shown in Figure 3.14. After 10 minutes of exposure to the H_2O_2, the viable *B.subtilis* spore count on these surfaces had been reduced to below the detectable limit (4.5 orders of disinfection).

Although multi-target kinetics were originally developed to describe the disinfection rate of micro-organisms exposed to UV, they were applied to the data shown in Figure 3.12 to provide a direct comparison of parameters between the disinfection data obtained for UV disinfection and that obtained for disinfection using H_2O_2. The parameters obtained are shown in Table 3.4.
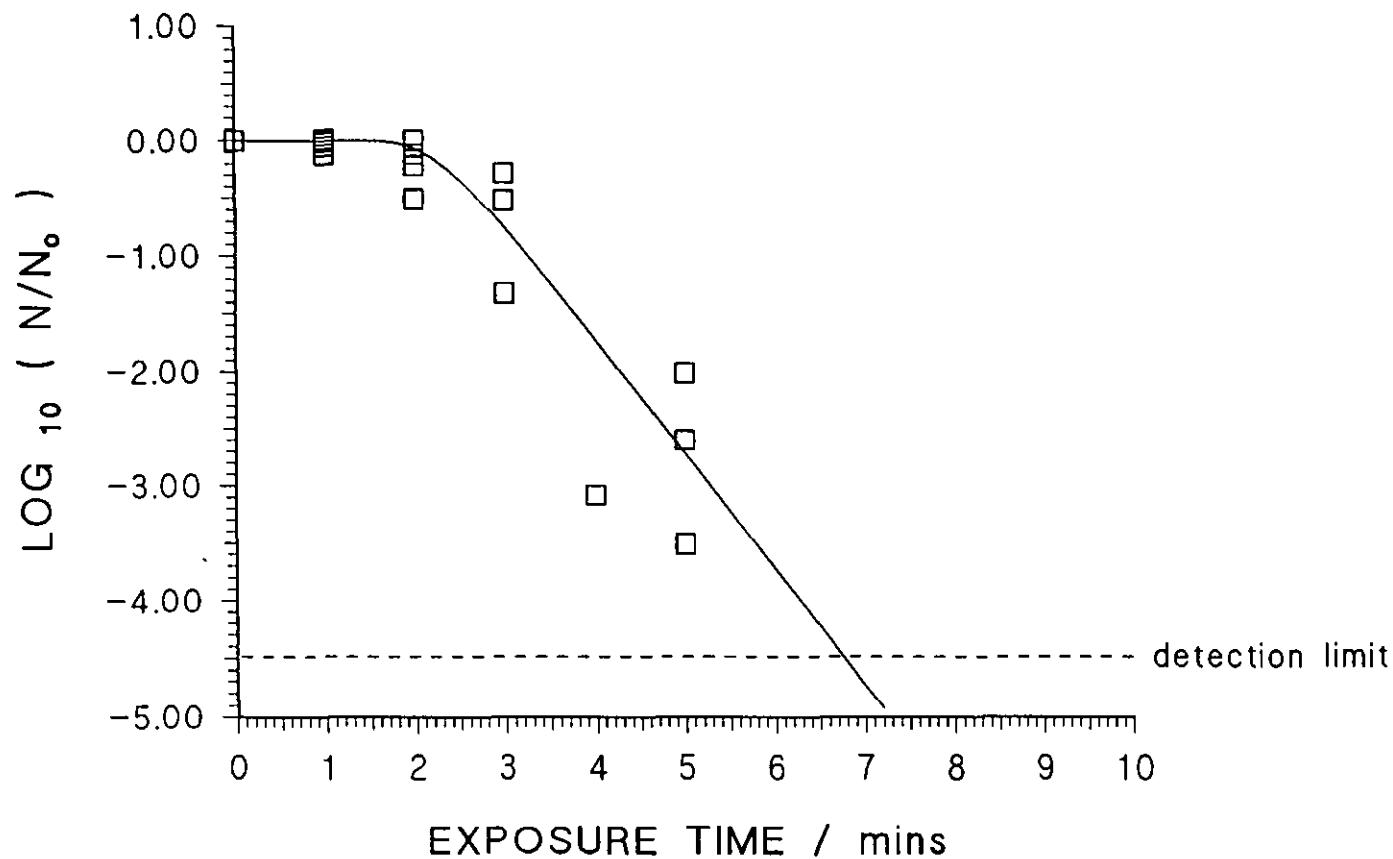
FIGURE 3.12   Exposure of *B.subtilis* spores on PTFE coupons to 29 w/v% H_2O_2
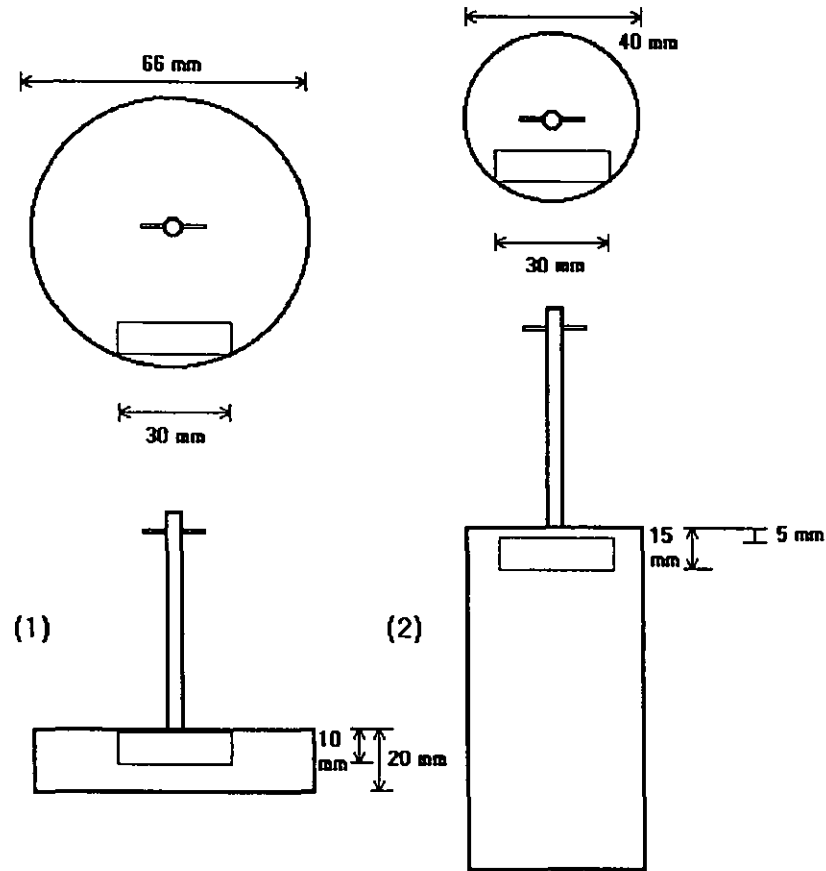
FIGURE 3.13 Arrangement of *B.subtilis* spore impregnated Grade 2 filter paper strips on the disc and cylindrical objects for confirming experimentally-determined kinetics
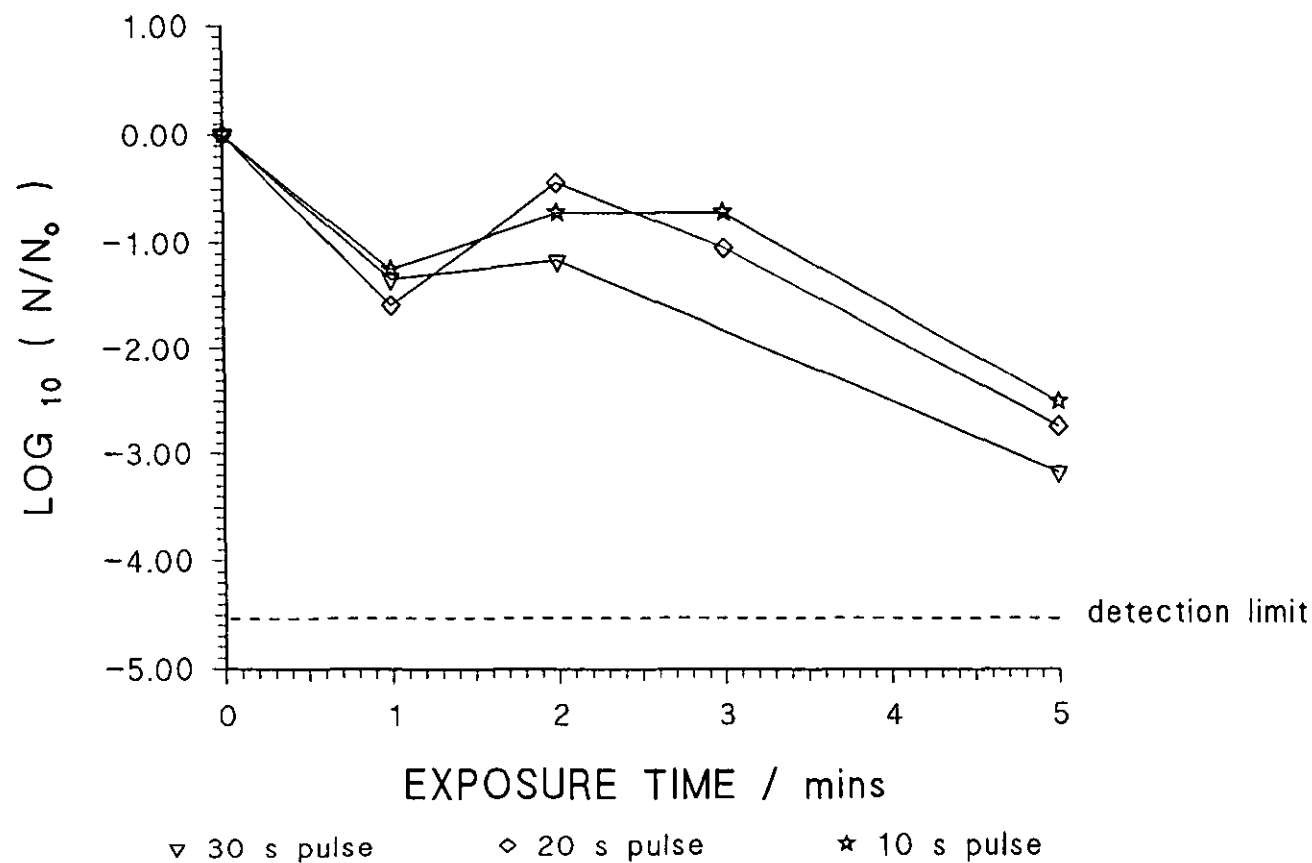
FIGURE 3.14 *B.subtilis* spores on stainless steel coupons exposed to sprays of 29w/v% H_2O_2

Species	Inactivation rate constant / s^{-1}	Target number	Reference
B.subtilis (ATCC 6633)	3.81×10^{-2}	172	This work
B.subtilis (ATCC SA22)	5.32×10^{-2}	1.78	Toledo (1973)
B.subtilis var. globigii	1.94×10^{-2}	39.8	Toledo (1973)
B.subtilis var. globigii (heat shocked)	3.56×10^{-2}	1000	Toledo (1973)
B.coagulens	2.31×10^{-2}	8.91	Toledo (1973)
B.stearothermophilus	2.55×10^{-2}	5.01	Toledo (1973)

Table 3.4   Summary of multi-target parameters for *Bacillus* spores exposed to 25.8% or 29% H_2O_2

3.3.3 Discussion

The data obtained here shows that 29 w/v% H_2O_2 was an effective sporicide at room temperature and was capable of reducing surface counts rapidly after the notable initial shoulder. The results also demonstrate the suitability of the methods developed to the investigation of spray disinfection.

The disinfection data obtained with 29 w/v% H_2O_2, shown in Figures 3.12 and 3.14, was prone to a greater degree of scatter than that for UV disinfection. This was most likely attributable to the variation in area which the dried *B.subtilis* spore film occupied on the coupon surface. Despite attempts at standardising spore deposition and rates of drying, as fully described in section 2.2.4, visual inspection revealed significant differences. Whilst the coupons used in the experiments shown in Figures 3.12 and 3.14 were subjected to a quantity of spray sufficient to wet the entire area of the spore film, variations in spore film depth would have offered varying degrees of protection to sub-surface layer spores and caused the observed disinfection rate to vary.

Figure 3.12 shows that consistent disinfection data was obtained using PTFE coupons, whilst Figure 3.14 shows that the disinfection curve obtained on stainless steel coupons was variable. Iron is known to catalyse the generation of free radicals from H_2O_2 and the combination of Fe^{2+} ions and H_2O_2 is known as 'Fenton's reagent' (Lunak and Sedlak, 1992). Disinfection rates in the presence of Fe^{2+} ions are considerably enhanced and it is possible that Fenton's Reagent was formed, though not consistently, during the spray experiments reported here. Visible spots of rust were observed to have formed on the stainless steel coupons some hours following treatment with H_2O_2 sprays.

Table 3.4 presents results obtained in this study together with the parameters for multi-target kinetics which were fitted to the results obtained by Toledo et al. (1973). Although these workers did not obtain any disinfection data for spores of B.subtilis (ATCC 6633), they did obtain results using spores from other species of Bacillus, including a different strain of B.subtilis. Toledo et al. used 25.8% H_2O_2 at 24°C and their data were thus obtained at slightly different operating conditions to those employed here (29% H_2O_2 at 23°C). However these conditions were relatively close to each other to permit useful comparisons to be made.

The table shows that the first-order disinfection rates (k values) obtained are all within the same order of magnitude. However, large discrepancies are revealed in the values of the exponent n which relates directly to the size of the initial shoulder. The results that provided the closest agreement with those obtained in the course of this work are those for heat shocked B.subtilis var. globigii spores. Toledo et al. (1973) showed that length and severity of the heat shocking process affected the resistance of B.subtilis spores to H_2O_2. Toledo et al. employed a heat shock of 80°C for 20 minutes compared to the 70°C for 30 minutes used in this work. The n value shows that a much larger initial shoulder was found for disinfection with 29 w/v% H_2O_2 compared to disinfection with UV.

3.4 Combined UV and H_2O_2 disinfection

3.4.1 Introduction

Combined treatment with UV and H_2O_2 has been widely reported to bring about a synergistic disinfection effect (Bayliss and Waites, 1979, 1980, 1982). The objective of the experiments reported here was to establish whether these synergistic effects could be demonstrated to occur at the surfaces of materials. In addition to these studies, work is also presented on the related issue of the influence of UV intensity on disinfection rate/efficiency in combined treatment.

Confirmation was sought that the kinetic equations developed from laboratory-generated data could predict the disinfection performance in the spray chamber. Two sets of experiments were conducted in the spray chamber to assess the disinfection rates for the combined UV + 1.0 w/v% H_2O_2 disinfection process at spatial locations of known UV intensity. The concentration of H_2O_2 used was that claimed by Bayliss and Waites (1979a) to result in maximal synergistic inactivation. More concentrated aqueous solutions of H_2O_2 absorbed UV at 254 nm and resulted in a diminution of UV intensity and a comcomitant decrease in lethality. The first experiment involved placing strips of Grade 2 filter paper coated with *B.subtilis* spores onto two objects of different geometries. The locations of the filter paper strips on the objects were as shown in Figure 3.13. Forty microlitres of 1.0 w/v% H_2O_2 was pipetted onto the filter paper strips, the object suspended in the spray chamber and the object exposed to 10 seconds of UV irradiation from 2 of the 4 UV lamps. The filter paper strips were sampled to determine the reduction in spore viability for each filter paper strip location. The experiment was repeated a further two times. The UV intensities at the filter paper strip locations had been previously determined by using the bioassay method employing Grade 2 filter paper strips (see section 2.6.3). Equation (3.2a) was then used to predict the disinfection performance obtained with UV + 1.0 w/v H_2O_2 in the spray chamber at the determined UV intensities.

An additional test of whether the laboratory-determined disinfection kinetics were valid under the conditions that existed in the larger-scale spray chamber was to compare the disinfection rates obtained for spray disinfection within the spray chamber for the UV + 1.0 w/v% H_2O_2 process with those obtained on the laboratory-scale. Aluminium coupons were attached to the disc object as shown in Figure 3.13. The surviving fraction was determined 3 times for each exposure time in each experiment.

3.4.2 Results

Experiments were conducted with strips of spore-laden Grade 2 filter paper impregnated with H_2O_2, as described in section 2.3.3. The H_2O_2 solutions employed ranged in concentration from 0.1 to 5.0 w/v% at a UV intensity of 4.7 Wm^{-2}. The results are presented in Figure 3.15 and show that the highest levels of disinfection were achieved at concentrations of H_2O_2 in the range of 0.5 to 1.0 w/v%.

Figure 3.16 shows inactivation data for *B.subtilis* spores on Grade 2 filter paper strips exposed to UV light of different intensities (I), either alone (using wet filter paper) or in combination with 1.0 w/v% H_2O_2. The disinfection rate with UV and H_2O_2 combined was faster than for UV alone. There is some tailing of the disinfection curve for the combined sterilants at fluences over 100 Jm^{-2}. The results of Figure 3.16 also show that the disinfection level achieved depended on the fluence received and was independent of the UV intensity.

The kinetics of disinfection of *B.subtilis* spores by the combination of UV and H_2O_2 are adequately described by first order kinetics as Figure 3.16 shows; the rate constant (k) being 0.102 $(Jm^{-2})^{-1}$.

The graph plots LOG$_{10}$ (N/N$_o$) on the y-axis (ranging from 0.00 to -3.00) against H$_2$O$_2$ CONCENTRATION / w/v% on the x-axis (0.1, 0.5, 1.0, 2.0, 5.0). A dashed line near the top indicates the disinfection performance of 47 Jm^{-2} of UV. UV intensity = 4.7 Wm^{-2}.
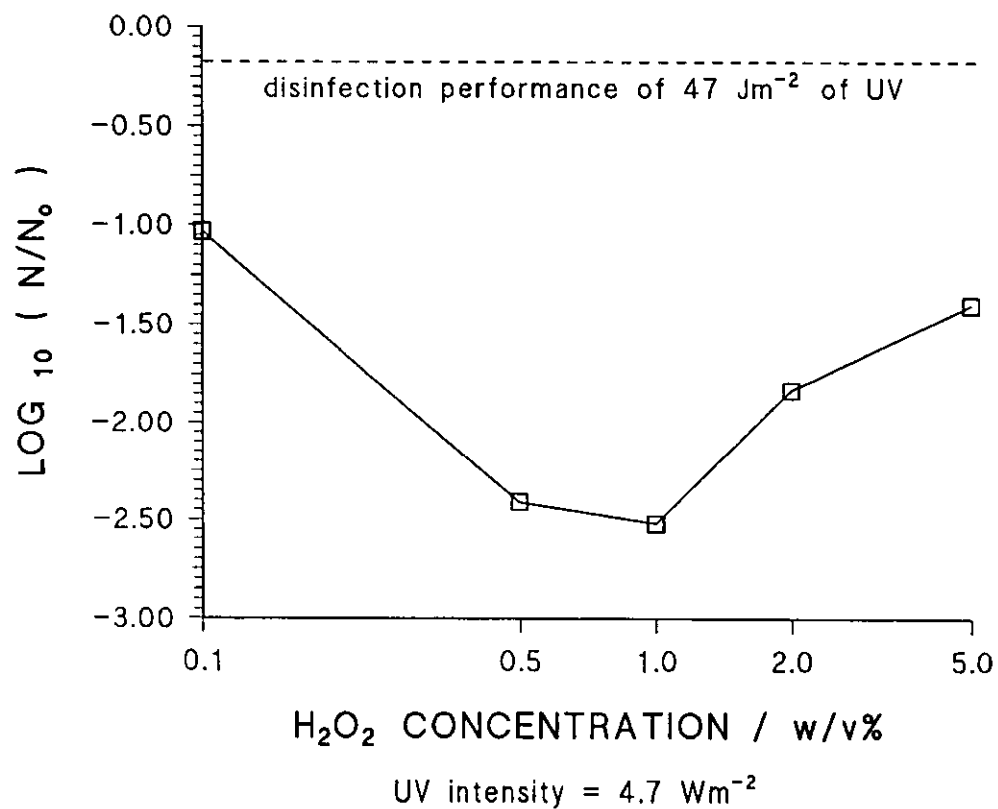
FIGURE 3.15 Disinfection performance for *B.subtilis* spores on Grade 2 filter paper exposed to UV and a range of concentrations of H$_2$O$_2$
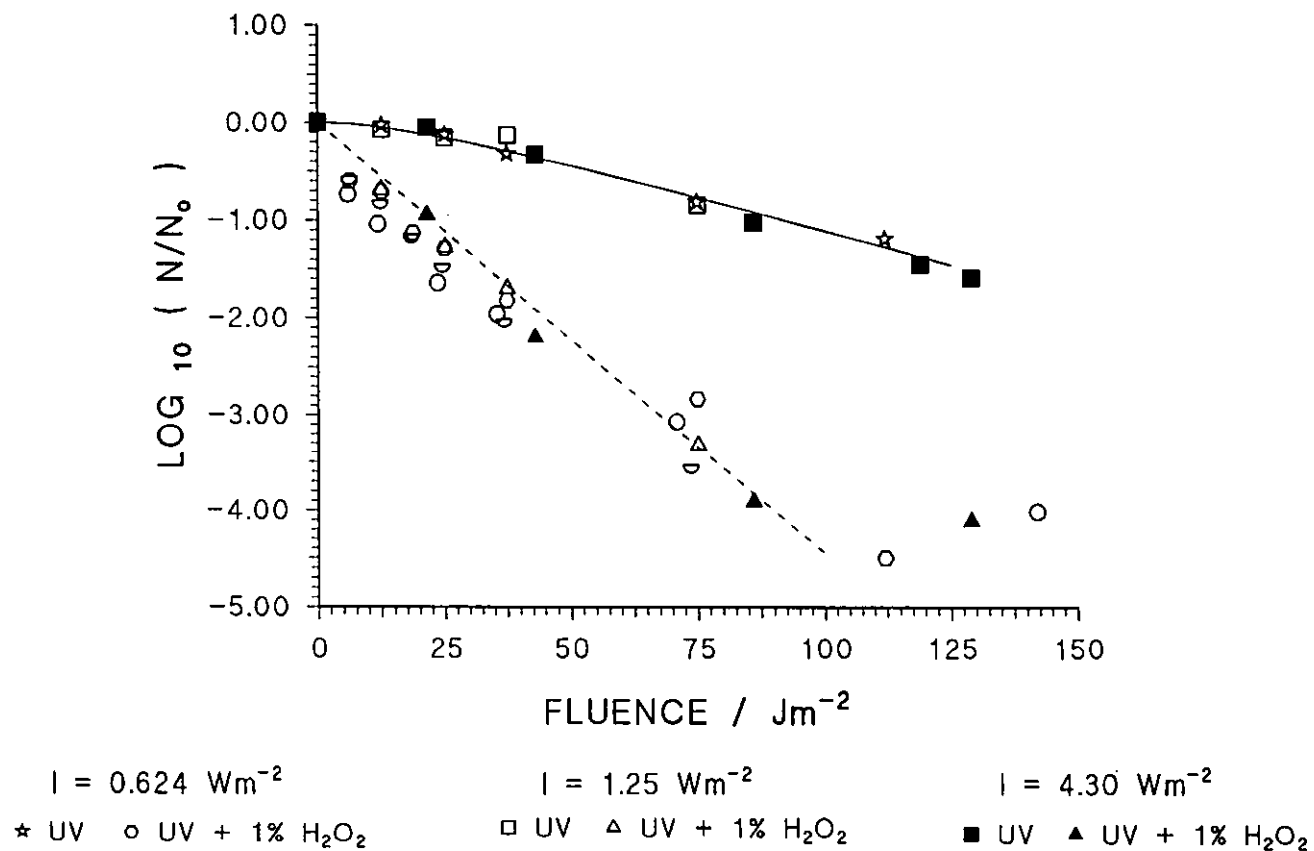
FIGURE 3.16   Exposure of *B.subtilis* spores on Grade 2 filter paper to UV + 1.0 w/v% H_2O_2
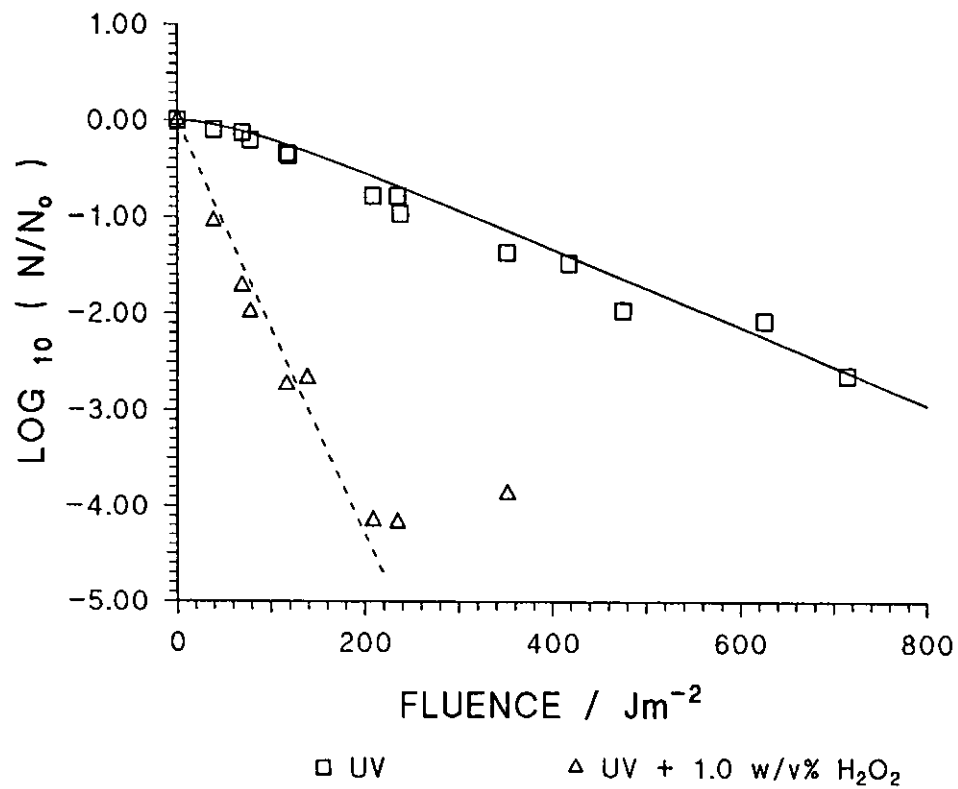
FIGURE 3.17 Exposure of *B.subtilis* spores on Grade 6 filter paper to UV and UV + 1.0w/v% H_2O_2

Figure 3.17 shows inactivation data for *B.subtilis* spores in Grade 6 filter paper exposed to UV light and also to combined UV and 1.0 w/v% H_2O_2. Again, an increased disinfection rate is observed for the combined process. First order kinetics were fitted to the inactivation data for the combined process, where k = 4.95 x 10^{-2} $(Jm^{-2})^{-1}$.

Figure 3.18 shows inactivation data of *B.subtilis* spores deposited on aluminium coupons exposed to UV solely and UV combined with H_2O_2 in the spray sterilisation chamber. This data confirms that synergism was achieved with 1.0 w/v% H_2O_2 sprays when combined with UV in the spray chamber.

Different spray pulse durations were investigated to establish whether reducing the mass of H_2O_2 on the surface altered the disinfection rate. Figure 3.19 shows the results for 3 separate experiments using different spray pulse durations. It is seen that the disinfection level obtained was independent of the duration that the spray was applied to the coupons. Therefore the impact from a spray application of 10 seconds was sufficient to coat the coupons so that the maximum UV + 1.0 w/v% H_2O_2 disinfection rate was obtained.

Table 3.5 shows data for combined UV + 1% H_2O_2 treatment of filter paper strips in the UV chamber. Column 3 of the table represents estimates of UV intensities obtained by bioassay. The values of UV intensities thus obtained were used in equation (3.1) to enable estimates of log reductions to be made (presented in column 5). The experimentally determined disinfection levels were slightly higher than the predicted levels. However errors in the exposure time (due to the finite time taken to rotate the brass tubes covering the UV lamps) might easily have accounted for this discrepancy.
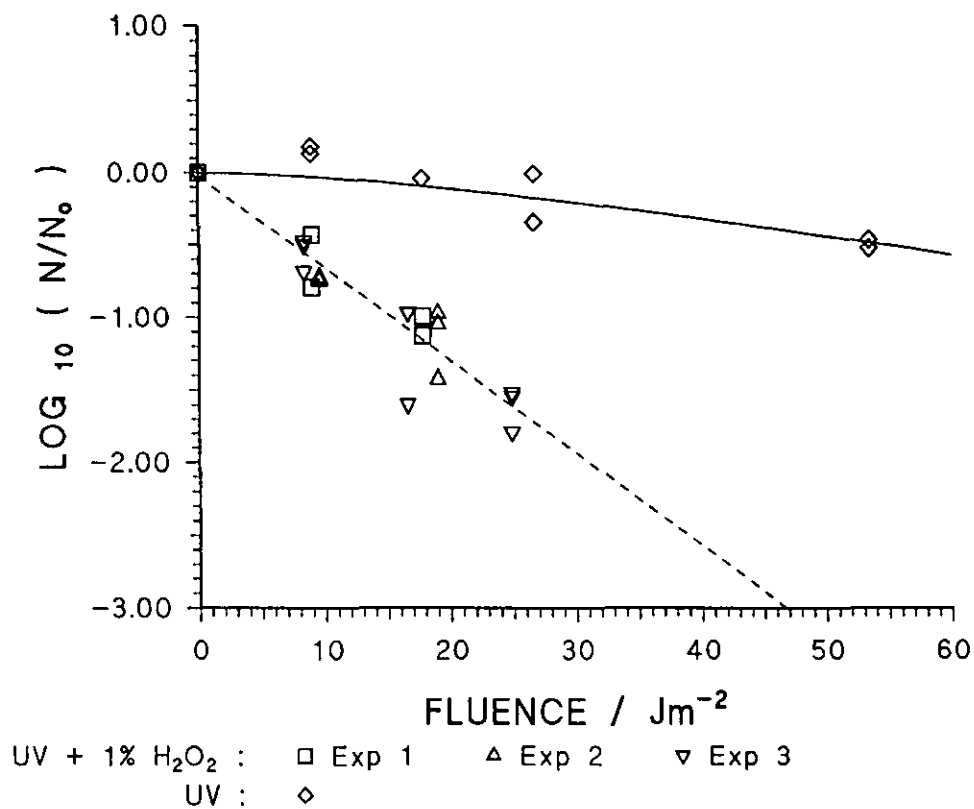
FIGURE 3.18 Exposure of *B.subtilis* spores on aluminium coupons to UV + 1.0 w/v% H_2O_2 in the spray chamber
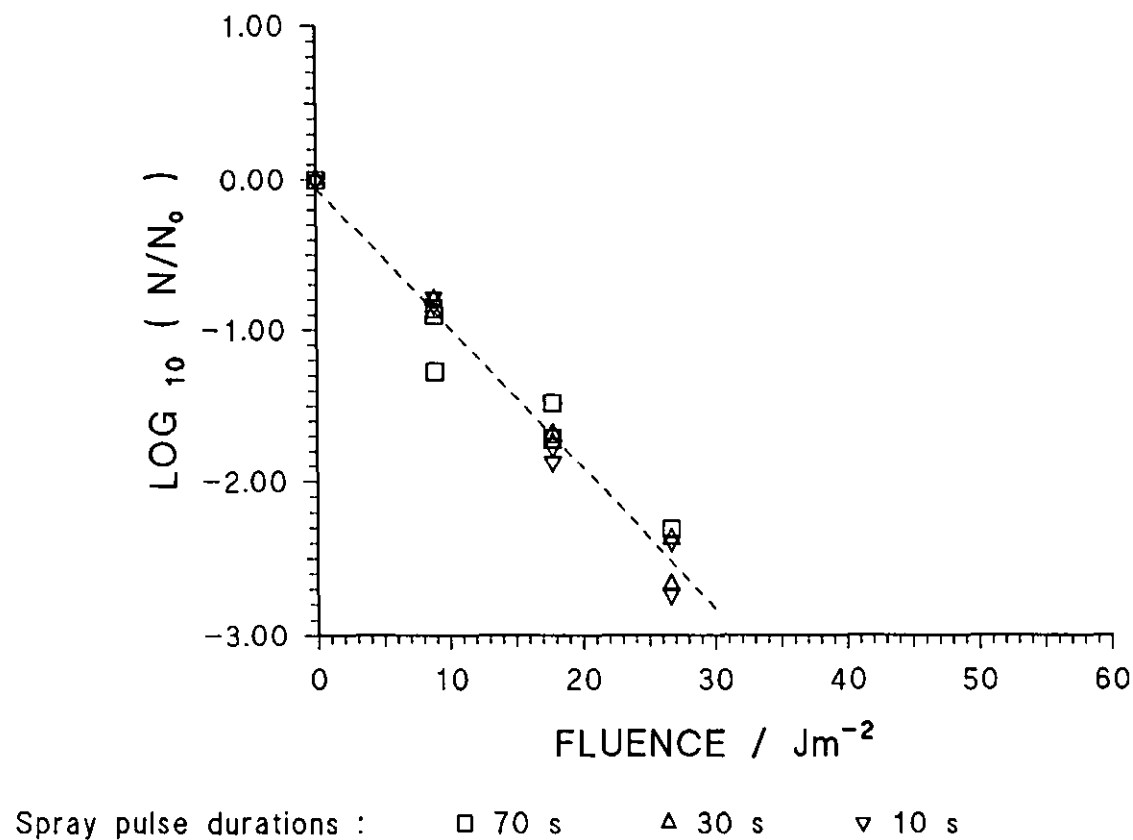
FIGURE 3.19 **Effect of spray pulse duration on disinfection performance for *B.subtilis* spores on aluminium coupons exposed to UV + 1.0 w/v% H$_2$O$_2$ in the spray chamber**

OBJECT	LOCATION	UV INTENSITY / Wm⁻² (*1)	EXPERIMENTALLY OBTAINED LOG REDUCTION ($LOG_{10}\{N/N_0\}$) A	PREDICTED LOG REDUCTION (*2) B	A/B
DISC	SIDE	2.71	-1.36	-1.21	1.12
DISC	TOP	4.97	-2.50	-2.21	1.13
CYLINDER	SIDE	3.44	-1.87	-1.53	1.22
CYLINDER	TOP	4.30	-2.12	-1.91	1.11

Table 3.5   Comparison of experimentally-determined disinfection levels to predicted disinfection levels from laboratory-based kinetics

*1   Determined by bioassay (method described in section 2.6.3)

*2   for 10 seconds exposure from equation (3.2a)

3.4.3 Discussion

Figure 3.15 shows that the most effective combined disinfection performance was achieved with H_2O_2 solutions of concentrations in the range 0.5 to 1.0 w/v%. This agrees with the results of Bayliss and Waites (1979). The criterion for synergism is satisfied as the disinfection level obtained with the combined treatment is greater than the sum of the individual effects of UV (shown in Figure 3.15) and 1.0 w/v% H_2O_2 (no effect).This latter result confirms the findings of Stevenson and Shafer (1983) that 1% H_2O_2 is not sporicidal.

None of the data obtained for combined UV + 1.0 w/v% H_2O_2 treatment revealed the presence of an initial shoulder (see Figures 3.16 - 3.19) and therefore first-order disinfection kinetics could justifiably be applied. Bayliss and Waites (1979) also found first-order disinfection kinetics to be appropriate for combined UV + 1.0 w/v% H_2O_2 treatment for *B.subtilis* (NCDO 2129) spores. These workers also reported 'tailing' of

the curves at between 4 and 5 orders of reduction in spore viability, as was also displayed in the results obtained here. This phenomenon is possibly attributable to the existence of clumps of spores which would result in the spores near the centres of the these clumps receiving a lower UV intensity than spores near the outer periphery of such clumps.

Comparison of the rate constants obtained for Grade 2 and Grade 6 filter paper strips revealed disinfection rates to be higher in the former case both for UV alone and also for UV in combination with H_2O_2 (Table 3.6) and this finding suggests that surface shielding effects are significant in both cases.

First order kinetics were seen to be applicable to spore-coated aluminium coupons when exposed to a combination of UV and 1.0 w/v% H_2O_2 in the spray chamber (Figure 3.18) where $k = 0.129$ $(Jm^{-2})^{-1}$. Bayliss and Waites (1979) investigated the use of the identical combination of treatments against spores of a number of *Bacillus* species including *B.subtilis* (NCDO 2129) and presented their disinfection data plotted against the exposure time. By using the stated UV intensity from later studies of theirs which employed an identical experimental arrangement (Bayliss and Waites, 1981), it was possible to determine the fluence at which the disinfection data had been obtained. Fitting first-order kinetics to their data for the combined process and multi-target kinetics to their data for UV disinfection, kinetic parameters were obtained for their results and are shown in Table 3.6 together with results obtained in this study. A comparison of the data obtained here with that of Bayliss and Waites (1981) was made by taking the ratio of rate constants for UV irradiation alone and for UV treatment in combination with H_2O_2. This procedure allows differences in kinetic responses of the spores in the two studies to be ignored whilst at the same time allowing some useful comparisons to be made. The ratios obtained are shown in Table 3.6, with values ranging from 3.17 to 5.66.

	UV multi-target kinetics		UV + 1.0 W/V% H_2O_2 first-order kinetics	
Medium	Inactivation rate coefficient / $(Jm^{-2})^{-1}$	Target number	Inactivation rate coefficient / $(Jm^{-2})^{-1}$	Ratio of inactivation rate coefficients
Wet Grade 2 filter paper	3.22×10^{-2}	2.00	1.02×10^{-1}	3.17
Wet Grade 6 filter paper	9.34×10^{-3}	2.00	4.95×10^{-2}	5.30
Aluminium coupons	2.28×10^{-2}	1.00	1.29×10^{-1}	5.66
Distilled water (Bayliss and Waites, 1979)	2.74×10^{-2}	2.03	1.31×10^{-1}	4.78

Table 3.6   Comparison of kinetic parameters for the UV and UV + 1.0 %
H_2O_2 process on different surfaces and in distilled water
(see Appendix 3 for standard deviations)

Figure 3.19 also reveals that changing the duration of the initial spray pulse (and hence the mass of spray deposited on the coupons) had no effect on disinfection performance over the range investigated. The coupons were observed to be saturated with spray droplets in each case, thus giving the same disinfection results. Therefore the spray regimes employed in this work were suitable for effective surface disinfection. (The mass of spray deposited in these experiments is estimated in Appendix 2).

3.5 Disinfection using ozone and ozone combined with UV

3.5.1 Introduction

Ozone is a powerful oxidant and has been widely used in water treatment, both alone and in combination with UV, to remove organic pollutants (Legrini *et al.*, 1993). In contrast, relatively little work has been done on the use of aqueous ozone as a disinfectant. In this section the disinfection performance of aqueous ozone both alone and in combination with ultraviolet light on *B.subtilis* spores on filter paper strips is described. In these experiments, aqueous ozone (40 µL) was pipetted directly onto each strip and these were then immediately irradiated using the high intensity UV source. In addition, results from experiments in which the sporicidal activity of gaseous ozone was investigated using an enclosed 1 litre vessel in which spore-coated aluminium coupons were exposed are reported.

3.5.2 Results

Disinfection studies were initially undertaken with aqueous ozone concentrations of between 0.23 to 0.55 mg/L, these concentrations had previously been claimed to be sporicidal (Meltzer, 1993). No sporicidal effect was detected for exposure times of up to 10 minutes (results not shown). Consequently it was decided to use a significantly higher concentation of ozone. Figure 3.20 shows the results of treatment of Grade 2 filter paper strips coated with *B.subtilis* spores with a saturated ozone solution maintained at 2 °C. The concentration of ozone in this solution was 43.8 mg/L, as determined by the iodometric techniques described in Section 2.8. The aqueous ozone produced only minimal inactivation of *B.subtilis* spores within the exposure time investigated. Further, Figure 3.20 shows that no synergism was obtained between ozone and UV.
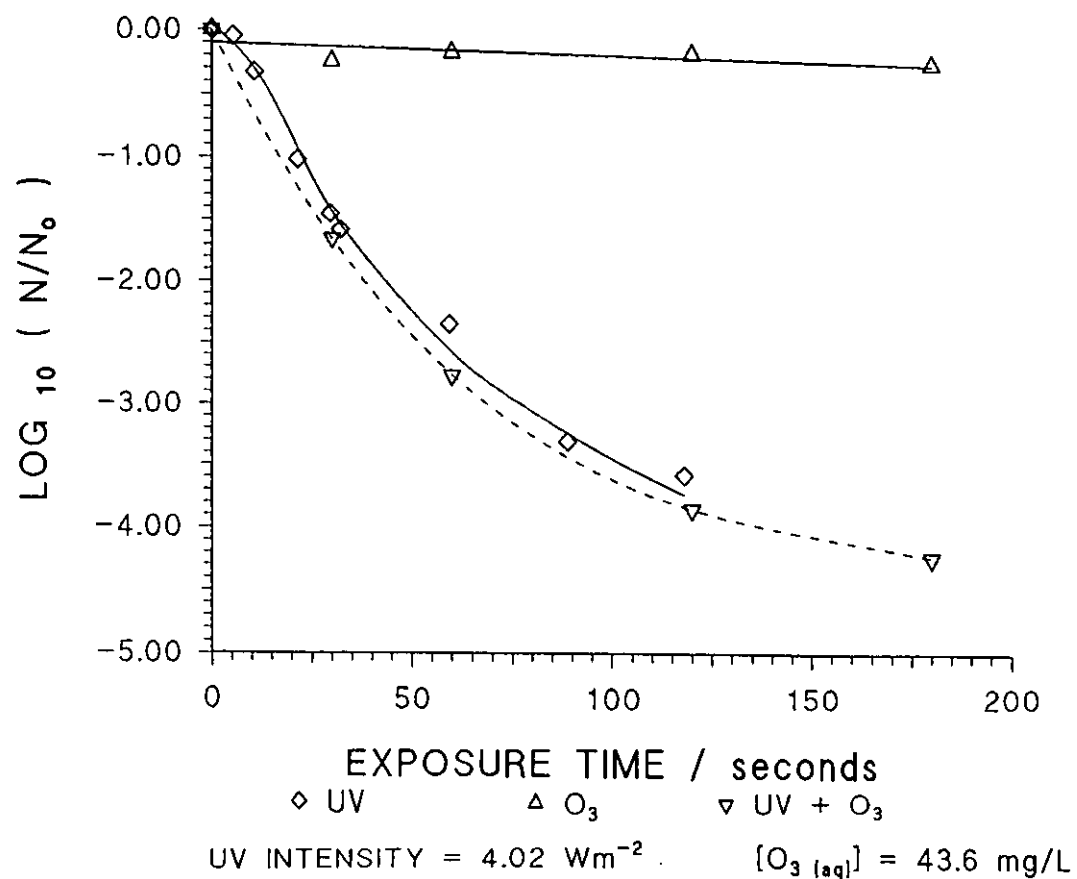
FIGURE 3.20 *B.subtilis* spores on Grade 2 filter paper exposed to UV and aqueous O₃

In order to compare the disinfection performance of aqueous and gaseous ozone, spores were deposited onto aluminium coupons and exposed to the output from an air-fed ozoniser as described in section 2.3.4 for exposure times of up to 30 minutes. The results are shown in Figure 3.21; only a modest amount of inactivation was achieved over the 30 minute exposure period.

3.5.3 Discussion

Ozone solutions did not exert any significant lethal effects against spores of *B.subtilis* on filter paper. Rickloff (1987) showed 10 mg/L aqueous ozone at 20°C to be sporicidal against *B.subtilis* spores dried onto porcelain cylinders when immersed in aqueous ozone. The absence of lethal effects might have been due to the thermal decomposition of the ozone immediately following application to the filter strips. It is known that aqueous ozone is unstable and decomposes to water, H_2O_2 and dissolved oxygen (Staehelln and Hoigne, 1985). The saturated aqueous ozone that was produced did not decompose when kept in the glass Dreschel bottle in an ice bucket (see section 2.9) for up to 20 minutes after the supply of gaseous ozone had been turned off but some decomposition was evident by 50 minutes. However, smaller volumes of aqueous ozone proved to be much less stable: for example, transferring 4 ml of 7 mg/l aqueous ozone from the Dreschel bottle to a silica cuvette and observing its absorbance at 258 nm (using a UV spectrophotometer) showed the aqueous ozone concentration to be falling rapidly. Within 2 minutes the aqueous ozone concentration had fallen to below 0.05 mg/l. This was attributed to a combination of thermal decomposition and ozone mass transfer to the air. The average temperature of the filter paper strips was approximately 23°C. The decomposition of aqueous ozone in filter paper could therefore be expected to be even faster than in the silica cuvettes because of the greater surface area to volume ratio.

It is also possible that ozone was being decomposed by a non-thermal mechanism: in a protocol for the detection of aqueous ozone, Anon. (1977), cautioned against the use of sintered glass spargers, remarking that when these were used the final concentration
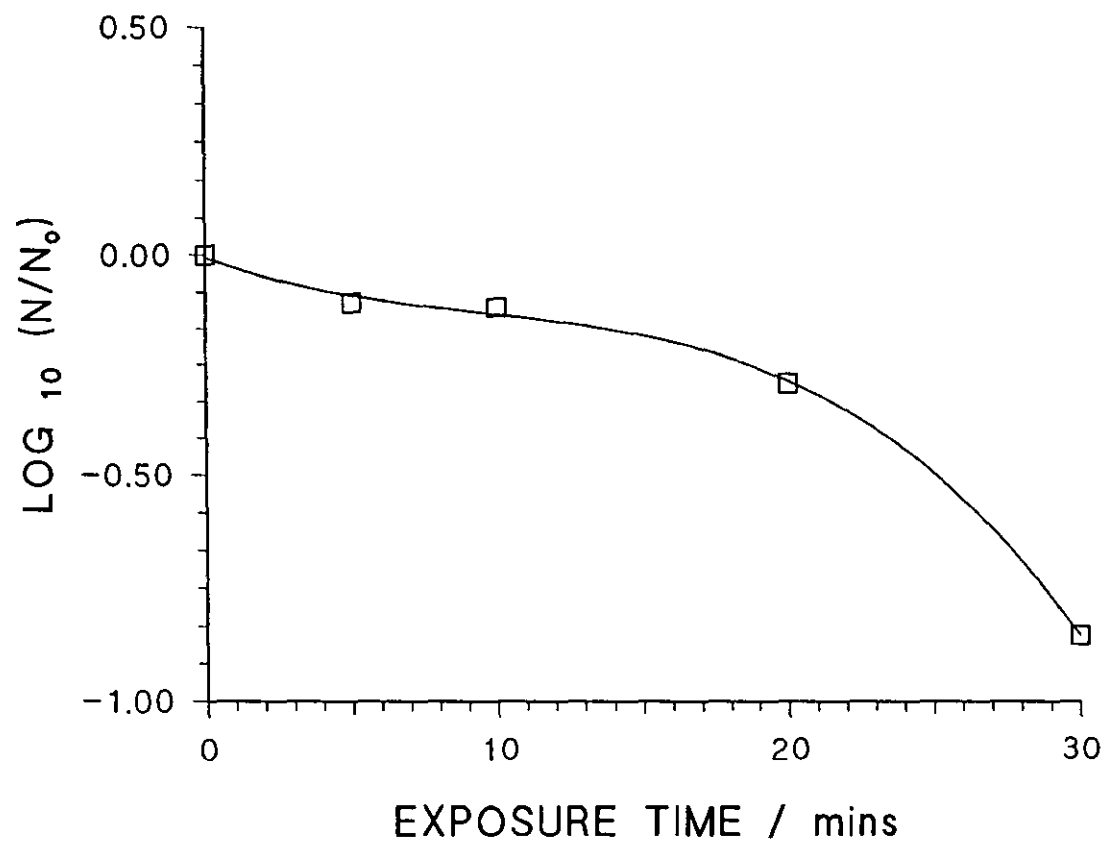
FIGURE 3.21 *B.subtilis* spores on aluminium coupons exposed to gaseous O_3 (1.2%v/v)

of aqueous ozone obtained was always less than in their absence. Moreover, the reason put forward for this phenomenon was attributed to unspecified "surface-catalysed decomposition".

In contrast to the results for aqueous ozone, the results for gaseous ozone proved more encouraging (Figure 3.21). Aluminium coupons were employed in this work because the surface needed to be resistant to the highly oxidising nature of ozone. The thin aluminium oxide layer that coated the aluminium coupons rendered them inert to ozone gas. Also, aluminium has not been previously reported to have catalysing properties when used in conjunction with oxidising compounds such as H_2O_2, unlike copper or iron. Ishizaki *et al.* (1986) also demonstrated that gaseous ozone was sporicidal to *B.subtilis* spores, with disinfection levels of up to 5 orders of magnitude obtained within 1.5 hours at 95% relative humidity using a gaseous ozone concentration of 3.0 mg/L. Direct comparison with the results of Ishizaki are not possible as relative humidity was not determined in the experiments conducted here.

In practical terms the use of aqueous ozone possesses obvious advantages over the use of gaseous ozone. However the results reported here, though of limited scope, have highlighted potential difficulties in the use of aqueous ozone for treating objects at ambient temperatures.

3.6 Disinfection experiments employing electrostatically-charged sprays

3.6.1 Introduction

A series of experiments is described here in which an electric charge was applied to the spray nozzle whilst at the same time earthing the target, or object, against which the spray was directed. It was reasoned that operation in this way would result in enhanced coverage of the target as individual spray droplets would acquire charge and would

migrate towards the earthed object. This offered the prospect of improving coverage of the object and also of minimising consumption of the liquid oxidant (H_2O_2). Grade 2 filter paper strips were employed in these experiments because of their relatively high liquid absorbance compared to aluminium coupons, thereby slowing the rate of coverage of the surface. The filter paper strips were attached to the outside surface of the hollow stainless steel cylindrical object (Figure 3.22) by means of adhesive tape and the object was then suspended in the spray chamber. In this way, a direct earth connection was made to the cylinder. Sprays were generated using a stainless steel air-atomising nozzle which was connected to a power supply and charged to a negative potential of 15 kV. The spray was administered in pulses of 5 seconds duration per minute.
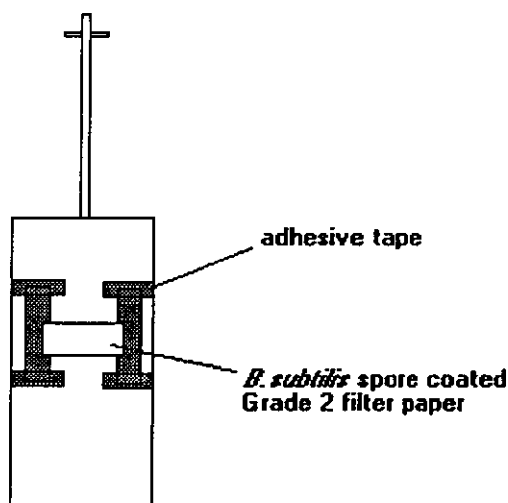
Figure 3.22 Filter paper arrangement on hollow cylinder for electrostatic spraying experiments

Concentrated H_2O_2 (29 w/v%) was employed in these experiments as previous work had shown that combined UV and 1.0 w/v% H_2O_2 treatment would have resulted in rapid disinfection and posed problems in sampling from the chamber. Another advantage of operating in this way was that interpretation of results would be facilitated by not having to account for UV effects.

3.6.2 Results

Experiments using a charged nozzle were conducted over a 4 day period and in all, three experiments were performed. On each occasion a control experiment was performed with the spray nozzle uncharged. Exposure of spore-laden strips to H_2O_2 in the chamber resulted in only low levels of inactivation. The results from the first experiment are shown in Figure 3.23 and show that charging the nozzle resulted in an enhanced disinfection effect. This effect was also demonstrated in the subsequent experiments (results not shown). However repetitive handling of the H_2O_2 caused the concentration to be reduced to unknown levels, thereby decreasing the disinfection performance at each repetition of the experiment.

3.6.3 Discussion

An increase in the disinfection rate using the charged nozzle is observed in the results of Figure 3.23 when using charged sprays, this infers that a greater impact of H_2O_2 spray on the filter paper strips occurred when using charged sprays. Once a surface is fully coated with H_2O_2 then further increases in the impact of spray should not affect the disinfection level. Therefore it can be concluded that the Grade 2 filter paper strips were not saturated with H_2O_2, otherwise they would have had identical disinfection curves.

Whilst the results in Figure 3.23 show that a greater deposition of spray occurred when using electrostatically-charged sprays, the data does not enable the increase in impact of the spray on the target to be determined. The 'Impact Test' methods (described in section 2.7) were developed to determine the mass of spray deposited on a surface and were employed in investigating electrostatically-charged sprays in further detail. The results are discussed in Appendix 2.

106
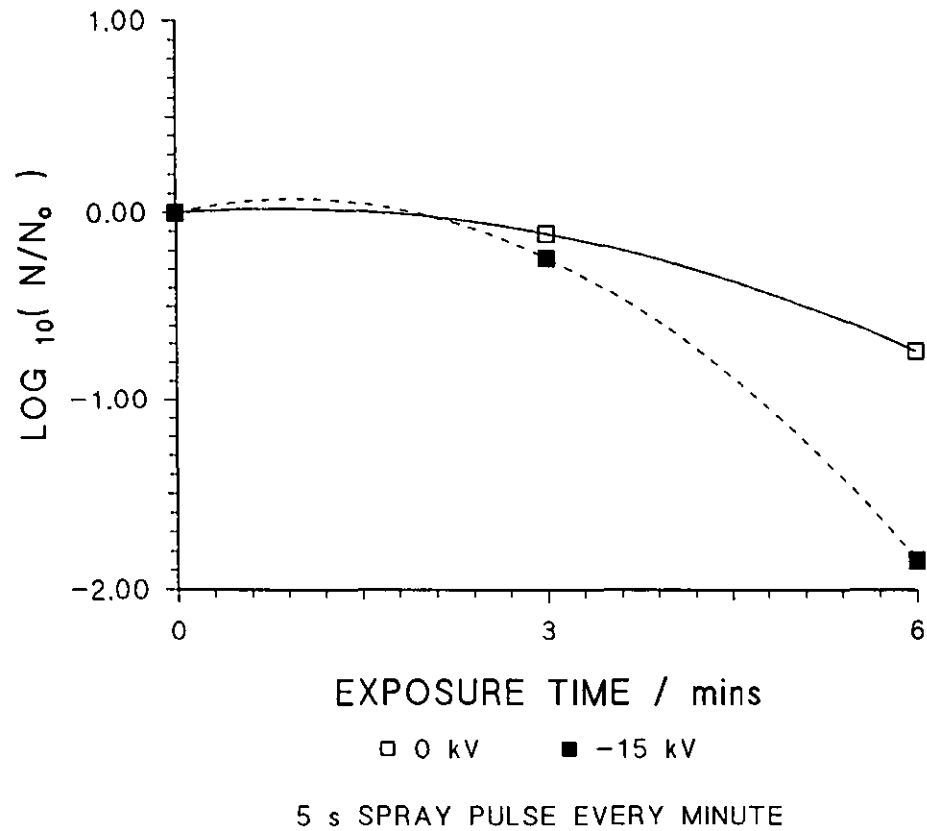
FIGURE 3.23 *B.subtilis* spores on Grade 2 filter paper strips exposed to
electrostatically-charged sprays of 29 w/v% H_2O_2

3.7 Overall Discussion and Conclusions

The choice of materials and method of introducing the spores on to the surface of those materials were important considerations in the studies described here. Filtration media such as filter papers and membranes provided a relatively straightforward way of depositing spores onto the surface. In the former case the relatively absorbent nature of the filters permitted known volumes of spore suspension to be carefully deposited directly on to the surface. Whereas in the latter case, spore deposition was achieved by filtering a suspension of the spores through the membrane. Experimental results of generally good quality were obtained using a variety of materials of different surface characteristics in UV irradiation experiments.

Moreover, useful experimental data was obtained with filter media in experiments with H_2O_2 when the latter could be applied in discrete quantities as in the experiments conducted using the laboratory mounted UV sources. In particular, synergistic disinfection effects between H_2O_2 and UV were clearly revealed. However, the absorbent nature of filter papers was seen as undesirable in experiments involving liquid disinfecting agents such as H_2O_2 and aqueous ozone solutions in the spray chamber. It was reasoned that differential absorption of the peroxide during UV irradiation would have resulted in complex disinfection kinetics. A quest for alternative materials (such as aluminium, stainless steel and PTFE) ultimately revealed other difficulties: whilst aluminium and stainless steel could be employed under conditions such that they bore no surface charge (i.e. by earthing) even distribution of spores was never achieved. Considerations of surface charge was of particular concern in experiments in which the spray nozzle was charged but even spray droplets produced by uncharged nozzles are known to bear a charge (J.I.T. Stenhouse, Chemical Engineering Dept., Loughborough University; personal communication).

One very important finding resulting from the use of a diverse range of materials was that the materials offered varying degrees of protection from the incident UV light to

the spores associated with those surfaces. The implications of this are considered fully in Chapter 4.

4. Mathematical Modelling of Surface Shielding

4.1. Introduction

The experimental data of Chapter 3 indicated that the inactivation kinetics of *B.subtilis* spores were influenced by the nature of the material on which the spores were irradiated. This was in part revealed by the variation in form of the inactivation curves (see Figures 3.1 to 3.11). With the exception of the stainless steel coupons, where it was suggested that Fenton's Reagent might have been generated, the materials chosen were relatively inert, that is, it could be assumed that spore inactivation was not affected by interactions with the constituents of the surface and that the intrinsic UV resistance of the spores remained constant. Direct visual evidence, in the form of SEM photographs, was however obtained to show that the physical structure of materials onto which spores were deposited might constitute an important factor in determining inactivation kinetics. For example, on materials such as glass microfibre filters (Figure 3.8), spores were revealed in spatial locations which appear remote from the surface and surrounded by the relatively large glass microfibres. The extent of penetration of spores into the body of the material would clearly influence the amount of radiant UV light 'seen' by the spores. Spore penetration would be intimately linked to the structure of the material and in the example cited above, the fibres can be visualised as offering shielding to the spores to an extent which depended on the precise nature of the association of any particular spore and adjacent fibres. The analysis presented in this chapter is based on the experimental data of Chapter 3 and constitutes an attempt to categorise materials which were employed as supports for the spores by quantifying the extent of protection or shielding offered to the spores. This was done by assuming the surface of each material to comprise a finite number of zones. It was further assumed that each zone provided a definable degree of shielding as represented by a unique value of a so-called 'Exposure Factor', which is defined below. In addition, the population of spores is visualised as being distributed among these zones (see Figure 4.1). The theory developed here provides a method of determining both the 'exposure factor' and the fractional distribution of the spore population among the zones, the number of which is set

(a) Distribution of spores in a
    matrix which provides
    shielding from incident
    UV light

(b) Zonal model showing
    distribution of spores into two
    zones, each with a characteristic
    exposure factor, α,
    and each containing a
    fraction, f, of the total microbial
    population
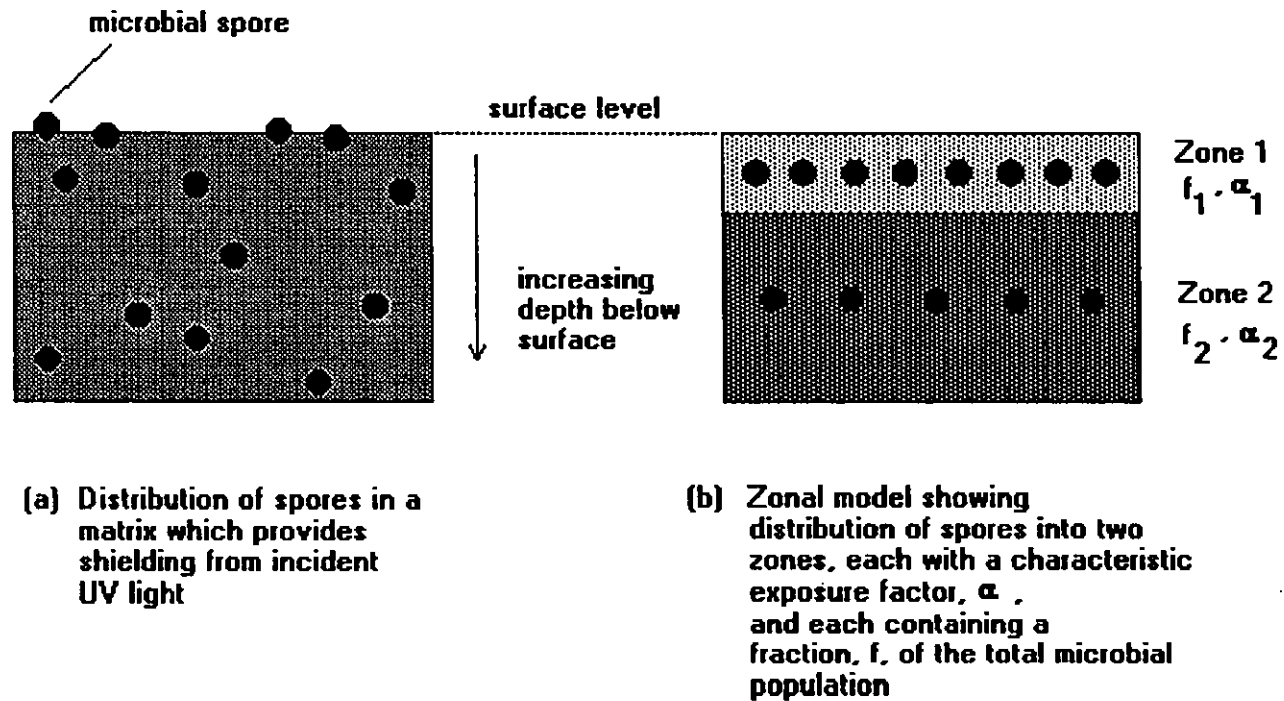
FIGURE 4.1 Example of the application of the zonal shielding model

by the user. In order to achieve this, 'unshielded' inactivation data was required for the spores, that is data obtained under conditions such that the spores received no, or only negligible, shielding from the surface layers of the material.

A search through the literature revealed experimental data pertaining to the UV irradiation of beef steaks (Stermer *et al.*, 1987) in a form which was amenable to analysis by the methods developed in this chapter and the application of the zonal shielding model to this data is also considered here.

4.2 Mathematical description

The fraction of the UV intensity incident on a surface which the micro-organisms present on that surface can receive is defined by an 'Exposure Factor', α, such that :

$$\alpha = \frac{\text{UV intensity received by microorganisms}}{\text{UV intensity incident on surface}} \qquad \textbf{(4.1)}$$

The product of the UV intensity incident on the surface, I_s, and the exposure time, t, of the surface to UV defines the surface fluence, F_s :

$$F_s = I_s.t \qquad \textbf{(4.2)}$$

From equation (4.1), the UV intensity received by micro-organisms on the surface can be defined as :

$$I = I_s.\alpha \qquad \textbf{(4.3)}$$

The unshielded inactivation kinetics are fitted to a suitable function such that :

$$\left(\frac{N}{N_o}\right) = g(F) \qquad \textbf{(4.4)}$$

Equation (4.4) can be any expression that provides a good fit to the experimental disinfection data obtained on a surface that provides no, or minimal, shielding. For example, if the unshielded disinfection data are fitted with multi-target kinetics then equation (4.4) takes the form :

$$g(F) = 1 - (1 - e^{-kF})^n \qquad \textbf{(4.4a)}$$

In this study, relatively rapid disinfection data was obtained for spores irradiated on the surface of both aluminium and PTFE coupons and also Anodisc membranes. Therefore the disinfection kinetics developed on all of these surfaces could be used to provide the 'unshielded' disinfection kinetics. The disinfection kinetics for Anodisc membranes were chosen for use because scanning electron microscope (SEM) images were available for this surface and clearly showed the *B.subtilis* spores present only on the surface on the membrane (see Figure 3.6).

Unshielded inactivation kinetics can be applied to an area of the surface that provides surface shielding by rewriting equation (4.3) as

$$F = F_s . \alpha$$

Thus equation (4.4) becomes :

$$\left(\frac{N}{N_o}\right) = g(F_s . \alpha) \qquad \textbf{(4.5)}$$

The surface is treated as being comprised of a finite number of zones, n_z, in which the exposure factor, α, and the fraction of the total number of micro-organisms on the whole surface present in the zone, f, are specified. The f and α values are parameters that are chosen to provide a good fit to the experimental data.

The following notation is introduced :

f_j = fraction of the total number of micro-organisms on the surface present in zone j

α_j = exposure factor in zone j

The following abbreviation is introduced here :

$$y = \left(\frac{N}{N_o}\right) \tag{4.6}$$

To obtain the disinfection kinetics for the total surface, unshielded inactivation kinetics are applied to each zone on the surface using equation (4.5). By summing the number of viable micro-organisms present in each zone, the number of viable micro-organisms present on the surface is determined :

$$\overline{N} = \sum_{j=1}^{n_z} f_j \cdot N_j \tag{4.7}$$

where $\overline{N}$ = number of viable micro-organisms per unit surface area present on the entire surface

Combining (4.5) and (4.7) yields

$$\overline{N} = \sum_{j=1}^{n_z} f_j N_o \cdot g(F_s \cdot \alpha_j)$$

114

Therefore, assuming the initial microbial concentration is constant over the whole surface,

$$\overline{y} = \left(\frac{\overline{N}}{N_o}\right) = \sum_{j=1}^{n_z} f_j \cdot g\left(F_s \cdot \alpha_j\right) \tag{4.8}$$

From the definitions of f and α, equation (4.8) is subject to the following constraints :

$$\sum_{j=1}^{n_z} f_j = 1.0 \tag{4.9}$$

and

$$1.0 \geq f_j \geq 0.0 \qquad \text{for all j} \tag{4.10}$$

$$1.0 \geq \alpha_j \geq 0.0 \qquad \text{for all j}$$

Equation (4.8) can be fitted to experimental inactivation data obtained on a surface that provides surface shielding by the selection of values for f and α in each zone. This selection can be performed by applying least squares regression.

With n_p data points for the inactivation of a micro-organism on a surface providing surface shielding, the sum of the square of the errors, S, can be defined as :

$$S = \sum_{k=1}^{n_p} (LOG_{10}\overline{y_k} - LOG_{10}\overline{y_{exp_k}})^2 \tag{4.11}$$

where $\overline{y_k}$ = value of $\overline{y}$ predicted by equation (4.8) for same value of F_s as at k th

data point (F_{s_k})

i.e.
$$\overline{y_k} = \sum_{j=1}^{n_z} f_j \cdot g(F_{s_k} \cdot \alpha_j)$$

The best fit of equation (4.11) to the experimental data is found when S is minimised :

$$\text{min } S \quad \text{subject to equality constraint (4.9) and inequality constraints (4.10)}$$

(4.12)

Due to the presence of constraints, equation (4.12) forms a nonlinear programming problem.

4.3 Solving the model

The nonlinear programming problem (4.12) was solved using a computer program ZONESHLD which searches for a Karesh-Kuhn-Tucker point. A detailed description of the program is given in Appendix 1.

A 'Karesh-Kuhn-Tucker point' is a local minimum of the 'Lagrangian function', L (Bazarra *et al.*, 1993). The Lagrangian function combines the function to be minimised together with the products of the equality and inequality constraints with their 'Lagrangian multipliers', λ and μ, such that:

$$L(\underline{x}) = f(\underline{x}) + \sum_{j=1}^{n_e} \lambda_j h_j(\underline{x}) + \sum_{\substack{i=1 \\ where \\ i \in J_A}}^{n_i} \mu_i g_i(\underline{x})$$

(4.13)

where $\mu \geq 0$, $\underline{x}$ is the vector of parameters to be solved for, h is the matrix of equality constraints, and μ is the matrix of inequality constraints. J_A is the set of active inequality constraints.

116

At a local minimum subject to the constraints, there exist values for the multipliers such that

$$\nabla L(\underline{x}) = \nabla f(\underline{x}) + \sum_{j=1}^{n_e} \lambda_j \nabla h_j(\underline{x}) + \sum_{\substack{i=1 \\ \text{where} \\ i \in J_A}}^{n_i} \mu_i \nabla g_i(\underline{x}) = 0 \quad \text{(4.14)}$$

A local minimum is found by applying the following iterative strategy :

STEP 1.
Make all inequalities inactive and set all Lagrangian multipliers for the inequality constraints to zero.

STEP 2.
Solve $\nabla L = 0$

STEP 3.
If all the inequality constraints are not violated and there are no Lagrangian multipliers for the inequality constraints that are < 0 then STOP - a Kuhn-Tucker point has been found.

STEP 4a.
Remove the inequality constraint with the largest negative multiplier.

STEP 4b.
Add all violated inequalities to the active set.

Applying the above equations to the case of surface shielding :

$\underline{x}$ = f and α in each of the n_z zones

$f(\underline{x})$ = S, the sum of the square of the errors, defined in equation (4.12)

$g(\underline{x})$ = inequality constraints, defined in equation (4.9)

$h(\underline{x})$ = equality constraint, defined in equation (4.10)

Step 2 of the iterative set strategy, the solution of $\nabla L = 0$, is the rate-determining step of

the process. The program ZONESHLD uses the Newton method (Bajpai *et al.*, 1988) to find the minimum value of the Lagrangian function. The method used to complete Step 2 will be discussed in further depth in Appendix 1.

On exit from the computer program ZONESHLD, the parameters f and α in each zone were given.

4.4 Results

Figures 4.2 - 4.4 show the disinfection data previously described in Chapter 3 for respectively, dry Grade 2 filter paper, dry Grade 6 filter paper and glass microfibre filter paper, along with the curves fitted from equation (4.8). Exposure factors were calculated for *B.subtilis* spores on these surfaces and are shown in Table 4.1. The sum of the square of the errors, S, divided by n_p, the number of data points (not those at the origin), is also displayed in Table 4.1; the lower this value, the 'better' the fit of the zonal shielding model to the experimental results. The results from the zonal shielding model are also shown in histogram format in Figure 4.5.

Surface	n_z	n_p	f	α	S / n_p
Dry Grade 2 filter paper	2	26	0.440 0.560	1.00 0.211	0.065
Dry Grade 6 filter paper	3	16	0.426 0.229 0.345	0.303 0.278 0.0138	0.003
Glass microfibre filter paper	3	19	0.131 0.721 0.148	0.637 0.0883 0.0271	0.124

Table 4.1 Exposure factors for zonal shielding model

As explained earlier, it was also possible to estimate the exposure factors on beef steaks from the results of Stermer *et al.* (1987) who investigated the application of UV as a disinfectant for meat. By culturing the natural microbial flora of beef on agar plates and irradiating these cultures under a UV source, they were obtaining data under conditions in
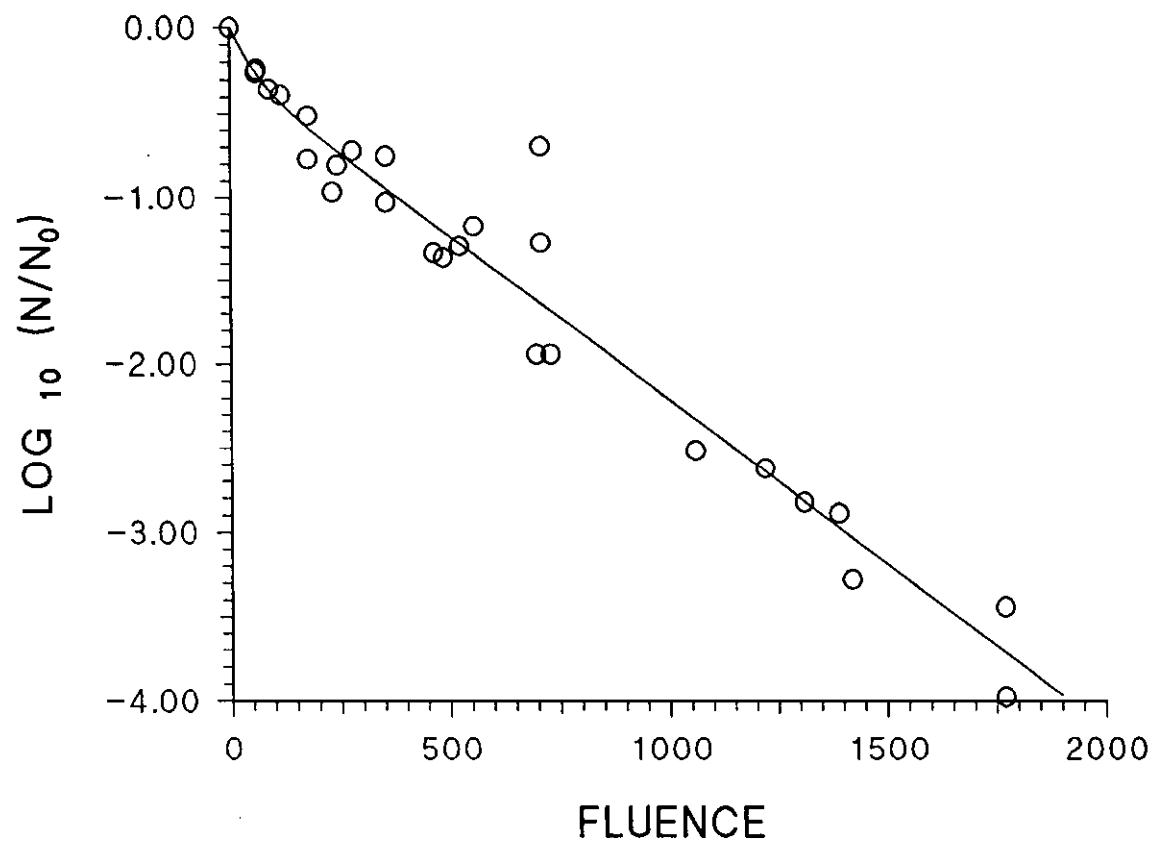
FIGURE 4.2   **Application of surface shielding model to the UV disinfection results obtained on dry Grade 2 filter paper strips**
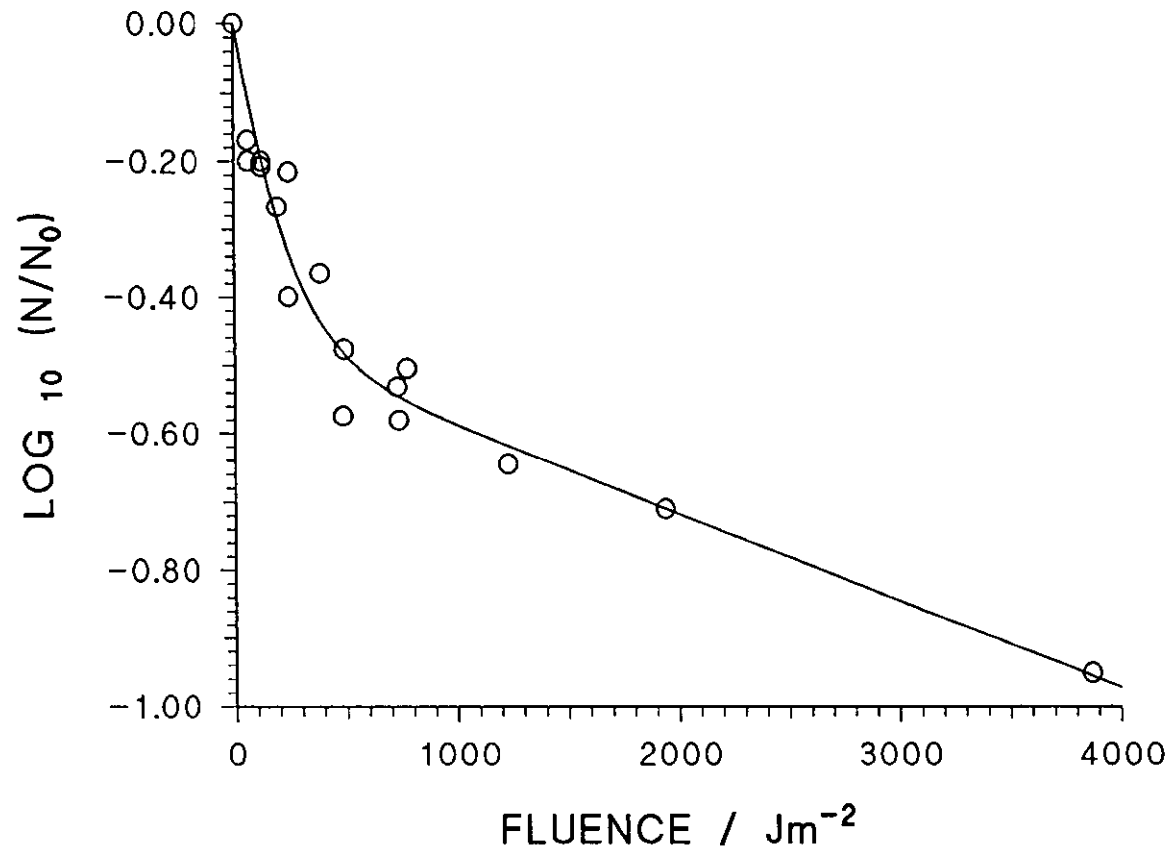
FIGURE 4.3   **Application of surface shielding model to UV disinfection results obtained on dry Grade 6 filter paper strips**
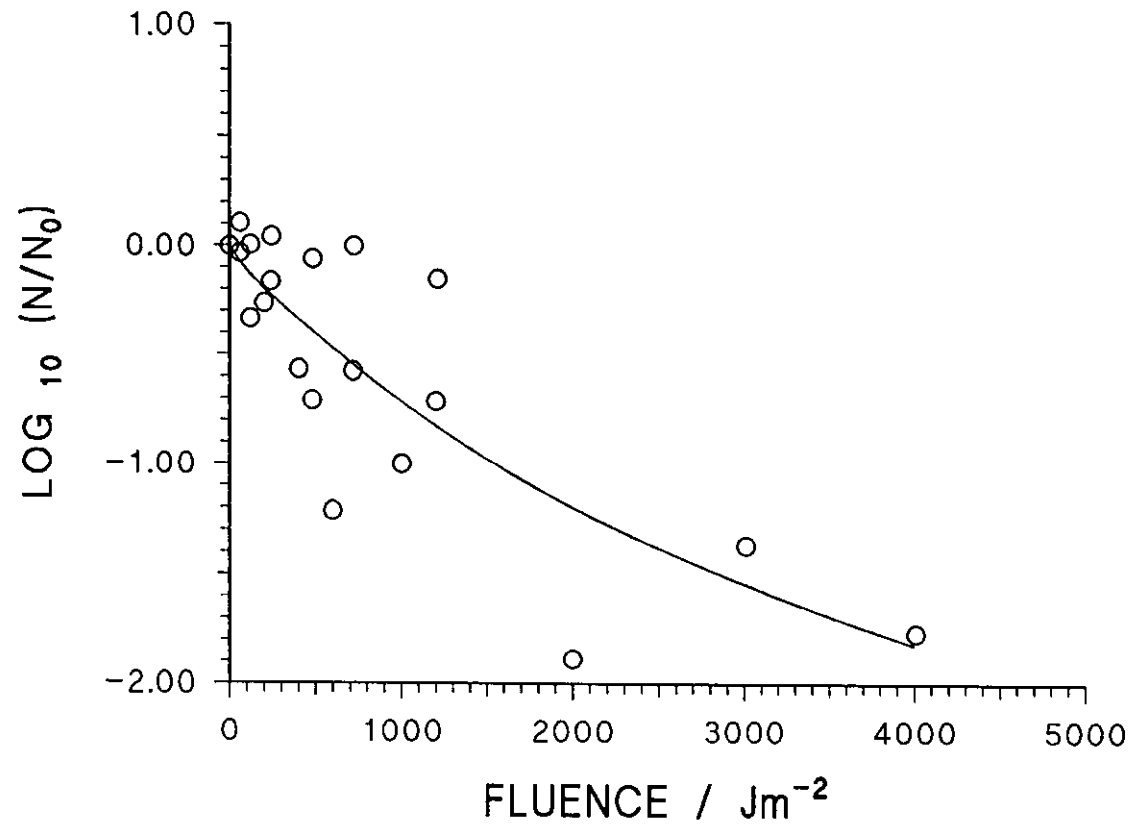
FIGURE 4.4   Application of surface shielding model to UV disinfection results obtained on Glass microfibre filter paper
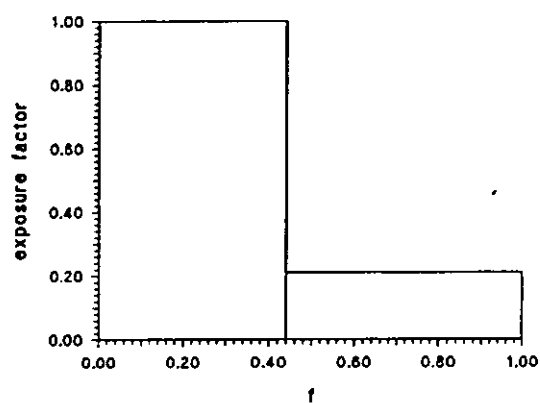
(a) Dry Grade 2 filter paper
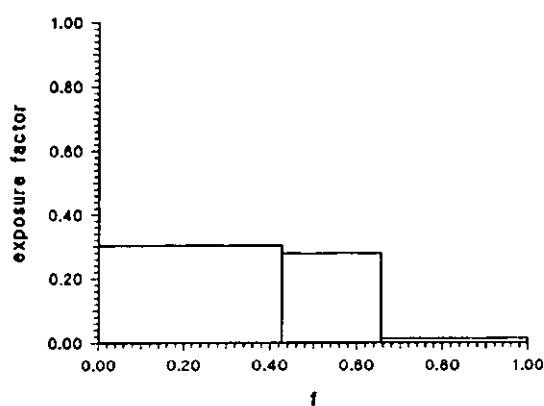
(b) Dry Grade 6 filter paper
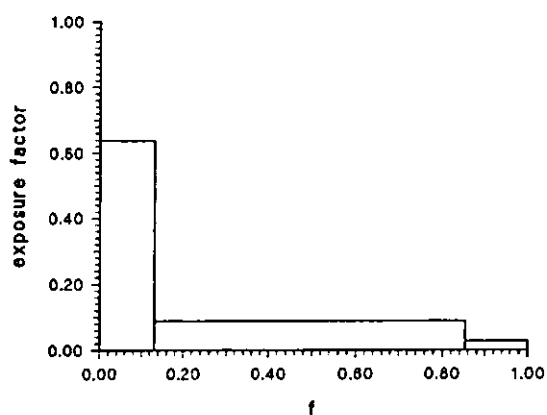
(c) Glass microfibre filter paper

FIGURE 4.5   Exposure factors for surfaces providing surface shielding

122

which the microbial colonies received little or no shielding from the incident UV, i.e. the inactivation kinetics of this microbial flora constitutes the unshielded kinetics as previously defined (see Figure 4.6). First order kinetics were fitted to the data by regression (using the computer program FigP, Biosoft) ($k = 0.153$ $(Jm^{-2})^{-1}$).

Stermer *et al.* also presented data for the irradiation of beef steaks under the same UV source (see Figure 4.7). The curve fitted to the data shown in Figure 4.7 was determined by equation (4.8) and the parameters are given in Table 4.2 below. The following results were obtained with a 3 zone model :

Parameter	ZONE 1	ZONE 2	ZONE 3
Population fraction, f	0.260	0.725	0.0156
Exposure factor, α	0.749	0.517	0.00352

Table 4.2   Results from the application of the zonal shielding model to beef steaks

4.5 Discussion

The strategy adopted using the program ZONESHLD was to increase the number of zones until no further improvement in the solution could be made. The sum of the square of the errors was used to quantify the quality of the fit of the zonal shielding model to the experimental data. In certain instances it was found that increasing the number of zones resulted in a solution in which the additional zone bore an identical value of α to the previously obtained solution, i.e. a zone had in effect been split into two zones having identical values of the exposure factor. Such solutions offered no advantages and so were ignored.

Three zones were required for accurate representation of the disinfection curves obtained on the materials offering a higher level of shielding, i.e. dry Grade 6 filter paper and glass microfibre filter paper. Also included in this category were the beef steak results of Stermer
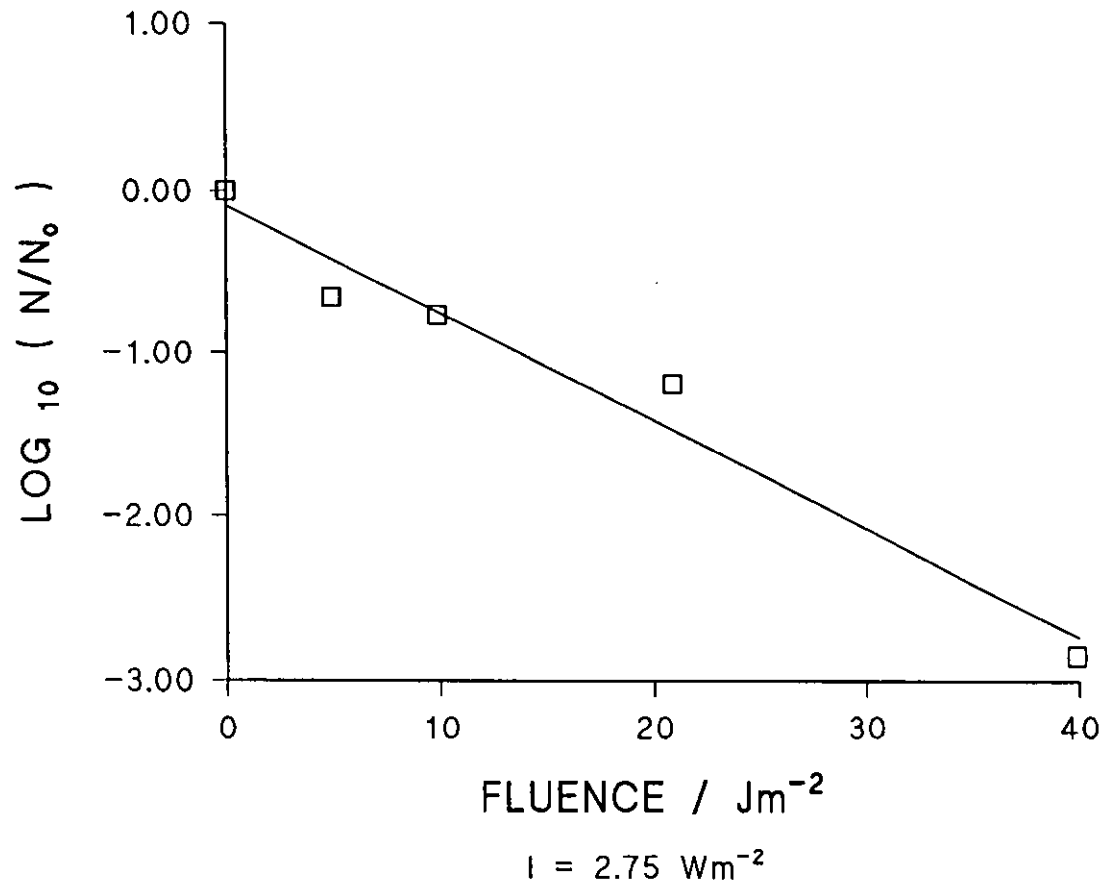
FIGURE 4.6 'Unshielded' disinfection data for beef flora (from the paper by Stermer *et. al*, 1987)
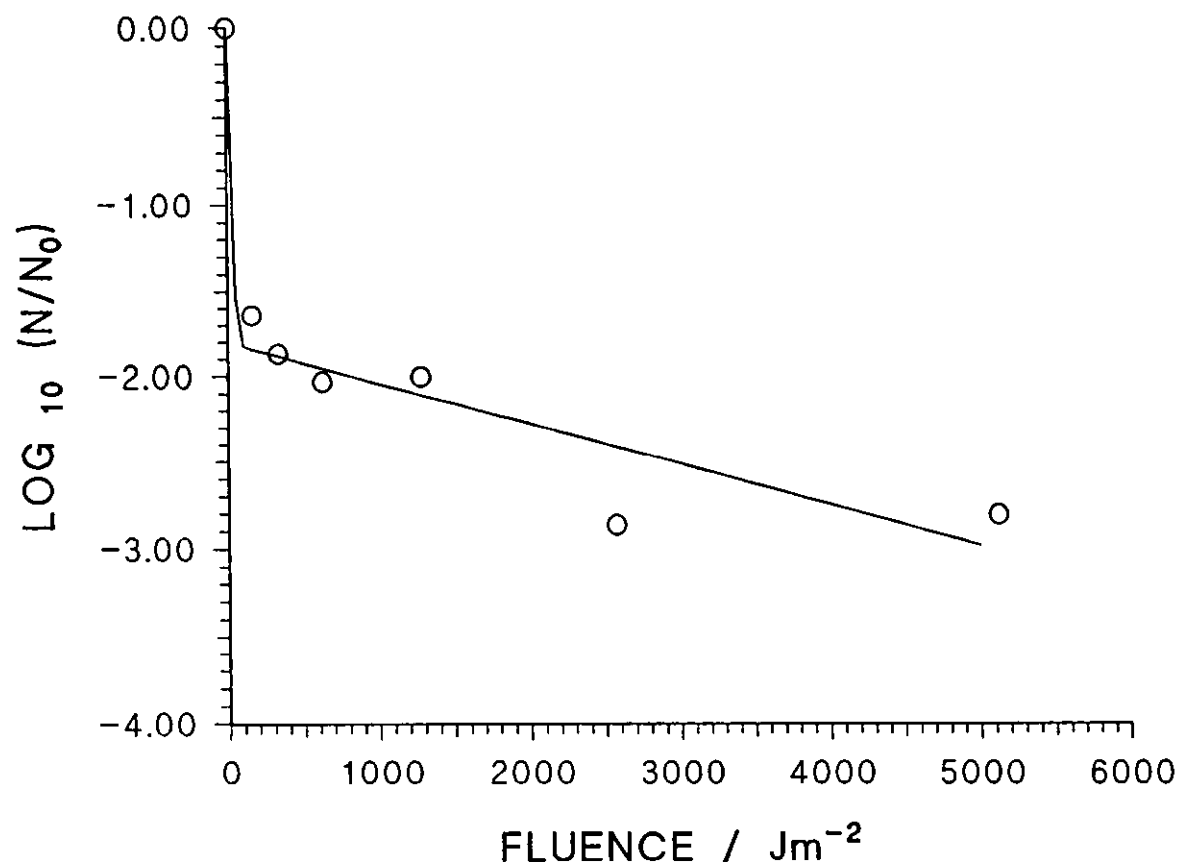
FIGURE 4.7 Disinfection data for beef steaks exposed to UV (from Stermer *et. al*, 1987)

et al. (1987). Some of the exposure factors tend to zero for these surfaces which implies total protection from UV. The lowest factors were observed for beef steaks. The disinfection curve for this material tailed off at about 2 - 3 orders of disinfection (see Figure 4.7), which is reflected in the value for α in the third zone (where $\alpha = 0.00352$).

Initially it was reasoned that increasing the number of zones beyond 3 might offer better solutions of the zonal shielding model. However this tends to lead to the formation of zones in which the exposure factor to tends towards zero; in addition the spore population occupying these zones would be very low indeed. This created difficulties in convergence towards a solution because in general a large range of values for f and α over multiple zones renders the system of equations describing the model ill-conditioned. In practice therefore, all the inactivation data obtained were described using three zones or less.

Whilst the zonal model developed here proved useful in describing inactivation data caution should be observed in interpreting the results obtained too literally. In reality, the surfaces of materials are unlikely to contain a fixed number of discrete zones each having characteristic shielding properties but rather a distribution of areas with less well defined characteristics. A further advantage of the model is that it allows the disinfection kinetics due to UV to be described by the same equations that were used for unshielded surfaces.

It is also seen that this technique can be successfully applied to data other than that obtained in this work. However, an exhaustive search through the literature revealed only one study (that of Stermer *et al.* (1987)) having data in a form amenable to analysis by the methods described here. One example of a study not providing data in form required is that of Huang and Toledo (1982) who investigated the use of UV as a disinfectant for the external surfaces of whole fish. They obtained disinfection data for the natural flora on the fish skin when exposed to UV but unfortunately they did not provide any data for the disinfection rate of the natural flora when exposed to UV on an unshielded surface. However they did find that the disinfection rate obtained on smooth-surfaced fish, such as mackerel, was greater than that obtained on rough-surfaced fish, such as mullet.

4.6 Conclusions

A zonal shielding model was developed to account for the protection offered to surface-associated spores from incident UV light by virtue of surface.topography. Application of the model to the experimental inactivation data obtained in this work and also to the data of Stermer *et al.* (1987) yielded expressions which described the data well.

Application of the model to materials offering a relatively high degree of shielding from incident UV light revealed zones which displayed relatively low values of the exposure factor, α. This was an interesting result and suggests that spores would continue to remain protected as the UV fluence was increased. Experiments were not conducted to establish whether this was indeed the case but it is clearly one area for future studies.

Another intriguing question raised is that once a particular surface has been characterised by conducting experiments with a model organism (e.g. *B.subtilis* spores) what is the minimum additional data that would allow predictions to be made about inactivation kinetics for different microbial species ? In particular, would unshielded inactivation data for the different microbial species be sufficient ? Investigations of this nature were outside the scope of the work described here but again, this could well prove a fruitful area for future work.

4.7 Notation

F	UV fluence
F_s	surface fluence
f	fraction of the total number of micro-organisms present in a particular zone
g(F)	unshielded inactivation kinetics equation (see equation (4.4))
I_s	UV intensity incident on surface
j	zone number
N	number of viable micro-organisms per unit surface area
N_o	initial value of N
$\overline{N}$	N for the whole surface
n_p	number of data points
n_z	number of zones
S	sum of the squares of the errors of the fit of equation (4.8) to the experimental data
t	exposure time of surface to UV
y	N/N_o
α	exposure factor due to surface shielding from UV

5. UV FIELD MODELLING

5.1 Introduction

A variety of mathematical models have been developed to predict the intensity field produced by a UV source (Alfano *et al.*, 1986). These models are either 'incidence' or 'emission' models. Incidence models require knowledge of values of the UV intensity close to (or inside) the region in which predictions of the UV intensity are required. This data is then used to extrapolate to other spatial locations based on equations describing the emission characteristics of the UV source. Emission models, on the other hand, can predict the UV intensity using a model for the emission characteristics of the source providing that the power output from the source at the wavelength range of interest is known. Manufacturers often provide such data.

UV intensity models can be further classified according to the method that they employ to describe the emission characteristics of the source. These are 'parallel-plane emission', 'spherical emission' and 'diffuse emission'. The simplest model is the parallel-plane emission model. This model assumes that each differential volume of the source only emits light in a plane parallel to the point of emission, i.e. that it is 2-dimensional. The spherical emission model describes 3-dimensional emission. In this model, each differential volume of the UV source approximates to a point which is assumed to emit light evenly in all directions. The equation describing such emission from a point source is known as Lambert's law (Jacob and Dranoff, 1970) :

$$I(\rho) = \frac{\cdot S_p}{4\pi\rho^2} \cdot e^{-\mu\rho} \tag{5.1}$$

where I = UV intensity / Wm^{-2}

       S_p = Power output from point source / W

       ρ = distance from point source / m

       μ = attenuation coefficient / m^{-1}

Diffuse emission models consider the emission from a UV source to be produced in every direction, that is in a diffuse way.

The physical dimensions of the source are sometimes approximated to a line (uni-dimensional) in order to simplify the form of the equation describing the emission characteristics of the source. Such models are referred to as 'line source' models. Where the source is considered to be 3 dimensional and to emit light evenly throughout the volume of the source, the model is described as an 'extense source' model (Alfano *et al.*, 1986).

The equations previously described predict the 'point UV intensity'. This is the UV intensity at a given point in space which receives the total energy of every ray of light intersecting it. The point UV intensity is therefore applicable when considering spatial locations in gases or liquids. On a surface however, the angle of the surface relative to the emission source needs to be known in order to calculate the UV intensity at the surface. This is because the quantity of UV energy received by a surface depends on its projected area, not the actual area of the surface. The projected area divided by the actual area of a surface is known as the 'view factor' (Bennett and Myers, 1983). The intensity on a surface will be less than the point UV intensity if the surface is not directly facing the point source (an example is shown in Figure 5.1). It was not possible to integrate analytically the UV emission models when taking account of view factors and hence computer programs based on numerical methods must be written to solve them.

surface

UV point
source
$$\bar{I} = I$$

UV point
source

$$\bar{I} = I_\bullet \frac{A_p}{A} = I_\bullet (\cos \alpha)$$
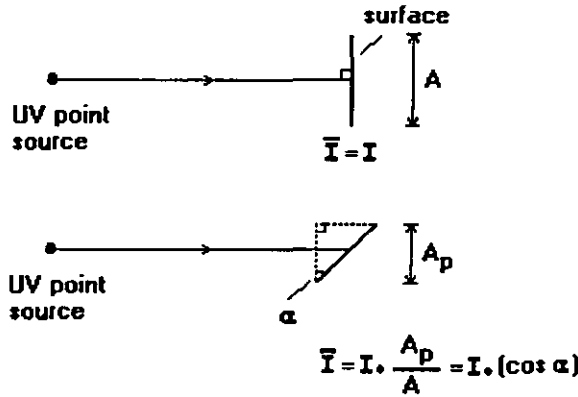
Figure 5.1 Demonstration of view factors

130

The power output from the UV sources employed in the spray disinfection chamber was known from manufacturer's data for the power output at 253.7 nm, which is the emission line from a mercury vapour source that produces the principal germicidal effect. This value was 13.1 W. As the power output was known, an emission model was employed to predict the UV intensity at a wavelength of 253.7 nm. No previously developed mathematical models were available that could have been easily applied to the case of predicting the UV intensity on objects within the spray disinfection chamber. Therefore an extense source with spherical emission (ESSE) model was created that took the view factors into account.

5.2 Mathematical description

The building block of the mathematical model used here is Lambert's law, the equation for the point UV intensity produced by a point source. Air and water do not absorb UV light of 253.7 nm wavelength and hence for modelling the UV field in the spray chamber it can be confidently stated that the attenuation coefficient, $\mu = 0$. Therefore equation (5.1) can be rewritten as:

$$I(\rho) = \frac{S}{4\pi\rho^2}$$

(5.2)

In the spray chamber, the UV sources were located close enough to the test object that changing the distance between the UV sources and the test object by the diameter of the UV sources would provide a significant change in the UV intensity received by the test object. Therefore it was necessary to use a model of the source which took account of the finite dimensions of the source. The model used was based on the Extense Source with Spherical Emission (ESSE) model in cylindrical polar co-ordinates (Alfano et al., 1986). This model not only took account of the finite volume of the UV source but it assumed that UV light was being emitted evenly throughout the volume along the arc length of the source.

The model assumes that the volume of the source is comprised of elements of differential

volume $dV = rd\theta.dr.dl$. As $d\theta,dr,dl$ all tend to zero, the differential volume tends to a point and hence the equation for a point source can be used to describe the emission characteristics of a differential volume of a UV source. By integrating over the emitting volume of the UV source, the point UV intensity at a given spatial location (r_1,l_1,θ_1) can be calculated from the following equation :

$$I(r_1,l_1,\theta_1) = \int_{l=0}^{l=L}\int_{r=0}^{r=r_L}\int_{\theta=0}^{\theta=2\pi} \frac{S_v}{4\pi \rho^2}.r.d\theta.dr.dl \qquad (5.3)$$

where

$$S_v = \frac{S}{V_L}$$

and

$$\rho^2 = (r\sin\theta - r_l\sin\theta_l)^2 + (r\cos\theta - r_l\cos\theta_l)^2 + (l - l_l)^2$$

Equation (5.3) can be integrated analytically in one dimension with integration in the two remaining dimensions having to be performed numerically. If equation (5.3) is integrated along the length of the source then it becomes a summation of line sources with spherical emission. This model is suitable to determine the point intensity in non-absorbing liquids or air.

To determine the UV intensity at a surface the view factors must be taken into account. The example shown in Figure 5.1 is for two dimensions. The quantity $(\cos\alpha)$ is termed a 'view factor' and is the fraction of the point UV intensity that the surface receives due to its orientation relative to the UV source. When considered in three dimensions, a second view factor must be introduced for the perpendicular plane. Hence the equation describing the UV intensity received by a differential area of surface from a point UV source is :

$$\bar{I}(\rho) = \frac{S_p}{4\pi \rho^2}.(\cos\alpha).(\cos\beta) \qquad (5.4)$$

Using equation (5.4) in place of equation (5.2) causes the ESSE model to take the form:

132

$$\bar{I}(r_1,l_1,\theta_1) = \int\limits_{l=0}^{l=L} \int\limits_{r=0}^{r=r_1} \int\limits_{\theta=0}^{\theta=2\pi} \frac{S_v}{4\pi\rho^2}.(\cos\alpha).(\cos\beta).rd\theta.dr.dl \qquad (5.5)$$

$(\cos\alpha)$ and $(\cos\beta)$ are functions of the coordinates of the UV point sources and the point on the surface, as well as the orientation of the surface. Consequently equation (5.5) cannot be integrated analytically. It can be solved numerically by assuming that the UV source consists of a finite number of point UV sources, N_p. The sum of the power output from the point UV sources equates to the power output from the UV source :

$$N_p.S_p = S \qquad (5.6)$$
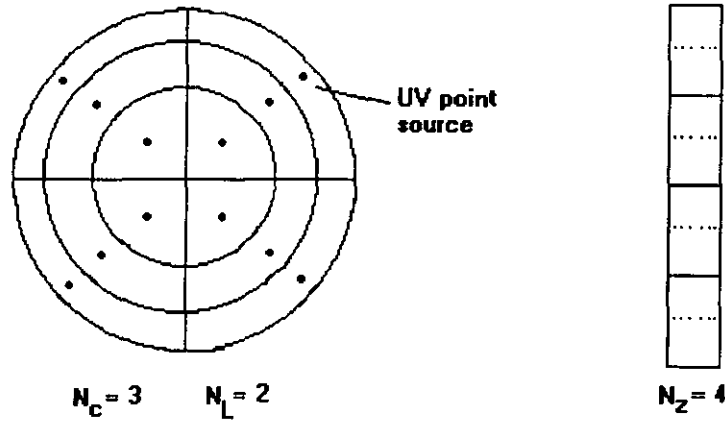
Figure 5.2 Location of point sources in the UV source model

The volume of the UV source can be divided into elements of equal volume using the scheme shown in Figure 5.2. The length of the UV source is divided into a number of zones, N_z, of equal length. The cross-sectional area of the UV source is divided into a number of concentric circles of equal areas by a number of lines, N_L, separated by an angle of $\dfrac{\pi}{N_L}$. By placing a point source at the center of each finite volume element comprising the UV source, equation (5.5) can be rewritten as :

133

$$\bar{I}(r_l, l_l, \theta_l) = \frac{S_p}{4\Pi} \sum_{i=1}^{N_t} \sum_{j=1}^{N_L} \sum_{k=1}^{N_x} \frac{1}{\rho^2} \cdot (\cos\alpha) \cdot (\cos\beta) \tag{5.7}$$

where $\rho^2 = (r_i \cos\theta_j - r_l \cos\theta_l)^2 + (r_i \sin\theta_j - r_l \sin\theta_l)^2 + (l_k - l_l)^2$

$(\cos\alpha)$ and $(\cos\beta)$ are calculated from the known surface orientation (at which the UV intensity is being determined) to the UV point sources. $\rho^2, (\cos\alpha), (\cos\beta)$ are calculated for every point UV source.

5.3 Verifying the mathematical models

To verify the emission form of the ESSE model developed, it was necessary to obtain UV intensity data at known spatial locations produced by unshielded UV lamps. Such data was not available from the spray chamber because the UV lamps within the spray chamber were located inside the brass tubes and meshes which significantly reduced the UV output from the UV lamps into the spray chamber. The manufacturer of the Voltarc G30 sources employed in the spray chamber quoted that a UV intensity of 120 μW/cm^2 (for 254 nm wavelength) should be obtained at a distance of 1 m from the UV source. The ESSE model predicts a UV intensity of 109 μW/cm^2 based on the manufacturer's quoted power output at 254 nm of 13.1 W. The manufacturer's estimated power output cannot be used to predict the UV intensity in the experimental spray chamber because the UV sources are located behind meshes which reduce the UV intensity. However by using the ESSE model to estimate the effective power output of the UV sources based on UV intensity measurements within the chamber, it is possible to predict the UV intensity field within the experimental chamber. In effect, this is converting the ESSE model into an incidence model.

A UV radiometer was located inside the spray sterilisation chamber using the arrangement shown in Figure 5.3. As the location of the UV radiometer was known in relation to the

UV sources in the spray chamber, it was possible to use the ESSE model to calculate the power output of the UV sources from the intensity measurements taken using the radiometer. By re-arranging equation (5.7) to calculate S_p for each UV intensity measurement made with the radiometer, $\overline{I}(r_1, l_1, \theta_1)$, the effective power output from the UV source can then be determined from equation (5.6) which would produce the UV intensity measured at the given spatial location. A computer program was written to perform these calculations - POWER.FOR (see Appendix 1). The 'apparent' power output for one UV source in the spray disinfection chamber was estimated at between 0.491W - 0.528W at 254 nm when placed inside a UV source holder. Errors in determining the precise spatial location of the radiometer sensor can account for the slight variation in the estimated 'apparent' power output from one UV source.
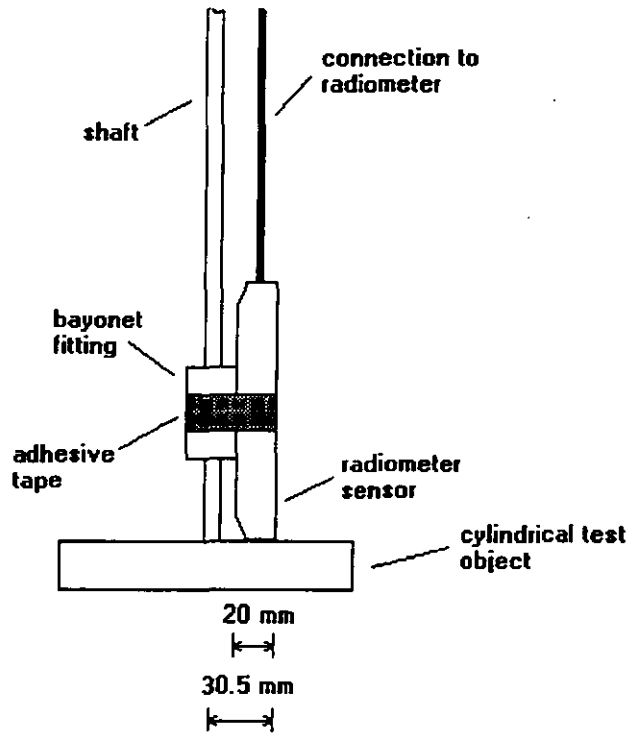
Figure 5.3   Arrangement for UV intensity measurements in the spray disinfection chamber using the radiometer

In addition to employing a UV radiometer to provide UV intensity measurements within the spray chamber, the dry Grade 2 filter paper bioassay technique (see section 2.6.3) was employed to provide UV intensity measurements. As the disinfection data on which the

bioassay curve is based was produced independently from the series of experiments conducted within the spray chamber, this technique for providing UV intensity measurements was used to verify the predicted UV intensity field within the spray chamber.

Three experiments using the disc test object and the cylindrical test object were undertaken in the spray chamber using the dry Grade 2 filter paper bioassay to determine the average UV intensity over areas covered by filter paper strips on the surfaces of the objects (see section 2.6.3). The locations of these areas are shown in Figure 5.4. The UV field model was used to generate average UV intensities within these same areas and the results compared. The results of the bioassays and model predictions are shown in Table 5.1. It is seen that the intensity predicted by the model is 75-95% of the intensity determined by the bioassay. This shows reasonable agreement.

A possible source of error was the effect of the mesh. It was assumed that the mesh reduced the UV intensity by the same proportion no matter what the spatial location within the rig. However, the reduction in UV intensity will change depending upon the angle from which the mesh is viewed. For simplicity this effect has been ignored and the comparison between experimental and model results would suggest that the effect can be neglected.

5.4 Predicting UV intensity fields on surfaces

It is possible to predict the UV intensity fields for a wide range of UV lamp arrangements and object geometries. In this section are presented a small selection of results obtained from applying the ESSE model. As has been previously mentioned, each object geometry will produce a unique set of view factors at the object surface and therefore separate computer programs must be written to solve for different object geometries. Two object geometries are considered here - cylindrical and slab geometries.

Object (see below)	Location	UV intensity / Wm^{-2}			Model
		Experimental			
		Average	Low	High	
1	SIDE	2.46	2.08	3.13	2.09
1	TOP	4.52	4.33	4.71	3.75
2	SIDE	3.27	2.71	3.54	2.48
2	TOP	4.09	4.00	4.17	3.85
3	H1	4.92	4.53	5.53	4.38
3	H2	4.83	4.53	5.00	4.00
3	H3	3.42	3.20	3.58	2.69

Table 5.1   **Comparison of model results and bioassay results for the UV intensity in the spray chamber at different locations**

Note: Refer to figure below for object number and location
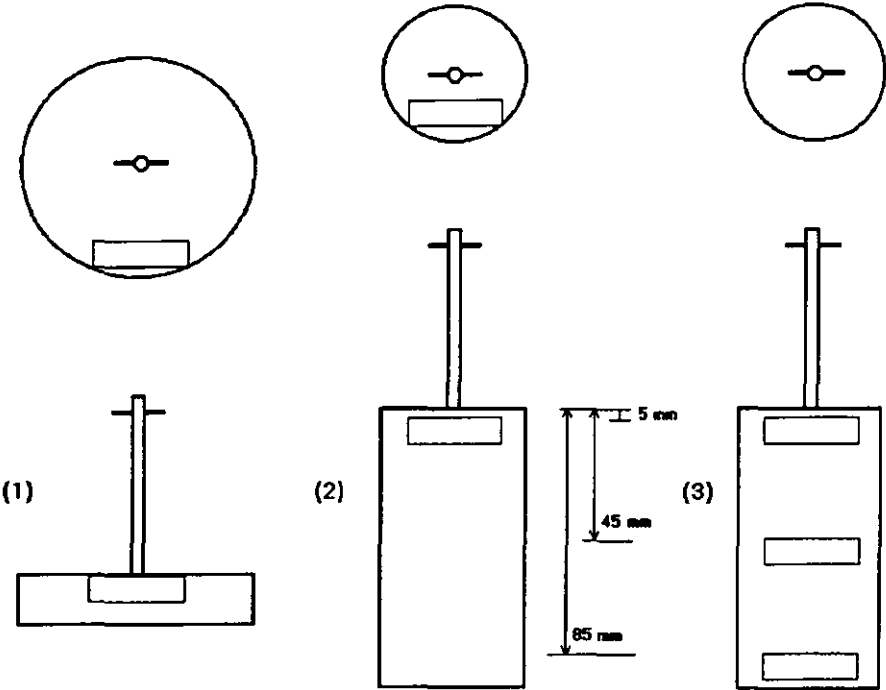
FIGURE 5.4   **Locations of Grade 2 filter paper strips for bioassay intensity measurements**

5.4.1 Cylindrical geometry

The disinfection studies that were performed during this work were conducted on the disc test object. Therefore it was valid to consider the UV intensity fields that would be produced on a cylinder within the spray chamber.

Predictions for the UV intensity fields produced on the disc test object in its experimental location (i.e. with the top surface level with the bottom of the windows in the brass tubes and suspended from the shaft along the axis of the spray chamber - see Figure 5.5) were made using three computer programs - VOLTARC, VERT and MULTIVOL. The programs VOLTARC and VERT were employed to calculate the UV intensities produced on the top and side of a cylindrical object exposed to the output of one UV source respectively. Once the UV intensity field produced by one UV source was known, the UV intensity field produced by many UV sources could be predicted by summing the intensity fields produced from each UV source. The program MULTIVOL was used to perform the summation calculation. The listings for these computer programs are given in Appendix 1.

Figures 5.6 - 5.9 show the UV intensity fields on the disc test object in the spray chamber irradiated by either 1, 2, 3 or 4 UV sources respectively. (The UV sources were equidistant from one another). For the side intensity profile, the UV intensity around the circumference of the side of the disc at the top edge is shown. For the top surface, the UV intensity at a radial distance of 27 mm is shown. This radial distance was the location of the centre of the *B.subtilis* spore-coated coupons on the top surface of the disc test object during the disinfection experiments described in Chapter 3. The manufacturer's power output of 13.1 W was used in generating these results.

The figures 5.6 - 5.9 show that increasing the number of UV sources not only increases the UV intensity produced on the disc but also creates a more even UV intensity field, particularly on the side of the disc which will be shielded from the output of some of the UV lamps at certain orientations. Figure 5.7(a) shows that the UV intensity fell to only approximately 80% of its maximum value during the disinfection experiments.
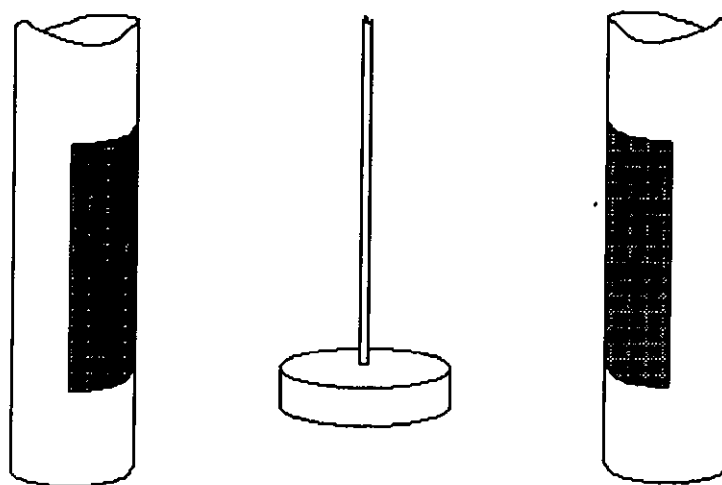
(a) Cylindrical geometry
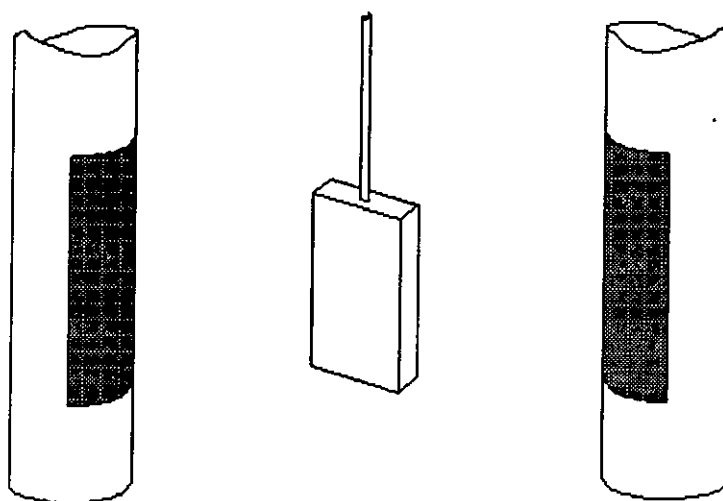
(b) Slab geometry

FIGURE 5.5   Object geometries in the spray disinfection chamber
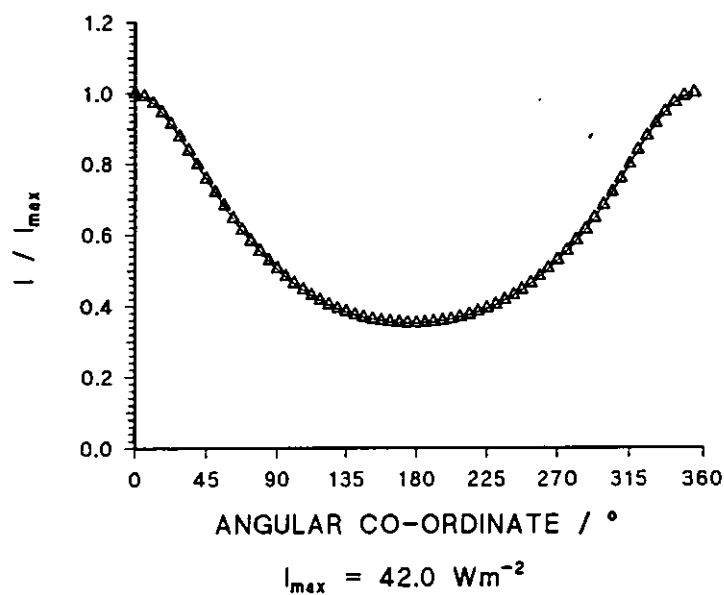
(a) Top surface
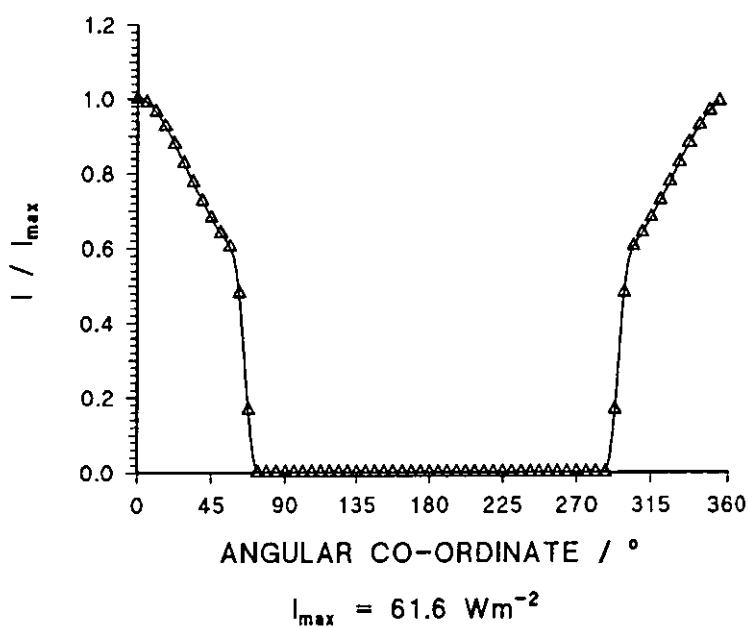
(b) Side

FIGURE 5.6 UV intensity profiles on disc test object in the spray chamber produced by a single UV source

(a) Top surface

$I_{max} = 56.7 \ Wm^{-2}$

(b) Side

$I_{max} = 61.6 \ Wm^{-2}$
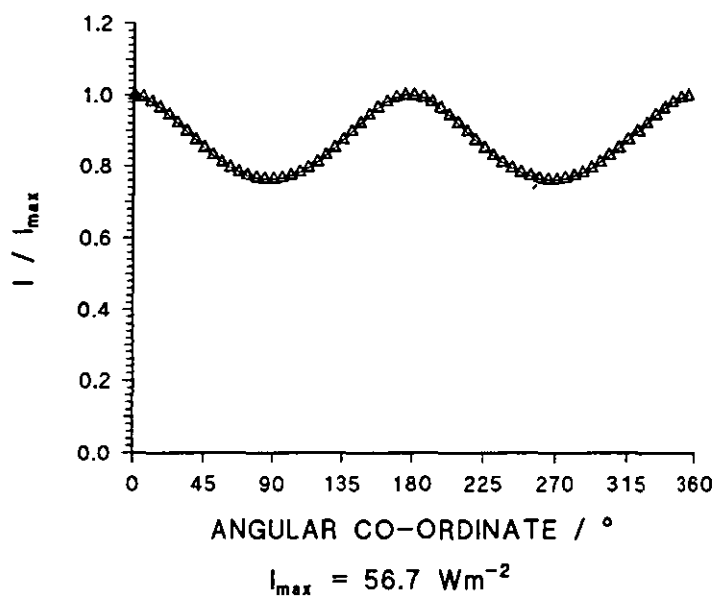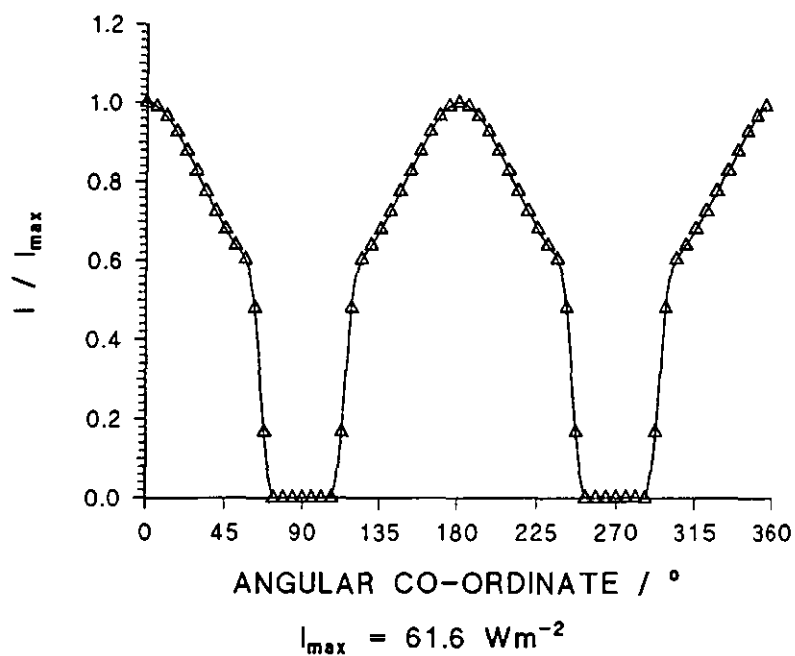
FIGURE 5.7 UV intensity profiles on disc test object in the spray chamber produced by 2 sources

$I_{max} = 77.1 \ Wm^{-2}$

(a) Top surface

$I_{max} = 71.6 \ Wm^{-2}$
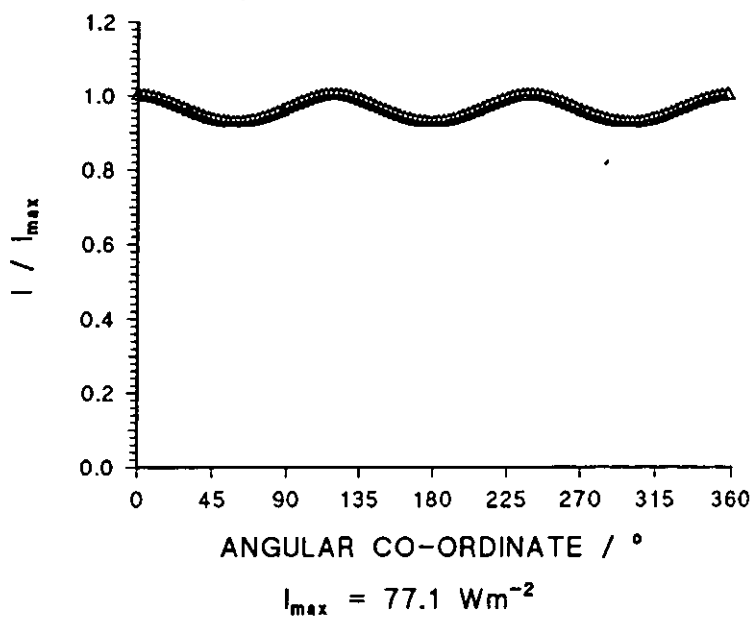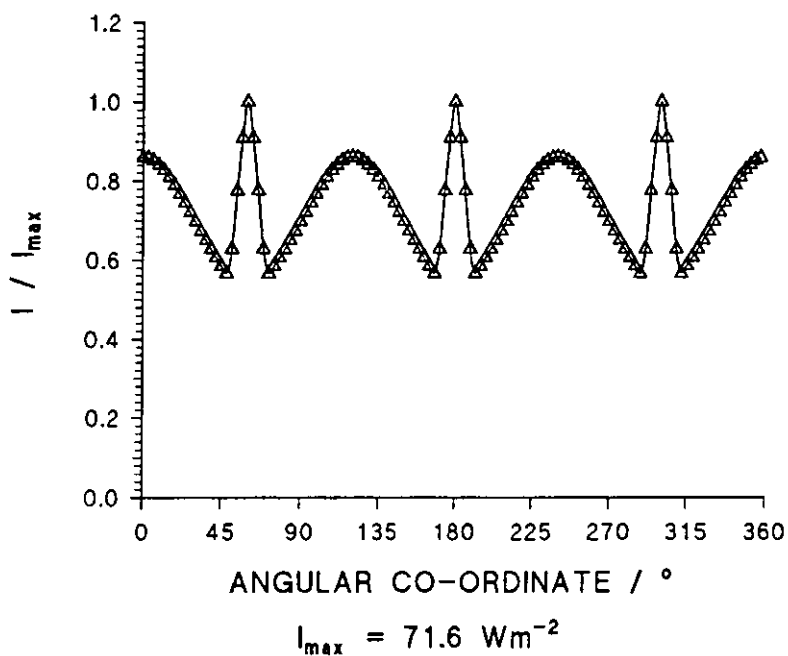
(b) Side

FIGURE 5.8   UV intensity profiles on disc test object in the spray chamber produced by 3 UV sources

142

$$I_{max} = 100 \text{ Wm}^{-2}$$

(a) Top surface

$$I_{max} = 84.9 \text{ Wm}^{-2}$$
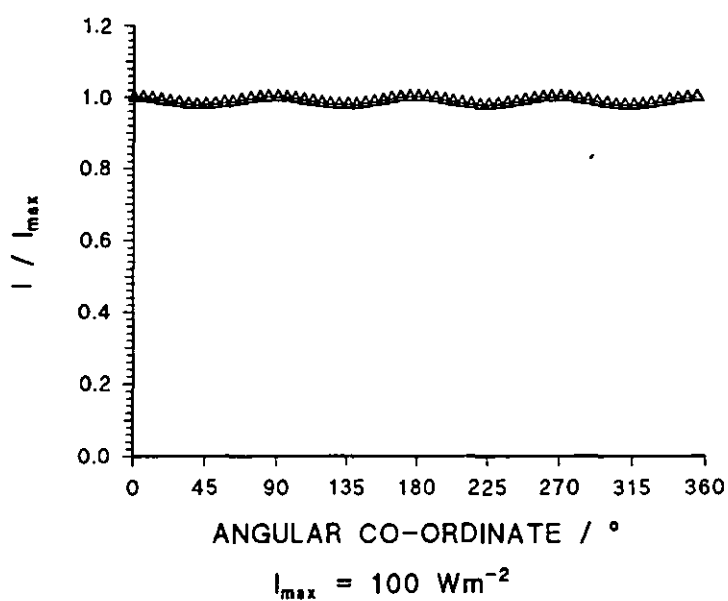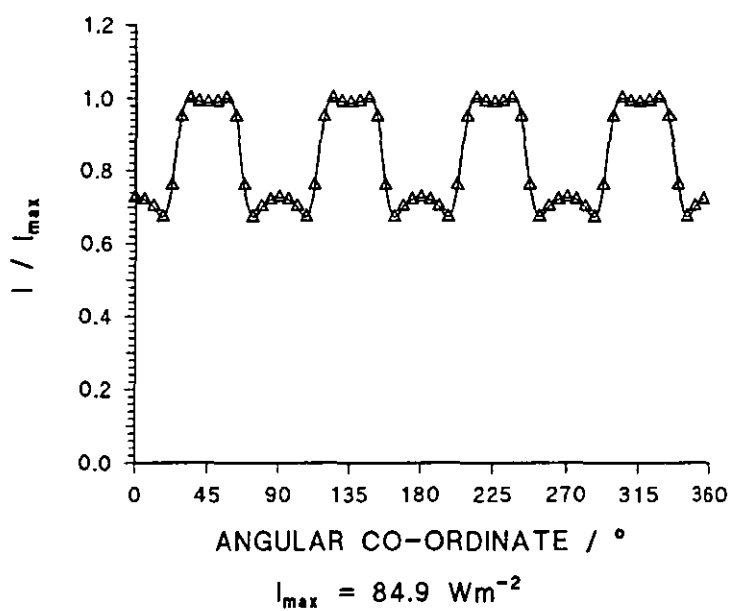
(b) Side

FIGURE 5.9   **UV intensity profiles on disc test object in the spray chamber produced by 4 UV sources**

143
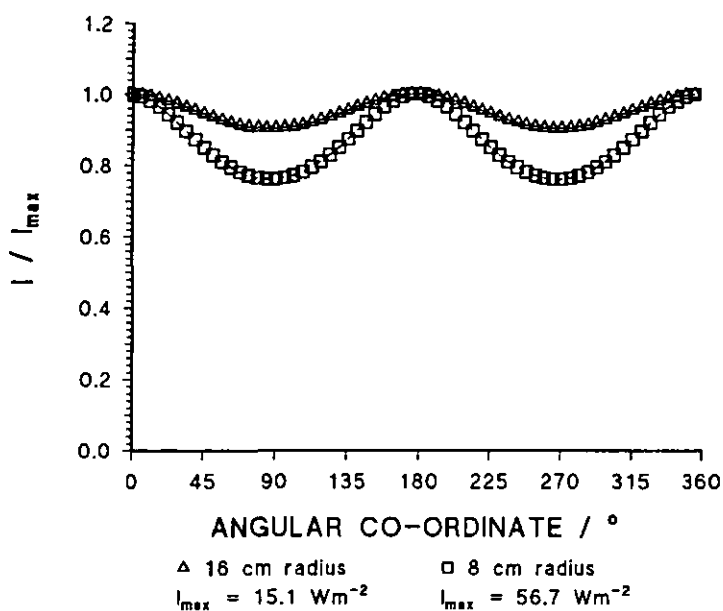
(a) Top surface
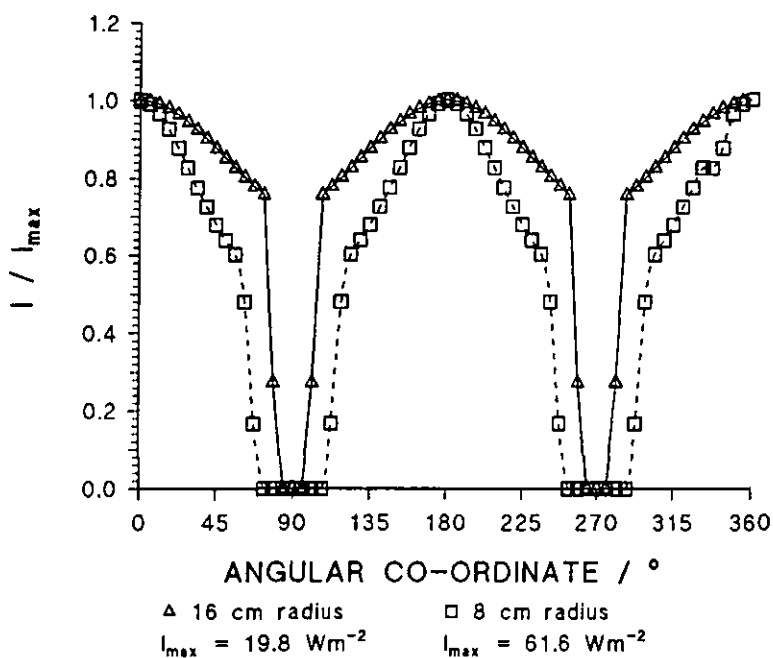
(b) Side

FIGURE 5.10   UV intensity profiles on disc test object in the spray chamber produced by 2 UV lamps

Figure 5.10 compares predicted UV intensity fields for the disc when using 2 UV sources which are located 16 cm from the centre of the disc, compared to 8 cm in the case shown in Figure 5.7. It is seen that the UV intensity is lower than the case in Figure 5.7 but the UV intensity field shows less variation for both the top and side of the object.

5.4.2 Slab geometry

No disinfection experiments were conducted with a test object of slab geometry but this geometry provided an interesting comparison to the cylindrical geometry previously described. UV intensity fields were produced for a cube of dimensions 66 mm x 66 mm x 66 mm located at the axis of the spray chamber and at a height where the centre of the cube was level with the middle of the windows in the brass tubes (see Figure 5.5). The location of the cube was chosen so that the intensity fields on the sides would be the same and those on the top and bottom of the cube would be identical. The manufacturer's data of 13.1W was used for the power output of the lamp.

Figures 5.11 shows the UV intensity fields produced on the sides and top/bottom of the cube when the sides of the cube are facing the UV lamps, i.e.
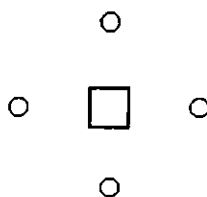
The origin of the Cartesian co-ordinates is located at the centre of the cube. The highest intensities on the top and bottom surfaces were achieved at the four corners, whereas for the sides, maximum intensity was attained along a line traversing the centre.

145
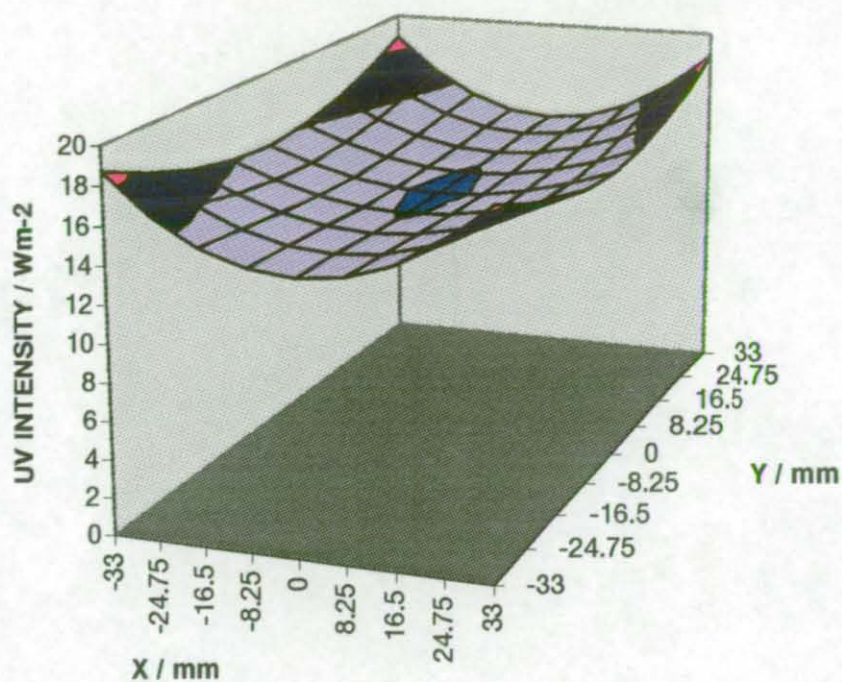
(a) Top / bottom surfaces
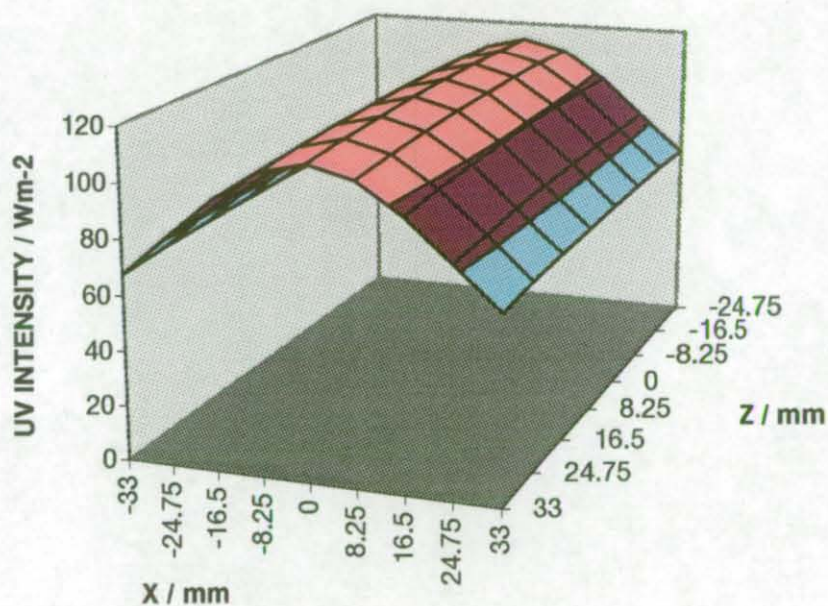
(b) Sides

FIGURE 5.11   UV intensity profiles on a cube in the spray chamber produced by 4 UV lamps facing the center of each side
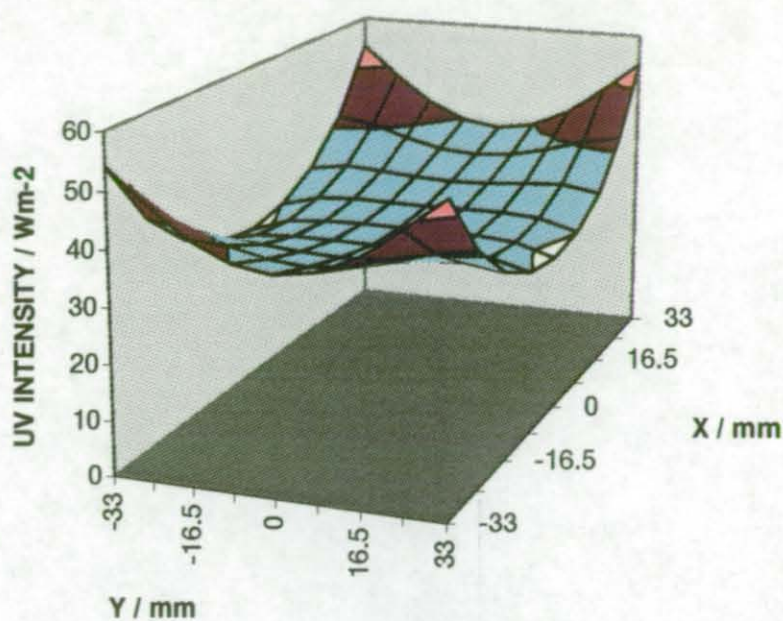
(a) Top / bottom surfaces
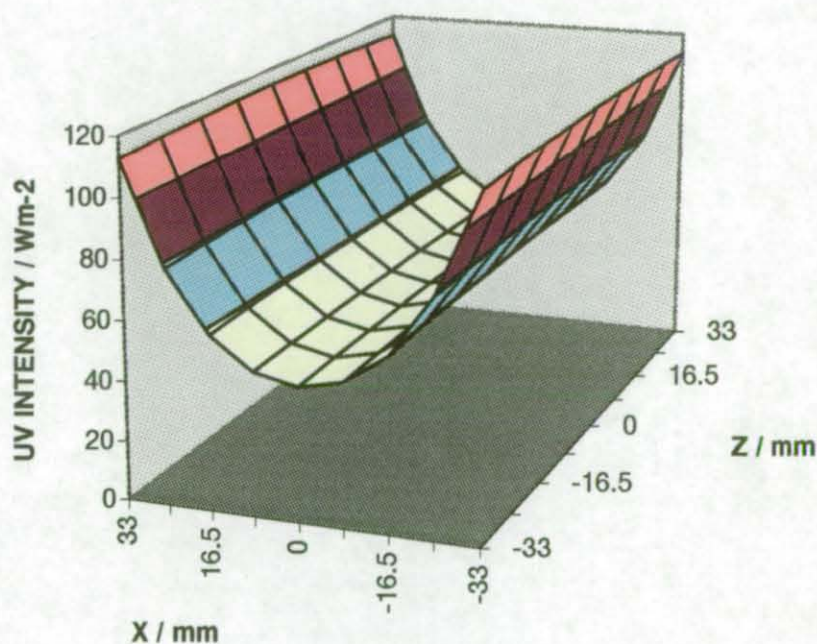
(b) Sides

FIGURE 5.12 UV intensity profiles on a cube in the spray chamber produced by 4 UV lamps facing the edges between the sides of the cube

Figure 5.12 shows the UV intensity fields produced on the cube when it is rotated through 45° around its central axis, i.e.
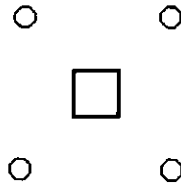
As for the previous configuration, maximum intensities on the top and bottom surfaces of the cube were achieved at the corners, however a greater variation in intensity is apparent. In contrast to the previous configuration, the maximum intensity attained on the side faces occurred along the edges, with the maximum intensity now being at the centre.

5.5 Conclusions

The UV intensity field generated by the arrangement of sources in the spray chamber was modelled by creating an extense source with spherical emission model. This enabled the intensities on the surfaces of objects of different geometrical form suspended in the UV field to be predicted. Although the routines established permitted consideration of a wide variety of shapes, particular attention was focused on cylinder and slab geometries. The versatility of the developed models was further demonstrated by examining the effects of irradiation by either 1, 2, 3 or 4 sources and of increasing the distance between object and source.

Where practicable, verification of model predictions and radiometer and bioassay measurements were made, and these gave acceptable levels of agreement. This agreement provided justification for further developments of the model and its application as described in Chapter 6 to situations in which objects are being sprayed with hydrogen peroxide whilst undergoing UV irradiation.

5.6 Notation

I	point UV intensity
$\bar{I}$	UV intensity on a surface
L	arc (emitting) length of UV source
N_C, N_L, N_Z	number of circles and lines dividing the UV source cross-sectional area, and the number of lines dividing the length of the UV source, respectively, into equi-volume elements (see Figure 5.2)
r, l, θ	cylindrical polar coordinates
r_L	radius of UV source
S	Power output from UV source
S_P	power output from a point UV source
S_V	power output from UV source per unit emitting volume
V_L	emitting volume of UV source
ρ	distance from point source
μ	(Base e) attenuation coefficient for UV in a medium
$(\cos\alpha), (\cos\beta)$	Surface view factors

6. Combined UV-H$_2$O$_2$ Disinfection Model

6.1 Introduction

Kinetic equations describing the disinfection kinetics of *B.subtilis* spores when exposed to UV, either alone or in combination with H$_2$O$_2$, were obtained from experimental results in Chapter 3 and models describing the UV intensities produced on an object in a UV field were developed in Chapter 5. Combining these two models together could enable the degree of disinfection that could be achieved for a solid object undergoing spraying with 1% H$_2$O$_2$ in a UV field to be predicted.

A method of achieving this combination is described in this chapter and is illustrated with reference to a specific example. The example chosen for analysis comprises a tunnel with UV sources located on the walls; an object, in this case a slab pre-sprayed with H$_2$O$_2$, is imagined to move through the tunnel at constant velocity. Predictions are obtained and presented here of the disinfection of the surfaces of the object as it moves through the tunnel.

6.2 Model description

6.2.1 General equations

It was seen in Chapter 3 that the disinfection kinetics of *B.subtilis* spores exposed to UV could be represented by first order kinetics :

$$\left(\frac{N}{N_0} \right) = e^{-kF}$$

(3.1a)

This was also the case for UV + 1% H_2O_2 :

$$\left(\frac{N}{N_0}\right) = e^{-k_1 F}$$

(3.1b)

Equations (3.1a) and (3.1b) are in one sense limiting cases. To predict the disinfection performance in which a fraction of the surface, f_c, was covered by 1% H_2O_2 spray, equations (3.1a) and (3.1b) can be combined to produce:

$$\left(\frac{N}{N_0}\right) = f_c \cdot e^{-k_1 F} + (1 - f_c) \cdot e^{-kF}$$

(6.1)

A zonal shielding model was developed in Chapter 4; this allowed equation (3.1) to be applied to surfaces which shielded micro-organisms to incident UV. Denoting the kinetic disinfection function in generalised terms as g, i.e. :

$$\left(\frac{N}{N_0}\right) = g(F)$$

the disinfection performance can be predicted for a surface represented by n_z zones in which the fraction of the total number of micro-organisms on the surface, f_j, and the surface view factor, α_j, are known in each zone :

$$\left(\overline{\frac{N}{N_0}}\right) = \sum_{j=1}^{n_z} f_j \cdot g(F_s \cdot \alpha_j)$$

(4.8)

where F = $F_s \alpha_j$

             F_s =   UV fluence incident on surface

151

The UV intensity model developed in Chapter 5 allowed the UV intensity incident on a surface, I_s, to be calculated. For a given exposure time, t, the UV fluence received on the surface of the object is

$$F_s = I_s . t$$

Once the fluence received by the surface is known then equation (4.8) can be applied.

In most real applications, the UV intensity will vary over the surface of an object. In such situations, in order to apply equation (4.8) it will be necessary to know the UV intensity distribution on the object surface. Methods of achieving this are described in Chapter 5 in which UV intensity field models were solved numerically. It was seen that in order to apply the model, the object surface must be divided into areas in which the UV intensity is considered to be uniform. The UV intensity is calculated at the centres of these areas, e.g.
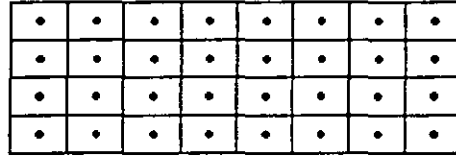
Figure 6.1 Surface area zones of constant UV intensity

Once I_s was calculated for each of these surface areas by the UV intensity field model, the survival after a specified exposure time, t, in each of these surface areas was calculated by equation (4.8) :

$$\overline{y} = \left(\overline{\frac{N}{N_0}}\right) = \sum_{j=1}^{n_z} f_j . g(I_s . t \alpha_j) \qquad (4.8')$$

If these surface areas are equal then the survival for the whole surface, comprised of n_{sp} surface areas, is calculated by the following equation:

$$\overline{y}_{surf} = \frac{\sum_{i=1}^{n_{sp}} \overline{y}_i}{n_{sp}} \qquad (6.2)$$

For an object comprising n_{so} surfaces, the survival on the whole object is given by :

$$\overline{y}_{obj} = \sum_{k=1}^{n_{so}} a_k \cdot \overline{y}_{surf_k} \qquad (6.3)$$

where a_k =   <u>surface area of surface k</u>
                                         surface area of object

6.2.2 Example

The system of equations thus described are versatile enough to enable them to be applied to any geometrically defined object present in any UV field. To demonstrate the application of the equations a specific example is considered below.

Previously in Chapter 5 only stationary objects in stationary UV fields were considered. In this example an object having the geometry of a slab is assumed to travel through a spray disinfection field which is an open-ended 'tunnel' comprised of two walls either side of the object. The object travels at constant velocity through this tunnel. The tunnel is 10 metres in length and each wall is made up from 10 panel sections, each 1 metre in length, which have an identical arrangement of UV lamps, as shown in Figure 6.2.

The model micro-organism present on the surface of the slab is taken to be *B.subtilis* spores, allowing the application of equations (3.1a) and (3.1b) using the parameters
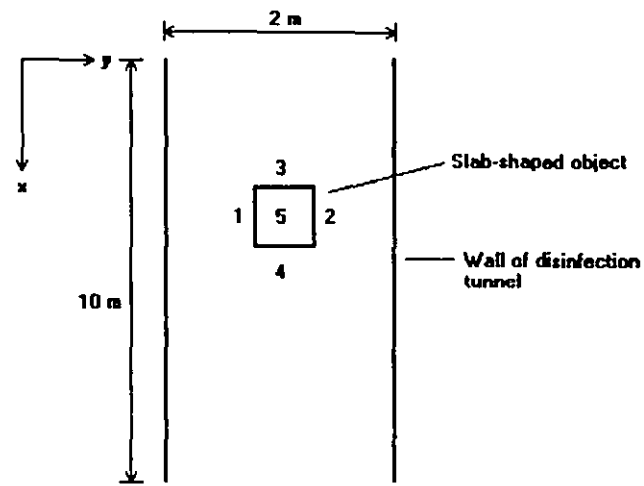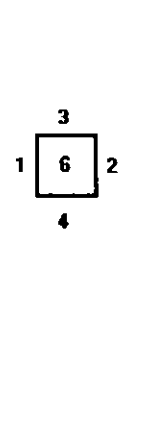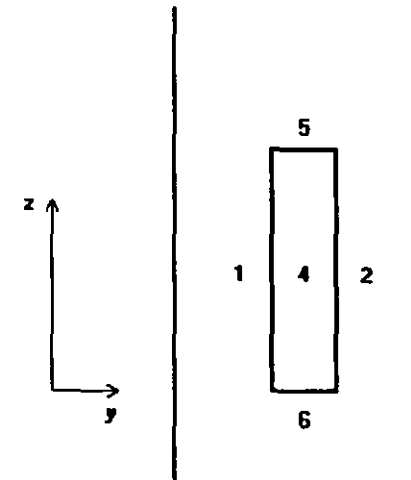
FIGURE 6.2 Disinfection tunnel arrangement

determined from the experiments described in Chapter 3; ($k = 2.13 \times 10^{-2}$ $(Jm^{-2})^{-1}$; $k_1 =$ 0.129 $(Jm^{-2})^{-1}$).

The slab-shaped object is assumed to travel down the centre of the tunnel. The 6 surfaces of the slab have been numbered for reference. The slab has a height of 2 metres with a width and breadth of 0.25 metres each. A Cartesian system of co-ordinates has been applied to the disinfection tunnel with $z = 0$ being level with the bottom of the slab. The origin is located at the start of the tunnel on the left hand wall (see Fig. 6.2a). The slab-shaped object and the UV sources have been located so as to achieve a symmetrical UV intensity field on the object. This means that the opposite surfaces of the slab, i.e. sides 1 & 2, sides 3 & 4, and sides 5 & 6 have identical UV intensity patterns.

The UV sources used in the disinfection chamber are considered to be Voltarc G30 UV sources, as used in the experimental disinfection chamber described in Chapter 2 and used to generate the results in Chapter 3. These sources have an arc length of 0.35 m, a diameter of 1.5 cm and emit 13.1W at 254 nm. The model had a provision for altering the arrangement of the UV sources on the wall panels. The first arrangement used is shown in Figure 6.3. This shows 2 UV sources positioned horizontally on the wall panel, each 0.25 m above and below the top and bottom of the slab, i.e. 2.50 m apart.

In the example considered below, the slab-shaped object will travel through the disinfection chamber for periods of time necessary to achieve certain levels of disinfection and the residence time in the disinfection chamber will affect the UV fluence received. In addition to investigating the effect of residence time on disinfection performance, the effect of changing the arrangement of UV lamps in the chamber by increasing the number of evenly-spaced UV lamps on each wall section will be investigated. Also, the effect of changing the orientation of the UV lamps from horizontal to vertical will be considered.

UV source

direction of motion

slab

0.25 m

z

2 m

z = 0

0.25 m

x

0.25 m

Repeatable tunnel wall section

0.35 m

1 m

x_end

x_start
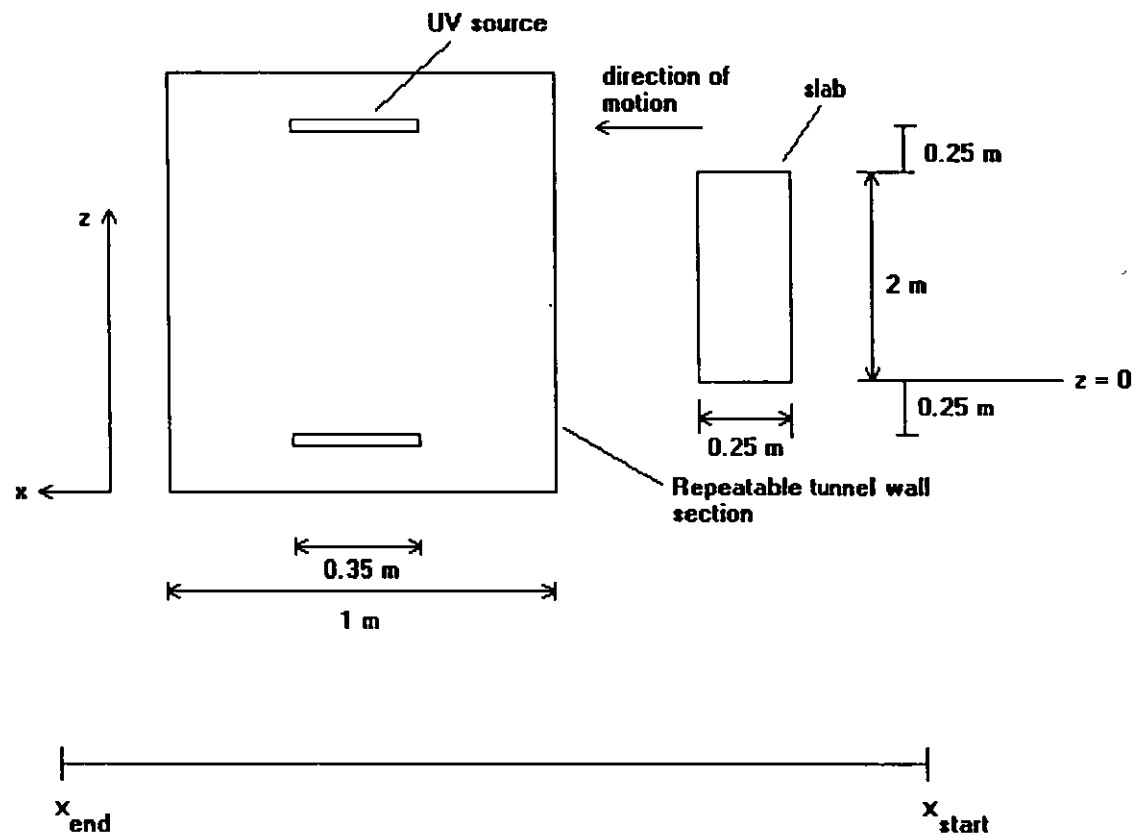
FIGURE 6.3 UV source arrangement on disinfection tunnel wall

In order to apply equation (6.3) it was necessary to know the UV fluence that each surface zone has received during its passage through the disinfection chamber. The UV intensities on the object surface will change as the object moves through the disinfection chamber. As the equations cannot be integrated it is necessary to solve the equations numerically. This is done by assuming that the object passes through sections of the disinfection tunnel in which the UV intensity is constant. This is shown in Figure 6.4. The greater the number of these sections the better the approximation. The UV intensity at specified points on the object surface is then calculated using the program
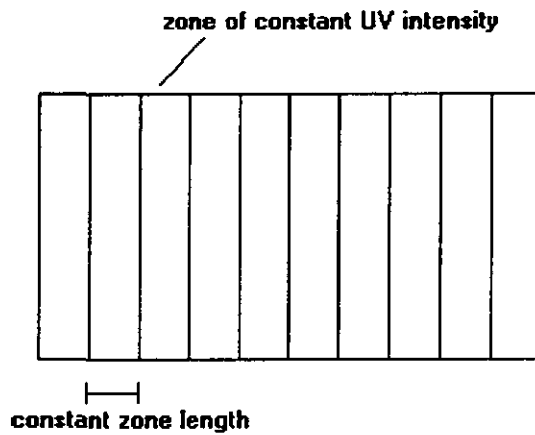
Figure 6.4 Division of the disinfection tunnel into sections of constant UV intensity

SLABAV (Appendix 1) which places the object at the centre of each section of constant UV intensity. By specifying the number of sections of constant UV intensity in the disinfection tunnel, n_{sc} , SLABAV calculates the UV fluence, $\overline{F}$, received by a surface area on the object during passage through the disinfection chamber from the summation of the fluences received in each section of the tunnel :

$$\overline{F} = \sum_{a=1}^{n_{sc}} F_a$$

(6.4)

If the object is travelling at a constant velocity through sections of disinfection chamber which are of equal length then equation (6.4) can be rewritten as :

$$\overline{F} = t_s \sum_{a=1}^{n_{sc}} I_a \qquad\qquad \text{(6.5)}$$

where t_s =   residence time in a section of disinfection chamber where the UV intensity is constant

          I_a =   UV intensity in tunnel section a

Equation (6.5) can be re-written as

$$\overline{F} = t_c . \overline{I} \qquad\qquad \text{(6.6)}$$

where $\overline{I} = \dfrac{\displaystyle\sum_{a=1}^{n_{sc}} I_a}{n_{sc}} \qquad\qquad \text{(6.7)}$

          $\overline{I}$ =   average UV intensity on the surface area during the passage through the disinfection chamber

          t_c =   residence time of the object in the disinfection chamber

The computer program SLABRES (Appendix 1) uses the calculated fluence from equation (6.6) to determine the surviving fraction of micro-organisms in a surface area using equation (6.1). The program then determines the overall surviving fraction on each side of the slab and the whole surface of the slab using equations (6.2) and (6.3).

6.3 Results

From the arrangement of UV sources shown in Figure 6.3, the computer program SLABAV calculated the average UV intensity, $\bar{I}$, over the surfaces of the slab-shaped object and the results are shown in Figure 6.5. The vertical surfaces facing the UV sources, sides 1 and 2, have a UV intensity approximately double the UV intensity on the other 4 surfaces of the slab, with the UV intensity decreasing towards the centre of the slab. The other surfaces of the slab have a more even UV intensity across their surfaces.

The Cartesian co-ordinates used in this figure are local co-ordinates to the slab surfaces. The origin of these co-ordinates is located in the top left hand corner of each surface. The greatest variation of UV intensity occurs on sides 1 and 2. By varying the residence time spent in the disinfection tunnel, t_c, the program SLABRES predicted the disinfection levels on each of the 6 surfaces of the object and the object as a whole. These results are shown in Figure 6.6 which shows the residence times necessary to achieve a given disinfection performance. As the UV intensity field is identical on opposite surfaces of the slab, the disinfection level for these opposite surfaces will be identical.

The results shown in Figure 6.6 are for an object whose surfaces provide no shielding to incident UV. It is possible to use the surface shielding parameters estimated for various surfaces in Chapter 4 to predict the disinfection performance that would be achieved if the surfaces of the slab-shaped object exhibited various degrees of shielding against incident UV. Figure 6.7 shows the disinfection level that would be produced for the object if its surfaces provided the same degree of shielding to UV as beef steaks (from the results of Stermer *et al.*, 1987) and dry Grades 2 and 6 filter papers (Whatman). The disinfection performance for surfaces providing no shielding is also shown for comparison.

159
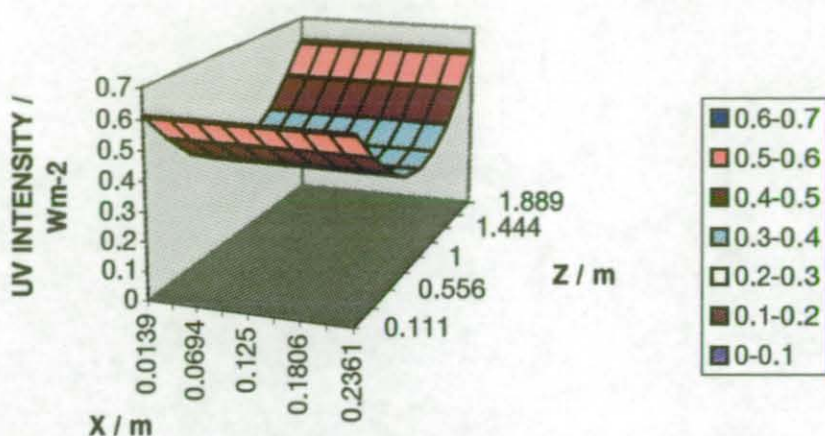
(a) Sides 1 and 2
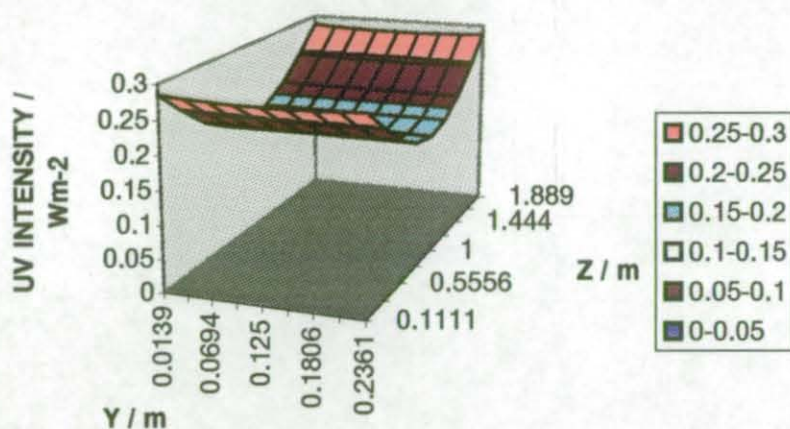
(b) Sides 3 and 4
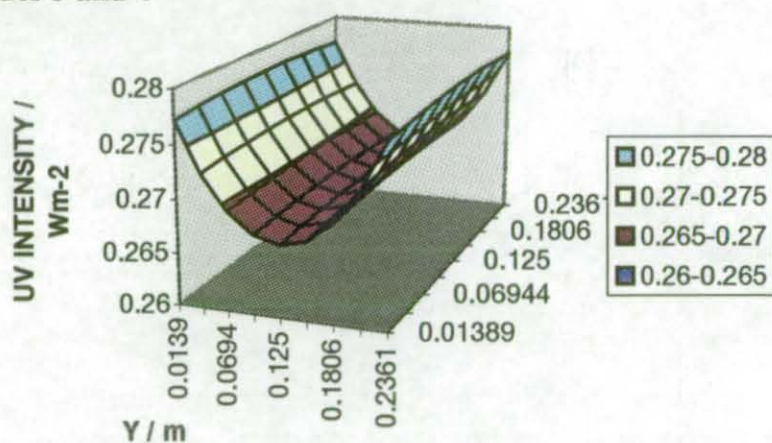
(c) Sides 5 and 6

FIGURE 6.5 **UV intensity fields on surfaces of the slab in the disinfection tunnel**
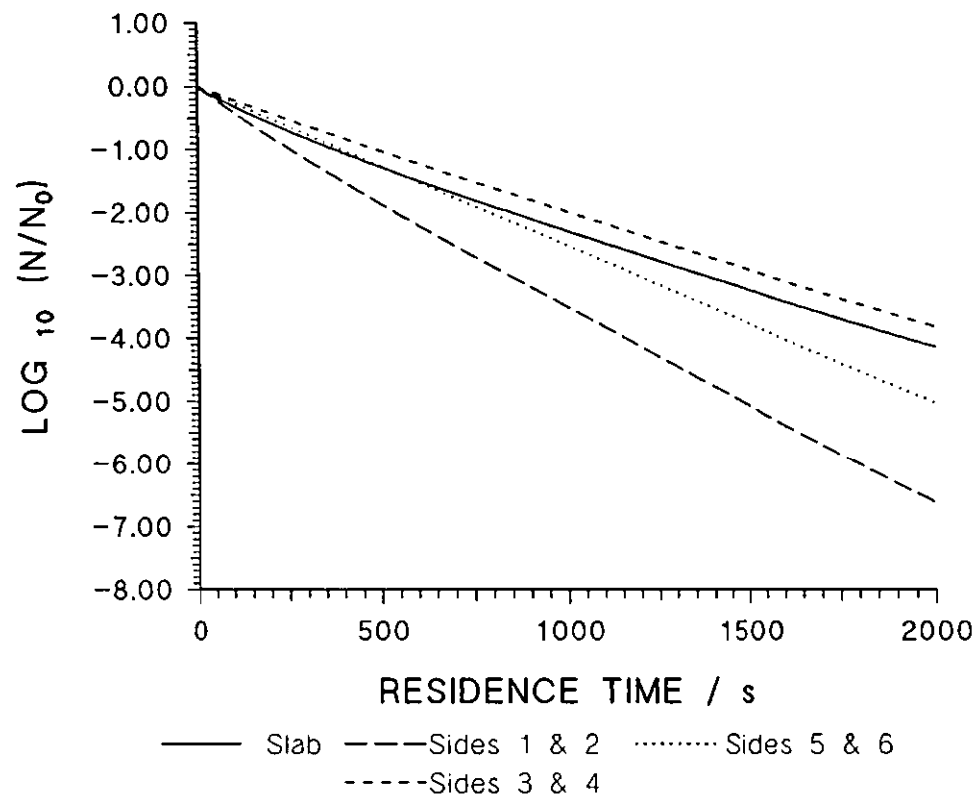
FIGURE 6.6   **Disinfection level produced on slab-shaped object in disinfection chamber employing horizontal UV source arrangement**
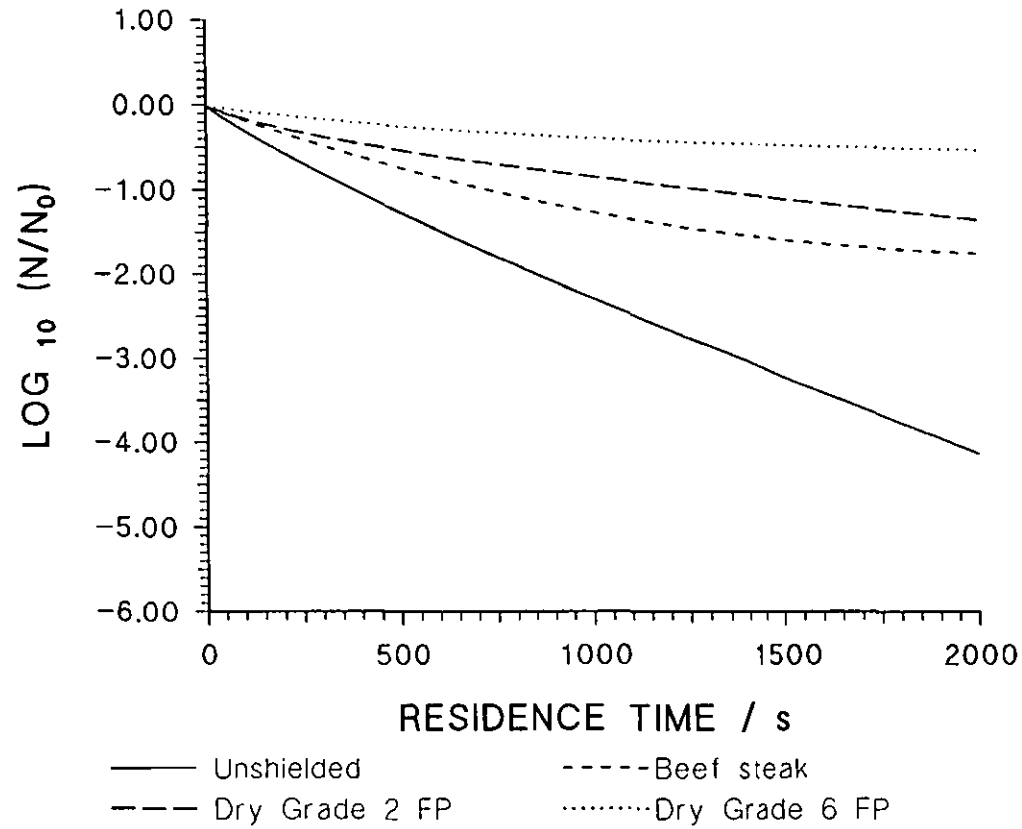
FIGURE 6.7   **Disinfection levels produced on slab-shaped object exposed to UV in the disinfection chamber for different surface exposure factors**

In order to see the effect of only partial coverage of a surface with 1% H_2O_2 spray on disinfection performance, the degree of coverage by spray was varied between 0 and 100%. It was assumed that the object provided no shielding to micro-organisms on the surface. The results are shown in Figure 6.8 and show that as coverage is increased from 0 to 100%, the residence time in the tunnel necessary to achieve identical levels of disinfection decreases to approximately 0.17 times the previous value.

As previously mentioned, the arrangement of the UV sources on the walls of the disinfection tunnel could be varied. Many variations could have been accommodated by the model but in the example described below the effect of increasing the number of horizontal UV sources on the walls was considered. The arrangement used, shown in Figure 6.9, was similar to that shown in Figure 6.3 except that the top and bottom UV sources were located 2 metres above and below the top and bottom surfaces of the slab respectively. Additional UV sources could be evenly distributed between the top and bottom UV sources. The number of UV sources per tunnel section of constant UV intensity was varied between 4 (i.e. 2 per wall) and 20 for a constant residence time in the disinfection chamber of 1000 seconds. The results are shown in Figure 6.10 where it is seen that increasing the number of sources above 8 makes no difference to the disinfection performance for the whole slab.

A further variation in the arrangement of the UV sources was considered. The orientation of the UV sources was changed so that the UV sources were vertically positioned on the walls of the disinfection chamber. Two UV sources per wall per unit tunnel section were employed with the centres of the UV lamps level with the top and bottom of the slab-shaped object in the centre of each 1m wall panel section. Using this arrangement, the average UV intensity for each surface area was calculated using SLABAV and the disinfection levels produced calculated using SLABRES. The UV intensity fields produced on the object's surfaces are shown in Figure 6.11. The disinfection level produced on the slab-shaped object when there is no shielding to incident UV is shown in Figure 6.12.
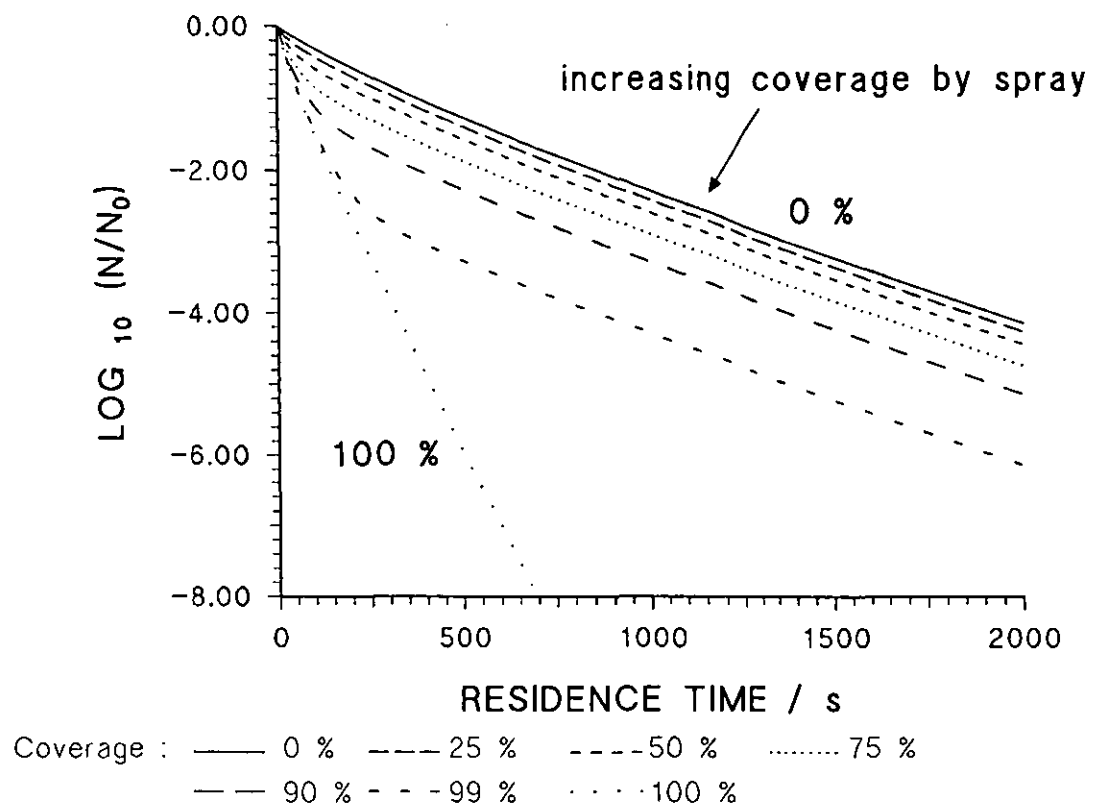
FIGURE 6.8 Disinfection level produced on slab-shaped object in the disinfection chamber when exposed to UV and 1.0 w/v% H$_2$O$_2$ spray of differing fractional surface coverage
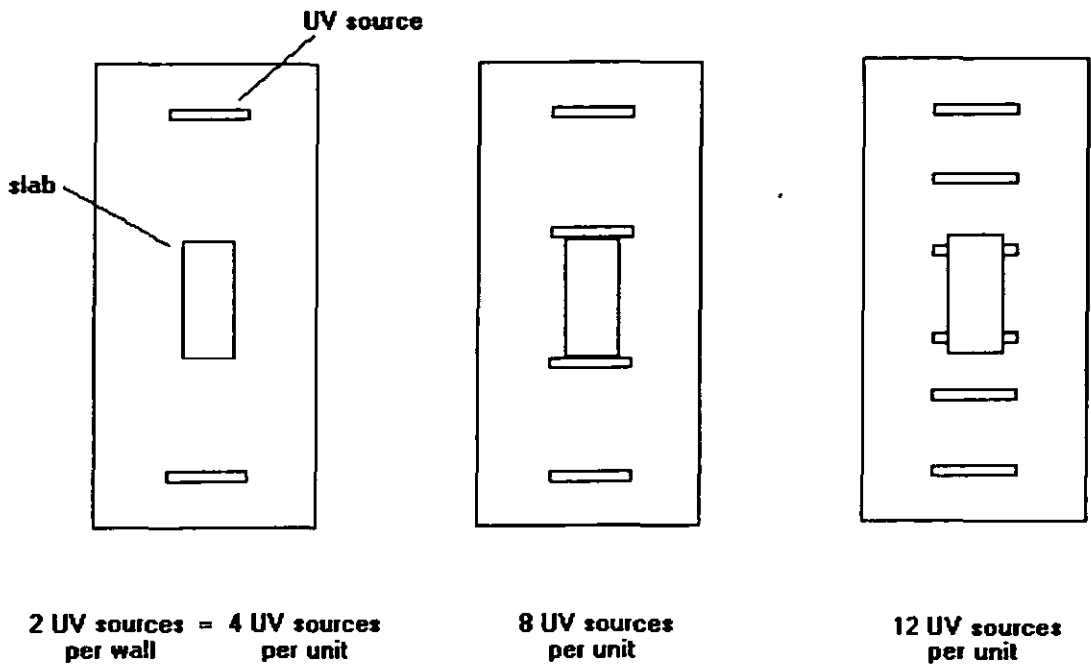
Figure 6.9   Increasing the number of evenly-distributed UV sources on the walls of the disinfection tunnel

6.4 Discussion

Two arrangements of UV source orientation were considered - horizontal and vertical. A comparison of Figures 6.6 and 6.12 shows that the horizontal UV source arrangement produced the greater overall disinfection performance for the same residence time. The disinfection rates on the individual surfaces using the horizontal arrangement showed less variation than was the case with the vertical UV source arrangement. Figure 6.12 shows that the disinfection rates on the vertical surfaces of the object (sides 1 - 4) were faster using the vertical source arrangement than the corresponding disinfection rates for the horizontal arrangement. However as the UV intensity on the top and bottom surfaces (sides 5 and 6) produced was far lower, the disinfection rate for the whole object tends to that of sides 5 and 6 as the survival level

165
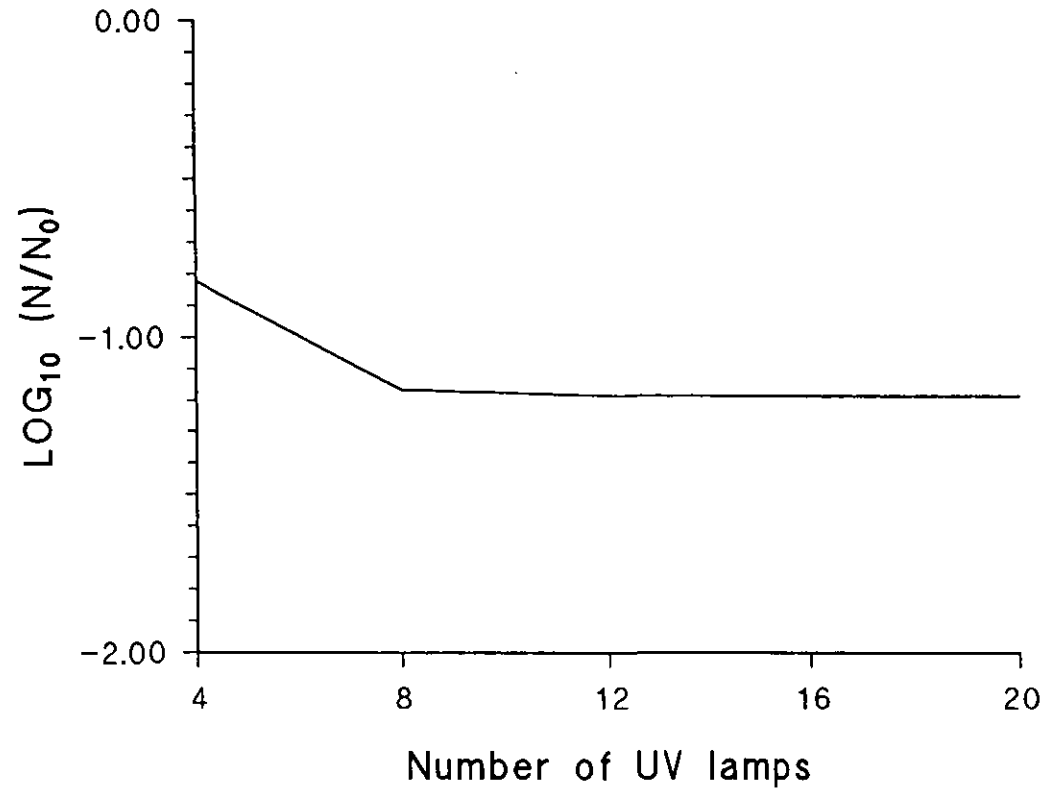
FIGURE 6.10 Disinfection level achieved in disinfection tunnel using different numbers of UV lamps per repeatable tunnel section
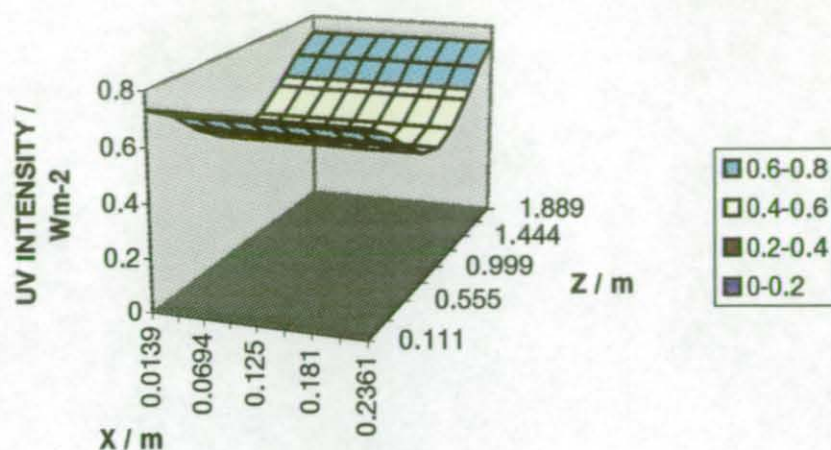
(a) Sides 1 and 2
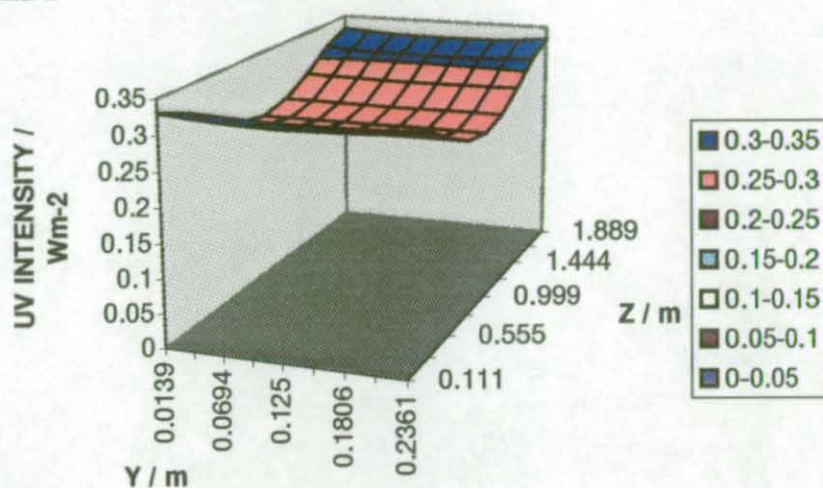
(b) Sides 3 and 4
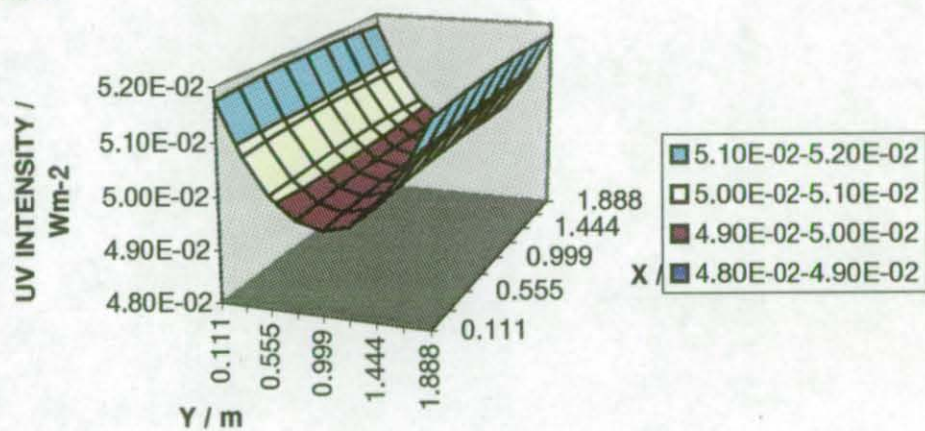
(c) Sides 5 and 6

FIGURE 6.11   UV intensity on slab-shaped object in disinfection chamber using vertical UV source arrangement
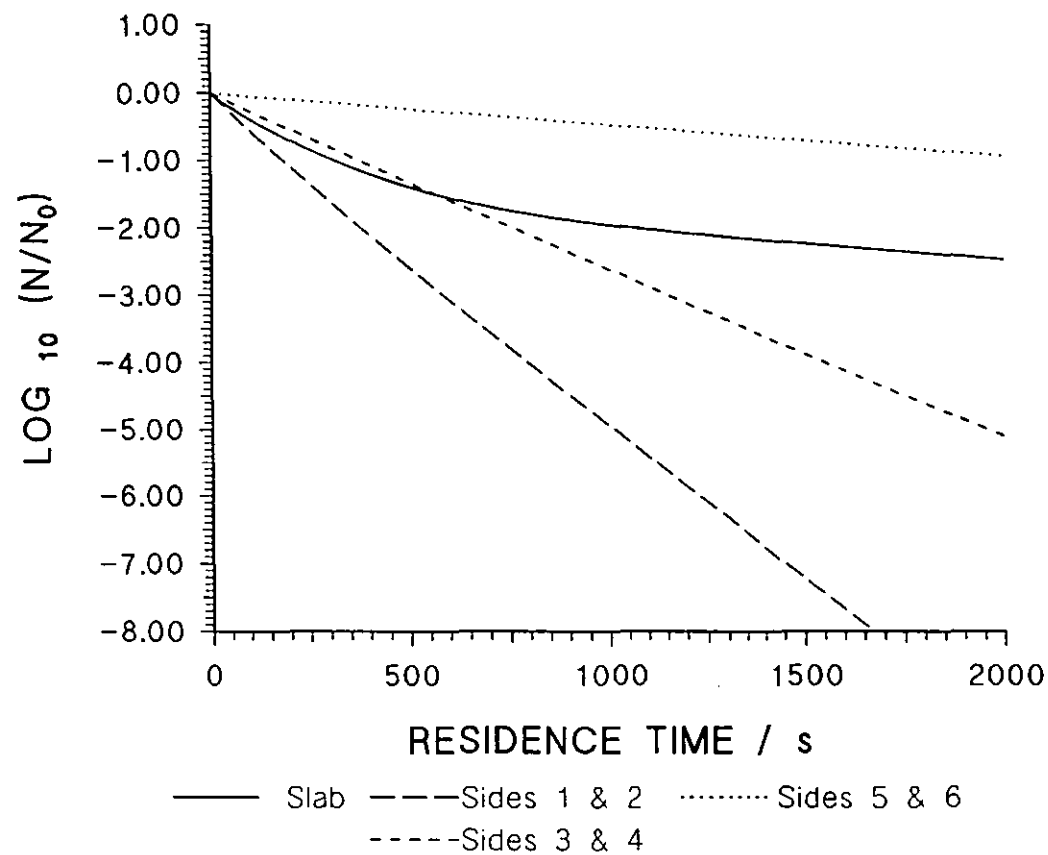
FIGURE 6.12 Disinfection rate on slab using vertical UV source arrangement in disinfection tunnel

on the other 4 sides of the slab tends to zero. This result demonstrates that it is important to chose an arrangement of UV sources leading to approximately even UV intensities on the object surfaces. This avoids the situations occurring where overall disinfection rate is limited by individual surfaces.

These results show that the UV sources are best employed in a vertical arrangement for the vertical surfaces of the slab (sides 1 - 4) and best employed in a horizontal arrangement for the horizontal surfaces of the slab (sides 5 - 6). Therefore a prudent design would include both horizontal and vertical UV sources to ensure a more even UV intensity over the surfaces of the object.

Figures 6.6 and 6.12 show the disinfection level produced by a specified residence time within the disinfection chamber. The disinfection level shown is based on a calculated UV fluence. Thus the effect of doubling the UV intensity is to produce the same disinfection levels at half the residence time. Therefore the disinfection curves shown can be used to predict the disinfection levels that would be achieved for different UV intensities using the same UV source arrangement. However if the number of UV sources or their locations are changed then the UV intensity fields must be recalculated.

Figure 6.10 shows an example of where increasing the number of UV sources does not produce a great improvement in the disinfection level. In the case considered, increasing the number of UV sources had relatively little effect on the top and bottom surfaces of the slab. Thus the disinfection levels on the vertical surfaces become much greater but the overall disinfection rate for the object becomes limited by the top and bottom surfaces whose disinfection rates are not increasing with additional UV sources. One possibility not considered here was to situate UV sources on the floors and ceiling of the tunnel.

Figure 6.7 showed the effect of surface shielding from incident UV on the disinfection level obtained. It is seen that in the cases considered, the disinfection level obtained was greatly reduced where surface shielding occurred. It is also seen from Figure 6.7 that the disinfection rate becomes smaller at higher fluences and tends to 'tail off' to a plateau region. In these cases increasing the UV intensity on the object, either by increasing the number of UV sources or the residence time, will produce little to no additional disinfection of the object. One example of this is the surface of beef steaks (from the results of Stermer *et al.*, 1987). The zonal shielding model fitted a third zone in which the micro-organisms were virtually completely shielded from incident UV. Therefore the number of viable micro-organisms in this zone will be fairly insensitive to the UV dose applied. This again shows that simply increasing the number of UV sources will not necessarily increase the disinfection performance. A slight increase in disinfection performance may not be economically worthwhile when balanced against the capital and operating costs of additional UV sources. Thus a designer should chose the UV source arrangement carefully.

Figure 6.8 shows that the fraction of the object's surfaces covered by 1% H_2O_2 spray when in the presence of UV greatly influences the disinfection level obtained. It was seen in Chapter 3 that the disinfection rate for *B.subtilis* spores exposed to UV + 1% H_2O_2 was greater than that when the spores were exposed to UV alone. If a surface is not fully covered with H_2O_2 spray then the covered surface areas are disinfected more quickly and the microbial count tends to zero in those areas. The remaining uncovered areas are disinfected less quickly and as the microbial count in the spray-covered surface areas tends to zero, the disinfection rate tends to that in the uncovered surface areas. This is clearly seen in Figure 6.8 for surfaces with uncovered areas. The gradient of the disinfection curve for these surfaces tends to that of the disinfection curve for UV alone as the residence time increases.

This result shows that it is very important to obtain full coverage of the object's surfaces with H_2O_2 spray because the disinfection performance is very sensitive to the

fractional coverage of the surface, e.g. note the difference between 99% and 100% coverage of the surface on the disinfection level obtained. The sensitivity of the disinfection performance to the fractional coverage of the surface can also explain why the experimental disinfection results obtained with peroxide sprays within the disinfection chamber (see Chapter 3) were more variable than those obtained with UV as the sole disinfectant.

6.5 Conclusions

It is seen from this example that it is possible to predict the disinfection rate for a specific micro-organism on an object if the incident UV intensity and surface shielding are known. All the predictions made here assumed that the surfaces were contaminated with *B.subtilis* spores which Toledo *et al.* (1973) claimed was one of the most resistant micro-organisms to H_2O_2. Real surfaces are therefore likely to be contaminated with more susceptible organisms and therefore the predictions here are conservative.

This approach is quite intensive and would only be used as a more detailed design stage after initial calculations using simpler line source with spherical emission (LSSE) UV intensity models which would not take into account such factors as the view factors and surface shielding factors on an object surface when calculating the disinfection level. These would be sufficient to provide very approximate values of disinfection levels.

The example considered here demonstrated that it is important to avoid large differences in the disinfection rates on the object as the disinfection rate tends to the lowest disinfection rate as the overall survival is reduced. This can be ensured with careful arrangement of the UV sources. The UV intensity field models can be applied to any object geometry and provide a useful tool in ensuring an even UV intensity field

pattern across the surfaces of the object. When using the combined UV + 1% H_2O_2 spray disinfection system, the results obtained showed that it was important to achieve full coverage of the object surface in order to avoid variable disinfection rates. This must be balanced against over use of peroxide spray due to legal limits on the levels of hydrogen peroxide that are permitted in foodstuffs for example, which is 0.1 ppm (Toledo *et al.*, 1973).

6.6 Notation

a_k = fraction of total surface area of object on surface k

f_c = fraction of surface covered by spray

f_j = fraction of micro-organisms in zone j (zonal shielding model)

F_s = fluence incident at surface

$g(F)$ = function giving fractional survival in terms of fluence received by micro-organisms

I_s = UV intensity incident on surface

k = multi-target equation rate coefficient

k_1 = first-order rate coefficient

N = microbial surface concentration

N_0 = initial microbial surface concentration

n = number of targets in multi-target equation

n_{sc} = number of sections of constant UV intensity comprising the disinfection tunnel

n_{so} = number of surfaces on an object

n_{sp} = number of surface areas of constant UV intensity comprising a surface

n_z = number of zones (zonal shielding model)

t = exposure time

t_c = residence time in disinfection tunnel

y	=	fractional survival
$\bar{y}$	=	overall fractional survival
$\bar{y}_{obj}$	=	overall fractional survival on an object
$\bar{y}_{surf}$	=	overall fractional survival on a surface
α_j	=	surface view factor in zone j (zonal shielding model)

7. OVERALL CONCLUSIONS AND SUGGESTIONS FOR FURTHER WORK

7.1 Overall Conclusions

1. The experimental techniques developed in this work enabled the inactivation of *B.subtilis* spores associated with solid surfaces to be investigated. Spore inactivation was brought about by UV irradiation, peroxidation and ozonation applied either singly or in combination. No single method of spore deposition was universally applicable either for all surfaces or for all the disinfection treatments examined.

2. Kinetic models, either first order or multi-target, were fitted to the experimental data and enabled comparisons of the disinfection treatments to be made. Combinations of UV and H_2O_2 were shown to act synergistically in inactivating spores and the greatest synergy was displayed at a H_2O_2 concentration of 1.0% w/v.

3. Ozone exhibited sporicidal activity against surface-associated *B.subtilis* spores when in gaseous form but not as a saturated aqueous solution. This was thought to be due to an interaction between the surface and aqueous ozone.

4. UV was shown to be more effective against *B.subtilis* spores on surfaces such as membranes than on others such as fibrous filter papers. This was attributed to the micro-topography of the surface affording the spores a measure of protection from incident UV.

5. A zonal shielding model was developed in which surface associated micro-organisms were assumed to be distributed between a finite number of zones each having a characteristic Exposure Factor which defined the degree of protection from incident UV afforded by that zone. Non-linear programming techniques were employed to

obtain solutions of the microbial distribution and of the Exposure Factors for each zone. In practice it was found that in all cases three zones were sufficient to describe the experimental data.

6. A mathematical UV field model was developed to predict the surface intensities on objects of regular geometry located within a UV field. Bioassay results and radiometer readings showed good agreement with the model.

7. The combination of the UV field model with experimentally obtained disinfection kinetics allowed predictions to be made of the rate of inactivation of *B.subtilis* spores on the surfaces of objects known geometry treated with either UV or UV and H_2O_2. The model developed was sufficiently versatile to enable application to any object of regular geometry in UV fields generated by various combinations of UV sources.

7.2 Suggestions for further work

7.2.1 Deposition of Test Micro-organisms on Surfaces

Whilst enabling useful kinetic data to be obtained for the inactivation of *B.subtilis* spores on a variety of surfaces, the experimental techniques employed here did reveal some limitations. Loss of spores occurred from surfaces due to physical wash-off by aqueous hydrogen peroxide but also occurred under conditions when washoff could not have been the cause. The actual cause was never determined but was related to the use of the air-atomising nozzle and might possibly have involved electrostatic forces.

A method of immobilising a test organism in a suitable matrix could eliminate these difficulties. One possible contender in this regard is pectin. The test organism would need to be suspended in pectin whilst the latter was in molten form. The pectin would then be sprayed onto solid objects whereupon it would harden to produce a gel, in a manner similar to that employed in the food industry to glaze confectionery. Following

175

irradiation, the gel film would be peeled off and the organism recovered by treating with the enzyme pectinase. Preliminary studies have shown that *B.subtilis* spore viability was not adversely affected by pectinase. In addition to reducing, or even eliminating, physical loss of the test organism, the possibility also exists that the matrices produced would be similar to the biofilms found in natural environments in which micro-organisms are present both on the surface and throughout the depth of the film (Blenkinsopp and Costerton, 1991). Moreover, the UV absorptive properties of the films could be modified by, for example, incorporating inert solid material such as talc. Another possibility is the prospect of employing species other than *B.subtilis* spores as test organisms. The use of micro-organisms more representative of the microflora of natural surfaces would enable more accurate estimates to be made of the conditions necessary to achieve required levels of disinfection. Spores are in general more resistant than vegetative forms (Block, 1983). Preliminary results obtained during the course of this work showed that a number of common surface-associated micro-organisms were unable to survive the desiccation which occurred during deposition of the organisms onto the test surfaces, but entrapment of such organisms within an aqueous gel might well significantly improve their survival.

7.2.2 Verification of the Zonal Shielding Model

The application of the zonal shielding model to materials providing a relatively high degree of shielding yielded solutions which implied the existence of discrete zones characterised by Exposure Factors which approached zero. Whilst it was acknowledged in Chapter 4 that surfaces would in reality comprise a distribution of exposure factors, the model nonetheless, predicates the existence of a fraction of the microbial population which would remain viable even at very high UV fluences. This prediction would need to be experimentally verified using materials which offered different degrees of surface shielding and would require the exposure of these materials to UV fluences of increasing magnitude whilst determining microbial survival.

7.2.3 Electrostatic Spraying

The work carried out here to investigate the effect of charging sprays of disinfectants on the disinfection levels obtained on surfaces was encouraging but inconclusive. This was primarily due to the shortcomings in the design of the disinfection chamber which promoted charge leakage and which resulted in a highly turbulent air flow pattern. Whilst use of the chamber provided necessary containment of the oxidising sprays, a fundamental redesign of the chamber would need to be undertaken to enable consistent results to be obtained with charged sprays. In particular, both the nozzle and the object would need to be more remote from surrounding structures which might provide a conduit to earth.

7.2.4 Predicting impact rates from spray nozzles

In order to predict the impact rate of sprays from a nozzle on a target surface, it would be necessary to have a model which could predict the spray density, drop size distribution and velocities at any given spatial location. If an air-atomised nozzle was used then the effect of the surrounding air on the spray droplets would increase with decreasing drop size until they are dominated by the surrounding air, as was the case with atomised sprays (Boothroyd, 1971). Further complications would arise when the air flow from the nozzle became turbulent at a given distance from the nozzle. To predict the impact on an object, it would be necessary to know the air-flow pattern around the object.

Commercially available computational fluid dynamic (CFD) packages could be used to solve the time-averaged Navier-Stokes equations describing the coupled air-spray droplet system. Certain parameters would need to be experimentally determined for the model. These include the drop size distribution of the spray at known distances from the nozzle, the droplet density across the spray angle and the velocity distribution of the drops. The model would allow the effects of variations in key design parameters

such as distance between nozzle and target, feed air pressure to the nozzle, electrostatic-charging of the nozzle etc. on disinfection performance to be investigated.

APPENDIX 1 - Computer programs

A1.1 Zonal Shielding model

A1.1.1 Background

The program ZONESHLD attempts to find a Karesh-Kuhn-Tucker point which solves the nonlinear programming problem described in Chapter 4. This listing of ZONESHLD uses first-order kinetics to describe unshielded UV disinfection kinetics for *B.subtilis* spores. However it is possible to employ other kinetic expressions. These should be placed in the OBJFUN subroutine (at the end of the program).

The number of variables to be solved for will depend on the number of active inequality constraints. The matrix, $\underline{X}$, of the variables to be solved for consists of the values of f and α in each of the n_z zones, λ, the Lagrangian multiplier for the equality constraint (4.9) and the Lagrangian multipliers, μ, for the active inequality constraints (4.10).

$$\underline{X} = \begin{bmatrix} f_1 \\ \vdots \\ f_{n_z} \\ \alpha_1 \\ \vdots \\ \alpha_{n_z} \\ \lambda \\ \mu_1 \\ \vdots \\ \mu_{2n_z} \end{bmatrix}$$

Thus $\underline{X}$ can contain between $(2n_z + 1)$ and $(4n_z + 1)$ variables to be solved for.

The form of equation (4.11) which describes the sum of the square of the errors, S, does not readily lend itself to differentiation. Approximate values of the derivatives were obtained using centre-spaced finite difference methods, which are derived from the Taylor series (Bajpai *et al.*, 1988). The first and second derivatives of the Lagrangian, L, with respect to two variables, x_1 and x_2, are given by the following equations :

179

$$\left(\frac{\partial L}{\partial x_1}\right) \approx \frac{L(x_1 + h) - L(x_1 - h)}{2h} \qquad \text{(A1.1)}$$

$$\left(\frac{\partial^2 L}{\partial x_1^2}\right) \approx \frac{L(x_1 + h) - 2L(x_1) + L(x_1 - h)}{h^2} \qquad \text{(A1.2)}$$

$$\left(\frac{\partial^2 L}{\partial x_1 \partial x_2}\right) \approx \frac{L\left(\frac{x_1 + h}{x_2 + h}\right) - L\left(\frac{x_1 - h}{x_2 + h}\right) + L\left(\frac{x_1 - h}{x_2 - h}\right) - L\left(\frac{x_1 + h}{x_2 - h}\right)}{4h^2} \qquad \text{(A1.3)}$$

where h is the finite difference mesh spacing. Consistent results were obtained with values of h between 10^{-3} and 10^{-5}.

The nonlinear simultaneous equations, $\nabla L = 0$, must be solved by iterative methods. Using Newton's method (Bajpai *et al.*, 1988), the following equations can be written :

$$\nabla^2 L(\underline{X}_k) \cdot \underline{p}_k = -\nabla \underline{L}(\underline{X}_k) \qquad \text{(A1.4)}$$

$$\underline{X}_{k+1} = \underline{X}_k + \underline{p}_k \qquad \text{(A1.5)}$$

where $\underline{p}_k$ is the step to be taken from the k th approximation to $\underline{X}$.

The initial values of $\underline{X}$ are set by random numbers in the INIT subroutine. At each approximation to $\underline{X}$, $\nabla^2 \underline{L}(\underline{X}_k)$ and $\nabla \underline{L}(\underline{X}_k)$ can be determined using equations (A1.1) - (A1.3). Equation (A1.4) is then solved for p_k using Gaussian elimination (Bajpai *et al.*, 1987) and the next approximation to $\underline{X}$ is then calculated using equation (A1.5). Successive approximations to $\underline{X}$ are determined by this method until the root geometric mean of the residuals of $\nabla L = 0$ is less than or equal to a specified tolerance, CONVTOL.

If the program is successful then the final value of $\underline{X}$ is displayed, together with the value of S and the root geometric mean of the residuals. During processing, if the program cannot proceed further due to encountering a singular matrix or an infeasible point (e.g. a point which required the log of a negative number to be calculated) then the program will terminate and display the point at which lowest value of the sum of the square of the errors, S, was encountered.

ZONESHLD was written in a compilable BASIC language called POWERBASIC

180

(Spectra Publishing, Sunnyvale, CA, USA) and run on a Pentium PC.

A1.1.2 Program listing

```
REM                                                              .
REM         ZONESHLD
REM
REM         A program to solve the Zonal Shielding model by searching for
REM         Karesh-Kukn-Tucker points.
REM
            $DYNAMIC   ·
            DEFDBL A-Z          'default to double precision
REM
            F = 0.000   'objective function (Lagrangian)
            S = 0.000   'sum of the square of the errors
REM
            NAC% = 0            'number of active constraints
            NZ% = 4            'number of zones
            N% = 2*NZ%+1+NAC%        'number of variables on which objective function
REM                                  'depends
REM
            NMAX% = 4*NZ%+1                    'maximum number of variables that may be solved for
REM
REM         Active constraints
REM
            DIM AC%(2*NZ%)
            DIM G(4*NZ%)
REM
REM         Experimental data (shielded surface)
REM
            NP%=26                    'number of data points
            DIM FS(NP%)               'surface fluence at each data point
            DIM YEXP(NP%)             'log10 survival at each data point
REM
            K1 = 2.13E-2                  '1st order constant for unshielded kinetics
            KL = 0.434294481    'log base conversion factor
REM
            DIM X(NMAX%)                      'variables (maximum number possible)
REM
            DIM DF(NMAX%)                     '1st derivatives
            DIM D2F(NMAX%,NMAX%)             '2nd derivatives
REM
            ONE = 0.000            'objective function at each of the 4 points
            ONW = 0.000            'used to calculate the second derivatives
            OSE = 0.000
            OSW = 0.000
REM
            FE = 0.000            'objective function at the 2 points used for 1st
            FW = 0.000            'derivative
REM
            DIM XE(NMAX%)    'working arrays
            DIM XW(NMAX%)
REM
            DIM XNE(NMAX%) 'working arrays
            DIM XNW(NMAX%)
            DIM XSE(NMAX%)
            DIM XSW(NMAX%)
REM
REM         ********* finite difference mesh spacing **************
            H = 1E-5
REM         ****************************************************
REM
            DIM P(NMAX%)      'step direction from Newton-Raphson method
REM
            RGM = 0.0            'root geometric mean
```

181

```
        CONVTOL = 2E-2    'convergence tolerance
        TOL = 1E-3        'variable tolerance
REM
        DIM F1(NMAX%)     'working variable
        DIM X1(NMAX%)     'ditto
REM
        DIM PR(NMAX%)     'residuals adjustments to search direction
        DIM R(NMAX%)      'residuals
REM
        DIM A(NMAX%,NMAX%)        'matrices for Gaussian elimination
        DIM B(NMAX%)
REM
        DIM A0(NMAX%,NMAX%)       'array to store original A matrix
        DIM B0(NMAX%)             'array to store original B matrix
REM
        DIM XBEST(NMAX%)          'variables to record best point encountered
        RGMBEST = 1E6
        SBEST = 1E6
REM
REM     Define error trapping code (declaratives)
REM
        ON ERROR GOTO 9000
REM
REM     ********************************************************************
REM               INITIATE VARIABLES
REM     ********************************************************************
REM
REM     Set up the experimental survival data for the shielded surface
REM
        CALL EXPER(FS(),YEXP(),NP%)
REM
REM     Set up the initial point
REM
        CALL INIT(X(),N%)
REM
REM     ********************************************************************
REM               STEP 1
REM     ********************************************************************
REM
REM     Set the flags to 0  ( 0 = no, 1 = yes )
REM
        SOLFLAG%=0        'solution reached flag
        ERRFLAG%=0        'error encountered flag
REM
        ITER2% = 1
REM
        DO WHILE SOLFLAG% = 0
REM
                N% = 2*NZ%+1+NAC%           'number of variables to solve for
REM
                CLS
                LOCATE 1,1
                PRINT "Pass number ";ITER2%; " through the main loop"
                PRINT
                PRINT NAC%; " active inequality constraints"
                PRINT
                INPUT Z9
                IF Z9 <> 0 THEN STOP
REM
                ITER% = 1              'counter for iterations performed in step 2 loop
REM
REM
REM     Find df(X) at the point at the start of the step 2 loop
REM
                GOSUB 1000            'calculate 1st order differentials
REM
                CALL CONVRESD(DF(),N%,RGM)
REM
REM
```

182

```
REM        Main loop - perform this loop until the residuals of df(X)=0 have
REM        been reduced to within the specified tolerance
REM
REM        ••••••••••••••••••••••••••••••••••••••••••••••••••••••••••••••••••
REM                    STEP 2
REM        ••••••••••••••••••••••••••••••••••••••••••••••••••••••••••••••••••
REM
                   DO WHILE RGM > CONVTOL
REM                                                                    .
REM

                        CLS
                        LOCATE 1,1
                        PRINT "Iteration:"; ITER%; " in step 2 loop"
                        LOCATE 3,1
                        PRINT "RGM = ";RGM
                        LOCATE 5,1
                        PRINT "Current X matrix is"
                        PRINT
                        FOR K%=1 TO N%
                                PRINT K%,X(K%)
                        NEXT K%
                        IF ERRFLAG% = 1 THEN
                                PRINT
                                PRINT "Error encountered on last iteration - continuing from best point"
                                ERRFLAG% = 0
                        END IF
                        PRINT
                        PRINT "Hit enter to continue"
                        INPUT Z1
                        IF Z1 <> 0 THEN STOP
REM
REM        Not reached the solution. Thus must perform another iteration.
REM
                        IF S < SBEST THEN
                                FEAS%=1
                                FOR I%=1 TO 2*NZ%
                                        IF X(I%) < -TOL OR X(I%) > ( 1.000 + TOL ) THEN
                                                FEAS%=0
                                        END IF
                                NEXT I%
                                IF FEAS% = 1 THEN 'no bounds violated
                                        RGMBEST = RGM
                                        SBEST = S
                                        FOR J%=1 TO N%
                                                XBEST(J%) = X(J%)
                                        NEXT J%
                                END IF
                        END IF
                   END IF
REM
REM        Calculate the 2nd derivatives of the equations using finite differences
REM
                        GOSUB 2000          'calc 2nd order derivatives
REM
REM
REM        Solve for the step direction using Gaussian elimination
REM
REM        First set up -df(X) in F1 array
REM
                        FOR K%=1 TO N%
                                F1(K%) = -DF(K%)
                        NEXT K%
REM
REM        Now call the Gaussian elimation routine to solve for P
REM
                        GOSUB 5000          'Gaussian elimination routine
REM
REM        Determine how far to move in the search direction and then perform
REM        the move
REM
```

183

```
                              CALL STEPSIZE(X(),P(),N%)
REM
REM
REM        Calculate df(X)
REM
                        GOSUB 1000            'calc 1st order derivatives
                        CALL CONVRESD(DF(),N%,RGM)            'determine RGM
REM
REM                                                                    '
                        ITER% = ITER% + 1
REM
REM
REM        End of stage 2
REM
                LOOP                                     .
REM
REM        ••••••••••••••••••••••••••••••••••••••••••••••••••••••••••••••••
REM                    STAGE 3
REM        ••••••••••••••••••••••••••••••••••••••••••••••••••••••••••••••••
REM
REM
REM    Step 3 of the iterative set strategy
REM
REM        Set up flags ( 0 = no, 1 = yes )
REM
300                GFLAG%=0                    'inequality constraints violated
                   MUFLAG%=0                   'negative multipliers for inequality constraints
REM
REM
REM        Check to see if any inequality constraints have been violated
REM
                FOR I%=1 TO NZ%
REM
REM        Check lower bounds
REM
                        IF X(I%) < -TOL OR X(I%+NZ%) < -TOL THEN
                                GFLAG%=1
                        END IF
REM
REM        Check upper bounds
REM
                        IF X(I%) > (1.0000 + TOL) OR X(I%+NZ%) > (1.0000 + TOL) THEN
                                GFLAG%=1
                        END IF
REM
                NEXT I%
REM
REM        Check to see if there are any negative Lagrangian multipliers for
REM        active inequality constraints.
REM
                IF NAC% > ZERO THEN
REM
                        FOR I%=1 TO NAC%
                                IF X(2*NZ%+1+I%) < -TOL THEN
                                        MUFLAG%=1
                                END IF
                        NEXT I%
                END IF
REM
REM        Check to see if solution reached
REM
                IF GFLAG%=0 AND MUFLAG%=0 THEN
                        SOLFLAG%=1
                        GOTO 500            'display final results and stop
                END IF
REM
REM        ••••••••••••••••••••••••••••••••••••••••••••••••••••••••••••••••
REM                    STEP 4A
REM        ••••••••••••••••••••••••••••••••••••••••••••••••••••••••••••••••
REM
```

184

.

```
REM        Step 4a of the iterative set strategy
REM        ( Remove the inequality constraint with the largest negative multiplier)
REM
REM

                    LNM% = 0              'number of the largest negative multiplier
                    VLNM = 0             ' value of the largest negative multiplier
REM
                    IF NAC% > ZERO AND MUFLAG% = 1 THEN
REM
REM        Find largest negative Lagrangian multiplier
REM
                         FOR I%=1 TO NAC%
                              IF X(2*NZ%+1+I%) < VLNM THEN
                                        VLNM = X(2*NZ%+1+I%)
                                        LNM% = I%
                              END IF
                         NEXT I%
REM
REM        Remove this multiplier from the active set
REM
                         IF LNM% < 2*NZ% THEN
REM
REM        Shift constraints up 1 in the matrix
REM
                              FOR I%=LNM% TO NAC%
                                   K% = 2*NZ%+1
                                   X(K%+I%) = X(K%+I%+1)
                                   AC%(I%) = AC%(I%+1)
                              NEXT I%
                         END IF
REM
                         X(4*NZ%+1) = 0.000000
                         AC%(2*NZ%) = 0.000000
REM
                         NAC% = NAC% - 1
REM
                    END IF
REM
REM ************************************************************
REM             STEP 4B
REM ************************************************************
REM
REM        Step 4b of the iterative set strategy
REM        ( Add all violated inequalities to the active set )
REM
REM
REM        Check lower bounds
REM
                    FOR I%=1 TO 2*NZ%
REM
                         IF X(I%) < -TOL THEN
REM
REM        add to active set
REM
                              NAC% = NAC% + 1
                              AC%(NAC%) = I%
REM
REM        set the variable to the bound value and its Lagrangian multiplier to 1
REM
                              X(I%) = 0.0000
                              X(2*NZ%+1+NAC%) = 1.0000
                         END IF
                    NEXT I%
REM
REM        Check upper bounds
REM
                    FOR I%=1 TO 2*NZ%
REM
                         IF X(I%) > (1.000 + TOL) THEN
```

185

```
REM
REM        add to active set
REM
                                    NAC% = NAC% + 1
                                    AC%(NAC%) = I%+2*NZ%
REM
REM        set the variable to the bound value and its Lagrangian multiplier to 1
REM
                                    X(I%) = 1.00000
                                    X(2*NZ%+1+NAC%) = 1.00000
                        END IF
                NEXT I%
REM
REM
REM        Reset inital estimates of all active multipliers to 1
REM
                X(2*NZ%+1) = 1.00000
REM
                FOR I% = 1 TO 2*NZ%
                        X(I%+2*NZ%+1) = 0.0000
                NEXT I%
REM
                FOR I%=1 TO NAC%
                        X(2*NZ%+1+I%) = 1.00000
                NEXT I%
REM
REM        Return to Step 2
REM
                ITER2% = ITER2% + 1
REM
        LOOP
REM
        STOP
REM
REM        ***********************************************************
REM                SOLUTION REACHED - DISPLAY RESULTS
REM        ***********************************************************
REM
500     CLS
        PRINT "Solution reached after ";ITER2%;" iterations"
        PRINT
        PRINT "RGM= ";RGM; "        S = ";S
        PRINT
REM
        FOR I%=1 TO 2*NZ%
                PRINT I%,X(I%)
        NEXT I%
REM
        STOP
REM
REM        *********************************************************
REM                CALCULATE 1st ORDER DIFFERENTIALS
REM        *********************************************************
REM
1000    H1 = 0.5 / H
REM
        FOR I%=1 TO N%
REM
                FOR J%=1 TO N%
                        XE(J%) = X(J%)
                        XW(J%) = X(J%)
                NEXT J%
REM
                XE(I%) = XE(I%) + H
                XW(I%) = XW(I%) - H
REM
                CALL OBJFUN(FE,XE())
                CALL OBJFUN(FW,XW())
REM
```

186

```
                        DF(I%) = ( FE - FW ) * H1
            NEXT I%
REM
            RETURN
REM
REM     ••••••••••••••••••••••••••••••••••••••••••••••••••••••••••••••
REM               CALCULATE 2nd ORDER DIFFERENTIALS
REM     ••••••••••••••••••••••••••••••••••••••••••••••••••••••••••••••
REM
REM     Calculate the diagonal first (d2f/dxi2)
REM
2000    H2D = 1 / (H^2)
REM
        FOR I% = 1 TO N%
                FOR J%=1 TO N%
                        XE(J%) = X(J%)
                        XW(J%) = X(J%)
                NEXT J%
REM
                XE(I%) = XE(I%) + H
                XW(I%) = XW(I%) - H
REM
                CALL OBJFUN(FE,XE())
                CALL OBJFUN(FW,XW())
                CALL OBJFUN(F,X())
REM
                D2F(I%,I%) = ( FE - 2*F + FW ) * H2D
        NEXT I%
REM
REM     Now calculate the rest of the 2nd order differentials
REM
        H2 = 0.25 / (H^2)
REM
        FOR I% = 1 TO N%
                FOR J% = 1 TO N%
                        IF I% <> J% THEN
REM
                                FOR A%=1 TO N%
                                        XNE(A%) = X(A%)
                                        XNW(A%) = X(A%)
                                        XSE(A%) = X(A%)
                                        XSW(A%) = X(A%)
                                NEXT A%
REM
                                XNE(I%) = XNE(I%) + H
                                XNE(J%) = XNE(J%) + H
REM
                                XNW(I%) = XNW(I%) - H
                                XNW(J%) = XNW(J%) + H
REM
                                XSW(I%) = XSW(I%) - H
                                XSW(J%) = XSW(J%) - H
REM
                                XSE(I%) = XSE(I%) + H
                                XSE(J%) = XSE(J%) - H
REM
                                CALL OBJFUN(ONE,XNE())
                                CALL OBJFUN(ONW,XNW())
                                CALL OBJFUN(OSW,XSW())
                                CALL OBJFUN(OSE,XSE())
REM
                                D2F(I%,J%) = ( ONE - ONW + OSW - OSE ) * H2
REM
                        END IF
                NEXT J%
        NEXT I%
REM
        RETURN
```

187

```
REM
REM         ••••••••••••••••••••••••••••••••••••••••••••••••••••••••••••
REM               GAUSSIAN ELIMINATION
REM         ••••••••••••••••••••••••••••••••••••••••••••••••••••••••••••
REM
REM         SEARCH for the step direction
REM
REM         A general program to perform gaussian elimination with pivoting
REM         on the system  A.P = B.
REM
REM         First set up the A and B matrices from the values specified
REM
REM         Save the original A and B matrices - need these for residuals calculation
REM
5000        FOR I% = 1 TO N%
                    FOR J% = 1 TO N%
                            A(I%,J%) = D2F(I%,J%)
                            A0(I%,J%) = A(I%,J%)
                    NEXT J%
REM
                    B(I%) = F1(I%)
                    B0(I%) = B(I%)
            NEXT I%
REM
REM         Enter main loop
REM
            FOR L% = 1 TO (N% - 1)
REM
REM         Perform the pivotting
REM
                    CALL PIVOT(A(),B(),P(),N%,L%)
REM
REM         Now have the rows in the correct order after pivotting. Now perform
REM         Gaussian elimination to eliminate another variable.
REM
                    CALL GAUSS(A(),B(),P(),N%,L%)
REM
            NEXT L%
REM
REM         Finished the Gaussian elimination - calculate the results
REM
            P(N%) = B(N%) / A(N%,N%)
REM
            FOR I% = N%-1 TO 1 STEP -1

                    T1 = 0.00   'working variable
                    FOR J%=I%+1 TO N%
                            T1 = T1 + A(I%,J%) * P(J%)
                    NEXT J%
                    P(I%) = (B(I%) - T1) / A(I%,I%)
            NEXT I%
REM
REM         Restore A and B matrices for residuals calc
REM
            FOR I% = 1 TO N%
                    FOR J% = 1 TO N%
                            A(I%,J%) = A0(I%,J%)
                    NEXT J%
REM
                    B(I%) = B0(I%)
            NEXT I%
REM
REM         Calculate the residuals
REM
            CALL RESID(A(),B(),P(),R(),N%)
REM
REM
REM         Enter main loop
REM
```

```
          FOR L% = 1 TO (N% - 1)
REM
REM       Perform the pivotting
REM
                  CALL PIVOT(A(),R(),PR(),N%,L%)
REM
REM       Now have the rows in the correct order after pivotting. Now perform
REM       Gaussian elimination to eliminate another variable.
REM
                  CALL GAUSS(A(),R(),PR(),N%,L%)
REM
          NEXT L%
REM
REM       Finished the Gaussian elimination - calculate the results and exit
REM
          PR(N%) = R(N%) / A(N%,N%)
REM
          FOR I% = N%-1 TO 1 STEP -1

                  T1 = 0.00   'working variable
                  FOR J%=I%+1 TO N%
                          T1 = T1 + A(I%,J%) * PR(J%)
                  NEXT J%
                  PR(I%) = (R(I%) - T1) / A(I%,I%)
REM
                  P(I%) = P(I%) - PR(I%)
          NEXT I%
REM
REM       end of routine
REM
          RETURN
REM
REM
REM       *****************************************************************
REM           ERROR HANDLING (declaratives)
REM       *****************************************************************
REM
REM       An error occured - possibly division by zero, or trying to take the log
REM       of a non-positive number. Program has to stop. Show the user the
REM       point at which the lowest value of S, the sum of the square of the
REM       errors, was found.
REM
9000      CLS
          PRINT "Program terminated with error ";ERR
          PRINT
          PRINT "The point at which the lowest sum of the square of the errors was encountered was :"
          PRINT
          FOR I%=1 TO 2*NZ%
                  PRINT I%,XBEST(I%)
          NEXT I%
REM
          PRINT "S = ";SBEST; "      RGM = ";RGMBEST
REM
          STOP
REM
REM
          SUB INIT(X(),N%)
REM
REM       Set up the initial random values of X
REM
                  SHARED NZ%,NAC%
REM
REM       Randomize the number of seconds there have been since midnight.
REM       This should give a different set of initial values each time
REM       the program is run.
REM
                  RANDOMIZE TIMER
REM
REM       Randomized - now select the initial point
```

189

```
REM
                FLAG%=0
                DO WHILE FLAG%=0
                        T1 = 0.000
                        FOR I%=1 TO NZ%-1
                                X(I%) = RND
                                T1 = T1 + X(I%)
                        NEXT I%
REM
                        X(NZ%) = 1.000 - T1
                        IF X(NZ%) >= 0.000 AND X(NZ%) <= 1.000 THEN
                                FLAG%=1
                        END IF
                LOOP
REM
REM     Set alpha values
REM
                FOR I%=1 TO NZ%
                        X(I%+NZ%) = RND
                NEXT I%
REM
                X(N%) = 1.000                   'initial estimate of lamda
REM
REM     Set the Lagrangian multipliers for the inequality constraints
REM     to zero.
REM
                FOR I% = 2*NZ%+2 TO 4*NZ%+1
                        X(I%) = 0.0000
                NEXT I%
REM
                CLS
                PRINT "initial values:"
                PRINT
                FOR I%=1 TO N%
                        PRINT I%,X(I%)
                NEXT I%
                PRINT
                INPUT Z9
REM
        END SUB
REM
REM
        SUB EXPER(FS(),YEXP(),NP%)
REM
REM     Set up the experimental data to determine the sum of squares of the
REM     errors by
REM
                RESTORE 9998
REM
                FOR K%=1 TO NP%
                        READ FS(K%), YEXP(K%)
                        YEXP(K%) = LOG10(YEXP(K%))
                NEXT K%
REM
9998            DATA 177,0.3090, 354,0.1774
                DATA 708,0.0537, 1770,3.631E-4
REM
                DATA 88.5,0.4446, 177,0.1702
                DATA 354,0.09419, 708,0.2032, 1060,3.069E-3
                DATA 1420,5.30E-4, 1770,1.059E-4
REM
                DATA 523,0.05129, 1310,1.514E-3
REM
                DATA 278,0.1905, 556,0.0678, 1390,1.303E-3
REM
                DATA 60.8,0.578, 243,0.1567, 486,4.365E-2
                DATA 729,0.01148, 1220,2.40E-3
REM
                DATA 58.1,0.557, 116,0.412
```

190

DATA 232,0.1086, 464,0.04677, 697,0.01148

REM
    END SUB
REM
REM
    SUB PIVOT(A(),B(),X(),N%,L%)
REM
REM   Pivot the rows around so that the row with the largest coefficient
REM   for the variable about to be eliminated appears in the top row.   .
REM
REM   Find the row with the largest coefficient in the column of the
REM   A matrix for the variable that is to be eliminated.
REM
    DIM AT(N%)
    ROW% = 0
REM
    FOR I% = L%+1 TO N%
        IF ABS(A(I%,L%)) > ABS(A(L%,L%)) THEN
            ROW%=I%
        END IF
    NEXT I%
REM
    IF ROW% > 0 THEN
REM
REM   Need to pivot
REM
REM   Save the old top row in a temporary array and then swap the rows
REM   around.
REM
    FOR J%=1 TO N%
        AT(J%) = A(L%,J%)
        A(L%,J%) = A(ROW%,J%)
        A(ROW%,J%) = AT(J%)
    NEXT J%
REM
    BT = B(L%)
    B(L%) = B(ROW%)
    B(ROW%) = BT
    END IF
REM
    END SUB
REM
REM
    SUB GAUSS(A(),B(),X(),N%,L%)
REM
REM   Have pivotted the A matrix if necessary. Now must perform the
REM   Gaussian elimination step to eliminate the variable in the L%
REM   column.
REM
REM   Want to eliminate this variable from the subsequent N%-L% rows
REM   which contain it.
REM
    FOR I% = L% + 1 TO N%
REM
REM   Calc the elimination factor
REM
    ELIM = A(I%,L%) / A(L%,L%)
REM
    FOR J%=L% TO N%
        A(I%,J%) = A(I%,J%) - ELIM * A(L%,J%)
    NEXT J%
REM
    B(I%) = B(I%) - ELIM * B(L%)
    NEXT I%
REM
    END SUB
REM
REM
    SUB RESID(A(),B(),X(),R(),N%)

191

```
REM
REM        Calculate the residuals from the solution of the Gaussian elimination
REM
                   FOR I%=1 TO N%
REM
REM        Calculate A.X - B = R   (where X is the solution vector)
REM
                       R(I%) = 0.0000
REM
                       FOR J%=1 TO N%
                               R(I%) = R(I%) + A(I%,J%) * X(J%)
                       NEXT J%
REM
                       R(I%) = R(I%) - B(I%)
               NEXT I%
           END SUB
REM
REM
REM
           SUB STEPSIZE(X(),P(),N%)
REM
REM        Must determine a suitable step size in the search direction. Choose
REM        one which minimises the objective function
REM
                   BETA = 1.000
REM
REM        Chosen the step size - now perform the step
REM
                   FOR I%=1 TO N%
                           X(I%) = X(I%) + BETA * P(I%)
                   NEXT I%
REM
           END SUB
REM
REM
REM
           SUB CONVRESD(DF(),N%,RGM)
REM
REM        Calculate the root geometric mean
REM
                   RGM = 0.000
REM
                   FOR I%=1 TO N%
                           RGM = RGM + DF(I%)^2
                   NEXT I%
REM
                   RGM = SQR(RGM)
REM
           END SUB
REM
           SUB OBJFUN(F,X())
REM
REM        Calculate the objective function at X
REM
                   SHARED YEXP(),FS(),N%,NZ%,K1,KL,NP%
                   SHARED NAC%,G(),AC%(),S
REM
                   F = 0.00000
REM
                   FOR K%=1 TO NP%
REM
REM        Calculate Y (N/No) at the kth data point
REM
                       T1 = 0.000              'working variable
REM
                       FOR J%=1 TO NZ%
                               T1 = T1 + X(J%)*EXP( -K1 * X(J%+NZ%) * FS(K%) )
                       NEXT J%
REM
```
192

```
                        IF T1 > ZERO THEN
                                T1 = LOG10(T1)
                        ELSE
                                T1 = -10.000
                        END IF
REM
                        YK = T1
REM
                        F = F + ( YK - YEXP(K%) )^2          .
                NEXT K%
REM
                        S = F
REM
REM     Add the equality constraint's contribution to the Lagrangian
REM
                        T1 = 0.000
REM
                FOR I%=1 TO NZ%
                        T1 = T1 + X(I%)
                NEXT I%
REM
                        T1 = T1 - 1.00000
REM
                        F = F + X(2*NZ%+1) * T1
REM
REM     Add the contribution from the inequality constraints
REM
                FOR I%=1 TO 2*NZ%
                        G(I%) = -X(I%)
                        G(I%+2*NZ%) = X(I%) - 1.0000
                NEXT I%
REM
                T2 = 0.000
                IF NAC% > ZERO THEN
                        FOR J%=1 TO NAC%
                                T2 = T2 + X(2*NZ%+1+J%) * G(AC%(J%))
                        NEXT J%
REM
                        F = F + T2
                END IF
REM
REM
                END SUB
REM
                STOP
                END
```

A1.2 UV intensity programs

A1.2.1 Introduction

The ESSE model developed in Chapter 5 is a versatile model capable of predicting the UV intensity on a surface produced by a UV lamp of known emission power. The model can be re-arranged so that if the UV intensity on a surface is known then the power output of the lamp can be estimated. This is demonstrated in section A1.2.2. Section A1.2.3 details the programs used to calculate the UV intensities on objects of cylindrical geometry. Section A1.2.4 details the programs used to generate the results from Chapter 6 (for the

'disinfection tunnel').

A1.2.2 Determination of UV lamp power output

(a) Background

The program POWER.FOR is a Fortran 77 program which is used to calculate the power output of a UV lamp. When a UV intensity measurement is known at a given spatial location, it is possible to estimate the power output of the UV lamp that would give such an intensity if the UV lamp's emission characteristics can be described by the ESSE model (see equation 5.5).

The user must provide the UV intensity measurement, I, taken using the UV radiometer at the cylindrical-polar coordinate (r_1, l_1, θ_1). The user must specify the number of point sources which will comprise the UV source by setting the N_C, N_L and N_Z parameters (see Figure 5.2). On completion, the program will display the estimate of the power output of the UV lamp.

(b) Program listing

```
C
C   POWER.FOR
C
C   Extense source model employed to provide an estimate of
C   the power output of a lamp
C
C   By D.Gardner  (8/95)
C
C   The model assumes volumetric emmision from the lamp.
C
C   The program calculates the dimensionless intensity at a point
C   specified by the user (r1,l1,t1), which is merely the sum of the
C   dimensionless intensities from the individual point sources
C   which are evenly spaced throughout the lamp volume. This program
C   is for a non-absorbing medium.
C
    REAL*8 S,RL,LL,SP
    REAL*8 ISUM,I,R1,L1,T1,R,L,T,PI,RHOS
    REAL*8 RHO,EF,Z5
    REAL*8 X,X1,Y,Y1
C
    INTEGER NL,NC,NP,NZ
C
    PARAMETER (NC=10)
    PARAMETER (NL=10)
    PARAMETER (NZ=20)
C
```

194

```
C   Calculate number of point sources
C
    NP=2*NL*NC*NZ
C
    PI=3.141593
C
C   Define cylindrical polar co-ordinates at which UV intensity
C   was determined
C
    R1=(0.08 - 30.5E-3)
    T1=0
    L1=41E-3
C
C   UV lamp parameters
C
    I=6.29
    RL=7.5E-3
    LL=0.20
C
C
C   Sum intensities from individual point sources
C
    ISUM=0
C
    DO 100 J=1,NZ
            DO 200 K=1,NC
                    DO 300 M=1,2*NL
C
C   Calculate cylindrical co-ordinates of the point source
C
                            T=(M-1)*PI/NL
                            R=SQRT((K-0.5)*RL**2/NC)
                            L=(J-0.5)*LL/NZ
C
C   Calculate the square of the distance between the point source
C   and the point at which the intensity is being determined
C
                            RHOS=(R*SIN(T)-R1*SIN(T1))**2
                            RHOS=RHOS+(R*COS(T)-R1*COS(T1))**2
                            RHOS=RHOS+(L-L1)**2
C
C   Calculate cartesian forms
C
                            X=R*SIN(T)
                            Y=R*COS(T)
                            X1=R1*SIN(T1)
                            Y1=R1*COS(T1)
C
C   Calculate view factors
C
                            V1=ATAN(ABS(X1-X)/ABS(Y1-Y))
                            V1=COS(V1)
C
                            V2=ATAN(ABS(L1-L)/ABS(Y1-Y))
                            V2=COS(V2)
C
                            ISUM=ISUM+1/RHOS*V1*V2
C
C
C
C
300         CONTINUE
200     CONTINUE
100  CONTINUE
C
C
    SP=I*4*PI/ISUM
    S=SP*NP
C
```

195

```
      PRINT*,'THE POWER OUTPUT IS'
      PRINT*,S
C
C
      STOP
      END
```

A1.2.3 UV intensities on objects of cylindrical geometry

(a) Background

Two programs, VERT and VOLTARC, calculate the UV intensities at specified points on the vertical and horizontal surfaces of an object of cylindrical geometry respectively. For both programs only one UV source is specified. The results from these programs are then used by a third program, MULTIVOL, which is used to sum the UV fields produced by individual UV lamps in a multi-lamp system.

The view factors can be calculated by simple geometry. For example, for the vertical surface of a cylinder the view factors, (cos α) and (cos β), are calculated as follows :
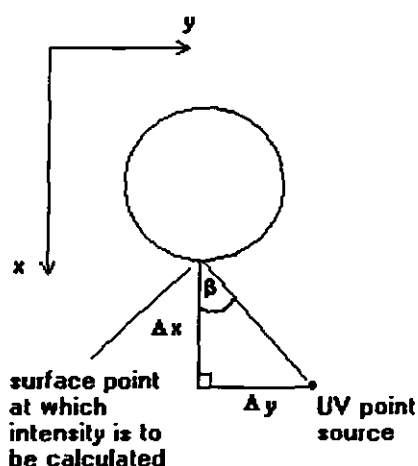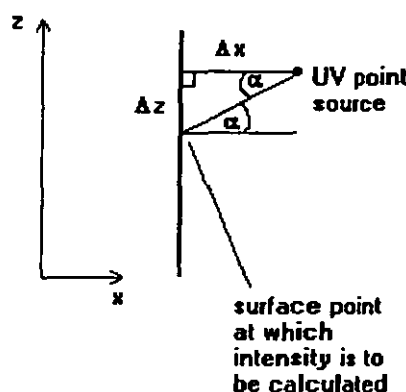
$$(\cos\beta) = \frac{\Delta x}{\sqrt{(\Delta x^2 + \Delta y^2)}} \qquad\qquad (\cos\alpha) = \frac{\Delta x}{\sqrt{(\Delta x^2 + \Delta z^2)}}$$

Once the view factors are known then equation (5.7) can be applied.

(b) Program listings

```
REM     VERT.BAS
REM
REM     A program to calculate the UV field, produced by 1 Voltarc source
```
196

```
REM        located in the rig, for the side of a cylindrical object.
REM
REM        PARAMETER LIST
REM
           PI=3.141592654
REM
REM     Cylinder
REM
           NA%=1
           NP%=120
REM
REM
REM        Voltarc lamp
REM
           NC%=3
           NL%=5
           NZ%=20
REM
REM        DEFINE INTENSITY STORAGE ARRAY
REM
           $DYNAMIC
REM
           DIM IO(NA%,NP%)
REM
REM        VARIABLE SET-UP
REM
REM        Lamp parameters
REM
           S=13.1
           AL=0.35
           WL=0.20
           RL=7.5E-3
           RD=0.08
REM
           NPS%=2*NL%*NC%*NZ%
           SP=S*WL/(AL*NPS%)
REM
REM        Object parameters
REM
           ORAD=0.033
           OH=0.000
           OSZ=0.00
REM
           CLS
           LOCATE 1,1
           PRINT "NUMBER OF POINT SOURCES SELECTED = "
           LOCATE 1,36
           PRINT NPS%
           LOCATE 3,1
           PRINT "NUMBER OF LAMP ZONES = "
           LOCATE 3,24
           PRINT NC%
           LOCATE 3,30
           PRINT "NUMBER POINTS IN EACH LAMP ZONE = "
           LOCATE 3,65
           PRINT NL%*2
REM
REM
REM        LAMP LOOPS - the contribution from each point source comprising the UV source
REM        must be taken into account
REM
           FOR L%=1 TO NC%
                   FOR M%=1 TO 2*NL%
REM

                           LOCATE 8,1
                           PRINT L%
                           LOCATE 8,10
                           PRINT M%
REM
```

197

```
REM        Calculate the radial and theta co-ordinates of the point source
REM

                    LR=SQR((L%-0.5)*RL^2/NC%)
                    LT=(M%-1)*PI/NL%
REM
REM        Calculate cartesian forms
REM

                    LX=RD+LR*COS(LT)
                    LY=LR*SIN(LT)
REM
REM        Establish limits for the object points able to see the UV
REM        point source output - calculate theta A and theta 1
REM

                    TA=ATN(LY/LX)
                    T1=ATN(SQR(LX^2 + LY^2 - ORAD^2)/ORAD)
REM
REM        First OBJECT loop - angular co-ordinate
REM

                FOR J%=1 TO NP%
                        OBT=(J%-1)*2*PI/NP%
REM
REM        Calculate object cartesian co-ordinates
REM

                        OX=ORAD*COS(OBT)
                        OY=ORAD*SIN(OBT)
REM
REM        Calculate delta x and delta y
REM

                    DX=LX - OX
                    DY=LY - OY
REM
REM        Limit calculations to those object points that receive some
REM        UV point source output
REM

                    IF OBT >= (TA-T1+2*PI) OR OBT <= (TA+T1) THEN
REM
REM        Final LAMP LOOP - height co-ordinate
REM

                    FOR K%=1 TO NZ%
                            LZ=(K%-0.5)*WL/NZ%
REM
REM        Select object point height
REM

                            FOR I%=1 TO NA%
                                IF NA%=1 THEN
                                        OBZ=OH
                                ELSE
                                        OBZ=OSZ - (I%-1)*OH/(NA%-1)
                                END IF
REM
                                DZ=OBZ - LZ
REM
REM        Calculate view factors
REM

                                VFA=ABS(DX)/SQR(DX^2 + DZ^2)
                                VFB=ABS(DX)/SQR(DX^2 + DY^2)
REM
REM        Calculate UV point source contribution to the object point, corrected
REM        for the view factors
REM

                                RHOS=DX^2 + DY^2 + DZ^2
                                IO(I%,J%)=IO(I%,J%)+(1/RHOS)*VFA*VFB
                            NEXT I%
                        NEXT K%
                    END IF
                NEXT J%
            NEXT M%
        NEXT L%
REM
```

198

```
REM        Multiply IO array through by the constant to obtain actual intensities
REM

           IMAX=0
REM

           FOR I%=1 TO NA%
                   FOR J%=1 TO NP%
                                  IO(I%,J%)=IO(I%,J%)*SP/(4*PI)
                                  IF IO(I%,J%)>IMAX THEN
                                               IMAX=IO(I%,J%)
                                  END IF
                          NEXT J%
                   NEXT I%
REM
REM        Save intensity measurements in sequential file
REM

           OPEN "INTENSE.DAT" FOR OUTPUT AS #1
           WRITE #1 , NA% , NP%
           FOR Y%=1 TO NA%
                   FOR Z%=1 TO NP%
                                  WRITE #1, IO(Y%,Z%)
                          NEXT Z%
                   NEXT Y%
           CLOSE #1
           OPEN "DIMEN.DAT" FOR OUTPUT AS #1
           WRITE #1, NA% , NP% , IMAX
           FOR Y%=1 TO NA%
                   FOR Z%=1 TO NP%
                                  WRITE #1, IO(Y%,Z%)/IMAX
                          NEXT Z%
                   NEXT Y%
           CLOSE #1
REM
REM

           STOP
           END




REM        VOLTARC.BAS
REM
REM        A program to calculate the UV field produced by 1 Voltarc source
REM        located in the rig for a circular disc-shaped object.
REM
REM
REM        PARAMETER LIST
REM

           PI=3.141592654
REM
REM        Circular disc
REM

           NA%=1
           NP%=64
REM
REM        Voltarc lamp
REM

           NC%=3
           NL%=5
           NZ%=20
REM
REM        DEFINE INTENSITY STORAGE ARRAY
REM

           $DYNAMIC
REM

           DIM IO(NA%,NP%)
REM
REM        VARIABLE SET-UP
REM
REM        Lamp parameters
REM
```

199

```
                 S=13.1
                 AL=0.35
                 WL=0.20
                 RL=7.5E-3
                 RD=0.16
                 OBZ=0.00
REM
                 NPS%=2*NL%*NC%*NZ%
                 SP=S*WL/(AL*NPS%)
REM
REM      Object parameters
REM
                 ORAD=0.033
REM
                 CLS
                 LOCATE 1,1
                 PRINT "NUMBER OF OBJECT POINTS CHOSEN = "
                 LOCATE 1,34
                 PRINT NA%*NP%
                 LOCATE 3,1
                 PRINT "ANULUSES = "
                 LOCATE 3,12
                 PRINT NA%
                 LOCATE 3,30
                 PRINT "POINTS IN EACH ANULUS = "
                 LOCATE 3,56
                 PRINT NP%
REM
REM      OBJECT LOOPS - the UV intensity is caluclated for each point on the object
REM      top in turn.
REM
                 FOR I%=1 TO NA%
                         FOR J%=1 TO NP%
REM
REM      Show object point number
REM
                 LOCATE 8,1
                 PRINT I%
                 LOCATE 8,10
                 PRINT J%
REM
REM      Calculate object point cylindrical polar co-ordinates
REM
                         OBT=(J%-0.5)*2*PI/NP%
REM                      OBR=ORAD*(I%-0.5)/NA%
                         OBR=27E-3
REM
REM
REM      Set intensity summation to zero for new object point
REM
                         ISUM=0
                         IMAX=0
REM
REM      LAMP LOOPS - the contribution from each point source comprising
REM      the UV source must be taken into account.
REM
                 FOR K%=1 TO NZ%
                         FOR L%=1 TO NC%
                                 FOR M%=1 TO 2*NL%
REM
REM      Calculate cylindrical polar co-ordinates of the point source
REM
                                         LT=(M%-1)*PI/NL%
                                         LR=SQR((L%-0.5)*RL^2/NC%)
                                         LL=(K%-0.5)*WL/NZ%
REM
REM      Calculate distance from UV point source to point on object
REM
                                         DX=RD+LR*COS(LT)-OBR*COS(OBT)
```

200

```
                                                    DY=LR*SIN(LT)-OBR*SIN(OBT)
                                                    DZ=LL - OBZ
REM

                                                    RHOS=DX^2 + DY^2 + DZ^2
                                                    RHO=SQR(RHOS)
REM
REM        Calculate UV intensity, corrected for the view factor, and add to
REM        sum total for the object point
REM
                                                    VF=DZ/RHO
                                                    ISUM=ISUM+(1/RHOS)*VF
                                NEXT M%
                        NEXT L%
                NEXT K%
REM
REM        Complete UV intensity calculation
REM
                        ISUM=ISUM*SP/(4*PI)
REM
REM        STORE UV INTENSITY
REM
                        IO(I%,J%)=ISUM
REM
                        IF ISUM > IMAX THEN
                                IMAX=ISUM
                        END IF
REM
                NEXT J%
        NEXT I%
REM
REM        Save intensity measurements in sequential file
REM
        OPEN "INTENSE.DAT" FOR OUTPUT AS #1
        WRITE #1 , NA% , NP%
        FOR Y%=1 TO NA%
                FOR Z%=1 TO NP%
                        WRITE #1, IO(Y%,Z%)
                NEXT Z%
        NEXT Y%
        CLOSE #1
        OPEN "DIMEN.DAT" FOR OUTPUT AS #1
        WRITE #1, NA% , NP% , IMAX
        FOR Y%=1 TO NA%
                FOR Z%=1 TO NP%
                        WRITE #1, IO(Y%,Z%)/IMAX
                NEXT Z%
        NEXT Y%
        CLOSE #1
REM
REM
        STOP
        END


REM
REM        MULTIVOL.BAS  - a program to manipulate the data output from
REM        VOLTARC.BAS  and  VERT.BAS in order to model the case of more than one lamp
REM
REM
REM        Load the data from VOLTARC.BAS - the sequential file INTENSE.DAT
REM
        OPEN "INTENSE.DAT" FOR INPUT AS #1
        INPUT #1, NA% , NP%
        $DYNAMIC
        DIM IO(NA%,NP%)
        DIM MIO(NA%,NP%)
        FOR I%=1 TO NA%
                FOR J%=1 TO NP%
                        INPUT #1, IO(I%,J%)
```

201

```
                NEXT J%
        NEXT I%
        CLOSE #1
REM
REM
REM     Copy the IO array into MIO
REM
        FOR I%=1 TO NA%
                FOR J%=1 TO NP%
                        MIO(I%,J%)=IO(I%,J%)
                NEXT J%
        NEXT I%
REM
REM     Define the number of lamps
REM
        NLA%=2
REM
        NR%=NP%/NLA%
        IMAX=0
REM
REM     CONVERT THE DATA TO THE SPECIFIED MULTI-LAMP SYSTEM
REM
        FOR I%=1 TO NLA%-1
                FOR J%=1 TO NP%
                        C%=J%+NR%*I%
                        IF C%>NP% THEN
                                C%=C%-NP%
                        END IF
                        FOR K%=1 TO NA%
                                MIO(K%,C%)=MIO(K%,C%)+IO(K%,J%)
                                IF MIO(K%,C%)>IMAX THEN
                                        IMAX=MIO(K%,C%)
                                END IF
                        NEXT K%
                NEXT J%
        NEXT I%
REM
REM
REM     Save the multi-lamp intensity data in INTENSE2.DAT
REM
        OPEN "INTENSE2.DAT" FOR OUTPUT AS #1
        WRITE #1, NA% , NP%
        FOR Y%=1 TO NA%
                FOR Z%=1 TO NP%
                        WRITE #1, MIO(Y%,Z%)
                NEXT Z%
        NEXT Y%
        CLOSE #1
        OPEN "DIMEN.DAT" FOR OUTPUT AS #1
        WRITE #1 , NA% , NP% , IMAX
        FOR Y%=1 TO NA%
                FOR Z%=1 TO NP%
                        WRITE #1 , MIO(Y%,Z%)/IMAX
                NEXT Z%
        NEXT Y%
        CLOSE #1
REM
REM
        STOP
        END
```

A1.2.4 UV disinfection tunnel

(a) Background

A computer program, SLABAV, was written to calculate the average UV intensity at specified points on the surface of a slab-shaped object travelling through a 'tunnel' of UV lamps. The computer program SLABRES uses the results from SLABAV to determine the survival of micro-organisms on the 6 surfaces of the slab after passing through the disinfection tunnel in a specified time, T. (See section 6.2.2 for further information).

(b) Program listings

```
REM
REM       SLABAV.BAS
REM
REM       A program to calculate the UV intensity profile on an object
REM       of slab geometry within a tunnel-shaped chamber of UV lamps.
REM
REM       Parameter set-up
REM
REM       UV lamp parameters
REM
          S=13.1                'power output from one UV lamp /W
          LL=0.35               'length of the UV lamp /m
          RL=7.5E-3             'radius of the UV lamp /m
REM
          NC%=3                 'parameters to divide the UV lamp up into finite
          NL%=2                 'zones. At the centre of each finite zone there
          NZ%=10                'is a point UV source.
REM
REM       UV lamp locations
REM
          NUVL%=4                        'number of UV lamps
REM
          DIM UVF%(NUVL%)                 'flag to determine whether the UV lamp is suspended
REM                                       'vertically (0) or horizontally (1)
REM
          DIM UVX(NUVL%)  'cartesian co-ordinates of the top end of the UV lamps
          DIM UVY(NUVL%)  ' (or end with lower x co-ordinate in the case of
          DIM UVZ(NUVL%)  '  horizontal lamps)
REM
REM       Note:   x = distance from start of tunnel
REM               y = distance from wall
REM               z = height above the floor
REM
          RESTORE 1000
          FOR X%=1 TO NUVL%
                  READ UVF%(X%)
                  READ UVX(X%)
                  READ UVY(X%)
                  READ UVZ(X%)
          NEXT X%
REM
          NP%=2*NC%*NL%*NZ%       'number of point sources comprising 1 UV lamp
REM
```

203

```
          SP=S/NP%                    'power output of one point UV source
REM
          PI=3.141593
REM
REM
REM       Slab parameters
REM
          SLABH = 2.00                'slab height /m      (z dimension)
          SLABW = 0.25                'slab width /m       (x dimension)          .
          SLABB = 0.25                'slab breadth /m     (y dimension)
REM
REM
REM       Define the number of locations along the tunnel at which the
REM       surface intensities are to be calculated.
REM
          NTUN%=10                    'number of positions along the tunnel at which
REM                                   the UV intensity is to be calculated.
          NLI1%=10                            'number of points in length of influence #1 (before tunnel)
          NLI2%=10                    'number of points in length of influence #2 (after tuneel)
REM
          NPOS%=NTUN% + NLI1% + NLI2%        'number of positions at which intensity is calculated
REM
REM
          LTUN = 1.000                'length of repeatable section of tunnel
REM
          LENPOS = LTUN/(NTUN%)       'length between positions in the tunnel
REM
REM       Define the number of points on each slab surface at which the UV
REM       intensity is to be calculated.
REM
REM
          N1Z%=9
          N1X%=9
          N2Z%=9
          N2X%=9
          N3Z%=9
          N3Y%=9
          N4Z%=9
          N4Y%=9
          N5X%=9
          N5Y%=9
          N6X%=9
          N6Y%=9
REM
REM       Define the arrays containing the UV intensity profiles for each
REM       of the 6 surfaces of the slab
REM
          DIM S1(NPOS%,N1Z%,N1X%)         'surface 1
          DIM S2(NPOS%,N2Z%,N2X%)         'surface 2
          DIM S3(NPOS%,N3Z%,N3Y%)         'surface 3
          DIM S4(NPOS%,N4Z%,N4Y%)         'etc.
          DIM S5(NPOS%,N5X%,N5Y%)
          DIM S6(NPOS%,N6X%,N6Y%)
REM
REM
REM       Specify the cartesian co-ordinates of the centre of the slab
REM
          SCXB = -(NLI1%-0.5)*LENPOS          'beginning x co-ordinate of slab centre
          SCXE = LTUN + (NLI2%-0.5)*LENPOS    'end x co-ordinate of slab centre
          SCY=1.00 'y co-ordinate
          SCZ=1.00 'z co-ordinate
REM
REM
REM       Main loop - determine slab location in the tunnel
REM
          SCREEN 0
          CLS
          LOCATE 1,1
          PRINT "Slab position no."
```

```
          LOCATE 1,25
          PRINT "/";NPOS%
REM
          FOR P%=1 TO NPOS%
REM
               LOCATE 1,20
               PRINT USING "##";P%
REM
               SCX = SCXB + (P%-1)*LENPOS                    ·
REM
REM       Pick each surface point and calculate the UV intensity at it.
REM
REM       Surface 1
REM
REM
               IAV=0.0000                    'average UV intensity on surface
REM
               FOR I%=1 TO N1Z%
                    FOR J%=1 TO N1X%
REM
REM       State surface point co-ordinates
REM
                         SX=(J%-0.5)*SLABW/N1X% - SLABW/2 + SCX
                         SY=SCY - SLABB/2
                         SZ=-(I%-0.5)*SLABH/N1Z% + SCZ + SLABH/2
REM
                         SURF%=1
                         ISUM=0.0000
REM
                         CALL INTENSE(SURF%,SX,SY,SZ,ISUM)
REM
                         S1(P%,I%,J%) = ISUM
                    NEXT J%
               NEXT I%
REM
REM
REM       Surface 2
REM
               IAV=0.00000
REM
               FOR I%=1 TO N2Z%
                    FOR J%=1 TO N2X%
                         SX=-(J%-0.5)*SLABW/N2X% + SCX + SLABW/2
                         SY=SCY + SLABB/2
                         SZ=SCZ+SLABH/2 - (I%-0.5)*SLABH/N2Z%
REM
                         SURF%=2
                         ISUM=0.0000
REM
                         CALL INTENSE(SURF%,SX,SY,SZ,ISUM)
REM
                         S2(P%,I%,J%) = ISUM
REM
                    NEXT J%
               NEXT I%
REM
REM
REM       Surface 3
REM
               IAV=0.0000
REM
               FOR I%=1 TO N3Z%
                    FOR J%=1 TO N3Y%
                         SX=SCX - SLABW/2
                         SY=SCY + SLABB/2 - (J%-0.5)*SLABB/N3Y%
                         SZ=SCZ + SLABH/2 - (I%-0.5)*SLABH/N3Z%
REM
                         SURF%=3
                         ISUM=0.000
```

205

```
REM
                                    CALL INTENSE(SURF%,SX,SY,SZ,ISUM)
REM
                                    S3(P%,I%,J%) = ISUM
                            NEXT J%
                    NEXT I%
REM
REM
REM     Surface 4
REM
                    IAV = 0.00000
REM
                    FOR I%=1 TO N4Z%
                            FOR J%=1 TO N4Y%
                                    SX=SCX + SLABW/2
                                    SY=SCY - SLABB/2 + (J%-0.5)*SLABB/N4Y%
                                    SZ=SCZ + SLABH/2 - (I%-0.5)*SLABH/N4Z%
REM
                                    SURF%=4
                                    ISUM=0.0000
REM
                                    CALL INTENSE(SURF%,SX,SY,SZ,ISUM)
REM
                                    S4(P%,I%,J%) = ISUM
                            NEXT J%
                    NEXT I%
REM
REM
REM     Surface 5
REM
                    IAV = 0.0000
REM
                    FOR I%=1 TO N5X%
                            FOR J%=1 TO N5Y%
                                    SX=SCX - SLABW/2 + (I%-0.5)*SLABW/N5X%
                                    SY=SCY - SLABB/2 + (J%-0.5)*SLABB/N5Y%
                                    SZ=SCZ + SLABH/2
REM
                                    SURF%=5
                                    ISUM=0.000
REM
                                    CALL INTENSE(SURF%,SX,SY,SZ,ISUM)
REM
                                    S5(P%,I%,J%) = ISUM
                            NEXT J%
                    NEXT I%
REM
REM
REM     Surface 6
REM
                    IAV = 0.00000
REM
                    FOR I%=1 TO N6X%
                            FOR J%=1 TO N6Y%
                                    SX=SCX + SLABW/2 - (I%-0.5)*SLABW/N6X%
                                    SY=SCY - SLABB/2 + (J%-0.5)*SLABB/N6Y%
                                    SZ=SCZ - SLABH/2
REM
                                    SURF%=6
                                    ISUM=0.0000
REM
                                    CALL INTENSE(SURF%,SX,SY,SZ,ISUM)
REM
                                    S6(P%,I%,J%) = ISUM
                            NEXT J%
                    NEXT I%
REM
REM
            NEXT P%
```

206

```
REM
REM
REM         Write results to sequential files
REM
REM

            SCREEN 0
            CLS
REM
            LOCATE 1,1
            PRINT "Calculations complete - writing sequential files containing results"
REM
REM         Surface 1
REM
            OPEN "SURF1.DAT" FOR OUTPUT AS #1
REM
            WRITE #1,NPOS%
            WRITE #1,NTUN%
            WRITE #1,NLI1%
            WRITE #1,NLI2%
            WRITE #1,LTUN
            WRITE #1,LENPOS
REM
            WRITE #1,N1Z%
            WRITE #1,N1X%
REM
            FOR P%=1 TO NPOS%
                    FOR I%=1 TO N1Z%
                            FOR J%=1 TO N1X%
                                    WRITE #1,S1(P%,I%,J%)
                            NEXT J%
                    NEXT I%
            NEXT P%
REM
            CLOSE #1
REM
REM         Surface 2
REM
            OPEN "SURF2.DAT" FOR OUTPUT AS #1
REM
            WRITE #1,NPOS%
            WRITE #1,NTUN%
            WRITE #1,NLI1%
            WRITE #1,NLI2%
            WRITE #1,LTUN
            WRITE #1,LENPOS
REM
            WRITE #1,N2Z%
            WRITE #1,N2X%
REM
            FOR P%=1 TO NPOS%
                    FOR I%=1 TO N2Z%
                            FOR J%=1 TO N2X%
                                    WRITE #1,S2(P%,I%,J%)
                            NEXT J%
                    NEXT I%
            NEXT P%
REM
            CLOSE #1
REM
REM         Surface 3
REM
            OPEN "SURF3.DAT" FOR OUTPUT AS #1
REM
            WRITE #1,NPOS%
            WRITE #1,NTUN%
            WRITE #1,NLI1%
            WRITE #1,NLI2%
            WRITE #1,LTUN
            WRITE #1,LENPOS
```

```
REM
        WRITE #1,N3Z%
        WRITE #1,N3Y%
REM
        FOR P%=1 TO NPOS%
                FOR I%=1 TO N3Z%
                        FOR J%=1 TO N3Y%
                                WRITE #1,S3(P%,I%,J%)
                        NEXT J%
                NEXT I%
        NEXT P%
REM
        CLOSE #1
REM
REM     Surface 4
REM
        OPEN "SURF4.DAT" FOR OUTPUT AS #1
REM
        WRITE #1,NPOS%
        WRITE #1,NTUN%
        WRITE #1,NLI1%
        WRITE #1,NLI2%
        WRITE #1,LTUN
        WRITE #1,LENPOS
REM
        WRITE #1,N4Z%
        WRITE #1,N4Y%
REM
        FOR P%=1 TO NPOS%
                FOR I%=1 TO N4Z%
                        FOR J%=1 TO N4Y%
                                WRITE #1,S4(P%,I%,J%)
                        NEXT J%
                NEXT I%
        NEXT P%
REM
        CLOSE #1
REM
REM     Surface 5
REM
        OPEN "SURF5.DAT" FOR OUTPUT AS #1
REM
        WRITE #1,NPOS%
        WRITE #1,NTUN%
        WRITE #1,NLI1%
        WRITE #1,NLI2%
        WRITE #1,LTUN
        WRITE #1,LENPOS
REM
        WRITE #1,N5X%
        WRITE #1,N5Y%
REM
        FOR P%=1 TO NPOS%
                FOR I%=1 TO N5X%
                        FOR J%=1 TO N5Y%
                                WRITE #1,S5(P%,I%,J%)
                        NEXT J%
                NEXT I%
        NEXT P%
REM
        CLOSE #1
REM
REM     Surface 6
REM
        OPEN "SURF6.DAT" FOR OUTPUT AS #1
REM
        WRITE #1,NPOS%
        WRITE #1,NTUN%
        WRITE #1,NLI1%
```

208

```
          WRITE #1,NLI2%
          WRITE #1,LTUN
          WRITE #1,LENPOS
REM
          WRITE #1,N6X%
          WRITE #1,N6Y%
REM
          FOR P%=1 TO NPOS%
                FOR I%=1 TO N6X%
                      FOR J%=1 TO N6Y%
                            WRITE #1,S6(P%,I%,J%)
                      NEXT J%
                NEXT I%
          NEXT P%
REM
          CLOSE #1
REM
REM
REM       Display results
REM
REM
          LOCATE 5,1
          PRINT "The results have been generated and stored in the sequential files:"
          PRINT
          PRINT "SURF1.DAT - SURF6.DAT for the 6 surfaces of the slab"
          LOCATE 15,1
          INPUT "Hit enter to stop ";S$
REM
REM
          STOP
REM
REM       Cartesian co-ordinates of UV lamps
REM
1000      DATA 0, 0.500,0.000,0.175              'UV lamp #1 (vertical)
          DATA 0, 0.500,0.000,2.175
          DATA 0, 0.500,2.000,0.175
          DATA 0, 0.500,2.000,2.175
REM
REM
          SUB INTENSE(SURF%,SX,SY,SZ,ISUM)
REM
                SHARED NUVL%,NC%,NL%,NZ%,PI,LL,RL,SP,UVX(),UVY(),UVZ()
                SHARED UVF%()
REM
                ISUM=0.00000
REM
                FOR A%=1 TO NUVL%                    'UV lamp loop
                      FOR J%=1 TO NZ%                'lamp height loop
                            FOR K%=1 TO NC%          'lamp circle loop
                                  FOR M%=1 TO 2*NL%  'lamp line loop
REM
REM       Calculate the local cylindrical-polar co-ordinates of the UV point source
REM       (r,l,theta)
                                        T=(M%-1)*PI/NL%
                                        R=SQR((K%-0.5)*RL^2/NC%)
                                        L=(J%-0.5)*LL/NZ%
REM
REM       Convert cylindrical-polar co-ordinates for the UV point source into
REM       cartesian co-ordinates. (X,Y,Z)
REM
                                        IF UVF%(A%)=0 THEN     'vertical lamp
                                              X=UVX(A%) - RL*COS(T)
                                              Y=UVY(A%) + RL*SIN(T)
                                              Z=UVZ(A%) - L
                                        ELSE                   'horizontal lamp
                                              X=UVX(A%) + L
                                              Y=UVY(A%) + RL*SIN(T)
                                              Z=UVZ(A%) + RL*COS(T)
                                        END IF
```

209

```
REM
REM     Calculate the square of the distance between the UV point source
REM     (X,Y,Z) and the point on the surface of the slab (SX,SY,SZ)
REM

                                    RHOS=(X-SX)^2 + (Y-SY)^2 + (Z-SZ)^2

REM
REM     Calculate the view factors
REM
                                    SELECT CASE SURF%
                                         CASE 1
                                         IF Y<SY THEN
                                                   T2=SQR((X-SX)^2+(Y-
SY)^2)
                                                   T1=ABS(Y-SY)
                                                   COSAL=T1/T2
                                                   T2=SQR((Y-SY)^2+(Z-
SZ)^2)
                                                   COSBE=T1/T2
                                         ELSE
                                                   COSAL=0.0000
                                                   COSBE=0.0000
                                         END IF
                                         CASE 2
                                         IF Y>SY THEN
                                                   T2=SQR((X-SX)^2+(Y-
SY)^2)
                                                   T1=ABS(Y-SY)
                                                   COSAL=T1/T2
                                                   T2=SQR((Y-SY)^2+(Z-
SZ)^2)
                                                   COSBE=T1/T2
                                         ELSE
                                                   COSAL=0.0000
                                                   COSBE=0.0000
                                         END IF
                                         CASE 3
                                         IF X<SX THEN
                                                   T1=ABS(X-SX)
                                                   T2=SQR((X-SX)^2+(Y-
SY)^2)
                                                   COSAL=T1/T2
                                                   T1=ABS(Y-SY)
                                                   T2=SQR((Y-SY)^2+(Z-
SZ)^2)
                                                   COSBE=T1/T2
                                         ELSE
                                                   COSAL=0.000
                                                   COSBE=0.000
                                         END IF
                                         CASE 4
                                         IF X>SX THEN
                                                   T1=ABS(X-SX)
                                                   T2=SQR((X-SX)^2+(Y-
SY)^2)
                                                   COSAL=T1/T2
                                                   T1=ABS(Y-SY)
                                                   T2=SQR((Y-SY)^2+(Z-
SZ)^2)
                                                   COSBE=T1/T2
                                         ELSE
                                                   COSAL=0.0000
                                                   COSBE=0.0000
                                         END IF
                                         CASE 5
                                         IF Z>SZ THEN
                                                   T1=ABS(Y-SY)
                                                   T2=SQR((X-SX)^2+(Y-
SY)^2)
                                                   COSAL=T1/T2
```

```
                                                    T1=ABS(Z-SZ)
                                                    T2=SQR((Y-SY)^2+(Z-
SZ)^2)

                                                    COSBE=T1/T2
                                        ELSE
                                                    COSAL=0.0000
                                                    COSBE=0.0000
                                        END IF
                            CASE 6    '
                            IF Z<SZ THEN
                                                    T1=ABS(Y-SY)
                                                    T2=SQR((X-SX)^2+(Y-
SY)^2)

                                                    COSAL=T1/T2
                                                    T1=ABS(Z-SZ)
                                                    T2=SQR((Y-SY)^2+(Z-
SZ)^2)

                                                    COSBE=T1/T2
                                        ELSE
                                                    COSAL=0.0000
                                                    COSBE=0.0000
                                        END IF
                            END SELECT
REM
REM

                                        ISUM=ISUM+1/RHOS *COSAL*COSBE
REM
REM
REM

                                    NEXT M%
                            NEXT K%
                      NEXT J%
                NEXT A%
REM
REM        Take the power output of the lamp into account
REM
                      ISUM=ISUM*SP/(4*PI)
REM
                END SUB
REM
REM

                END



REM
REM        SLABRES.BAS
REM
REM        A program to convert the intensity at the surfaces of a slab into
REM        average UV intensity, fluence and disinfection level given a velocity
REM        for the slab through the tunnel.
REM
                $DYNAMIC
REM
                DIM DISINFS(6)        'disinfection per side
REM
                TOTDISF = 0.000       'total disinfection level for the slab
REM
REM        Slab dimensions
REM
                SLABH = 2.00          'slab height / m  (z dimension)
                SLABW = 0.25          'slab width / m   (x dimension)
                SLABB = 0.25          'slab breadth / m (y dimension)
REM
REM        Calculate the fraction of the total surface area of the slab that
REM        each surface of the slab contributes.
REM
                A1 = SLABW * SLABH
                A2 = SLABW * SLABH
```

211

```
                A3 = SLABB * SLABH
                A4 = SLABB * SLABH
                A5 = SLABB * SLABW
                A6 = SLABB * SLABW
REM
                SAREA = A1 + A2 + A3 + A4 + A5 + A6
REM
                A1 = A1 / SAREA
                A2 = A2 / SAREA
                A3 = A3 / SAREA
                A4 = A4 / SAREA
                A5 = A5 / SAREA
                A6 = A6 / SAREA
REM
                CLS
                PRINT "COMMENCING CALCULATIONS"
REM
REM             Load the results from SLABAV.BAS
REM
REM             Surface 1
REM
                OPEN "SURF1.DAT" FOR INPUT AS #1
REM
                INPUT #1,NPOS%
                INPUT #1,NTUN%
                INPUT #1,NLI1%
                INPUT #1,NLI2%
                INPUT #1,LTUN
                INPUT #1,LENPOS
REM
                INPUT #1,N1Z%
                INPUT #1,N1X%
REM
                DIM S1(NPOS%,N1Z%,N1X%)
                DIM SAV1(N1Z%,N1X%)
                DIM D1(N1Z%,N1X%)
REM
                FOR P%=1 TO NPOS%
                        FOR I%=1 TO N1Z%
                                FOR J%=1 TO N1X%
                                        INPUT #1,S1(P%,I%,J%)
                                NEXT J%
                        NEXT I%
                NEXT P%
REM
                CLOSE #1
REM
REM
REM             Surface 2
REM
                OPEN "SURF2.DAT" FOR INPUT AS #1
REM
                INPUT #1,NPOS%
                INPUT #1,NTUN%
                INPUT #1,NLI1%
                INPUT #1,NLI2%
                INPUT #1,LTUN
                INPUT #1,LENPOS
REM
                INPUT #1,N2Z%
                INPUT #1,N2X%
REM
                DIM S2(NPOS%,N2Z%,N2X%)
                DIM SAV2(N2Z%,N2X%)
                DIM D2(N2Z%,N2X%)
REM
                FOR P%=1 TO NPOS%
                        FOR I%=1 TO N2Z%
                                FOR J%=1 TO N2X%
```

212

```
                              INPUT #1,S2(P%,I%,J%)
                       NEXT J%
                NEXT I%
         NEXT P%
REM
         CLOSE #1
REM
REM
REM    Surface 3
REM
         OPEN "SURF3.DAT" FOR INPUT AS #1
REM
         INPUT #1,NPOS%
         INPUT #1,NTUN%
         INPUT #1,NLI1%
         INPUT #1,NLI2%
         INPUT #1,LTUN
         INPUT #1,LENPOS
REM
         INPUT #1,N3Z%
         INPUT #1,N3Y%
REM
         DIM S3(NPOS%,N3Z%,N3Y%)
         DIM SAV3(N3Z%,N3Y%)
         DIM D3(N3Z%,N3Y%)
REM
         FOR P%=1 TO NPOS%
                FOR I%=1 TO N3Z%
                       FOR J%=1 TO N3Y%
                              INPUT #1,S3(P%,I%,J%)
                       NEXT J%
                NEXT I%
         NEXT P%
REM
         CLOSE #1
REM
REM
REM    Surface 4
REM
         OPEN "SURF4.DAT" FOR INPUT AS #1
REM
         INPUT #1,NPOS%
         INPUT #1,NTUN%
         INPUT #1,NLI1%
         INPUT #1,NLI2%
         INPUT #1,LTUN
         INPUT #1,LENPOS
REM
         INPUT #1,N4Z%
         INPUT #1,N4Y%
REM
         DIM S4(NPOS%,N4Z%,N4Y%)
         DIM SAV4(N4Z%,N4Y%)
         DIM D4(N4Z%,N4Y%)
REM
         FOR P%=1 TO NPOS%
                FOR I%=1 TO N4Z%
                       FOR J%=1 TO N4Y%
                              INPUT #1,S4(P%,I%,J%)
                       NEXT J%
                NEXT I%
         NEXT P%
REM
         CLOSE #1
REM
REM
REM    Surface 5
REM
         OPEN "SURF5.DAT" FOR INPUT AS #1
```

213

```
REM
        INPUT #1,NPOS%
        INPUT #1,NTUN%
        INPUT #1,NLI1%
        INPUT #1,NLI2%
        INPUT #1,LTUN
        INPUT #1,LENPOS
REM
        INPUT #1,N5X%
        INPUT #1,N5Y%
REM
        DIM S5(NPOS%,N5X%,N5Y%)
        DIM SAV5(N5X%,N5Y%)
        DIM D5(N5X%,N5Y%)
REM
        FOR P%=1 TO NPOS%
                FOR I%=1 TO N5X%
                        FOR J%=1 TO N5Y%
                                INPUT #1,S5(P%,I%,J%)
                        NEXT J%
                NEXT I%
        NEXT P%
REM
        CLOSE #1
REM
REM
REM     Surface 6
REM
        OPEN "SURF6.DAT" FOR INPUT AS #1
REM
        INPUT #1,NPOS%
        INPUT #1,NTUN%
        INPUT #1,NLI1%
        INPUT #1,NLI2%
        INPUT #1,LTUN
        INPUT #1,LENPOS
REM
        INPUT #1,N6X%
        INPUT #1,N6Y%
REM
        DIM S6(NPOS%,N6X%,N6Y%)
        DIM SAV6(N6X%,N6Y%)
        DIM D6(N6X%,N6Y%)
REM
        FOR P%=1 TO NPOS%
                FOR I%=1 TO N6X%
                        FOR J%=1 TO N6Y%
                                INPUT #1,S6(P%,I%,J%)
                        NEXT J%
                NEXT I%
        NEXT P%
REM
        CLOSE #1
REM
REM
REM     Data now loaded. Start converting.
REM
        OPEN "DISINF1.DAT" FOR OUTPUT AS #1
        OPEN "DISINF2.DAT" FOR OUTPUT AS #2
        OPEN "DISINF3.DAT" FOR OUTPUT AS #3
        OPEN "DISINF4.DAT" FOR OUTPUT AS #4
        OPEN "DISINF5.DAT" FOR OUTPUT AS #5
        OPEN "DISINF6.DAT" FOR OUTPUT AS #6
        OPEN "DISINFS.DAT" FOR OUTPUT AS #7
REM
REM     Define the residence times at which survival to be calculated
REM
        FOR T = 0.000 TO 2000 STEP 20
REM
```

214

```
REM       Calculate the average UV intensity
REM
REM       Surface 1
REM
          DISINFS(1) = 0.000
REM
          FOR I%=1 TO N1Z%
                  FOR J%=1 TO N1X%
                          SAV1(I%,J%) = 0.0000
                          FOR P%=1 TO NPOS%
                                  SAV1(I%,J%) = SAV1(I%,J%) + S1(P%,I%,J%)
                          NEXT P%
REM
                          SAV1(I%,J%) = SAV1(I%,J%) / NPOS%
REM
REM       Have calculated the average UV intensity per surface point through
REM       the tunnel. Now calculate the disinfection per surface point
REM       achieved in a trip through a specified number of repeatable sections
REM       at a given velocity.
REM
                          CALL DISINF(SAV1(I%,J%),D1(I%,J%))
REM
                          DISINFS(1) = DISINFS(1) + D1(I%,J%)
                  NEXT J%
          NEXT I%
REM
REM       Calculate the disinfection (survival) level for side 1
REM       assuming an even initial microbial load
REM
          DISINFS(1) = DISINFS(1) / (N1Z% * N1X%)
REM
REM       Add to running total of disinfection level for the whole slab
REM
          TOTDISF = DISINFS(1) * A1
REM
REM
REM       Surface 2
REM
          DISINFS(2) = 0.000
          FOR I%=1 TO N2Z%
                  FOR J%=1 TO N2X%
                          SAV2(I%,J%) = 0.0000
                          FOR P%=1 TO NPOS%
                                  SAV2(I%,J%) = SAV2(I%,J%) + S2(P%,I%,J%)
                          NEXT P%
REM
                          SAV2(I%,J%) = SAV2(I%,J%) / NPOS%
REM
REM       Have calculated the average UV intensity per surface point through
REM       the tunnel. Now calculate the disinfection per surface point
REM       achieved in a trip through a specified number of repeatable sections
REM       at a given velocity.
REM
                          CALL DISINF(SAV2(I%,J%),D2(I%,J%))
REM
                          DISINFS(2) = DISINFS(2) + D2(I%,J%)
REM
                  NEXT J%
          NEXT I%
REM
          DISINFS(2) = DISINFS(2) / (N2Z% * N2X%)
REM
          TOTDISF = TOTDISF + DISINFS(2) * A2
REM
REM
REM       Surface 3
REM
          DISINFS(3) = 0.000
REM
```

```
            FOR I%=1 TO N3Z%
                    FOR J%=1 TO N3Y%
                            SAV3(I%,J%) = 0.0000
                            FOR P%=1 TO NPOS%
                                    SAV3(I%,J%) = SAV3(I%,J%) + S3(P%,I%,J%)
                            NEXT P%
REM

                            SAV3(I%,J%) = SAV3(I%,J%) / NPOS%
REM
REM         Have calculated the average UV intensity per surface point through
REM         the tunnel. Now calculate the disinfection per surface point
REM         achieved in a trip through a specified number of repeatable sections
REM         at a given velocity.
REM
                            CALL DISINF(SAV3(I%,J%),D3(I%,J%))
REM
                            DISINFS(3) = DISINFS(3) + D3(I%,J%)
REM
                    NEXT J%
            NEXT I%
REM
            DISINFS(3) = DISINFS(3) / (N3Z% * N3Y%)
REM
            TOTDISF = TOTDISF + DISINFS(3) * A3
REM
REM
REM         Surface 4
REM
            DISINFS(4) = 0.000
REM
            FOR I%=1 TO N4Z%
                    FOR J%=1 TO N4Y%
                            SAV4(I%,J%) = 0.0000
                            FOR P%=1 TO NPOS%
                                    SAV4(I%,J%) = SAV4(I%,J%) + S4(P%,I%,J%)
                            NEXT P%
REM
                            SAV4(I%,J%) = SAV4(I%,J%) / NPOS%
REM
REM         Have calculated the average UV intensity per surface point through
REM         the tunnel. Now calculate the disinfection per surface point
REM         achieved in a trip through a specified number of repeatable sections
REM         at a given velocity.
REM
                            CALL DISINF(SAV4(I%,J%),D4(I%,J%))
REM
                            DISINFS(4) = DISINFS(4) + D4(I%,J%)
REM
                    NEXT J%
            NEXT I%
REM
            DISINFS(4) = DISINFS(4) / (N4Z% * N4Y%)
REM
            TOTDISF = TOTDISF + DISINFS(4) * A4
REM
REM
REM         Surface 5
REM
            DISINFS(5) = 0.000
REM
            FOR I%=1 TO N5X%
                    FOR J%=1 TO N5Y%
                            SAV5(I%,J%) = 0.0000
                            FOR P%=1 TO NPOS%
                                    SAV5(I%,J%) = SAV5(I%,J%) + S5(P%,I%,J%)
                            NEXT P%
REM
                            SAV5(I%,J%) = SAV5(I%,J%) / NPOS%
REM
```

216

```
REM        Have calculated the average UV intensity per surface point through
REM        the tunnel. Now calculate the disinfection per surface point
REM        achieved in a trip through a specified number of repeatable sections
REM        at a given velocity.
REM
                        CALL DISINF(SAV5(I%,J%),D5(I%,J%))
REM
                        DISINFS(5) = DISINFS(5) + D5(I%,J%)
REM
                NEXT J%
        NEXT I%
REM
        DISINFS(5) = DISINFS(5) / (N5X% * N5Y%)
REM
        TOTDISF = TOTDISF + DISINFS(5) * A5
REM
REM
REM        Surface 6
REM
        DISINFS(6) = 0.000
REM
        FOR I%=1 TO N6X%
                FOR J%=1 TO N6Y%
                        SAV6(I%,J%) = 0.0000
                        FOR P%=1 TO NPOS%
                                SAV6(I%,J%) = SAV6(I%,J%) + S6(P%,I%,J%)
                        NEXT P%
REM
                        SAV6(I%,J%) = SAV6(I%,J%) / NPOS%
REM
REM        Have calculated the average UV intensity per surface point through
REM        the tunnel. Now calculate the disinfection per surface point
REM        achieved in a trip through a specified number of repeatable sections
REM        at a given velocity.
REM
                        CALL DISINF(SAV6(I%,J%),D6(I%,J%))
REM
                        DISINFS(6) = DISINFS(6) + D6(I%,J%)
REM
                NEXT J%
        NEXT I%
REM
        DISINFS(6) = DISINFS(6) / (N6X% * N6Y%)
REM
        TOTDISF = TOTDISF + DISINFS * A6
REM
REM
REM        Now write the results to sequential files
REM
        WRITE #1,LOG10(DISINFS(1))
        WRITE #2,LOG10(DISINFS(2))
        WRITE #3,LOG10(DISINFS(3))
        WRITE #4,LOG10(DISINFS(4))
        WRITE #5,LOG10(DISINFS(5))
        WRITE #6,LOG10(DISINFS(6))
        WRITE #7,LOG10(TOTDISF)
REM
        NEXT T
REM
        CLOSE #1
        CLOSE #2
        CLOSE #3
        CLOSE #4
        CLOSE #5
        CLOSE #6
        CLOSE #7
REM
        OPEN "SURFAV1.DAT" FOR OUTPUT AS #1
        OPEN "SURFAV2.DAT" FOR OUTPUT AS #2
```

217

```
                    OPEN "SURFAV3.DAT" FOR OUTPUT AS #3
                    OPEN "SURFAV4.DAT" FOR OUTPUT AS #4
                    OPEN "SURFAV5.DAT" FOR OUTPUT AS #5
                    OPEN "SURFAV6.DAT" FOR OUTPUT AS #6
REM
                    FOR I%=1 TO N1Z%
                            FOR J%=1 TO N1X%
                                    WRITE #1,SAV1(I%,J%)
                                    WRITE #2,SAV2(I%,J%)
                                    WRITE #3,SAV3(I%,J%)
                                    WRITE #4,SAV4(I%,J%)
                                    WRITE #5,SAV5(I%,J%)
                                    WRITE #6,SAV6(I%,J%)
                            NEXT J%
                    NEXT I%
REM
                    CLOSE #1
                    CLOSE #2
                    CLOSE #3
                    CLOSE #4
                    CLOSE #5
                    CLOSE #6
REM
                    LOCATE 10,1
                    PRINT "CALCULATIONS COMPLETE AND RESULTS WRITTEN TO FILES"
REM
                    STOP
REM
REM     Calculate the fractional survival per point for a specified
REM     UV intensity.
REM
                    SUB DISINF(IAV,YAV)
REM
                            SHARED LTUN,T
REM
REM     IAV = average UV intensity
REM     FAV = average UV fluence
REM     YAV = average microbial survival (fractional - NOT in log form)
REM
REM     Specify the slab velocity through the tunnel
REM
                            V = 0.20                 'velocity / m/s
REM
REM
                            RT = LTUN / V                 'residence time in a repeatable section
REM                                                       'of the tunnel.
REM
REM     Define the number of repeatable units which comprise the tunnel.
REM
                            NREPEAT% = 10
REM
REM     First calculate the average survival. Then correct for surface shielding
REM     if specified.
REM
                            FAV = IAV * T
REM
REM     Use surface shielding function.
REM
                            YAV = YACT(FAV)
REM
REM
                    END SUB
REM
REM
                    FUNCTION YACT(FAV)
REM
REM     This function gives the actual disinfection level, YACT, for a given
REM     surface fluence, FAV, when surface shielding parameters are specified.
REM
```

218

```
REM        Unshielded kinetic parameters - 1st order kinetics (UV only)
REM
                K = 2.13E-2
REM
REM        Unshielded kinetic parameters - 1st order kinetics (UV+1.0% H2O2)
REM
                K1 = 0.129
REM
REM        Surface shielding parameters
REM
                NZ% = 1                 'number of zones
                DIM FR(NZ%)             'fraction of m/o's in each zone
                DIM AL(NZ%)             'shielding factors in each zone
REM
                FR(1) = 1.000
REM             FR(2) = 0.2291
REM             FR(3) = 0.3449
REM
                AL(1) = 1.000
REM             AL(2) = 0.2784
REM             AL(3) = 0.01378
REM
REM
                YAC1=0.000
REM
                FOR J% = 1 TO NZ%
REM
REM        Calculate the survival in this zone, YZONE, for the actual fluence
REM        FACT.
REM
                    FACT = FAV * AL(J%)
REM
REM        Define the fraction of coverage of the surface by 1% H2O2 spray
REM
                    COV = 1.00
REM
                    YZONE = (1.0 - COV) * EXP(-K*FACT)
                    YZONE = YZONE + COV * EXP(-K1*FACT)
REM
REM        Add the contribution from this zone to the overall survival
REM
                    YAC1 = YAC1 + FR(J%) * YZONE
                NEXT J%
REM
                YACT = YAC1
REM
            END FUNCTION
REM
            STOP
            END
```

APPENDIX 2. IMPACT TESTS IN THE SPRAY CHAMBER

A2.1 Introduction

It was seen in Chapter 3 that an increase in the disinfection rate could be obtained if the spray was electrostatically-charged. It was proposed that this was due to an increase in the deposition of hydrogen peroxide spray on the test object. In order to investigate this proposition, impact tests were performed with electrostatically-charged sprays so as to directly measure the mass of spray deposited on the test object. The term 'impact tests' refers to the measurement of the mass of spray deposited on the object. Two methods of quantifying the mass of spray deposited on an object's surfaces were developed (see section 2.7). These methods involved collecting the spray deposited on the object in filter paper strips and determining the mass deposited using a precision balance.

A2.2 Impact rate

The spray impact rate on the test object when the spray was not charged was investigated first. Figures A2.1 - A2.3 show the mass of spray deposited on the top of the cylinder and disc objects when placed inside the spray chamber and exposed to an atomised spray of distilled water for various periods of time. Figure A2.2 shows the impact rate under identical conditions to those employed in the disinfection experiments detailed in Chapter 3. These figures show that the impact rate of spray on the top surfaces of the objects was constant over the duration of the experiments and for the particular arrangement employed.
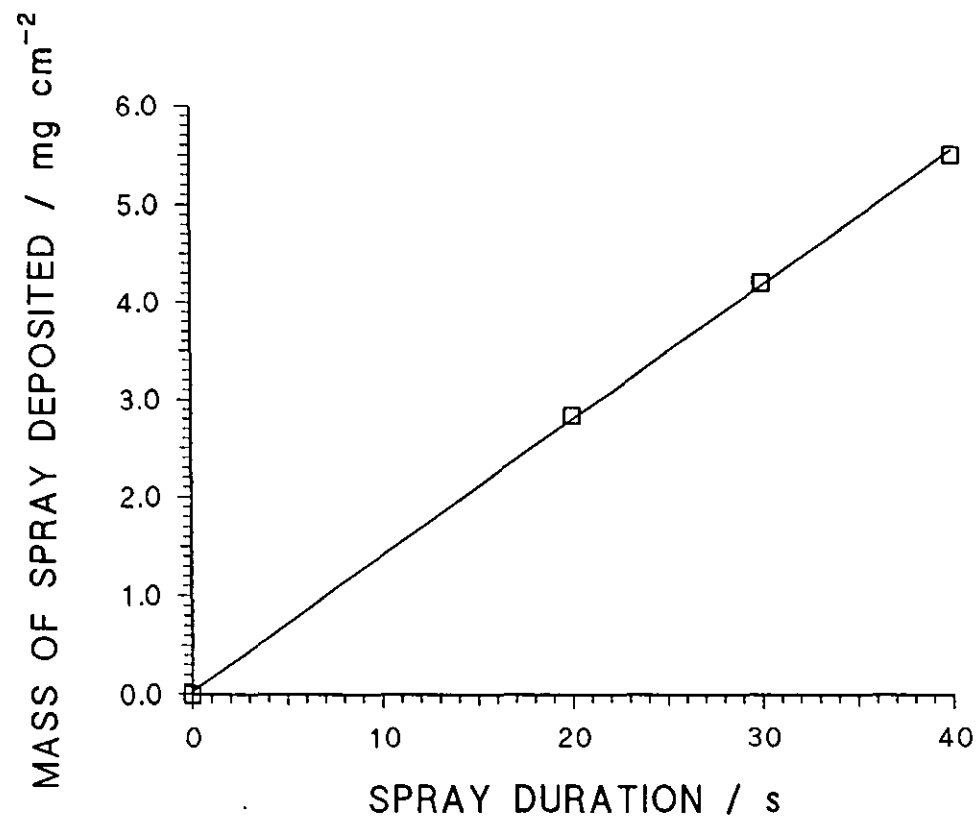
FIGURE A2.1 Spray impact on the top of the PVC cylinder (height = 10 cm, diameter = 4cm)

(Impact rate = 0.138 mg cm^{-2} s^{-1} , Spray rate = 0.30 ml s^{-1})

**FIGURE A2.2 Spray impact rate on top of disc object (height = 2 cm , diameter = 6.6 cm)
under disinfection experimental conditions**
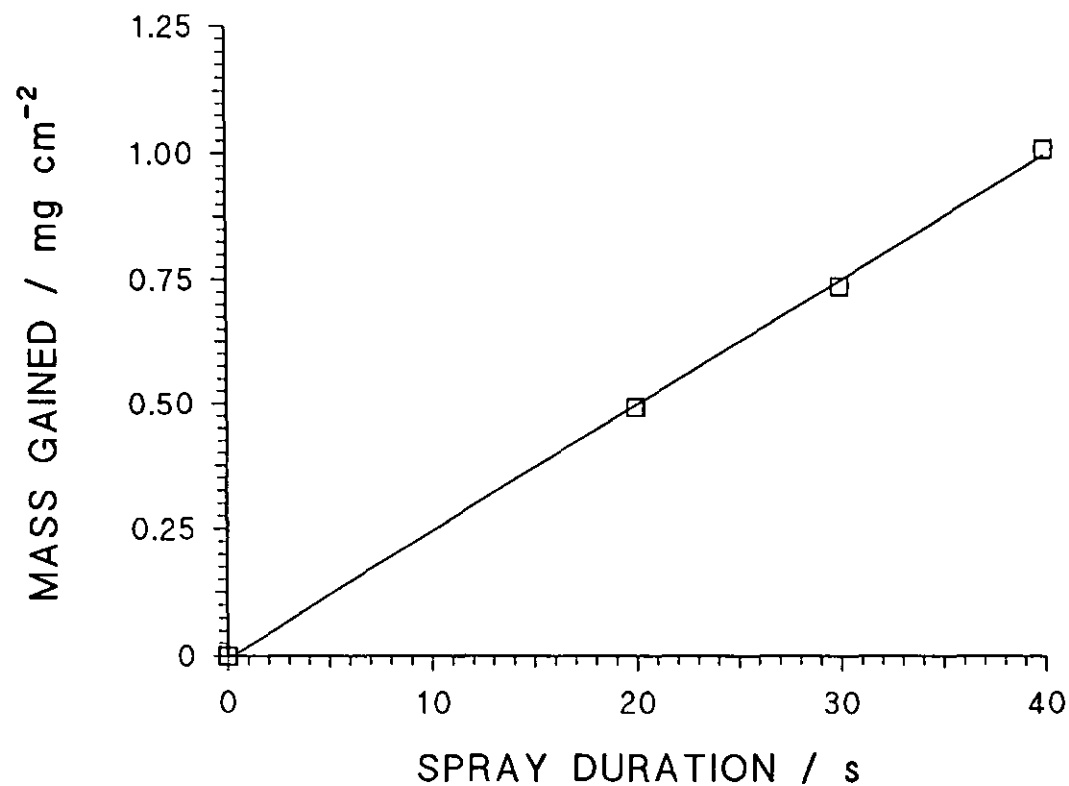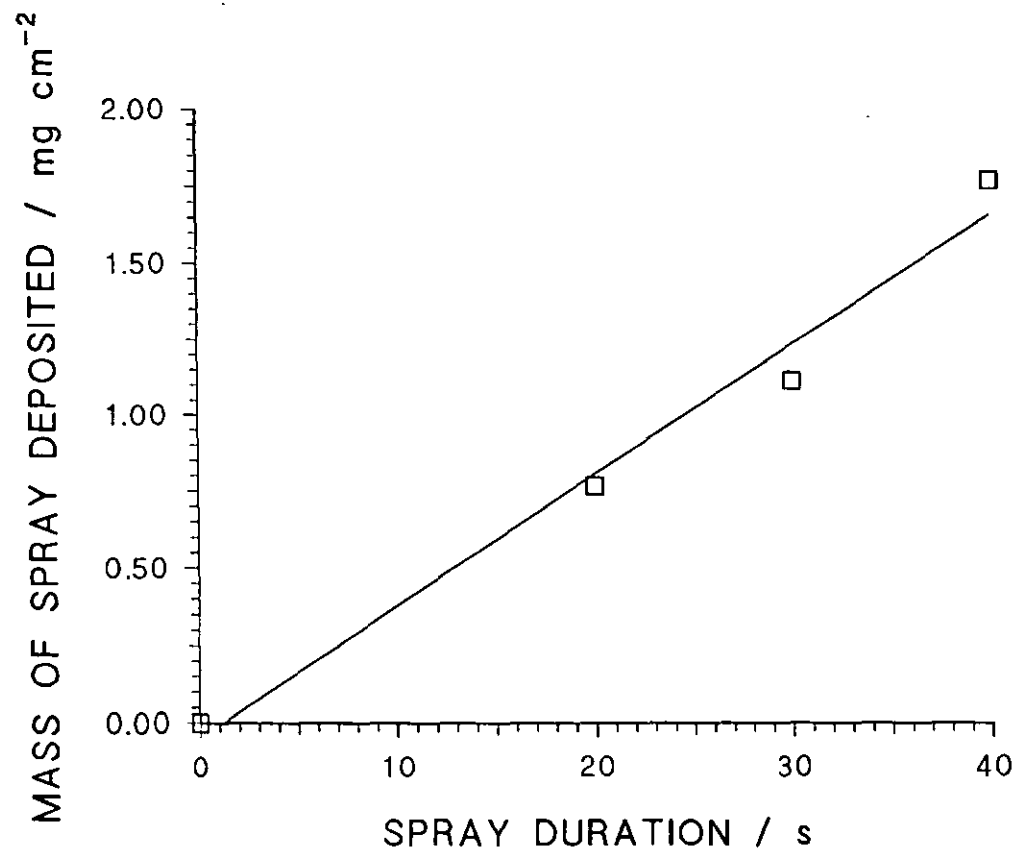(Impact rate = 0.0251 mg cm^{-2} s^{-1} , Spray rate = 0.30 ml s^{-1})

FIGURE A2.3 Spray impact on top of the disc object (height = 2 cm , diameter = 6.6 cm)
(Impact rate = 0.0427 mg cm^{-2} s^{-1} , Spray rate = 0.23 ml s^{-1})

A2.3 Electrostatic spraying

It was previously shown that the use of electrostatic sprays produced an increased disinfection performance (see section 3.6). In order to establish whether this could be attributed to increased deposition of spray on the object, impact tests were undertaken in the spray chamber using distilled water. Three objects were used in these studies - the PVC cylinder (hollow bottom), the PVC disc and the stainless steel hollow cylinder.

It was found that the highest potential that the nozzle could be raised to before a route to earth was created and charge lost (causing 'tripping' of the power supply) was about -16 kV. At this potential short-circuiting paths must have formed, probably by ionising the air in the spray chamber which allowed a circuit to be created from the nozzle through the air, through the QVF body of the spray chamber and finally through the support frame to earth. To avoid this the nozzle was charged to the highest potential (-15 kV) which resulted in stable operation.

Table A2.1 shows the quantity of spray deposited on filter paper strips attached to the side of the stainless steel cylindrical object. Three experiments were performed on two separate days and the table shows the average mass of spray deposited on the filter paper strips. The results show that by raising the nozzle to -15 kV potential, the mass of spray deposited was between 2.3 and 2.7 times greater than for an uncharged nozzle.

The results for the stainless steel and PVC cylinders are shown in Table A2.2. Whilst increased deposition of spray was observed for both objects when the nozzle was charged, the increase in spray deposition was much smaller than had previously been obtained (Table A2.1). The data in Table A2.2 shows only a 10-15% increase in deposition compared to the 130-170% increase in deposition shown in Table A2.1.

Experiment	0 kV NOZZLE	POTENTIAL	-15 kV NOZZLE	POTENTIAL	
	Average mass gained / mg cm^{-2} (A)	Range	Average mass gained / mg cm^{-2} (B)	Range	B / A
1	2.2	+/- 11%	5.0	+/- 17%	2.3
2	2.3	+/- 21%	6.3 '	+/- 19%	2.7

Spray parameters : 30 seconds spray pulse, 1.5 bar feed air pressure

TABLE A2.1   **Effect of electrostatically-charging the spray on the impact rate on the outside of the stainless steel hollow cylindrical object**

Object	Surface	Nozzle potential / kV	Mass gained / mg cm^{-2}	Ratio -15kV / 0 kV
PVC CYLINDER	SIDE	0	1.19	
PVC CYLINDER	SIDE	-15	1.34	1.13
PVC CYLINDER	TOP	0	3.23	
PVC CYLINDER	TOP	-15	3.56	1.10
STAINLESS STEEL CYLINDER	SIDE	0	1.23	
STAINLESS STEEL CYLINDER	SIDE	15	1.35	1.10

Spray parameters : 20 seconds spray pulse, 2.0 bar feed air pressure

TABLE A2.2   **Effect of electrostatically-charging the spray on the impact on surfaces of test objects**

The impact of an electrostatic spray on the disc object was investigated in the spray chamber. Table A2.3 shows the mass of spray deposited on the surfaces of the disc object. The largest increase in deposition on the disc object due to electrostatic spraying was on the side. This was the surface that in normal circumstances, i.e. when the nozzle was uncharged, received the lowest impact in the spray chamber. The bottom surface was directly facing the spray nozzle and the top surface acquired spray because of the settling of spray droplets due to gravity. By charging the spray and earthing the object, a force

component acting towards the centre of the spray chamber would have been created, aiding the deposition of spray droplets on the side of the object. The increase in deposition on the top and bottom of the object are comparable with those shown in Table A2.2. The increase in impact on the side of the cylinder is larger than that previously observed.

The impact rate of an electrostatically-charged spray on the side of the disc object is shown in Figure A2.4. This figure contrasts with Figures A2.1 - A2.3 which show a constant impact rate on the surfaces of the test objects. At low exposure times, the impact rate on the sides of the cylinder was low and only small quantities of spray were deposited. Under these circumstances, the losses due to evaporation from the side of the cylinder prior to sampling would have been appreciable. Therefore the measured mass deposited on the side of the cylinder for short exposure times is likely to have been underestimated.

SURFACE	MASS GAINED at 0 kV / mg cm^{-2}	MASS GAINED at -15 kV/ mg cm^{-2}	RATIO -15 kV / 0 kV
TOP	0.882	1.02	1.16
SIDE	0.053	0.311	5.86
BOTTOM	0.939	1.06	1.13

Spray parameters : 1.5 bar feed air pressure, 20 second spray pulse

TABLE A2.3   **Comparison of impact of spray on disc object using uncharged and electrostatically-charged sprays**

Figure A2.4 again demonstrates an increased deposition rate when the spray nozzle was raised to -15 kV potential. The ratio between the mass of spray deposited when the nozzle was charged compared to when the nozzle was uncharged decreased as more spray was deposited on the surface. As the mass of electrostatically-charged spray deposited onto the surface increased, so did the overall charge present, assuming that the object was not earthed. Repulsion between like charges will occur between the surface and the spray droplets, counteracting the force imposed on the spray droplets due to the electric field between the spray nozzle and the earthed bayonet socket fitting above the object. This will
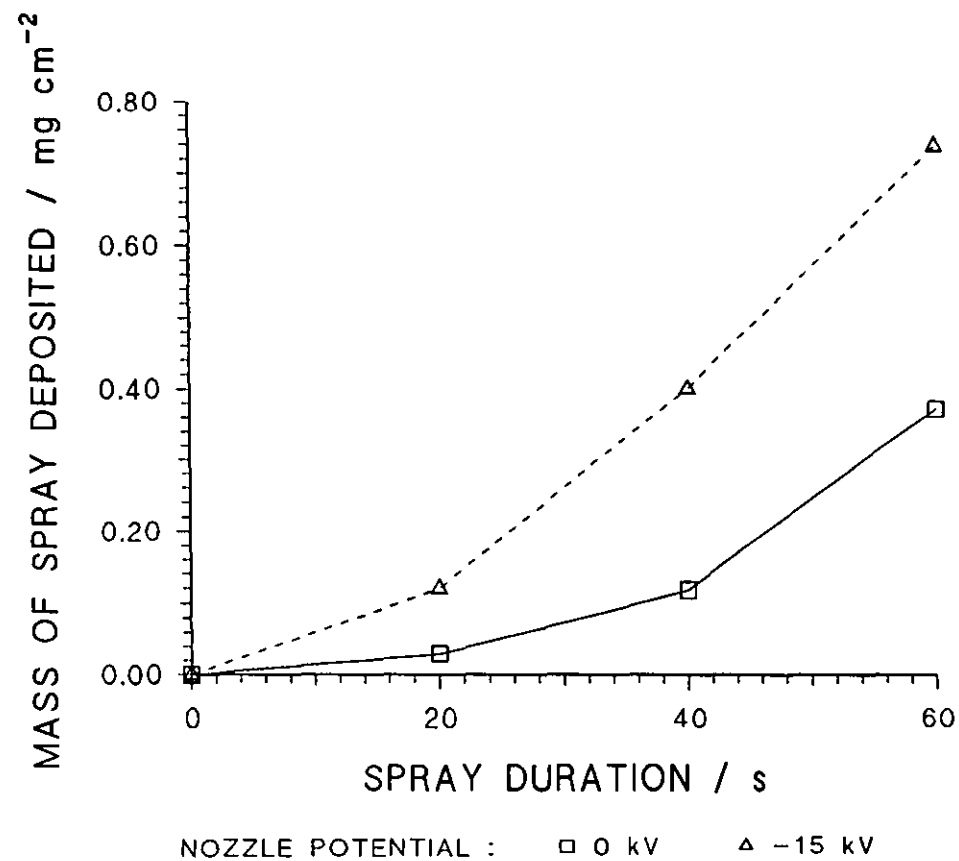
FIGURE A2.4 Impact on the side of the disc object from electrostatic and non-electrostatic sprays

have the effect of lowering the impact rate as spray is accumulated on the surface. This explains in part why on the other surfaces of the squat cylinder where higher impact was observed, i.e. the top and bottom surfaces, electrostatic charging of the spray did not produce so marked an effect.

The effect on enhancing deposition of spray by attractive electrostatic forces can be limited by the momentum of the entrained droplets in the air streams surrounding the object. For example, the data in Table A2.1 showed that an increased impact could be obtained on the outside of the hollow stainless steel cylindrical object using electrostatically-charged sprays. When uncharged sprays were employed, no impact was obtained inside the cylinder when the bottom of cylinder was sealed. Even when electrostatically-charged sprays were employed, no impact was obtained inside the cylinder. As air could not flow through the cylinder (because it was sealed at the bottom) droplets would have to leave the surrounding air streams to enter the hollow cylinder. The absence of deposited spray inside the hollow cylinder could be explained by the entrainment of spray droplets in the surrounding air streams.

The forces produced by the momentum of the air streams created by the air atomising nozzle in the spray sterilisation chamber often would generally act to lessen the effect of the attractive forces of the electrostatically-charged drops to the target. In the absence of the bulk air movement in the chamber, the effect of the electric field was seen by the rapidly clearing electrostatically-charged mist (taking about 5 seconds to clear) compared to the uncharged case where the mist in the chamber took about 2-3 minutes to settle due to gravity.

APPENDIX 3. STATISTICS

A3.1 Introduction

This appendix contains four tables originally shown in Chapter 3 to which have been added the standard deviations of the experimentally-determined parameters for first-order and multi-target disinfection kinetics. The table numbers in this appendix are the same as in Chapter 3, e.g. Table 3.1 is Table A3.1.

All comparisons of inactivation constants were assessed using the Student t-test (Chatfield, 1970) and were all found to be significant at the 99% level.

A3.2 Results

	INACTIVATION RATE CONSTANT $(Jm^{-2})^{-1}$		EXPONENT	LOG_{10} (EXPONENT)	
MEDIUM	Mean	Standard deviation	Mean	Mean	Standard deviation
Distilled water	1.65×10^{-2}	9.88×10^{-4}	2.65	0.423	0.156
Wet Grade 2 filter paper	3.22×10^{-2}	1.29×10^{-3}	2.00	0.301	5.09×10^{-2}
Wet Grade 6 filter paper	9.34×10^{-3}	7.11×10^{-4}	2.00	0.301	0.127

TABLE A3.1   Multi-target kinetic constants for *B.subtilis* spore inactivation by UV

	INACTIVATION RATE CONSTANT $(Jm^{-2})^{-1}$	
MEDIUM	Mean	Standard deviation
Glass microfibre filter paper	1.10×10^{-3}	1.78×10^{-4}
Impervious materials (PTFE, aluminium and stainless steel)	2.28×10^{-2}	1.74×10^{-3}
Anodisc membranes	2.13×10^{-2}	2.09×10^{-3}
Dry Grade 2 filter paper	4.79×10^{-3}	1.43×10^{-4}
Dry Grade 6 filter paper	8.77×10^{-4}	1.34×10^{-4}

TABLE A3.2   First-order kinetic constants for *B.subtilis* spore inactivation by UV

Species	Inactivation rate constant		Target number	LOG_{10} (Target number)		Reference
	Mean	SD		Mean	SD	
B.subtilis (ATCC 6633)	3.81×10^{-2}	9.47×10^{-3}	172	2.24	1.01	This work

TABLE A3.4   Summary of multi-target parameters for *Bacillus* spores exposed to 25.8% or 29% H_2O_2

	UV + 1.0 w/v% H_2O_2 first-order kinetics	
	Inactivation rate coefficient / $(Jm^{-2})^{-1}$	
Medium	Mean	Standard deviation
Wet Grade 2 filter paper	1.02×10^{-1}	4.90×10^{-3}
Wet Grade 6 filter paper	4.95×10^{-2}	2.71×10^{-3}
Aluminium coupons	1.29×10^{-1}	7.89×10^{-3}

TABLE A3.6   Comparison of kinetic parameters for the UV and UV + 1.0 % H_2O_2 process on different surfaces and in distilled water

REFERENCES

M. Adinarayana, E. Bothe and D. Schilte-Frohlinde (1988)
Hydroxyl radical-induced strand break formation in single-stranded polynucleotides and single-stranded DNA in aqueous solution as measured by light scattering and by conductivity. *International Journal of Radiation Biology* **54(5)** 723 - 737.

O.M. Alfano, R.L. Romero and A.E. Cassano (1986)
Radiation field modelling in photoreactors - I. Homogeneous media. *Chemical Engineering Science* **41(3)** 421 - 444.

S. Andrews (1996)
Evaluation of surface disinfection procedures for enumerating fungi in foods: a collaborative study. *International Journal of Food Microbiology* **29** 177 - 184.

T.C. Anestos (1988)
A theoretical model for electric field distribution and enhancement in air-atomised electrostatic spray painting. *Transactions on Industrial Applications* **1A-22(1)** 70 - 74.

Anon - APHA Intersociety Committee (1977)
Methods of air sampling and analysis. *Washington : Publication Office, American Health Association.*

Anon - ICMSF (1980)
Microbial ecology of foods. Volume 1 - Factors affecting life and death of microorganisms. *Academic Press, London.*

R. Bachmann (1975)
Sterilization by intense ultraviolet radiation. *Brown Boveri Review* **5** 206 - 209.

H. Bader and J. Hoigne (1981)
Determination of ozone in water by the indigo method. *Water Research* **15** 449 - 456.

A.G. Bailey (1986)
The theory and practice of electrostatic spraying. *Atomisation and Spray Technology* **2** 95 - 134

A.C. Bajpai, L.R. Mustoe and D. Walker (1987)
Engineering Mathematics. *John Wiley & Sons, Chichester.*

A.C. Bajpai, L.R. Mustoe and D. Walker (1988)
Advanced Engineering Mathematics. *John Wiley & Sons, Chichester.*

M. Baldry (1983)
The bactericidal, fungicidal and sporicidal properties of hydrogen peroxide and peracetic acid. *Journal of Applied Bacteriology* **54** 417 - 423.

231

F.J. Beltran, J.F. Garcia-Araya and B. Acedo (1994)
Advanced oxidation of azatrine in water - II. Ozonation combined with ultraviolet radiation. *Water Research* **28(10)** 2165 - 2174.

C.O. Bennett and J.E. Myers (1983)
Momentum, heat and mass transfer. *McGraw-Hill, London.*

Bergey's Manual of Determinative Bacteriology (Eighth Edition) (1974)
Williams and Wilkins, Baltimore, USA.

S.A. Blenkinsopp and J.W. Costerton (1991)
Understanding bacterial biofilms. *Trends in Biotech.* **9** 138 - 146.

S.S. Block (1983)
Disinfection, sterilization and preservation. *Lea and Febiger, Philadelphia, USA.*

S.F. Bloomfield and M. Arthur (1994)
Mechanisms of inactivation and resistance of spores to chemical biocides. *Journal of Applied Bacteriology (Symposium Supplement)* **76** 91S - 104S.

R.G. Boothroyd (1971)
Flowing gas-solids suspensions. *Chapman and Hall, London.*

O. Cerf and F. Metro (1977)
Tailing of survival curves of *Bacillus licheniformis* spores treated with hydrogen peroxide. *Journal of Applied Bacteriology* **42** 405 - 415.

J.C.H. Chang, S.F. Ossoff, D.C. Lobe, M.H. Dorfman, C.M. Dumais, R.G. Qualls, J.D. Johnson (1985)
UV inactivation of pathogenic and indicator microorganisms. *Applied and Environmental Microbiology* **49(6)** 1361 - 1365.

C. Chatfield (1970)
Statistics for technology. *Penguin, Harmondsworth.*

E. Dahi (1976)
Physiochemical aspects of disinfection of water by means of ultrasound and ozone. *Water Research* **10** 667 - 684.

M. Denis, G. Minon and W.J. Masschelein (1992)
Gas-liquid reactions in UV - ozone systems. *Ozone Science and Engineering* **14** 215 - 230.

M. Dirksen, W.F. Blakely, E. Holwitt and M. Dizdaroglu (1988),
Effect of DNA conformation on the hydroxyl radical-induced formation of 8,5'-cyclopurine 2'-deoxyribonucleoside residues in DNA. *International Journal of Radiation Biology*

54(2) 195 - 204.

L.M. Dorfman and G.E. Adam (1973)
Reactivity of the hydroxyl radical in aqueous solutions. *NSRDS - National Bureau of Standards - 46, U.S. Government Printing Office, Washington, D.C.*.

D.W. Duppler (1992)
Laparoscopic instrumentation, videoimaging, and equipment disinfection and sterilization. *Surgical Clinics of North America* **72(5)** 1021 - 1032.

A. Eisenstark, R.L. Buzard and P.S. Hartman (1986)
Inactivation of phage by near ultraviolet radiation and hydrogen peroxide. *Photochemistry and Photobiology* **44(5)** 603 - 606.

G.P. Ferrazza and E. Grabacki (1990)
The right spray demands the right nozzle. *Chemical Engineering* **(November)** 177 - 182.

D.W. Ferguson, M.J. McGuire, B. Koch, R.L. Wolfe and E.M. Aieta (1990)
Comparing peroxone and ozone for controlling taste and odour compounds, disinfection by-products and microorganisms. *Journal of the American Water Works Association* 181 - 191.

P. Francis, A. Gothard, K. Redhead and S. Pool (1988)
Disinfection with depyrogenation and removal of organics. *Environmental Engineering - Proceedings of the 1988 Joint CSCE - ASCE National Conference* 456 - 463.

A.H. Fu, J.G. Sebranek and E.A. Murano (1994)
Microbial and quality characteristics of pork cuts from carcasses treated with sanitizing sprays. *Journal of Food Science* **59(2)** 306 - 309.

W.H. Glaze, J. Kang and D.H. Chapin (1987)
The chemistry of water treatment processes involving ozone, hydrogen peroxide and ultraviolet radiation. *Ozone Science and Engineering* **9** 335 - 352.

G.G. Greer and S.D.M. Jones (1989)
Effects of ozone on beef carcus shrinkage, muscle quality and bacterial spoilage. *Canadian Institute of Food Science and Technology Journal* **22(2)** 156 - 160.

G.C. Gurzadyan, D.N. Nikogosyan, P.G. Kryukov, V.S. Letokhov, T.S. Balmukhanov, A.A. Belogurov and G.B. Zavilgelskij (1981)
Mechanism of high power picosecond laser UV inactivation of viruses and bacterial plasmids. *Photochemistry and Photobiology* **33** 835 - 838.

Harm, W. (1980a)
Biological effects of ultraviolet radiation. *Cambridge University Press, Cambridge,*

p43, 203.

Harm, W. (1980b) *ibid* p12

Harm, W. (1980c) *ibid* p45 - 49

Harm, W. (1980d) *ibid.* p23 - 39

Harm, W. (1980e) *ibid* p76

Harm, W. (1980f) *ibid* p97 - 100

Harm, W. (1980g) *ibid* p104 - 106

Harm, W. (1980h) *ibid* p43 - 45

Harm, W. (1980i) *ibid* p51 - 55

B.G. Harnulv and B.G. Snygg (1972)
Heat resistance of *Bacillus subtilis* spores at various water activities. *Journal of Applied Bacteriology* 35 615 - 624.

G.D. Harris, M. Asce, D. Adams, W.M. Moore and D.L. Sorensen (1987)
Potassium ferrioxalate as chemical actinometer in ultraviolet reactors. *Journal of Environmental Engineering* 113(3) 612 - 627.

K. Hirose, J. Hoya, K. Satomi and M. Yokoyama (1982)
Sterilization of sausage surface by high intensity UV-lamp system. *Nippon Shokuhin Kogyo Gakkaishi* 29(9) 518 - 521.

Y. Huang and R. Toledo (1982)
Effect of high doses of high and low intensity UV irradiation on surface microbial counts and storage-life of fish. *Journal of Food Science* 47 1667 - 1669.

T.W. Huber, R.A. Reddick and G.P. Kubica (1970)
Germicidal effect of ultraviolet irradiation on paper contaminated with mycobacteria. *Applied Microbiology* 19(2) 383 - 384.

K. Ikemizu, S. Morooka and Y. Kato (1987)
Decomposition rate of ozone in water with ultraviolet radiation. *Journal of Chemical Engineering of Japan* 20(1) 77 - 81.

H.A. Irazoqui, J. Cerda and A.E. Cassano (1973)
Radiation profiles in an empty annular photoreactor with a source of finite spatial dimensions. *AIChE Journal* 19(3) 460 - 467.

K. Ishizaki, N. Shinriki, and H. Matsuyama (1986)
Inactivation of *Bacillus* spores by gaseous ozone. *Journal of Applied Bacteriology* **60** 67 - 72.

S.M. Jacob and J.S. Dranoff (1970)
Light intensity profiles in a perfectly mixed photoreactor. *AIChemE Journal* **16(3)** 359 - 362.

G. Kaess and J.F. Wiedermann (1973)
Effects of ultraviolet irradiation on the growth of micro-organisms on chilled beef slices. *Journal of Food Technology* **8** 59 - 69.

P.B. Kenney, R.K. Prasai, R.E. Campbell, C.L. Kastner and D.Y.C. Fung (1995)
Microbiological quality of beef carcasses and vacuum-packaged subprimals: Process intervention during slaughter and fabrication. *Journal of Food Protection* **58(6)** 633 - 638.

N.A. Klapes and D. Vesley (1990)
Vapour-phase hydrogen peroxide as a surface decontaminant and sterilant. *Applied and Environmental Microbiology* **56(2)** 503 - 506.

M.C. Lagunas-Solar (1995)
Radiation processing of foods: An overview of scientific principles and current status. *Journal of Food Protection* **58(2)** 186 - 192.

S. Leaper (1984)
Comparison of the resistance to hydrogen peroxide of wet and dry spores of *B.subtilis SA22*. *Journal of Food Technology* **19** 695 - 702 .

B.H. Lee, S. Kermasha and B.E. Baker (1989)
Thermal, ultrasonic and ultraviolet inactivation of *Salmonella* in thin films of aqueous media and chocolate. *Food Microbiology* **6** 143 - 152.

A.H. Lefebvre (1989)
Atomisation and Sprays. *Hemisphere Publishing Corporation, London.*

O. Legrini, E. Oliveros and A.M. Braun (1993)
Photochemical processes for water treatment. *Chemical Review* 671 - 698.

S. Lunak and P. Sedlak (1992)
Photoinitiated reactions of hydrogen peroxide in the liquid phase. *Journal of Photochemistry and Photobiology A: Chemistry* **68** 1 - 33.

R.E. Marquis, J. Sim and S.Y. Shin (1994)
Molecular mechanisms of resistance to heat and oxidative damage. *Journal of Applied Bacteriology (Symposium Supplement)* **76** 40S - 48S.

H.R. Massie, H.V. Samis and M.B. Baird (1972)
The kinetics of degradation of DNA and RNA by H_2O_2. *Biochimica et Biophysica acta* **272** 539 - 548.

T.H. Meltzer (1993)
High purity water preparation - for the semiconductor, pharmaceutical, and power industries. *Tall Oaks Publishing Inc, USA..*

C.C.E. Meulemans (1987)
The basic principles of UV-disinfection of water. *Ozone Science and Engineering* **9** 299 - 314.

A.A. Miles and S.S. Misra (1938)
Estimation of the bactericidal power of the blood. *Journal of Hygene* **38** 732 - 748.

S. Morooka, K. Ikemizu and Y. Kato (1978)
Kagaku Kogaku Ronbushi **4** 377.

E.J. Morris (1972)
The practical use of ultraviolet radiation for disinfection processes. *Med. Lab. Technol.* **29** 41 - 47.

N. Munakata, M. Saito and K. Hieda (1991)
Inactivation action spectra of *Bacillus subtilis* spores in extended ultraviolet wavelengths (50 - 300 nm) obtained with synchrotron radiation. *Photochemistry and Photobiology* 761 - 768.

P. Muraca, J.E. Stout and V.L. Yu (1987)
Comparative assessment of chlorine, heat, ozone, and UV light for killing *Legionella pneumophilia* within a model plumbing system. *Applied Environmental Microbiology* **53(2)** 447 - 453.

H. Nakamura (1987)
Sterilisation efficiency of ultraviolet irradiation on microbial aerosols under dynamic airflow by experimental air conditioning systems. *Bulletin of Toyko Medical and Dental University* **34** 25 - 40.

K. Namba and S. Nakayama (1982)
Hydrogen peroxide - catalysed ozonation of refractory organics. I. Hydroxyl radical formation. *Bulletin of the Chemical Society of Japan* 3339 - 3340.

J.G. Padial and N.G. Osborne (1992)
Disinfection and sterilization of reusable endoscopic instruments. *Journal of Gynecologic Surgery* **8(4)** 261 - 263.

J.L. Peel and W.M. Waites (1983)
European patent number 0 022 801. *European Patent Office.*

R.G. Qualls and J.D. Johnson (1983)
Bioassay and dose measurement in UV disinfection. *Applied and Environmental Microbiology* 45 872 - 877.

J.O. Reagan, C.G. Smith and Z.L. Carpenter (1973)
Use of ultraviolet light for extending the retail caselife of beef. *Journal of Food Science* 38 929 - 931.

H. Rhaese and E. Freese (1968)
Chemical analysis of DNA alterations : I. Base liberation and backbone breakage of DNA and oligodeoxyadenylic acid induced by hydrogen peroxide and hydroxylamine. *Biochimica et Biophysica acta* 155 476 - 490.

H. Rhaese, E. Freese and M.S. Melzer (1968)
Chemical analysis of DNA alterations : II. Alteration and liberation of bases of deoxynucleotides and deoxynucleiosides induced by hydrogen peroxide and hydroxylamine. *Biochimica et Biophysica acta* 155 491 - 504.

J.R. Rickloff (1987)
An evaluation of the sporicidal activity of ozone. *Applied and Environmental Microbiology* 53(4) 683 - 686.

C. Ruef (1995)
Nosocomial transmission of methicillin-resistant *staphylococcus-aureus* (MRSA) - possible role of enviromental contamination. *Medical Microbiology Letters* 4(4) 189 - 196.

L.J. Sammartano and R.W. Tuveson (1985)
Hydrogen peroxide induced resistance to broad-spectrum near ultraviolet (300 - 400 nm) inactivation in *Escherichia coli. Photochemistry and Photobiology* 41(3) 367 - 370.

B.F. Severin, M.T. Suidan and R.S. Engelbrecht (1983)
Effects of temperature on ultraviolet light disinfection. *Environmental Science and Technology* 17 717 - 721.

G. Shama (1992)
Inactivation of *Escherichia coli* by ultraviolet light and hydrogen peroxide in a thin film contactor. *Letters in Applied Microbiology* 15 259 - 260.

G. Shama, D.W.M. Gardner, A.P. Martin and N.L. Mason (1994)
Disinfection of particles using ultraviolet light. *Trans IChemE* 72(part C - December) 197 - 200.

R. Sommer and A. Cabaj (1993)
Evaluation of the efficiency of a UV plant for drinking water disinfection. *Water Science and Technology* **27(3-4)** 357 - 362.

V.S. Springthorpe and S.A. Sattar (1990)
Chemical disinfection of virus-contaminated surfaces. *Critical Reviews in Environmental Control* **20(3)** 169 - 229.

J. Staehelln and J. Hoigne (1985)
Decomposition of ozone in water in the presence of organic solutes acting as promotors and inhibitors of radical chain reactions. *Environmental Science and Technology* **19** 1206 - 1213.

C.J. Stannard, J.S. Abbiss and J.M. Wood (1983)
Combined treatment with hydrogen peroxide and ultra-violet irradiation to reduce microbial contamination levels in pre-formed food packaging cartons. *Journal of Food Protection* **46(12)** 1060 - 1064.

P.E. Starke and J.L. Faber (1985)
Ferric iron and superoxide ions are required for the killing of cultered *hepatocytes* by hydrogen peroxide. *Journal of Biological Chemistry* **260(18)** 10099 - 10104.

R.A. Stermer, M. Lasater-Smith and C.F. Brassington (1987)
Ultraviolet radiation - an effective bactericide for fresh meat. *Journal of Food Protection* **50(2)** 108 - 111.

K.E. Stevenson and B.D. Shafer (1983)
Bacterial spore resistance to hydrogen peroxide. *Food Technology* **(Part 11)** 111 - 114.

T. Sugawara, M. Yoneya and H. Ohashi (1981)
Inactivation rate of *Bacillus subtilis* spores irradiated by ultraviolet rays. *Journal of Chemical Engineering of Japan* **14(5)** 400 - 405.

M. Teramoto, S. Imamura, N. Yatagai, Y. Nishikawa and H. Teranishi (1981)
Kinetics of the self-decomposition of ozone and the ozonation of cyanide ion and dyes in aqueous solutions. *Journal of Chemical Engineering of Japan* **14(5)** 383 - 388.

C.G.A. Thomas (1988)
Medical Microbiology. *Bailliere Tindall, London.*

R.T. Toledo, F.E. Escher and J.C. Ayres (1973)
Sporicidal properties of hydrogen peroxide against food spoilage organisms. *Applied Microbiology* **26** 592 - 597.

H.C. Urey, L.H. Dawsey and F.O. Rice (1929)
J. Am.Chem.Soc. **51** 1371

J.M. Van der Molen, J. Garty, B.W. Aardema and W.E. Krumbein (1980)
Growth control of algae and cyanobacteria on historical monuments by a mobile UV unit (MUVU). *Studies in Conservation* 25 71 - 77.

W.M. Waites, S.E. Harding, D.R. Fowler, S.H. Jones, D. Shaw and M. Martin (1988)
The destruction of spores of *Bacillus subtilis* by the combined effects of hydrogen peroxide and ultraviolet light. *Letters in Applied Microbiology* 7 139 - 140.
J. Wang and R.T. Toledo (1986)
Sporicidal properties of mixtures of hydrogen peroxide vapour and hot air. *Food Technology* (**Part 12**) 60 - 67.

G.B. Wickramanayake and O.J. Sproul (1988)
Ozone concentration and temperature effects on disinfection kinetics. *Ozone Science and Engineering* 10 123 - 135.

R.L. Wolfe, M.H. Stewart, S. Liang and M.J. McGuire (1989)
Disinfection of model indicator organisms in a drinking water plant using Peroxone. *Applied and Environmental Microbiology* 2230 - 2241.

E.J. Wolfrum, D.F. Ollis, P.K. Lim and M.A. Fox (1994)
The UV - H_2O_2 process: quantitative EPR determination of radical concentrations. *Journal of Photochemistry and Photobiology A:Chemistry* 78 259 - 265.

P. Yallaly and A. Eisenstark (1990)
Influence of DNA adenine methylase on the sensitivity of *Escherichia coli* to NUV and H_2O_2. *Biochemical and Biophysical Research Communications* **169(1)** 64 - 69.

A.E. Yousef and E.H. Marth (1988)
Inactivation of *Listeria monocytogenes* by ultraviolet energy. *Journal of Food Science* **53(2)** 571 - 573 .

H. Zhou and D. Smith (1994)
Kinetics of ozone disinfection in completely mixed system. *Journal of Environmental Engineering* **120(4)** 841 - 858.